4-1-2003

Theoretical Development of the Core-Drilling Method for Non destructive Evaluation of Stresses in Concrete Structures

Stephen Pessiki

Hakan T. Turker

Follow this and additional works at: http://preserve.lehigh.edu/engr-civil-environmental-atlss-reports

Recommended Citation

Pessiki, Stephen and Turker, Hakan T., "Theoretical Development of the Core-Drilling Method for Non destructive Evaluation of Stresses in Concrete Structures" (2003). ATLSS Reports. ATLSS report number 03-07:.
http://preserve.lehigh.edu/engr-civil-environmental-atlss-reports/28

THEORETICAL DEVELOPMENT OF THE CORE-DRILLING METHOD FOR NONDESTRUCTIVE EVALUATION OF STRESSES IN CONCRETE STRUCTURES

by

Hakan T. Turker

Stephen Pessiki

ATLSS Report No. 03-07

April 2003

THEORETICAL DEVELOPMENT OF THE CORE-DRILLING METHOD FOR NONDESTRUCTIVE EVALUATION OF STRESSES IN CONCRETE STRUCTURES

by

Hakan T. Turker
Graduate Research Assistant
Civil and Environmental Engineering

Stephen Pessiki
Associate Professor
Civil and Environmental Engineering

ATLSS Report No. 03-07

April 2003

ACKNOWLEDGMENTS

iii

TABLE OF CONTENTS

LIST OF FIGURES

ix

xi

LIST OF TABLES

ABSTRACT

This research establishes the theoretical basis for the core-drilling method for the nondestructive evaluation of in-situ stresses in the concrete in an existing structure. In the core-drilling method, a circular core-hole is drilled in to the concrete in a structure under stress, and the displacements that occur on the surface of the concrete as the core hole is drilled are measured. These measured displacements are then related to the in-situ stresses in the structure before drilling the hole.

Relieved displacement equations, equations for measured displacements from relieved displacements, and equations for in-situ stresses from measured displacements were derived for two stress states: (1) biaxial uniform normal and shear stress; (2) biaxial linear normal stress gradient and uniform shear stress. These closed-form equations are first developed for infinite plates in which these stresses were uniform through the plate thickness, and then applied to bounded objects. The closed-form equations were verified by finite element analyses. The evaluation of the applicability of the closed-form equations to objects with finite dimensions was conducted by finite element analyses

Semi-analytical equations were developed for objects with finite dimensions and a core-hole for in-situ stresses uniformly distributed through the object thickness. This development is done by introducing empirical coefficients called calibration constants. Accurate analytical definitions of calibration constants were defined with dimensionless coefficients that make calibration constants material independent.

In addition to first two in-situ states of stress that are uniformly distributed through the depth, a third in-situ stress state comprised of biaxial normal stress and shear stress that are non-uniform through depth is also considered in this research. The incremental core-drilling method is developed primarily for applications in which in-situ stresses are non-uniform through the drilling depth. The incremental core-drilling method involves measuring displacements after successive increments of core-hole depth. Then these measured displacements are related to the in-situ stresses that vary through the depth. Finite element analyses were performed to verify the incremental core-drilling method.

1

CHAPTER 1

INTRODUCTION

1.1. INTRODUCTION

A large percentage of the existing infrastructure in the United States and throughout the world is constructed of concrete. The in-situ stresses in a concrete structure can change over time due to a number of factors, including creep, shrinkage, deterioration, temperature variation, corrosion of embedded reinforcing steel, abnormal loading, and differential settlement of supports. *In-situ stresses* refers to the magnitude and direction of stresses in an existing structure.

Reliable information about the in-situ stresses in concrete in an existing structure is often needed to evaluate the structure. The evaluation may be performed to determine the load rating of the structure, or to decide whether to repair or replace the structure. As just one example, information about the in-situ stress in a prestressed concrete bridge girder can be used to estimate the effective prestress remaining in the girder. This information is useful in predicting the service load behavior and strength of the girder.

Because of so many factors that can affect in-situ stresses in an existing concrete structure, the in-situ state of stress is often difficult to predict analytically. In some cases, the in-situ stresses must be determined through measurements on the actual structure. However, few methods exist for the nondestructive evaluation of in-situ stresses in concrete structures. These existing methods have some limitations and a need exists for additional improved methods.

This research establishes the theoretical basis for a new nondestructive test method to assess the in-situ stresses in the concrete in an existing structure. The method is referred to as the *core-drilling method*. Potential applications of the method include the determination of in-situ stresses in a variety of reinforced concrete, prestressed concrete, and steel-concrete composite structures, including bridges, buildings, retaining walls, tunnels, and containment vessels.

The core-drilling method is similar to Hole-Drilling Strain-Gage Method (ASTM E 837 1994). The Hole-Drilling Strain-Gage Method is an American Society for Testing and Materials (ASTM) Standard Test Method. The method consists of measuring the strains at the surface of a specimen as a hole is drilled. The hole may be drilled completely through the structure. In this case, the hole is called a *through-hole*. A hole that does not penetrate completely through the thickness of the structure is called *blind-hole*. The Hole-Drilling Strain-Gage Method is often

used to determine residual stresses in isotropic linear elastic materials such as in steel structures. However, the method is not applicable to concrete structures because the heterogeneous nature of concrete prevents strain measurements over small gage lengths.

In the proposed core-drilling method, a circular core-hole is drilled in to the concrete in a structure under stress, and the displacements that occur on the surface of the concrete as the core hole is drilled are measured. The hole may be a through-hole, as shown in Figure 1.1. A core hole that does not penetrate completely through the thickness of the structure is called *core-hole*. In this hole, the material inside of the core-hole is not removed. Finally, the general term hole will refer to general case that could be either through-hole or core-hole.

Figure 1.1 illustrates the proposed method. Three points, a, b, and c are shown on the surface of the test object. As the core hole is drilled, each point a, b, c undergoes a relieved displacement (u_r, v_α) relative to the center of the hole. u_r is the radial component of this relieved displacement, and v_α is the tangential component of the relieved displacement. Displacement measurements, resulting from the relieved displacements, are taken between the points along L. The displacement measured between two points due to core-hole drilling is called *measured displacement* and denoted with U. The measured displacements are obtained by measuring the distance along L between two points before and after drilling the hole. These measured displacements U are then related to the in-situ stresses in the structure before drilling the hole. The core-drilling method is nondestructive if the ability of the structure to perform its intended function is not impaired and the core hole can be repaired.

1.1.1. Objective and Scope

The objective of this research is to establish the theoretical basis for the core-drilling method for the nondestructive evaluation of stresses in concrete structures.

Procedures are developed to calculate in-situ stresses from measured displacements for a variety of test configurations (Figure 1.1 is one example), test object geometries, and in-situ stress states. As explained in subsequent chapters, the equations are developed for 13 test configurations. The equations are first developed for infinite plates and then adapted to bounded objects (i.e. real structures). Both uniform and linearly varying stress states are treated. Some of the equations developed in this research are *closed-form* which means that the exact solution is analytically expressible. Other equations are called *semi-analytical* which are developed through a combined analytical and numerical approach.

1.1.2. Approach

In order to achieve the objective of this research, the following approach is taken:

1. Perform literature review of previous research and present techniques related to the measurement of in-situ stresses.

2. Develop closed-form equations for the relieved displacements due to a through-hole drilled in a thin plate in which the in-situ stresses are uniformly distributed through the plate thickness.

3. Develop closed-form equations for measured displacements in terms of relieved displacements.

4. Develop closed-form equations for in-situ stresses due to a through-hole drilled in a thin plate in which the in-situ stresses are uniformly distributed through the plate thickness. The equations express in-situ stresses in terms of measured displacements.

5. Verify the closed-form equations for relieved displacements and in-situ stresses through a comparison between results obtained from finite element analysis and results obtained from the closed-form equations.

6. Evaluate the applicability of the closed-form equations for relieved displacements and in-situ stresses to objects with finite dimensions, including bounded (finite) plates, three-dimensional objects and core-hole case.

7. Develop semi-analytical equations for the relieved displacements and in-situ stresses due to a core-hole drilled in three-dimensional objects in which in-situ stresses uniformly distributed through the object thickness. This is accomplished through the use of calibration constants, similar to what is done for the ASTM hole-drilling method.

8. Verify the equations for core-hole case by conducting finite element analyses.

9. Develop semi-analytical equations for relieved displacements due to a hole drilled in a three-dimensional object in which in-situ stresses are non-uniform through the thickness of the object.

10. Develop semi-analytical equations for in-situ stresses due to a hole drilled in a three-dimensional object in which in-situ stresses are non-uniform through the thickness of the object.

11. Verify the semi-analytical equations for non-uniform stress through thickness case by conducting finite element analyses.

1.2. ORGANIZATION OF THE REPORT

The remainder of this report is organized into seven chapters (Chapters 2-8) in accordance with the research approach summarized above. Chapter 2 presents a literature review of previous research (Task 1). This includes a review of techniques for the measurement of in-situ stresses in concrete and rock, and for the measurement of residual stresses in steel structures.

Chapter 3 presents the development of closed-form equations for relieved displacements, measured displacements and in-situ stresses (Task 2, 3 and 4). For the derivation of the equations, the problem is simplified as drilling a through-hole in an isotropic linear elastic

4

infinite plate in which in-situ stresses are uniformly distributed. This problem is treated as a two-dimensional problem of linear elasticity and equations are derived for plane stress and plane strain assumptions.

Chapter 4 presents the verification of the closed-form equations for relieved displacements and in-situ stresses (Task 5). This verification is done by conducting finite element analyses. The same problem considered for the derivation of the closed-form equations is modeled using finite elements. Then results obtained from the closed-form equations are compared with results obtained from finite element analyses.

Chapter 5 evaluates the applicability of the closed-form equations to objects with finite dimensions (Task 6). A series of finite element models are created to evaluate the closed-form equations for relieved displacements and in-situ stresses to bounded (finite) plates, three-dimensional objects, and core-hole. The width of the plate (W), thickness of the objects (T_p) and depth of the core-hole (h) are considered as parameters in the evaluation.

Chapter 6 presents semi-analytical equations for the core-hole case (Task 7). This development is done by introducing empirical coefficients called calibration constants. Chapter 6 also presents verification of the modified equations (Task 8).

Chapter 7 describes development of semi-analytical equations for relieved displacements and in-situ stresses for non-uniform stress distribution through thickness (Task 9, 10). Chapter 7 also presents verification of the semi-analytical equations (Task 11) for this case.

Finally, Chapter 8 presents the conclusions of this research and outlines the work needed to further the development of the core-drilling method.

1.3. NOTATION

The following is a summary of notation and acronyms used frequently in this report.

a	=	radius of the hole
a_c, b_c, c_c	=	dimensionless calibration coefficients for the uniform stress state
a_{ij}, b_{ij}, c_{ij}	=	dimensionless calibration coefficients for incremental core-drilling method
$a1_c, a2_c$	=	dimensionless calibration coefficients for the uniform stress state
$a1_c(i), a2_c(i)$	=	dimensionless calibration coefficients for the uniform stress state
$b1_c, b2_c$	=	dimensionless calibration coefficients for the uniform stress state
$b1_c(i), b2_c(i)$	=	dimensionless calibration coefficients for the uniform stress state
$c1_c, c2_c$	=	dimensionless calibration coefficients for the uniform stress state
$c1_c(i), c2_c(i)$	=	dimensionless calibration coefficients for the uniform stress state
cp_c	=	coefficients the functions that express in-situ stress variation through depth
h	=	depth of the hole
r	=	distance of any point to center of the hole
r_m	=	radius of the measurement circle
u_i	=	relieved displacement at point i
u_r	=	relieved displacement on radial direction

5

uR	=	normalized relieved displacement in radial direction $= u_r/r$
vR	=	normalized relieved displacement in tangential direction $= u_r/r$
z	=	distance of any point on z direction from the surface
A, B, C	=	calibration constants using the standard elastic laws
A_c, B_c, C_c	=	calibration constants for the geometry and loading
Cp	=	vector of the unknowns which are the coefficients of the assumed in-situ stress function
D_h	=	diameter of the hole
D_m	=	diameter of the fictitious measurement circle
G_A, G_B, G_C	=	influence functions
H	=	z/r_m
Kx	=	angle of the stress gradient, acting in y-z plane on x direction, from y-axis
Ky	=	angle of stress gradient, acting in x-z plane on y direction, from the x-axis
Li	=	distance between two points used to measure displacement Ui
P	=	mean pressure of the in-situ stresses
Q	=	conceptually represent the shear stress
T_p	=	thickness of the plate
U	=	measured displacement measured between two points
UR	=	relieved displacement readings vector
Ui	=	measured displacement between two points whose distance from each other is Li
Ul	=	measured displacement between two points whose distance from each other is Ll
W_p	=	width of the plate
α	=	angle measured counter-clockwise from the direction of x to the direction of u_r
α_l	=	angle measured counter-clockwise from the direction of σ_{max} to the direction of u_r
θ	=	angle measured counter-clockwise from direction of x to the direction of σ_{max}
ϕ_c	=	polynomial of degree c
ζ	=	h/r_m
μ	=	modules of rigidity
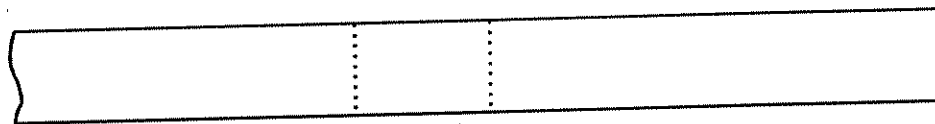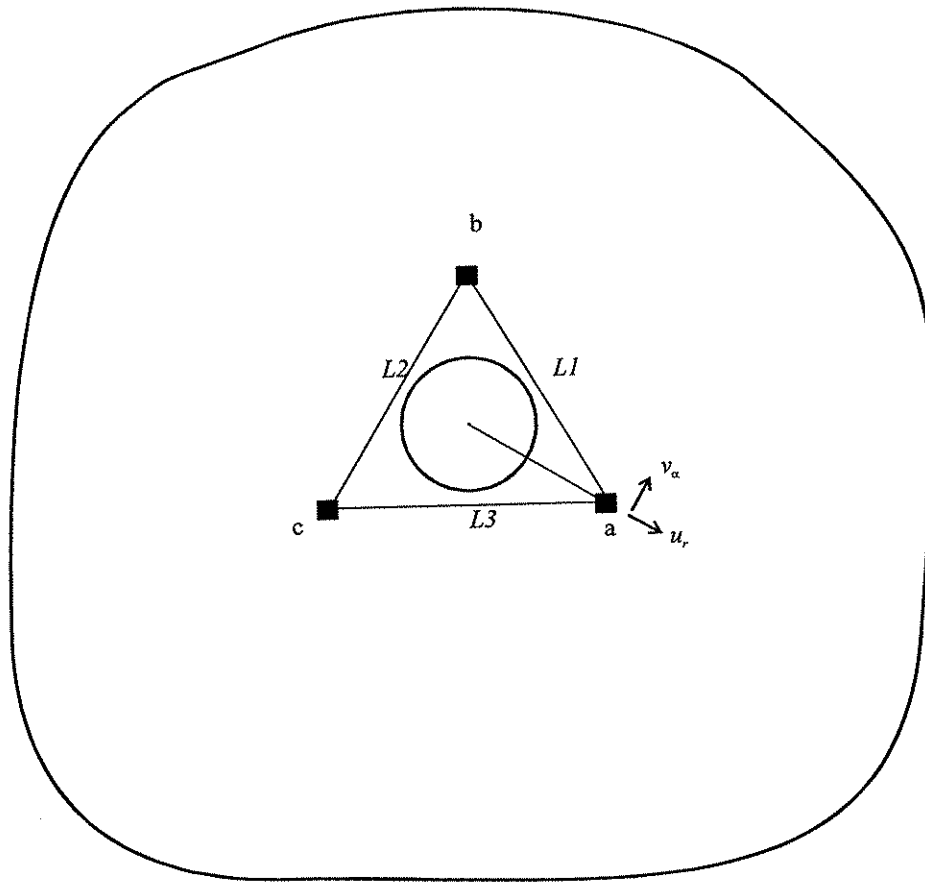
Figure 1.1 Illustration of the core-drilling method.

CHAPTER 2

BACKGROUND

2.1. INTRODUCTION

This chapter presents the results of the literature survey performed as part of Task 1. A review of techniques to measure in-situ stresses in concrete is given in Section 2.2. Section 2.3 describes the Overcoring Method (ASTM E 837 1994), which is an ASTM Standard Test Method for measuring in-situ stress in rock. A detailed description of Hole-Drilling Strain-Gage Method (hereafter referred to as the *hole-drilling method*), which is used mostly to determine residual stresses in linearly elastic, homogenous, materials such as steel, is given in Section 2.4 and Section 2.5. In this work, residual stresses are recognized as specific type of in-situ stresses. As discussed in Chapter 1, the hole drilling-method is an ASTM Standard Test Method which is developed for the cases in which residual stresses are uniform through the thickness of an object. The ASTM hole-drilling method is presented in Section 2.4. Section 2.5 discusses Incremental Hole-Drilling Methods, which are developed for the cases in which residual stresses vary through thickness. Three Incremental Hole-Drilling Methods are reviewed here. An overview of the Power Series Method is given in Section 2.5.1. Detailed descriptions of the Integral and Influence Function Methods are given in Sections 2.5.2 and Section 2.5.3, respectively.

In this chapter, information is presented in the original notation used in the literature to explain each technique. This causes some notations and symbols for similar quantities to vary between techniques in this chapter. In the rest of the chapters, the symbols and notations explained in Chapter 1 are used.

2.2. TECHNIQUES FOR CONCRETE

Two methods which have been developed for the evaluation of in-situ stresses in concrete are the flat jack method and the Nebraska method. These two methods are briefly described below.

2.2.1. Flat-Jack Method

In the flat jack method (Abduner 1982), the distance between two points on the surface of the structure is precisely measured. A slit is then cut into the structure between the two points perpendicular to the direction in which the stress is to be determined. The local stresses in the

8

structure are relieved as the slit is cut, and (for the case of compression) the relative distance between the two known points on the structure decreases. Next, a hydraulic jack (i.e. a flat jack) is inserted in to the slit, the jack is pressurized, and the pressure required to return the two points to their original relative separation is used to indicate the internal stress in the structure. One advantage of the flat jack method is that the elastic modulus of concrete is not needed to compute the value of the in-situ stress. One limitation of the method, which can lead to an error in the estimated value of in-situ stress, arises from the fact that the stress distribution applied by the flat jack may differ from the in-situ stress distribution that existed in the concrete prior to cutting the slit.

2.2.2. Nebraska Method

The Nebraska method (Keeler 1994) was originally developed for the evaluation of effective prestress force in prestressed concrete bridge girders. In the Nebraska method, a 25.4 mm diameter cylindrical hole is drilled in to the test structure, and a small crack is induced in the hole. This crack extends parallel to the direction in which the stress is to be determined. Next external stress is applied perpendicular to the crack, and the stress required to close the crack is determined. This applied stress is then related to the in-situ stress. Special hardware has been developed to clamp to the underside of the bridge girder and apply a transverse stress to cause crack closure. The need to apply this transverse stress may limit the applicability of the method in other applications, since it may be difficult to devise a method to apply the external stress perpendicular to the crack

2.3. OVERCORING METHOD

The Overcoring Method (ASTM D 4623 1996) (hereafter refer to as overcoring method) is a ASTM Standard Test Method for measuring in-situ stress in rock. In this method, a large diameter access hole is drilled to the depth at which the deformations are to be measured. Then a small diameter pilot borehole (38.1 mm) is drilled coaxial with the first access hole an additional distance of approximately 1 m. A specially designed deformation gage developed by U.S. Bureau of Mines is then inserted in the pilot borehole to measure change in dimension of the pilot borehole across three diameters of hole, spaced 60° apart. Then a larger diameter borehole (152.4 mm) with a thin walled core is drilled to over core the rock around the deformation gage in the pilot borehole. The displacements or deformations are recorded before and after the overcoring. At the end of the operation, the overcoring ring containing the measurement cell is removed. The geomechanical properties of the rock (Young's modulus E and Poisson's ratio v) are then determined by performing a biaxial test. With knowledge of the geomechanical properties of the rock, the measured borehole deformation can be related to the change in stress in plane perpendicular to borehole.

9

2.4. HOLE-DRILLING STRAIN GAGE METHOD

The hole-drilling method is a widely used method for measuring residual stresses near the surface of isotropic linearly elastic materials. As noted earlier, the hole-drilling method has been standardized as ASTM Standard Test Method E837 (ASTM E 837 1994).

The basic principle of the hole-drilling method is the measurement of the elastic strains that are relieved while a small diameter hole is drilled in a stressed material. Then these measured strains are related to residual stresses. The method permits the magnitudes and principal directions of residual stresses at the hole location to be determined. A specially designed three-gage rosette shown in Figure 2.1 is used to measure the relieved strains.

In principle, the experimental procedure is simple. The three-gage rosette shown in Figure 2.1 is fixed to the surface of the specimen under consideration. A hole is drilled in the center of the rosette, either completely through the specimen thickness, or to a depth exceeding approximately 40% of the mean diameter of the strain gage circle, as the surface strains are assumed to be fully released at this depth (ASTM E 837 1994). Readings of strains are taken both before and after the hole is drilled. Then these measured relieved strains are related to residual stresses at the hole location. Using the terminology introduced in Chapter 1, a hole drilled through the plate thickness is called a *through-hole*, and a hole which does not extend completely through the plate thickness is called a *blind-hole*.

The hole-drilling method is reported to give good results for the conditions listed below (ASTM E 837 1994):

- Isotropic, linear elastic material
- Residual stresses do not exceed 0.5 yield strength
- Variations of stress within the boundaries of the hole are small
- Stresses do not vary significantly with depth
- Plane stress conditions hold
- Large plate compared to hole size

As mentioned in Chapter 1, the hole-drilling method is not applicable to concrete structures because the heterogeneous nature of concrete prevents strain measurements over small gage lengths.

In most practical applications of the hole-drilling method, a blind-hole is drilled since drilling the hole through thickness is not possible or not feasible. No closed-form solution is available from theory of elasticity for the calculation of residual stresses for the blind-hole geometry. Instead, a solution is obtained for an infinite plate with a through-hole. Then the solution is extended to the blind-hole case.

2.4.1. Through-Hole Analysis

The theoretical solution of the strain relaxation is derived as follows. An elastic plane stress solution for the case of a small hole in an infinite plate under uniform stress is considered to

10

derive the equations. Figure 2.2 shows a schematic representation of residual stresses and a typical surface strain relieved when a hole is drilled into a specimen. The theoretical solution for the radial strain relaxation is

$$\varepsilon = (A + B\cos\alpha)\sigma_{max} + (A - B\cos 2\alpha)\sigma_{min} \tag{2.1}$$

$$A = -\frac{1-\nu}{2E}\left(\frac{a}{r}\right)^2 \tag{2.2}$$

$$B = -\frac{1-\nu}{2E}\left(\frac{4}{1+\nu}\left(\frac{a}{r}\right)^2 - 3\left(\frac{a}{r}\right)^4\right) \tag{2.3}$$

where

σ_{max} = maximum principal stress;

σ_{min} = minimum principal stress;

a = hole radius;

r = general radius, $r > a$;

E = Young modulus;

ν = Poisson ratio;

α = angular coordinate measured counter clockwise from the maximum principal stress direction.

There are three unknowns (σ_{max}, σ_{min}, α) in Equation (2.1). Three equations are obtained by equilibrating the strain gage readings to Equation (2.1). Solving these equations for the unknowns for the strain gage rosette, the result is

$$\sigma_{max,min} = \frac{\varepsilon_1 + \varepsilon_3}{4A} \mp \frac{\sqrt{(2\varepsilon_2 - \varepsilon_1 - \varepsilon_3)^2 + (\varepsilon_1 - \varepsilon_3)^2}}{4B} \tag{2.4}$$

$$\beta = \frac{1}{2}\tan^{-1}\left(\frac{2\varepsilon_2 - \varepsilon_1 - \varepsilon_3}{\varepsilon_1 - \varepsilon_3}\right) \tag{2.5}$$

where

β = angle measured clockwise from the location of gage 1 to the direction of principal stress σ_{min};

11

ε_1, ε_2, ε_3 = relieved strains measured by three correspondingly numbered, radially oriented, strain gages as shown in Figure 2.1.

2.4.2. Blind-Hole Analysis

Equations (2.4) and (2.5) are derived for a through-hole in an infinite plate. However, the equations can also be applied to the case of a blind-hole rather than a through-hole and for measurement of strain over a finite gage area and not at a point. The constants A and B for a blind-hole differ from the values given by Equations (2.2) and (2.3) (ASTM E 837 1994). The constants for the blind-hole case, identified as $\overline{A}$ and $\overline{B}$, are termed calibration constants. They cannot be calculated directly from theoretical formula. However, they can be obtained by a calibration test or numerical procedures such as finite-element analysis.

Constants A and B in the through-hole case are a function of material properties (E, ν) and the non-dimensional distance of the measurement point from the center of the hole (r/D). In addition to these variables, constants $\overline{A}$ and $\overline{B}$ in blind-hole case are a function of the dimensionless hole depth, Z/D. Thus, in a generalized functional form, the coefficients can be expressed as

$$\overline{A} = f(E, \ \nu, \ r, Z/D) \tag{2.6}$$
$$\overline{B} = f(E, \ \nu, \ r, Z/D)$$

where D is diameter of the gage circle.

The constants $\overline{A}$ and $\overline{B}$ are material dependent. They have to be determined for each material to be studied. Alternative formulas which contain material independent constants are proposed for the given material properties, and for through-hole case and blind-hole situation (Schajer 1981).

$$\overline{A} = -\left(\frac{1+\nu}{2E}\right)\overline{a} \tag{2.7}$$

$$\overline{B} = -\left(\frac{1}{2E}\right)\overline{b} \tag{2.8}$$

$\overline{a}$ is material independent and $\overline{b}$ depends weakly only on Poisson's ratio. Schajer (1988a; 1988b) has determined from finite element analysis that for blind-holes, $\overline{a}$ and $\overline{b}$ vary by less than 2% for the range of Poisson's ratio from 0.25 to 0.35. These dimensionless coefficients are tabulated in ASTM E 837.

2.5. INCREMENTAL HOLE-DRILLING METHOD

The basic hole-drilling method described in the ASTM Standard is intended primarily for applications in which residual stresses are uniform through the drilling depth. In such cases, the method and calibration data can be used to calculate the residual stresses from the measured

strain relaxation. However, in practical application, significant variations of residual stresses are often observed. In such cases, the procedure and calibration data provided in ASTM E837 are not applicable.

There is no closed-form solution available for the case of non-uniform residual stress through thickness. However, several approximate calculation procedures have been developed. In these methods, the hole is drilled in successive increments and the strain gage responses are recorded at each increment. In general, these methods are called Incremental Hole-Drilling Methods. Using Incremental Hole-Drilling Methods, it is possible to obtain the residual stresses as a function of depth measured from the specimen surface. Many different stress calculation procedures for incremental hole drilling have been developed, including the Incremental Strain Method (Kelsey 1956), Average Stress Method (Nickola 1986), Power Series Method (Schajer 1981), Integral Method (Schajer 1981; 1988a; 1988b), and Influence Functions (Beghini 1998; 2000).

In all of these calculation methods, plane stress conditions are assumed, and the residual stress variation is therefore described by the variation of the in plane stresses through depth. The calibration constants are obtained by numerical methods. The experimental procedure in the incremental hole-drilling method is similar to the procedure for the basic hole-drilling method.

Schajer (1988a) compared the first four methods listed in his work and concluded that

> "The Integral Method is the most general of the four stress calculation procedures, and is suitable for calculations with irregular stress fields. The Power Series Method *(Schajer 1981)* is suitable for use with smoothly varying stress fields. It is relatively robust numerically because the least-square procedure used tends to smooth out the effects of random errors in the experimental strain data. It is shown that the Incremental Strain and Average Stress Method are simple approximations of the Integral Method. For slightly non-uniform stress fields, all stress calculation methods give satisfactory results. For more steeply varying stress fields, the Incremental Strain and Average Stress Methods become increasingly unreliable, particularly for the stress more remote from the specimen surface."

Beghini (1998; 2000) reported that the Influence Function method is superior to the Integral and Power Series Methods by overcoming the need of interpolation, which might be needed in Integral and Power series methods.

For the reasons explained above, only the Power Series, Integral and Influence Function Methods will be explained here. In this study, the Integral Method and Influence Function Method are modified for non-uniform stress state through the object thickness.

2.5.1. The Power Series Method

The power series method was proposed by Schajer (1981). In this method, the residual stress variation through thickness is represented by a polynomial function. An arbitrary stress field can be decomposed into an equibiaxial and a shear stress component. (Equibiaxial stress state means a stress field under equal biaxial normal stresses. Any stress field can be decomposed into

13

equibiaxial and shear stress components where equibiaxial stress components are defined with mean biaxial normal stresses). Consider the biaxial component given as

$$\sigma_b(h) = b_0 + b_1 h + b_2 h^2 + b_3 h^3 + \dots \tag{2.9}$$

where h is the hole depth and b_i are the unknown constants. The strain response at hole depth, corresponding to $\sigma_b(h)$ is given as follows

$$\varepsilon_b(h) = b_0 \lambda_0(h) + b_1 \lambda_1(h) + b_2 \lambda_2(h) + \dots \tag{2.10}$$

where $\lambda_i(h)$ are the strain responses to unit power series stress fields h. The $\lambda_i(h)$ constants are calculated by application of finite elements. By use of the equal biaxial part of the incrementally released strain and Equation (2.9), the b_i constants can be obtained by least squares analysis. Then, subsequently, the equibiaxial component of the residual stress variation can be calculated by Equation (2.9). By a similar calculation of shear stress component, the arbitrary stress field can be determined.

Unfortunately, only the first two terms of the polynomial give accurate results. Additional terms give results which are very sensitive to error. For the same reason, the maximum depth is limited to 0.5 r_m where r_m is radius of the strain gage rosette.

2.5.2. Integral Method

Initial developments of the Integral Method were done by Bijak-Zochawski (1978), and followed by several others (e.g. Flaman 1985; Niku-Lari 1985; Schajer 1981). Schajer provided a valuable contribution to development of a correct procedure for obtaining non-uniform residual stresses through thickness. Here in this study, the Schajer (1981; 1988a; 1988b) approach is adopted to explain the Integral Method.

Schajer (1988a) described transformed stress and strain variables that are convenient to work with. The stress components acting at depth H in terms of transformed stress variables P, Q, and T are

$$P(H) = \frac{\sigma_3(H) + \sigma_1(H)}{2} \tag{2.11}$$

$$Q(H) = \frac{\sigma_3(H) - \sigma_1(H)}{2} \tag{2.12}$$

$$T(H) = \tau_{13}(H) \tag{2.13}$$

where

$H = Z/r_m$ = non-dimensional depth from surface;

$Z =$ depth from surface;

$r_m =$ strain gage mean radius.

$\sigma_l(H)$, $\sigma_2(H)$, and $\tau_{13}(H)$ represent normal and shear stress components in the reference system aligned with the rosette in Figure 2.1. Similarly, the following terms of measured strain are defined in terms of transformed strain variables p, q, and t

$$p(h) = \frac{\varepsilon_3(h) + \varepsilon_1(h)}{2} \qquad\qquad (2.14)$$

$$q(h) = \frac{\varepsilon_3(h) - \varepsilon_1(h)}{2} \qquad\qquad (2.15)$$

$$t(h) = \frac{\varepsilon_3(h) + \varepsilon_1(h) - 2\varepsilon_2(h)}{2} \qquad\qquad (2.16)$$

where

$h=z/r_m =$ non-dimensional hole depth;

$z =$ hole depth.

$\varepsilon_1(h), \varepsilon_2(h)$, and $\varepsilon_3(h)$ are strain gage measurements when the blind-hole depth is h. Terms $P(H)$ and $p(h)$ are related to the equibiaxial residual stress-strain level, while $Q(H)$, $T(H)$ and $q(h)$, $t(h)$ are related to the stress-strain shear level.

In order to simplify the calculation, it is convenient to consider each transformed stress or strain independently. For example, consider the transformed stresses $P(H)$ alone distributed through the depth of the structure within the range $0 \leq H \leq h$. In order to define a general model, an infinite body made of a homogeneous isotropic linear elastic material is assumed. As shown in Figure 2.3, as a hole is drilled to a certain depth h, the stresses $P(H)$ at every distance H from surface to hole depth h contribute to relaxed strain measured at the surface. Thus measured transformed strain relaxation $p(h)$, because of drilling a hole of depth h can be obtained by integrating of the infinitesimal strain relaxation component from the stress at all depth increment from surface to the hole depth (in the range $0 \leq H \leq h$).

$$p(h) = \frac{1+\nu}{E} \int_0^h A(H,h)P(H)dH \qquad\qquad (2.17)$$

where $A(H,h)$ is the strain relaxation per unit depth caused by a unit stress at depth H, when the hole depth is h.

We can also write the Equation (2.17) in a form that is suitable for practice where strain relaxations are measured at each depth increment.

15

$$\sum_{j=1}^{j=i} \overline{a}_{ij} P_j = \frac{E}{1+v} p_i \qquad 1 \leq j \leq i < n \tag{2.18}$$

where

p_i = measured strain relaxation after the ith hole depth increment;

P_j = equivalent uniform stress within the jth hole depth increment;

$\overline{a}_{ij}$ = strain relaxation due to a unit stress within increment j of a hole i increments   deep (see Figure 2.4 for the physical explanation of $\overline{a}_{ij}$).

The constant $\overline{a}_{ij}$ is defined as

$$\overline{a}_{ij} = \int_{H_{j-1}}^{H_j} A(H,h_i)dH \tag{2.19}$$

In matrix notation, Equation (2.19) becomes

$$\overline{a}P = \frac{E}{(1+v)} p \tag{2.20}$$

where four increments

$$\overline{a} = \begin{bmatrix} \overline{a}_{11} & & & \\ \overline{a}_{21} & \overline{a}_{22} & & \\ \overline{a}_{31} & \overline{a}_{32} & \overline{a}_{33} & \\ \overline{a}_{41} & \overline{a}_{42} & \overline{a}_{43} & \overline{a}_{44} \end{bmatrix} \qquad P = \begin{bmatrix} P_1 \\ P_2 \\ P_3 \\ P_4 \end{bmatrix} \qquad p = \begin{bmatrix} p_1 \\ p_2 \\ p_3 \\ p_4 \end{bmatrix} \tag{2.21}$$

where P_j are the equivalent uniform transformed resulting stress within each hole depth increment. Figure 2.4 shows a physical interpretation of the constants of $\overline{a}_{ij}$ of matrix $\overline{a}$. Equation (2.20) and similarly the other transformed stresses can be written in matrix notation as follows.

$$\overline{a}P = \frac{E}{1+v} p \tag{2.22}$$

$$\overline{b}Q = Eq \tag{2.23}$$

$$\overline{b}T = Et \tag{2.24}$$

where $\overline{b}$ is

$$\overline{b}_{ij} = \int_{H_{j-1}}^{H_j} B(H,h_i)dH \tag{2.25}$$

16

where $B(H,h_i)$ is the strain relaxation function for hole-drilling into a pure shear stress field.

The stress components can be obtained as follows

$$\sigma_1(H) = P(H) - Q(H) \tag{2.26}$$

$$\sigma_3(H) = P(H) + Q(H) \tag{2.27}$$

$$\tau_{13}(H) = T(H) \tag{2.28}$$

And principal stresses are obtained as

$$\sigma_{max}, \sigma_{min} = P(H) \mp \sqrt{Q^2(H)T^2(H)} \tag{2.29}$$

$$\beta(H) = \frac{1}{2}\tan^{-1}\left[\frac{T(H)}{Q(H)}\right] \tag{2.30}$$

where the $\beta(H)$ is the angle measured clockwise from direction 3 (Figure 2.1) to the maximum principal stress direction at depth H.

2.5.2.1. Calculation Constants a_{ij} and b_{ij}

The constants $\bar{a}_{ij}$ and $\bar{b}_{ij}$ can be found by finite element analysis. It was found that finite element analysis gave reliable results for calculating residual stress (Schajer 1988a; Schajer 1988b). A separate finite element analysis is performed for each combination of hole depth and stress location to calculate each constant. The constant $\bar{a}_{ij}$ relates an equibiaxial stress acting in increment j, in a hole i increments deep, to relieved displacement response. The constants $\bar{b}_{ij}$ are, similarly, the correlation constants between pure shear stress and relieved displacement response. The constant $\bar{a}_{ij}$ is required to consider axisymmetrical part to which is applied axisymmetrical load. However, the coefficient $\bar{b}_{ij}$, corresponding pure shear stress, is required to consider non-axisymmetric loading.

2.5.3. Influence Functions Method

In the Power Series and Integral Methods, the structure analyzed is divided in to a finite number of intervals. Residual stresses are found approximately by a discontinuous stepping function. The constants of the stepping functions in these two methods are calculated by the finite element method and tabulated for a finite number of regularly spaced hole depths and positions along the hole surface. However, in application, the hole depths that are used could be different from the hole depths for which the constants have been tabulated. In that case, two-dimensional interpolation is required.

17

The Influence Function Method overcomes this drawback by introducing a continuous function, called influence function (Beghini (1998; 2000)). The influence function allows a general residual stress distribution to be found directly by reading the relaxed strains from the strain gage rosette. The influence function can be employed to evaluate the constants required for the application of Integral Method without interpolation of tabular values.

2.5.3.1. Theory of Influence Function Method for the Hole-Drilling Method

The theoretical formulation of the Influence Function Method for the hole-drilling method is similar to the Integral Method. The main difference between the Influence Function Method and the Integral Method is the definition of calibration constants. The calibration constants (A, B) in the Integral Method are replaced with continuous functions called influence functions (I_A, I_B). Similar to the hole-drilling Method, the Influence Function Method is formulated for a homogenous, isotropic, linear elastic material. The same standard strain gage rosette as shown in Figure 2.1 is used.

The Integral Method uses so called transformed stress variables

$$P(Z) = \frac{\sigma_x(Z) + \sigma_y(Z)}{2} \tag{2.31}$$

$$Q(Z) = \frac{\sigma_x(Z) - \sigma_y(Z)}{2} \tag{2.32}$$

$$T(Z) = \tau_{xy}(Z) \tag{2.33}$$

where

Z = depth from surface.

$\sigma_x(Z)$, $\sigma_y(Z)$, and $\tau_{xy}(Z)$ represent normal and shear stress components in the reference system aligned with the rosette in Figure 2.1. Similarly, the following terms of measured strain are defined in terms of transformed strain variables.

$$p(z) = \frac{\varepsilon_3(z) + \varepsilon_1(z)}{2} \tag{2.34}$$

$$q(z) = \frac{\varepsilon_3(z) - \varepsilon_1(z)}{2} \tag{2.35}$$

$$t(z) = \frac{\varepsilon_3(z) + \varepsilon_1(z) - 2\varepsilon_2(z)}{2} \tag{2.36}$$

where

18

z = hole depth.

$\varepsilon_1(z)$, $\varepsilon_2(z)$, and $\varepsilon_3(z)$ are strain gage measurements at depth Z. The terms $P(Z)$ and $p(z)$ are related to equibiaxial residual stress-strain level, while $Q(Z)$, $T(Z)$ and $q(z)$, $t(z)$ are related to the stress-strain shear level.

In Figure 2.5, assume that the strain $p(z)$ relieved on the surface after drilling the hole with depth of z, is the integral of infinitesimal strains due to the residual stresses $P(Z)$ acting in the entire depth. The following equations are written on the basis of superposition principle

$$p(z) = \int_0^z I_A(Z,z)P(Z)dZ \qquad (2.37)$$

Similarly, the following equations can be written for the residual stresses $Q(Z)$ and $T(Z)$

$$q(z) = \int_0^z I_B(Z,z)Q(Z)dZ \qquad (2.38)$$

$$t(z) = \int_0^z I_B(Z,z)T(Z)dZ \qquad (2.39)$$

where I_A and I_B are suitable influence functions, of geometry and material properties to be determined, which are proportional to the strain relieved on the surface due to the stress acting at depth z when the hole has a total depth of z. This formulation corresponds to Integral Method in the hole-drilling method. The calibration constants (A, B) in Integral Method are replaced with influence functions (I_A, I_B).

For the known influence functions and measured strains, we can find stress variations through the hole depth by Equations (2.37), (2.38), (2.39).

The following dimensionless influence functions are defined for the particular rosette shown in Figure 2.1, dimensionless hole diameter ϕ, and material properties (E, ν).

$$A(H,h) = r_m E I_A(Z,z) \qquad (2.40)$$

$$B(H,h) = r_m E I_B(Z,z) \qquad (2.41)$$

where,

$H = Z/r_m$;

$h = z/r_m$;

$\phi = D_o/r_m$;

r_m = strain gage mean radius.

$A(H,h)$ and $B(H,h)$ are defined by double-power expansions as follows

$$A(H,h) = \sum_{k=1}^{n} \sum_{l=1}^{m} \alpha_{kl} H^{k-1} h^{l-1} \qquad (2.42)$$

$$B(H,h) = \sum_{k=1}^{n} \sum_{l=1}^{m} \beta_{kl} H^{k-1} h^{l-1} \qquad (2.43)$$

where the constants α_{kl} and β_{kl} depend on ϕ, gage geometry and ν.

2.5.3.2. Calculation of Constants α_{kl} and β_{kl}

The constants α_{kl} and β_{kl} are obtained from the finite element analyses. In the analyses, the incremental hole-drilling process is simulated by removing subsequent layers of elements. For any partial hole depth $h_i = h_{max} i/N (i=1,...,N)$, a series of loading conditions is subjected as shown in Figure 2.6 by applying a compressive unit pressure to the hole surface in the interval depths $(0, h_j)$ with $j=1,..., I$ in order to simulate a positive residual stress relaxation.

Equations (2.42) and (2.43) are integrated to get the strain produced by relaxing a unit pressure from 0 to H in a hole having depth h.

$$\hat{A}(H,h) = \sum_{k=1}^{n} \sum_{l=1}^{m} \frac{\alpha_{kl}}{k} H^{k} h^{l-1} \qquad (2.44)$$

$$\hat{B}(H,h) = \sum_{k=1}^{n} \sum_{l=1}^{m} \frac{\beta_{kl}}{k} H^{k} h^{l-1} \qquad (2.45)$$

Equations (2.44) and (2.45) are written in discrete form as follows.

$$Ep_{ij} = \sum_{k=1}^{n} \sum_{l=1}^{m} \frac{\alpha_{kl}}{k} h_j^{k} h_i^{l-1} \qquad (2.46)$$

$$Eq_{ij} = \sum_{k=1}^{n} \sum_{l=1}^{m} \frac{\beta_{kl}}{k} h_j^{k} h_i^{l-1} \qquad (2.47)$$

Beghini discussed that $n=m=6$ (i.e. 36 coefficients for each Influence Function) offers a reasonable compromise between accuracy and numerical stability. Numerical stability refers to numerically stable algorithm for solving $Ax = b$ is guaranteed to compute an approximate solution y satisfying $(A + dA)y = (b+db)$ for some small perturbations dA and db. The numbers of unknowns are considerably smaller than the number of equations (about 820 for each function) and a least-squares solution is used to find the unknowns.

20
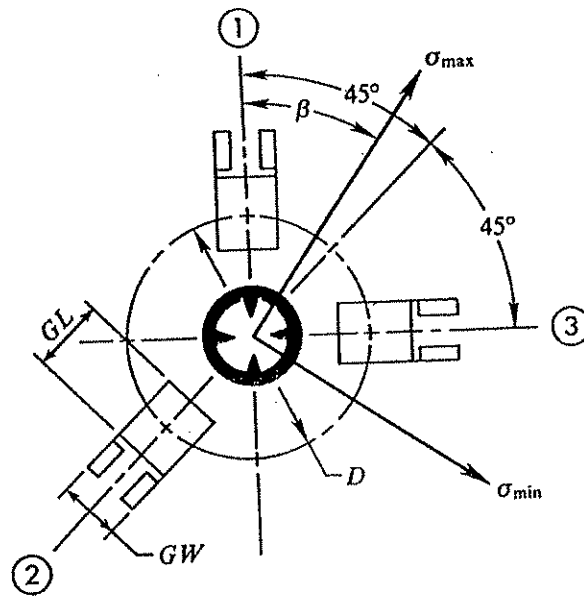
Figure 2.1 Typical standard rosette for hole-drilling residual stress calculation (ASTM E 837 1994).
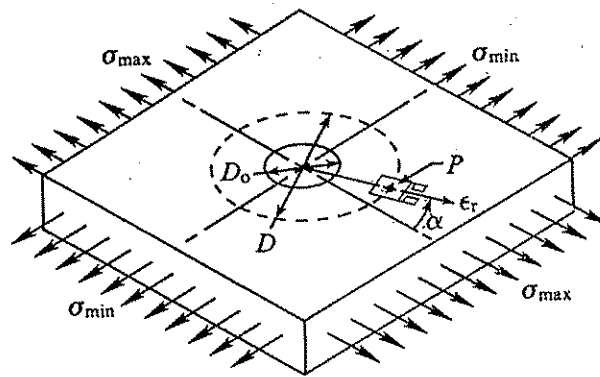
Figure 2.2 Stress state before hole is drilled (ASTM E 837 1994).
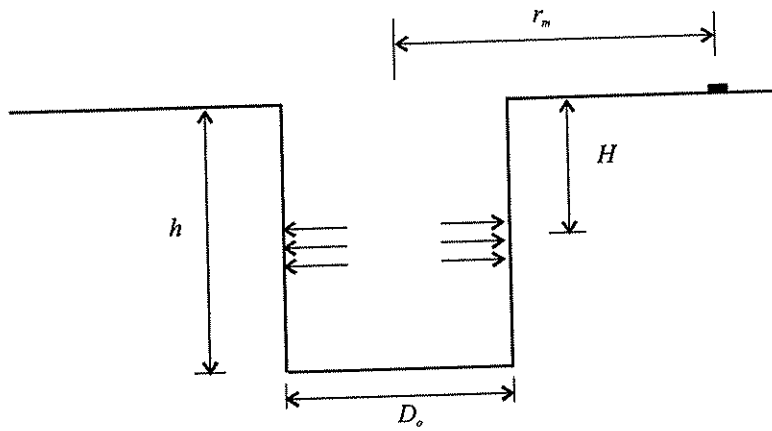
Figure 2.3 Integral Method definition of hole depth h and stress depth H.
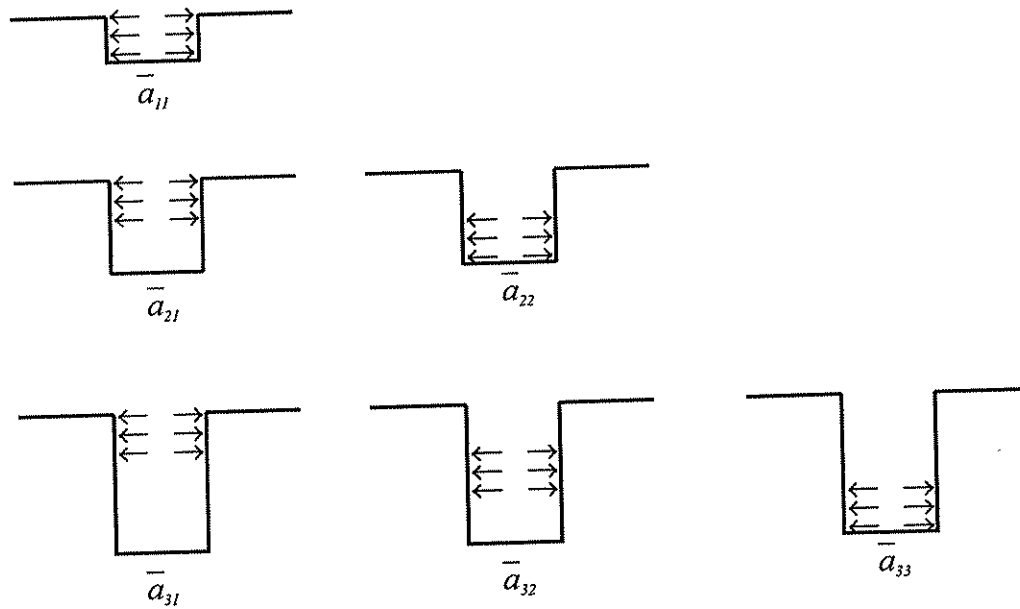
Figure 2.4 Stress loading corresponding to the coefficients $\bar{a}_{ij}$ of matrix $\bar{a}$ in the Integral Method.
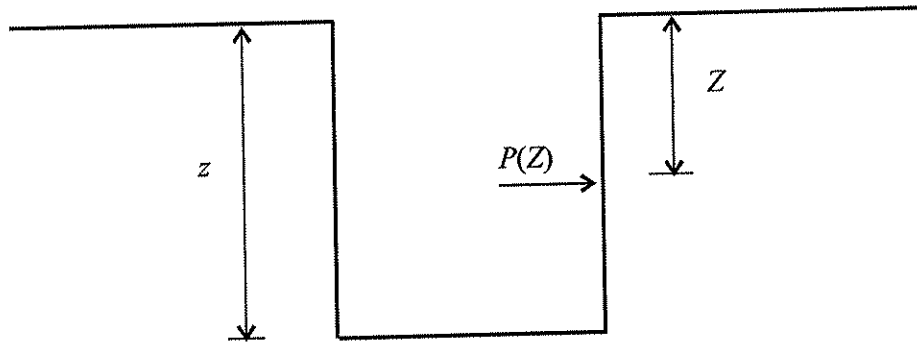
Figure 2.5 Illustration of hole depth z and stress depth Z in the Influence Function Method.
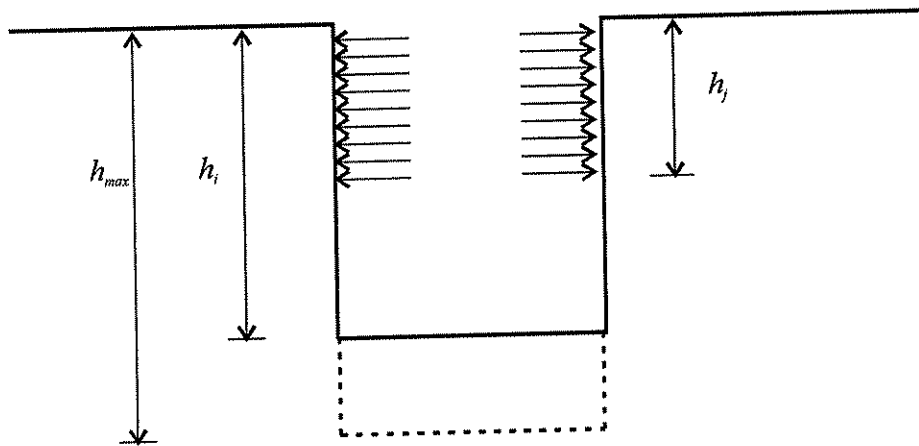
Figure 2.6 Scheme for finite element evaluation of the cumulative Influence Function.

CHAPTER 3

DERIVATION OF CLOSED-FORM IN-SITU STRESS EQUATIONS

3.1. INTRODUCTION

As explained before, in the core-drilling method, a core-hole is drilled in to a stressed area in a structure. As the core-hole is drilled, in-situ stresses are relieved and the displacements resulting from the core-hole drilling are measured. These measured displacements are related to in-situ stresses that existed before drilling the core-hole in the structure.

This chapter derives closed-form equations that form the theoretical basis for the core-drilling method. As defined in Chapter 1, closed-form equation means that the exact solution is analytically expressible. The main objective of this chapter is to derive closed-form equations that express in-situ stresses as a function of measured displacements U. The following paragraphs explain the scope of the derivations presented in this chapter.

Figure 3.1 shows a measurement location and in-situ stress before a core-hole is drilled in to a structure. Now imagine that a core-hole is drilled and the hole surface is subjected to equal stresses as previously existed, as shown in Figure 3.2(a). No stress and displacement change occurs under this condition. The equilibrium remains unchanged. The equilibrium stresses are radial (σ_r) and shear stress ($\tau_{r\alpha}$). In Figure 3.2 (b), equal and opposite stresses to those in Figure 3.2 (a) are applied at the core-hole. It is assumed that the material is linear elastic. The loading shown in Figure 3.2(b) can therefore be superposed with that in Figure 3.2(a), and the sum of these two, shown in Figure 3.2(c), is the resulting stress state after the core-hole is drilled. Thus, the loading in Figure 3.2(b), and the associated displacements, corresponds to the in-situ stress relaxation due to the drilling of the core-hole. The foregoing shows that the in-situ stress relaxation due to core-hole drilling, and the corresponding displacement relaxation, can be modeled as shown in Figure 3.2(b).

The illustration discussed in Figure 3.2 treats the core-hole case. Unfortunately, because of the complexity of the core-hole geometry, there is no closed-form solution available from the theory of elasticity. In order to solve this problem, it is simplified as an infinite thin plate with a hole drilled completely through the plate thickness (i.e. a through-hole) and loaded at the hole surface, as shown in Figure 3.3. N and T are the in-situ stresses that are relieved due to the through-hole drilling. These stresses are a function of α. If we know the in-situ state of stress

prior to hole drilling in the structure, we can calculate the stresses N and T that act on the through-hole surface.

Three different in-situ states of stress are considered in this research. The first in-situ state of stress is biaxial uniform normal and shear stress, shown in Figure 3.4. In this research, this in-situ state of stress is called the *uniform stress state*. The second in-situ state of stress considered in this research is biaxial linear normal stress gradient and uniform shear stress, shown in Figure 3.5. In this research, this in-situ state of stress is called the *linear gradient stress state*. Kx and Ky are the angles of linear stress gradients from the y and x-axes, respectively. All the stresses and angles in Figure 3.4 and Figure 3.5 are shown in the accepted positive sign convention. The linear gradient stress state case is the more general stress state. The uniform stress state is a specific case of the linear gradient stress state where $Kx = Ky = 0$. In the derivations, since linear gradient stress state involves more parameters to describe it, more measured displacements are needed to evaluate it. Third in-situ state of stress in this research is biaxial uniform normal and shear stress that are non-uniformly distributed through depth. In this research, this in-situ state of stress is called the *non-uniform stress state through depth*. The first two in-situ states of stress are considered for the derivation of the closed-form equations in this chapter. The non-uniform stress state through thickness is treated in Chapter 7.

The other assumptions made in the derivations presented in this chapter are that the material is linear elastic, isotropic, homogenous, and that the load is uniformly distributed through the plate thickness. Now this problem can be solved for the load calculated from in-situ state of stress. This problem is treated as two-dimensional problem of linear elasticity and solved for plane stress and plane strain assumptions.

In order to derive equations for in-situ stresses as function of measured displacements, the following steps are followed. First, equations for relieved displacements (u_r, v_a) are derived for both the uniform stress state and the linear gradient stress state. The relieved displacement equations (u_r, v_a) are then used to determine measured displacements (U). Then, equations are derived which express the in-situ stresses as a function of measured displacements. In this research, the term *in-situ stress equation* refers to an equation that expresses in-situ stresses as function of measured displacements. The equations that express uniform stress state as a function of measured displacements are called *uniform in-situ stress equations*. The equations that express the linear gradient in-situ stress state as a function of measured displacements are called *linear gradient in-situ stress equations*.

The organization of the remainder of this chapter is as follows. Section 3.2 derives equations for relieved displacements due to a through-hole in a thin plate for the uniform stress state. Section 3.3 derives equations for relieved displacements due to a through-hole in a thin plate for the linear gradient stress state. Section 3.4 explains how measured displacements are obtained from relieved displacements. Section 3.5 provides an overview of how the in-situ stress equations are derived from the measured displacements. Section 3.6 derives in-situ stress equations for the uniform in-situ stress state. Section 3.7 derives in-situ stress equations for linear gradient stress state.

3.2. RELIEVED DISPLACEMENT EQUATIONS FOR UNIFORM STRESS STATE

In this section, relieved displacement equations are derived for the uniform stress state, shown in Figure 3.4. As shown in Figure 3.4, this state is represented by either cartesian stress components (σ_{xx}, σ_{yy}, τ_{xy}) or principal stresses and principal stress direction (σ_{max}, σ_{min}, θ). In generalized functional form, the relieved displacement equations for the uniform stress state are expressed as follows.

$$u_r, \ v_\alpha = f(\sigma_{xx}, \sigma_{yy}, \tau_{xy}), \ f(\sigma_{xx}, \sigma_{yy}, \tau_{xy}) \tag{3.1}$$

$$u_r, \ v_\alpha = f(\sigma_{max}, \sigma_{min}, \theta), \ f(\sigma_{max}, \sigma_{min}, \theta) \tag{3.2}$$

where the u_r is relieved displacement on radial direction due to a hole drilled and v_α is relieved displacement on tangential direction due to a hole drilled.

First, closed-form equations for relieved displacements are derived in terms of the cartesian stress components (σ_{xx}, σ_{yy}, τ_{xy}) in Section 3.2.1. Then the closed-form equations for the relieved displacements are derived as a function of principal stresses and principal stress direction (σ_{max}, σ_{min}, θ) in Section 3.2.2.

3.2.1. Relieved Displacement Equations in Terms of Cartesian Stress Components

Figure 3.6 shows an infinite thin plate under the uniform stress state expressed in terms of cartesian stress components. Shown as dashed lines are the location where a through-hole will be drilled. Consider an infinitesimal point A on the dashed circle. The stress state on the infinitesimal point A is shown in Figure 3.6 (c). From the equilibrium of the stresses on the radial and tangential directions, we get normal (σ_r) and shear stress ($\tau_{r\alpha}$) components as shown below.

$$\sigma_r = \frac{\sigma_{xx} + \sigma_{yy}}{2} + \frac{\sigma_{xx} - \sigma_{yy}}{2}\cos 2\alpha + \tau_{xy}\sin 2\alpha \tag{3.3}$$

$$\tau_{r\alpha} = -\frac{\sigma_{xx} - \sigma_{yy}}{2}\sin 2\alpha + \tau_{xy}\cos 2\alpha \tag{3.4}$$

To obtain the relieved displacements, stresses of equal magnitude and opposite sign of these stresses are applied to the edge of the through-hole as was shown earlier in Figure 3.3. The normal (N) and the shear stresses (T) represent the relieved in-situ stresses after drilling the through-hole. The applied stresses are

$$N = -\sigma_r = -\frac{\sigma_{xx} + \sigma_{yy}}{2} - \frac{\sigma_{xx} - \sigma_{yy}}{2}\cos 2\alpha - \tau_{xy}\sin 2\alpha \tag{3.5}$$

26

$$T = -\tau_{r\alpha} = \frac{\sigma_{xx} - \sigma_{yy}}{2} \sin 2\alpha - \tau_{xy} \cos 2\alpha \tag{3.6}$$

Now the problem we need to solve is an infinite plate with a circular through-hole subjected to normal (N) and tangential (T) stresses at the edge of the through-hole as shown in Figure 3.3. The problem is solved for displacement using the potential function of complex method [see, for example Muskhelishvili (1953)].

The biharmonic equation as the governing equation for an isotropic material is given as

$$\nabla^4 U = \frac{\partial^4 U}{\partial x^4} + \frac{\partial^4 U}{\partial y^4} + 2\frac{\partial^4 U}{\partial x^2 \partial y^2} = 0 \tag{3.7}$$

This two-dimensional problem of the theory of elasticity can be solved by finding a biharmonic function $U(x, y)$ that satisfies boundary conditions.

It is known that the biharmonic function $U(x, y)$ can be expressed as

$$U(x, y) = \text{Re}[\bar{z}\varphi(z) + \kappa(z)] \tag{3.8}$$

where $\varphi(z)$ and $\chi(z)$ are analytic functions of complex variable z. $\bar{z}$ is conjugate of z,

where

$$z = x + iy = re^{i\alpha} \tag{3.9}$$

$$\bar{z} = x - iy = re^{-i\alpha} \tag{3.10}$$

where r and α define the cylindrical coordinate system. r is the radial distance of a point from the center. The displacement and stress equation for a polar coordinate system is given as (Muskhelishvili (1953))

$$2\mu(u_r + iv_\alpha) = e^{-i\alpha}\left\{\chi\varphi(z) - z\overline{\varphi'(z)} - \overline{\psi(z)}\right\} \tag{3.11}$$

$$X_n + iY = \varphi(z) + z\overline{\varphi'(z)} + \overline{\varphi(z)} \tag{3.12}$$

where

$$\chi = \frac{3-v}{1+v} \quad \text{for plane stress}$$

$$\chi = 3 - 4v \quad \text{for plane strain} \tag{3.13}$$

$$\mu = \frac{E}{2(1+v)} \quad \text{modulus of rigidity}$$

27

We now express $\varphi(z)$ and $\psi(z)$ for a region bounded by a circle as

$$\varphi(z) = \sum_{k=1}^{\infty} a_k z^{-k} \tag{3.14}$$

$$\psi(z) = \sum_{k=1}^{\infty} a_k' z^{-k} \tag{3.15}$$

where the a_k's and a_k''s are constants to be determined.

Writing the normal and tangential stresses in terms of these new holomorphic functions gives

$$\varphi(z) + z\overline{\varphi'(z)} + \overline{\varphi(z)} = \sum_{n=-\infty}^{\infty} A_n e^{in\alpha} = N - iT \tag{3.16}$$

The solution of an infinite plate with a through-hole subjected to stresses N and T is given below.

$$N - iT = \sum_{k=-\infty}^{\infty} A_k e^{ik\alpha} \tag{3.17}$$

Substituting Equations (3.5) and (3.6) in to Equation (3.17) we get

$$-\frac{\sigma_{xx} + \sigma_{yy}}{2} - \frac{\sigma_{xx} - \sigma_{yy}}{2} \cos 2\alpha - \tau_{xy} \sin 2\alpha$$
$$-i\left(\frac{\sigma_{xx} - \sigma_{yy}}{2} \sin 2\alpha - \tau_{xy} \cos 2\alpha \right) = \sum_{k=-\infty}^{\infty} A_k e^{ik\alpha} \tag{3.18}$$

Simplifying Equation (3.18) yields

$$-\frac{\sigma_{xx} + \sigma_{yy}}{2} - \frac{\sigma_{xx} - \sigma_{yy}}{2} e^{2i\alpha} - i\tau_{xy} e^{2i\alpha} = \sum_{k=-\infty}^{\infty} A_k e^{ik\alpha} \tag{3.19}$$

In extended form Equation (3.19) yields

$$-\frac{\sigma_{xx} + \sigma_{yy}}{2} - \frac{\sigma_{xx} - \sigma_{yy}}{2} e^{2i\alpha} - i\tau_{xy} e^{2i\alpha} = ... + A_{-3} e^{-3i\alpha} + A_{-2} e^{-2i\alpha} + A_{-1} e^{-1i\alpha}$$
$$+ A_0 e^0 + A_1 e^{i\alpha} + A_2 e^{2i\alpha} + A_3 e^{3i\alpha} + ... \tag{3.20}$$

From Equation (3.20) we get

28

$$A_{-k} = 0 \qquad k \geq 1$$

$$A_0 = -\frac{\sigma_{xx} + \sigma_{yy}}{2}$$

$$A_1 = 0$$

$$A_2 = -\frac{\sigma_{xx} - \sigma_{yy}}{2} + i\tau_{xy}$$

$$A_k = 0 \qquad k \geq 3$$

(3.21)

To find the coefficients a_o and a_o' we use the stresses at infinity. Since the stresses are zero at infinity, we have for large $|z|$

$$\Gamma = \Gamma' = 0$$

$$a_o = \Gamma = 0, \quad a_o' = \Gamma' = 0$$

(3.22)

The rest of the coefficients a_k s and a_k' s can be obtained from Equations (3.16), (3.21) and the single valuedness which is obtained from Equation (3.11) as $\chi a_1 + \overline{a}_1' = 0$

$$a_1 = \frac{\overline{A}_1 a}{1 + \chi} = 0 \quad , \quad a_1' = \frac{A_1 a}{1 + \chi} = 0$$

(3.23)

$$a_2 = \Gamma' a^2 + \overline{A}_2 a^2 = 0 - \frac{\sigma_{xx} - \sigma_{yy}}{2} a^2 - i\tau_{xy} a^2$$

$$a_2 = -\left(\frac{\sigma_{xx} - \sigma_{yy}}{2} + i\tau_{xy} \right) a^2$$

(3.24)

$$a_2' = 2\Gamma a^2 - A_0 a^2 = 0 - \left(-\frac{\sigma_{xx} + \sigma_{yy}}{2} a^2 \right)$$

$$a_2' = \frac{\sigma_{xx} + \sigma_{yy}}{2} a^2$$

(3.25)

$$\overline{a}_n = A_n a^n , \quad n \geq 3$$

$$\overline{a}_n = 0 \quad , \quad n \geq 3$$

(3.26)

$$a'_n = (n-1)a^2 a_{n-2} - a^n A_{-n+2} \quad , \quad n \geq 3$$

$$a'_3 = 0$$

$$a'_4 = 3a^2 a_2 - a^3 A_{-2}$$

$$a'_4 = -3\left(\frac{\sigma_{xx} - \sigma_{yy}}{2} + i\tau_{xy}\right)a^4 \tag{3.27}$$

$$a'_n = 0 \quad , \quad n \geq 5$$

Thus, expressions for $\varphi(z)$ and $\psi(z)$ can be found from Equation (3.14) as follows

$$\phi(z) = \sum_{k=0}^{\infty} a_k z^{-k} = a_2 \frac{1}{z^2} \tag{3.28}$$

Substituting the value of a_2 into Equation (3.28) we get

$$\phi(z) = -\left(\frac{\sigma_{xx} - \sigma_{yy}}{2} + i\tau_{xy}\right)a^2 \frac{1}{z^2} \tag{3.29}$$

$$\varphi(z) = \int \phi(z)dz = \sum a_k \frac{z^{-k+1}}{-k+1} \tag{3.30}$$

$$\varphi(z) = \left(\frac{\sigma_{xx} - \sigma_{yy}}{2} + i\tau_{xy}\right)a^2 \frac{1}{z} \tag{3.31}$$

$$\Psi(z) = \sum_{k=0}^{\infty} a_k' z^{-2} = a_2' z^{-2} + a_4' z^{-4}$$

$$= \frac{\sigma_{xx} + \sigma_{yy}}{2} a^2 \frac{1}{z^2} - \frac{3}{2}\frac{\sigma_{xx} - \sigma_{yy}}{z^4} a^4 - 3i\tau_{xy}\frac{a^4}{z^4} \tag{3.32}$$

$$\Psi(z) = \frac{\sigma_{xx} + \sigma_{yy}}{2} a^2 \frac{1}{z^2} - \frac{3}{2}\frac{\sigma_{xx} - \sigma_{yy}}{z^4} a^4 - 3i\tau_{xy}\frac{a^4}{z^4} \tag{3.33}$$

$$\psi(z) = \int \Psi(z)dz = \frac{\sigma_{xx} + \sigma_{yy}}{2} a^2 \frac{1}{z} + \frac{3}{2}\frac{\sigma_{xx} - \sigma_{yy}}{z^3} a^4 + 3i\tau_{xy}\frac{a^4}{z3} \tag{3.34}$$

The displacement equation is given as follows

$$2\mu(u_r + iv_\alpha) = e^{-i\alpha}\left\{\chi\varphi(z) - z\overline{\varphi'(z)} - \overline{\psi(z)}\right\} \tag{3.35}$$

After substituting Equations (3.34) and (3.31) in to (3.11) we get

30

$$2\mu(u_r + iv_\alpha) = e^{-i\alpha}\left\{\left(\frac{\sigma_{xx}-\sigma_{yy}}{2}+i\tau_{xy}\right)a^2\frac{1}{z}-z\left(-\left(\frac{\sigma_{xx}-\sigma_{yy}}{2}-i\tau_{xy}\right)a^2\frac{1}{\overline{z}^2}\right)\right.$$
$$\left.-\frac{\sigma_{xx}+\sigma_{yy}}{2}a^2\frac{1}{\overline{z}}+\frac{3}{2}\frac{\sigma_{xx}-\sigma_{yy}}{\overline{z}^3}a^4-3i\tau_{xy}\frac{a^4}{\overline{z}^3}\right\}$$

(3.36)

Now, from Equation (3.36), the radial and tangential relieved displacement equations (u_r, v_α) can be found as

$$u_r = \frac{\sigma_{xx}+\sigma_{yy}}{2}\frac{a^2}{2\mu r}+\frac{\sigma_{xx}-\sigma_{yy}}{2}\frac{1}{2\mu}\left(\frac{a^2}{r}+\frac{a^2}{r}\chi-\frac{a^4}{r^3}\right)\cos 2\alpha$$
$$+\tau_{xy}\frac{1}{2\mu}\left(\frac{a^2}{r}+\frac{a^2}{r}\chi-\frac{a^4}{r^3}\right)\sin 2\alpha$$

(3.37)

$$v_\alpha = \frac{\sigma_{xx}-\sigma_{yy}}{2}\frac{1}{2\mu}\left(\frac{a^2}{r}-\frac{a^2}{r}\chi-\frac{a^4}{r^3}\right)\sin 2\alpha$$
$$+\tau_{xy}\frac{1}{2\mu}\left(\frac{a^2}{r}-\frac{a^2}{r}\chi-\frac{a^4}{r^3}\right)\cos 2\alpha$$

(3.38)

Defining three constants A, B and C as follows

$$A = \frac{a^2}{2\mu r}$$

(3.39)

$$B = \frac{a^2\left(r^2(1+\chi)-a^2\right)}{2\mu r^3}$$

(3.40)

$$C = \frac{a^2\left(r^2(1-\chi)-a^2\right)}{2\mu r^3}$$

(3.41)

where μ and χ are defined earlier in to Equation (3.13).

The relieved displacement equation in the radial and tangential directions (u_r and v_α) become

$$u_r = \frac{\left(\sigma_{xx}+\sigma_{yy}\right)}{2}A+\frac{\left(\sigma_{xx}-\sigma_{yy}\right)}{2}B\cos 2\alpha+\tau_{xy}B\sin 2\alpha$$

(3.42)

$$v_\alpha = \frac{\left(\sigma_{xx}-\sigma_{yy}\right)}{2}C\sin 2\alpha-\tau_{xy}C\cos 2\alpha$$

(3.43)

31

For plane stress and plane strain conditions, the values of the constants A, B, and C are given in Table 3.1.

3.2.2. Relieved Displacement Equations in Terms of Principal Stresses

The relieved displacement equations given by Equations (3.42) and (3.43) are derived as a function of cartesian stress components, σ_{xx}, σ_{yy}, τ_{xy}. We express now the relieved displacements equations as a function of principal stresses σ_{max}, σ_{min}, θ. Figure 3.7 shows cartesian stress components and principal stresses. The relieved displacement Equations (3.42) and (3.43) are transformed to the x'-axis by taking $\tau = 0$, $\sigma_{xx} = \sigma_{max}$, $\sigma_{yy} = \sigma_{min}$ and $\alpha_1 = \alpha-\theta$ in the equations to get relieved displacement equations in terms of principal stresses. This leads to

$$u_r = A\frac{(\sigma_{max} + \sigma_{min})}{2} + B\frac{(\sigma_{max} - \sigma_{min})}{2}\cos 2\alpha_1 \tag{3.44}$$

$$v_\alpha = C\frac{(\sigma_{max} - \sigma_{min})}{2}\sin 2\alpha_1 \tag{3.45}$$

3.3. RELIEVED DISPLACEMENT EQUATIONS FOR LINEAR GRADIENT STRESS STATE

In this section, relieved displacement equations are derived for the linear gradient stress state. As shown in Figure 3.8 the linear gradient stress state (Figure 3.8(a)) is broken in to two parts (Figure 3.8(b) and (c)). The first part, the uniform stress state shown in Figure 3.8(b), has already been treated in the previous section. In this section, the relieved displacements equations are derived for the second part, shown in Figure 3.8(c). Then the superposition of the two parts is taken to get the relieved displacement equations for the linear gradient stress state.

The stress state shown in Figure 3.8(c) is called the *concentric linear gradient stress state*. All of the directions shown in this figure are assumed positive. *Kx* and *Ky* are the angles of the linear stress gradients to the y- and x-axes, respectively.

Similar to the previous sections, this problem is solved by considering an infinite plate with a through-hole loaded at the through-hole surface. The load applied at the through-hole surface is found by considering the initial in-situ state of stresses prior to drilling the through-hole. First, a uniaxial concentric linear gradient normal stress state is considered, as shown in Figure 3.9 (a). Then the solution will then be extended to a biaxial stress state case.

The dashed circle in Figure 3.9 (a) represents the location of the through-hole surface before drilling the through-hole. Normal (σ_r) and shear stress ($\tau_{r\alpha}$) around the dashed circle are calculated by taking the equilibrium of the stresses on an infinitesimal point A on the dashed circle, as shown in Figure 3.9 (c).

$$\sigma_r = Kx\,a\cos^2(\alpha)\sin(\alpha) \tag{3.46}$$

$$\tau_{r\alpha} = -Kx\,a\sin^2(\alpha)\cos(\alpha) \qquad (3.47)$$

where a is the radius of the through-hole. Kx is the angle of stress gradient. Now consider the case when the edge of the through-hole is subjected to normal (N) and tangential (T) stresses of equal magnitude and opposite sign to those computed in the equations above. It is also assumed that stresses vanish at infinity. The applied stresses are

$$N = -\sigma_r = -Kx\,a\cos^2(\alpha)\sin(\alpha) \qquad (3.48)$$

$$T = -\tau_{r\alpha} = Kx\,a\sin^2(\alpha)\cos(\alpha) \qquad (3.49)$$

Similar to Section 3.2, the problem we need to solve is an infinite plate with a circular through-hole subjected to normal (N) and tangential (T) stresses at the edge of the through-hole as shown in Figure 3.3. The problem is again solved for displacements using the function of complex method [see, for example Muskhelishvili (1953)].

The solution of an infinite plate with a through-hole subjected to stresses N and T due uniaxial uniform stresses is given below.

$$N - iT = \sum_{k=-\infty}^{\infty} A_k e^{ik\alpha} \qquad (3.50)$$

Substituting Equations (3.48) and (3.49) in to Equation (3.50) we obtain

$$Kx\,a\cos^2(\alpha)\sin(\alpha) - i\,Kx\,a\sin^2(\alpha)\cos(\alpha) = \sum_{k=-\infty}^{\infty} A_k e^{ik\alpha} \qquad (3.51)$$

$$\frac{Kx\,a}{4}i\,e^{3i\alpha} - \frac{Kx\,a}{4}i\,e^{-i\alpha} = \sum_{k=-\infty}^{\infty} A_k e^{ik\alpha} \qquad (3.52)$$

From Equation (3.52) we get

$$A_{-1} = -\frac{Kx\,a}{4}i \ , \ A_3 = \frac{Kx\,a}{4}i$$
$$A_{-k} = 0 \qquad k \geq 2$$
$$A_0 = A_1 = A_2 = 0$$
$$A_k = 0 \qquad k \geq 4 \qquad (3.53)$$

Since the stresses are zero at infinity, we have for the coefficients a_k s and a'_k as

$$\Gamma = \Gamma' = 0$$
$$a_0 = \Gamma = 0, \quad a'_0 = \Gamma' = 0 \qquad (3.54)$$

$$a_1 = \frac{\overline{A_1}a}{1+\chi} = 0 \ , \quad a_1' = \frac{A_1 a}{1+\chi} = 0 \tag{3.55}$$

$$a_2 = \Gamma' a^2 + \overline{A_2} a^2 = 0 \tag{3.56}$$

$$a_2' = 2\Gamma a^2 - A_0 a^2 = 0 \tag{3.57}$$

$$\overline{a}_n = A_n a^n \ , \quad n \geq 3$$
$$\overline{a}_3 = A_3 a^3 = -i\frac{Kx a^4}{4} \tag{3.58}$$
$$\overline{a}_n = 0 \quad , \quad n \geq 4$$

$$a_n' = (n-1)a^2 a_{n-2} - a^n A_{-n+2} \quad n \geq 3$$
$$a_3' = \frac{K a^4}{4} i$$
$$a_4' = 0 \tag{3.59}$$
$$a_5' = -i K a^6$$
$$a_n' = 0 \quad n \geq 6$$

Thus, expressions for $\varphi(z)$ and $\psi(z)$ can then be found from Equation (3.14) as follows

$$\phi(z) = \sum_{k=0}^{\infty} a_k z^{-k} = a_3 \frac{1}{z^3} \tag{3.60}$$

Substituting value of a_3 into Equation (3.60) we obtain

$$\phi(z) = -i\frac{K a^4}{4}\frac{1}{z^3} \tag{3.61}$$

$$\varphi(z) = \int \phi(z)dz = \sum a_k \frac{z^{-k+1}}{-k+1} \tag{3.62}$$

$$\varphi(z) = \frac{K a^4}{8}\frac{1}{z^2} \tag{3.63}$$

$$\Psi(z) = \sum_{k=0}^{\infty} a_k' z^{-2} = a_3' z^{-3} + a_5' z^{-5} = i\frac{K a^4}{2}\frac{1}{z^3} - i K a^6 \frac{1}{z^5} \tag{3.64}$$

$$\psi(z) = \int \Psi(z)dz = -i\frac{K a^4}{8}\frac{1}{z^2}i + \frac{K a^6}{4}\frac{1}{z^4} \tag{3.65}$$

34

$$\overline{\psi(z)} = i\frac{K\,a^4}{8}\frac{1}{\overline{z}^2} - i\frac{K\,a^6}{4}\frac{1}{\overline{z}^4} \tag{3.66}$$

The displacement equation is given as follows

$$2\mu(u_r + iv_\alpha) = e^{-i\alpha}\left\{\chi\varphi(z) - z\overline{\varphi'(z)} - \overline{\psi(z)}\right\} \tag{3.67}$$

After substituting Equations (3.63) and (3.66) in to Equation (3.67) we get

$$2\mu(u_r + iv_\alpha) = e^{-i\alpha}\left\{\chi i\frac{Kx\,a^4}{8}\frac{1}{r^2 e^{2i\alpha}} - re^{i\alpha}\left(i\frac{Kx\,a^4}{4}\frac{1}{r^3 e^{-3i\alpha}}\right)\right.$$
$$\left. -\left(i\frac{Kx\,a^4}{8}\frac{1}{r^2 e^{-2i\alpha}} - i\frac{Kx\,a^6}{4}\frac{1}{r^4 e^{-4i\alpha}}\right)\right\} \tag{3.68}$$

$$2\mu(u_r + iv_\alpha) = \frac{\chi Kx}{8}\frac{a^4}{r^2}(i\cos 3\alpha + \sin 3\alpha) - \frac{Kx}{4}\frac{a^4}{r^2}(i\cos 3\alpha - \sin 3\alpha)$$
$$-\frac{Kx}{8}\frac{a^4}{r^2}(i\cos\alpha - \sin\alpha) + \frac{Kx}{4}\frac{a^6}{r^4}(i\cos 3\alpha - \sin 3\alpha) \tag{3.69}$$

Now, from Equation (3.69), the radial and tangential relieved displacement equations (u_r, v_α) can be found as

$$u_r = Kx\left\{\frac{a^4}{16r^2\mu}\sin\alpha + \frac{a^4\left(r^2(2+\chi) - 2a^2\right)}{16\mu r^4}\sin 3\alpha\right\} \tag{3.70}$$

$$v_\alpha = Kx\left\{-\frac{a^4}{16r^2\mu}\cos\alpha + \frac{a^4\left(r^2(2-\chi) - 2a^2\right)}{16\mu r^4}\cos 3\alpha\right\} \tag{3.71}$$

Defining four constants F, H, I and J as follows

$$F = \frac{a^4}{16\mu r^2} \tag{3.72}$$

$$H = \frac{a^4\left(2a^2 - r^2(2+\chi)\right)}{16\mu r} \tag{3.73}$$

$$I = -\frac{a^4}{16\mu r^2} \tag{3.74}$$

35

$$J = \frac{a^4 \left(r^2 (2 - \chi) - 2a^2 \right)}{16 \mu r^4} \qquad (3.75)$$

The relieved displacement equations in the radial and tangential directions (u_r and v_α) are as follows.

$$u_r = Kx(F \sin \alpha + H \sin 3\alpha) \qquad (3.76)$$

$$v_\alpha = Kx(I \cos \alpha + J \cos 3\alpha) \qquad (3.77)$$

For plane stress and plane strain conditions, the values of F, H, I, and J are given in the Table 3.2.

Equations (3.76) and (3.77) for the uniaxial concentric linear gradient stress state are extended to the biaxial concentric linear gradient stress state as shown in Figure 3.10. Relieved displacement equations for the linear stress gradient in the y direction are obtained by replacing Kx with Ky and taking $\alpha = \alpha - \pi/2$ in Equations (3.76) and (3.77), namely

$$u_r = Ky(-F \cos \alpha + H \cos 3\alpha) \qquad (3.78)$$

$$v_\alpha = Ky(I \cos \alpha - J \cos 3\alpha) \qquad (3.79)$$

As shown in Figure 3.10, the superposition of Equations (3.76) and (3.78) give the equation for relieved radial displacement for the biaxial concentric linear gradient stress state. Similarly, the superposition of Equations (3.77) and (3.79) gives the equation for the relieved tangential displacement for the biaxial concentric linear gradient stress state.

$$u_r = Kx(F \sin \alpha + H \sin 3\alpha) + Ky(-F \cos \alpha + H \cos 3\alpha) \qquad (3.80)$$

$$v_\alpha = Kx(I \cos \alpha + J \cos 3\alpha) + Ky(I \sin \alpha - J \sin 3\alpha) \qquad (3.81)$$

Now we can obtain relieved displacement equations for the *linear gradient stress state* by superposing the relieved displacement Equations (3.42) and (3.43) for the uniform stress state and the relieved displacement Equations (3.80) and (3.81), as shown in Figure 3.8. The relieved displacement equations for the linear gradient stress state, shown in Figure 3.5, are as follows

$$u_r = A \frac{(\sigma_{xx} + \sigma_{yy})}{2} + B \frac{(\sigma_{xx} - \sigma_{yy})}{2} \cos 2\alpha + B\tau_{xy} \sin 2\alpha \\ + Kx(F \sin \alpha + H \sin 3\alpha) + Ky(-F \cos \alpha + H \cos 3\alpha) \qquad (3.82)$$

$$v_\alpha = \frac{\left(\sigma_{xx} - \sigma_{yy} \right)}{2} C \sin 2\alpha - \tau_{xy} C \cos 2\alpha Kx(I \cos \alpha + J \cos 3\alpha) \\ + Ky(I \sin \alpha - J \sin 3\alpha) \qquad (3.83)$$

36

3.4. MEASURED DISPLACEMENT

In the previous sections, the equations for the relieved displacements (u_r, v_α) were derived. Relieved displacement equations give the displacement of a point relative to the center of the through-hole. However, in practice, a displacement measurement might be taken between two points, neither of which are the center of the hole. As explained earlier, in this study, a displacement between two points is called *measured displacement* and shown with U. According to this definition, a relieved displacement can also be a measured displacement if one of the points is the center of the hole.

We can express measured displacements in terms of relieved displacements. Figure 3.11 is a representation of a displacement measurement between two measurement points due to hole drilling. The two measurement points are identified as i and j in the figure. *Measurement points* are to the points between which the displacement measurements are made. From the relieved displacement equation, we can find the relieved displacement (u_r, v_α) of each of these points. Relieved displacements of these points in the radial and tangential directions are noted in the figure. To find the measured displacement between these points, we need to take the projection of the relieved displacements on the line drawn between the two points. Thus, the measured displacement between the two measurement points is defined in terms of relieved displacements as follows

$$U = (u_i \cos(\theta_{ij}) - v_i \sin(\theta_{ij})) - (u_j \cos(\theta_{ji}) - v_j \sin(\theta_{ji}))$$

(3.84)

where

$$\theta_{ij} = \alpha_i + \beta$$

(3.85)

$$\theta_{ji} = \alpha_j + \beta$$

(3.86)

$$\beta = \frac{\pi - (\alpha_i + \alpha_j)}{2}$$

(3.87)

In this research, the length between the two measurement points is identified as L. Measured displacements are obtained by measuring the distance between the two measurement points before (L_{before}) and after (L_{after}) the hole is drilled. Then, taking the difference of these displacement values, we obtain the measured displacement (U)

$$U = L_{before} - L_{after}$$

(3.88)

3.5. OVERVIEW OF DERIVATION OF IN-SITU STRESS EQUATIONS

Relieved displacement Equations (3.42), (3.43), (3.82), (3.83) have been derived for two different in-situ states of stress: (1) uniform stress; and, (2) linear gradient stress. These two

states of stress were defined in Section 3.1 and shown in Figure 3.4 and 3.5. Measured displacements are obtained from relieved displacements using Equation (3.84).

The objective of this section and the remaining sections in this chapter is to derive equations for in-situ stress as a function of measured displacements (U).

In the generalized functional form, measured displacements for the uniform stress state can be expressed in terms of cartesian stress components and principal stresses as follows

$$U = f(\sigma_{xx}, \sigma_{yy}, \tau_{xy}) \tag{3.89}$$

$$U = f(\sigma_{max}, \sigma_{min}, \theta) \tag{3.90}$$

Similarly, in the generalized functional form, measured displacements for the linear gradient stress state can be expressed as follows

$$U = f(\sigma_{xx}, \sigma_{yy}, \tau_{xy}, Kx, Ky) \tag{3.91}$$

Now we want to express in-situ stress components, which are variables in Equations (3.89), (3.90) and (3.91), as a function of measured displacements. In order to achieve this goal, we first assume that the in-situ stresses in Equations (3.89), (3.90) and (3.91) as unknowns. There are three unknown in-situ stresses for the uniform stress state, and five unknown in-situ stresses for linear gradient stress state. To solve Equations (3.89) and (3.90) for in-situ stresses of the uniform stress state, three equations are needed. These three equations are obtained by making three displacement measurements ($U1$, $U2$, $U3$). Similarly, to solve Equation (3.91) for the linear gradient stresses, five equations are needed. We get these five equations by making five displacement measurements ($U1$, $U2$, $U3$, $U4$, $U5$).

In this research, equations that express in-situ stresses for the uniform stress state as a function of measured displacements are called *uniform in-situ stress equations*. Similarly, equations that express in-situ stresses for the linear gradient stress state as a function of measured displacements are called *linear gradient in-situ stress equations*.

In generalized functional form, uniform in-situ stresses equations in terms of cartesian stress components (σ_{xx}, σ_{yy}, τ_{xy}) and principal stresses (σ_{max}, σ_{min}, θ) are expressed as a function of measured displacements as follows

$$\sigma_{xx}, \sigma_{yy}, \tau_{xy} = f(U1, U2, U3), f(U1, U2, U3), f(U1, U2, U3) \tag{3.92}$$

$$\sigma_{max}, \sigma_{min}, \theta = f(U1, U2, U3), f(U1, U2, U3), f(U1, U2, U3) \tag{3.93}$$

The uniform in-situ stress equations are derived in Section 3.6.

In generalized functional form, linear gradient in-situ stress equations are expressed as

$$\sigma_{xx}, \sigma_{yy}, \tau_{xy}, Kx, Ky = f(U1,U2,U3,U4,U5), f(U1,U2,U3,U4,U5),$$
$$f(U1,U2,U3,U4,U5), f(U1,U2,U3,U4,U5), \tag{3.94}$$
$$f(U1,U2,U3,U4,U5)$$

The linear gradient in-situ stress equations are derived in Section 3.7

A total of 13 different Test Configurations are treated in this research. A test Configuration refers to a specific set of measured displacements. Eight of these Test Configurations are for the uniform stress state, and the remaining five Test Configurations are for the linear gradient stress state.

The 13 different Test Configurations are classified in to one of four different Types as shown in Figure 3.12. In each drawing, the core-hole is shown as a solid line circle, and the hole diameter is D_h. All the measurement points in the Test Configurations are placed on the same fictitious circle if the measurement point is not the center of the hole. This fictitious circle, whose radius and diameter are identified r_m and D_m, is termed *measurement circle*. In Figure 3.12, the measurement circle is shown with a dashed line. The radius and diameter of the measurement circle are termed *measurement circle radius* (r_m) and *measurement circle diameter* (D_m), respectively.

In Type I configurations (Figure 3.12(a)), for each measurement to be made, one measurement point is positioned at the center of the hole, and the second measurement point is outside of the diameter D_h. In Type II configurations (Figure 3.12(b)), for each measurement to be made, both measurement points are outside of the diameter D_h, and the measurement is made across the center of the hole. In Type III configurations (Figure 3.12 (c)), for each measurement to be made, both measurement points lie outside of the diameter D_h, and the measurement is made between the two points along a line which does not intersect the hole. Type IV configurations are comprised of any combinations of Type I, II and III measurements. An example of this is shown in Figure 3.12 (d).

The in-situ stress equations are derived as follows. First, for a particular Test Configuration, the measured displacements are written in terms of the relieved displacements. The resulting sets of linear equations are then solved for the in-situ stress components in terms of the measured displacements. For some of the Test Configurations, the derivations become quite cumbersome (if not impossible) to solve with hand calculations. In these instances, the linear equations are solved using MATHEMATICA (Wolfram 2000). MATHEMATICA is a general computer software system and language that uses numerical and symbolic calculations

3.6. DERIVATION OF UNIFORM IN-SITU STRESS EQUATIONS

As explained before, the uniform stress state is represented by either cartesian stress components σ_{xx}, σ_{yy}, τ_{xy} or principal stresses σ_{max}, σ_{min} and the principal stress direction θ. The objective of the formulation presented here is to express the uniform in-situ stress state in terms of the measured displacements. As shown in Equations (3.92) and (3.93), the displacements

39

may be used to compute the principal stresses directly, or to compute the rectangular components of these stresses.

Uniform in-situ stress equations are derived for the 8 different Test Configurations shown in Figure 3.12. Two sets of equations are derived for each Test Configuration. One set of equations calculates cartesian stress components σ_{xx}, σ_{yy}, τ_{xy}. The other set of equations calculates principal stresses σ_{max}, σ_{min} and direction θ. Columns 2 and 3 in Figure 3.12 shows the equation numbers of the equation for cartesian stress components and principal stresses for each Test Configuration. This is done to help reader locate equations that are of particular interest. The derivations presented in the following are grouped by Type of Test Configuration.

3.6.1. Type I

There are two Type I Test Configurations, A and B, as shown in Figure 3.13. The measurement points a, b, c are 45 degrees apart in Test Configuration A. In Test Configuration B, the measurement points are 60 degrees apart. For each configuration, we need to have measured displacement at points a, b and c relative the center of the hole at O. Since all displacement measurements are taken relative to the center of the hole, all measured displacement (U) values are equal to relieved displacements (u_r) values. Thus, the relieved displacement equation (u_r) directly gives the measured displacement values.

We can also calculate measured displacement using Equation (3.84). In measurement Type I, u_j and v_j are equal to zero since displacement at the center of the hole is zero. From Equation (3.87) we get

$$\beta = \frac{\pi - (\alpha i + (\alpha i + \pi))}{2} = -\alpha i$$

and when we substitute β into Equations (3.85) and (3.84), we get

$$\theta = \alpha i - \alpha i = 0$$

$$U = u_i \cos(0) - v_j \sin(0) = u_i \tag{3.95}$$

As seen from Equation (3.95), measured displacements in measurement Type I are equal to relieved displacements in the radial direction.

Relieved displacement equations were derived before as a function of cartesian stress components and principal stresses in Equations (3.42) and (3.44). The measured displacements for both Type I Test Configurations are expressed in terms of cartesian stress components and principal stresses as follows

$$U = u_r = A\frac{(\sigma_{xx} + \sigma_{yy})}{2} + B\frac{(\sigma_{xx} - \sigma_{yy})}{2}\cos 2\alpha + B\tau_{xy}\sin 2\alpha \tag{3.96}$$

40

$$U = u_r = A\frac{(\sigma_{max} + \sigma_{min})}{2} + B\frac{(\sigma_{max} - \sigma_{min})}{2}\cos 2\alpha_1 \tag{3.97}$$

where α is the angle measured counter-clockwise from direction of point a to u_r. $\alpha_1 = \alpha - \theta$. θ is the angle measured counter-clockwise from direction of point a to direction of principal stress σ_{max}.

3.6.1.1. Test Configuration A

Uniform In-situ Stress Equations in Terms of Cartesian Stress Components

The measured displacements Test Configuration A are expressed as a function of cartesian stress components by Equation (3.96). In this equation, there are three unknowns σ_{xx}, σ_{yy}, and τ_{xy}. To get these cartesian stress components, three displacement measurements are made. As shown in Figure 3.13, the three displacement measurements are *U1, U2, U3* at points *a, b, c* are required for Test Configuration A. Equation (3.96) is applied at three different locations *a, b,* and *c* shown in Figure 3.12 to obtain three measured displacements *U1, U2* and *U3*.

$$U1 = u_a = A\frac{(\sigma_{xx} + \sigma_{yy})}{2} + B\frac{(\sigma_{xx} - \sigma_{yy})}{2} \tag{3.98}$$

$$U2 = u_b = A\frac{(\sigma_{xx} + \sigma_{yy})}{2} + B\tau_{xy} \tag{3.99}$$

$$U3 = u_c = A\frac{(\sigma_{xx} + \sigma_{yy})}{2} - B\frac{(\sigma_{xx} - \sigma_{yy})}{2} \tag{3.100}$$

Equations (3.98), (3.99) and (3.100) express the three measured displacements *U1, U2* and *U3* in terms of the three desired stresses σ_{xx}, σ_{yy}, and τ_{xy}. Solving these three equations leads to three equations for stresses

$$\sigma_{xx} = \frac{A(-U1 + U3) + B(U1 + U3)}{2AB} \tag{3.101}$$

$$\sigma_{yy} = \frac{A(U1 - U3) + B(U1 + U3)}{2AB} \tag{3.102}$$

$$\tau_{xy} = \frac{U1 - 2U2 + U3}{2B} \tag{3.103}$$

41

Uniform In-situ Stress Equations in Terms of Principal Stresses and Direction

Here uniform in-situ stress equations in terms of principal stresses are derived as a function of measured displacements. The measured displacements for Test Configuration A are expressed as a function of principal stresses by Equation (3.97). In this equation, there are three unknowns σ_{max}, σ_{min}, and θ. To get these principal stresses, three displacement measurements are made. Equation (3.97) is applied to the Test Configuration A as shown in Figure 3.12 to obtain three measured displacements *U1*, *U2* and *U3*

$$U1 = u_a = A\frac{(\sigma_{max} + \sigma_{min})}{2} + B\frac{(\sigma_{max} - \sigma_{min})}{2}\cos 2(-\theta) \tag{3.104}$$

$$U2 = u_b = A\frac{(\sigma_{max} + \sigma_{min})}{2} + B\frac{(\sigma_{max} - \sigma_{min})}{2}\cos 2(-\theta + \pi/4) \tag{3.105}$$

$$U3 = u_c = A\frac{(\sigma_{max} + \sigma_{min})}{2} + B\frac{(\sigma_{max} - \sigma_{min})}{2}\cos 2(-\theta + \pi/2) \tag{3.106}$$

These equations are simplified as follows

$$U1 = u_a = A\frac{(\sigma_{max} + \sigma_{min})}{2} + B\frac{(\sigma_{max} - \sigma_{min})}{2}\cos 2\theta \tag{3.107}$$

$$U2 = u_b = A\frac{(\sigma_{max} + \sigma_{min})}{2} + B\frac{(\sigma_{max} - \sigma_{min})}{2}\sin 2\theta \tag{3.108}$$

$$U3 = u_c = A\frac{(\sigma_{max} + \sigma_{min})}{2} - B\frac{(\sigma_{max} - \sigma_{min})}{2}\cos 2\theta \tag{3.109}$$

Equations (3.107), (3.108) and (3.109) express the three measured displacements *U1*, *U2* and *U3* in terms of the principal stresses σ_{max}, σ_{min}, and the direction θ. Solving these three equations leads to three equations for principal stresses and direction

$$\sigma_{max} = \frac{U1 + U3}{2A} + \frac{\sqrt{(U1 - U3)^2 + (U1 + U3 - 2U2)^2}}{2B} \tag{3.110}$$

$$\sigma_{min} = \frac{U1 + U3}{2A} - \frac{\sqrt{(U1 - U3)^2 + (U1 + U3 - 2U2)^2}}{2B} \tag{3.111}$$

$$\theta = 1/2 \arctan\left[\frac{U1 + U3 - 2U2}{U1 - U3}\right] \tag{3.112}$$

42

Direct calculation of the angle θ using the common one argument *arctan* function can give an error of ± 90. The correct angle can be found by using the two-argument *arctan* function, where the signs of the numerator and denominator are taken into account.

Table 3.3 can be used to find the correct angle. A positive value of θ, say $\theta = \pi/3$, indicates that σ_{max} lies 60^0 anti-clockwise of the direction of measurement location a. A negative value of θ, say $\theta = -\pi/3$, indicates that that σ_{max} lies 60^0 clockwise of the direction of measurement location a. The case where both $U1 + U3 - 2U2 = 0$ and $U1 + U2 = 0$ corresponds to an equal biaxial stress field, for which the angle θ has no meaning.

3.6.1.2. Test Configuration B

Uniform In-situ Stress Equations in Terms of Cartesian Stress Components

As shown in Figure 3.13, three displacement measurements $U1$, $U2$, $U3$ at points a, b, c are required for Test Configuration B. Equation (3.96) is applied to Test Configuration B as shown Figure 3.13 to obtain three measured displacements $U1$, $U2$

$$U1 = u_a = \sqrt{3}B\tau_{xy} - (A - \frac{B}{2})\sigma_x + (A + \frac{B}{2})\sigma_y \tag{3.113}$$

$$U2 = u_b = \sqrt{3}B\tau_{xy} + (A - \frac{B}{2})\sigma_x + (A + \frac{B}{2})\sigma_y \tag{3.114}$$

$$U3 = u_c = -\sqrt{3}B\tau_{xy} + (A - \frac{B}{2})\sigma_x + (A + \frac{B}{2})\sigma_y \tag{3.115}$$

Equations (3.113), (3.114) and (3.115) express the three measured displacements $U1$, $U2$ and $U3$ in terms of the three desired stresses σ_{xx}, σ_{yy}, and τ_{xy}. Solving these three equations leads to three equations for stresses

$$\sigma_{xx} = \frac{A(2U1 - U2 - U3) + B(U1 + U2 + U3)}{3AB} \tag{3.116}$$

$$\sigma_{yy} = \frac{A(2U1 - U2 - U3) + B(U1 + U2 + U3)}{3AB} \tag{3.117}$$

$$\tau_{xy} = \frac{U2 - U3}{2\sqrt{3}B} \tag{3.118}$$

43

Equation (3.97) is applied to the points a, b, and c, to obtain three measured displacements $U1$, $U2$ and $U3$

$$U1 = u_a = (A + B\cos(2\theta))\sigma_{max} + (A - B\cos(2\theta))\sigma_{min} \tag{3.119}$$

$$U2 = u_b = (A - \frac{B}{2}\cos(2\theta) + \sqrt{3}\frac{B}{2}\sin(2\theta))\sigma_{max}$$
$$+ (A + \frac{B}{2}\cos(2\theta) - \sqrt{3}\frac{B}{2}\sin(2\theta))\sigma_{min} \tag{3.120}$$

$$U3 = u_c = \frac{B}{2}\cos(\frac{4\pi}{3} - 2\theta)\ (\sigma_{max} - \sigma_{min})$$
$$+ \frac{B}{2}\cos(\frac{10\pi}{3} - 2\theta)\ (\sigma_{max} - \sigma_{min}) + A(\sigma_{max} - \sigma_{min}) \tag{3.121}$$

Equations (3.119), (3.120) and (3.121) expres the three measured displacements $U1$, $U2$ and $U3$ in terms of the princial stresses and the direction. Solving the above equations, the in-situ state of stresses in terms of principal stresses σ_{max}, σ_{min}, and the direction θ are as follows

$$\sigma_{max} = \frac{U1 + U2 + U3}{3A} + \frac{2\sqrt{(U1^2 + U2^2 - U2\ U3 + U3^2 - U1(U2 + U3))}}{3B} \tag{3.122}$$

$$\sigma_{min} = \frac{U1 + U2 + U3}{3A} - \frac{2\sqrt{(U1^2 + U2^2 - U2\ U3 + U3^2 - U1(U2 + U3))}}{3B} \tag{3.123}$$

$$\theta = -arcsec\left[-\frac{2}{\sqrt{2 + \dfrac{2U1 - U2 - U3}{\sqrt{U1^2 + U2^2 - U2\ U3 + U3^2 - U1\ (U2 + U3)}}}} \right] \tag{3.124}$$

3.6.2. Type II

There are three Type II Test Configurations, C, D and E, as shown in Figure 3.13. As shown in the figure, measured displacements $U1$, $U2$, $U3$ are taken between two points across the center of the core hole. Using Equation (3.84), measured displacements are found as explained below.

Since displacement measurements are taken between two points 180 degrees apart from each other

44

$$\alpha_j = \alpha_i + \pi$$

$$\beta = \frac{\pi - (\alpha_i + \alpha_i + \pi)}{2} = -\alpha_i$$

$$\theta_{ij} = \theta_{ij} = \alpha_i + \beta = \alpha_i - \alpha_i = 0 \tag{3.125}$$

$$\theta_{ji} = \theta_{ij} = \alpha_j + \beta = (\alpha_i + \pi) - \alpha_i = \pi \tag{3.126}$$

Substituting the values of θ_{ij} *and* θ_{ji} into Equation (3.84) leads to

$$\begin{aligned} U &= (u_i \cos(\theta ij) - v_i \sin(\theta ij)) - (u_j \cos(\theta ji) - v_j \sin(\theta ji)) \\ &= (u_i \cos(0) - v_i \sin(0)) - (u_j \cos(\pi) - v_j \sin(\pi)) \\ &= u_i + u_j \end{aligned} \tag{3.127}$$

The relieved displacement equations were derived earlier as a function of cartesian stress components and principal stresses (Equations (3.42) to (3.44)). Thus, substituting Equations (3.42) and (3.44) into the Equation (3.127), the measured displacements for all Type II Test Configurations are expressed in terms of cartesian stress components and in terms of principal stresses, respectively, as follows:

$$U = u_i + u_j = A(\sigma_{xx} + \sigma_{yy}) + B\,(\sigma_{xx} - \sigma_{yy})\cos 2\alpha_i + 2B\tau_{xy}\sin 2\alpha_i \tag{3.128}$$

$$U = u_i + u_j = A(\sigma_{max} + \sigma_{min}) + B\,(\sigma_{max} - \sigma_{min})\cos 2\alpha_1 \tag{3.129}$$

3.6.2.1. Test Configuration C

Uniform In-situ Stress Equations in Terms of Cartesian Stress Components

As shown in Figure 3.13, three displacement measurements *U1, U2, U3* are required for Test Configuration B. Equation (3.128) is applied to Test Configuration B to obtain three measured displacements *U1, U2* and *U3*.

$$U1 = u_a + u_d = (A(\sigma_{xx} + \sigma_{yy}) + B(\sigma_{xx} - \sigma_{yy})) \tag{3.130}$$

$$U2 = u_b + u_e = 2A(\sigma_{xx} + \sigma_{yy}) + B\tau_{xy} \tag{3.131}$$

$$U3 = u_c + u_e = A(\sigma_{xx} + \sigma_{yy}) - B(\sigma_{xx} - \sigma_{yy}) \tag{3.132}$$

Equations (3.130), (3.131) and (3.132) express the three measured displacements *U1*, *U2* and *U3* in terms of the three desired stresses σ_{xx}, σ_{yy}, and τ_{xy}. Solving these three equations leads to three equations for stresses

$$\sigma_{xx} = \frac{A(-U1+U3)+B(U1+U3)}{4AB} \tag{3.133}$$

$$\sigma_{yy} = \frac{A(U1-U3)+B(U1+U3)}{4AB} \tag{3.134}$$

$$\tau_{xy} = \frac{U1-2U2+U3}{4B} \tag{3.135}$$

Uniform In-situ Stress Equations in Terms of Principal Stresses and Direction

Equation (3.129) is applied to Test Configuration C to get measured displacements *U1*, *U2*, *U3*.

$$U1 = u_a + u_d = ((A+B\cos(2\theta)\sigma_{max} + (A-B\cos(2\theta)\sigma_{max}) \tag{3.136}$$

$$U2 = u_b + u_e = 2((A+B\cos(2\theta)\sigma_{max} + (A-B\cos(2\theta)\sigma_{max}) \tag{3.137}$$

$$U3 = u_c + u_f = 2((A-B\cos(2\theta)\sigma_{max} + (A+B\cos(2\theta)\sigma_{max}) \tag{3.138}$$

Equations (3.136), (3.137) and (3.138) express the three measured displacements *U1*, *U2* and *U3* in terms of the three desired stresses σ_{max}, σ_{min}, and θ. Solving these three equations leads to three equations for stresses

$$\sigma_{max} = \frac{U1+U3}{4A} + \frac{\sqrt{(U1-U3)^2+(U1+U3-2U2)^2}}{4B} \tag{3.139}$$

$$\sigma_{min} = \frac{U1+U3}{4A} - \frac{\sqrt{(U1-U3)^2+(U1+U3-2U2)^2}}{4B} \tag{3.140}$$

$$\theta = \frac{1}{2} ArcCos\left[-\frac{U1-U3}{\sqrt{(U1-U3)^2+(U1-2U2+U3)^2}} \right] \tag{3.141}$$

46

3.6.2.2. Test Configuration D

Uniform In-situ Stress Equations in Terms of Cartesian Stress Components

As shown in Figure 3.13, three displacement measurements *U1*, *U2*, *U3* are required for Test Configuration D. Equation (3.128) is applied to the Test Configuration B to obtain three measured displacements *U1*, *U2* and *U3*.

$$U1 = u_a + u_d = A(\sigma_{xx} + \sigma_{yy}) + B\ (\sigma_{xx} - \sigma_{yy}) \tag{3.142}$$

$$U2 = u_b + u_e = 2\sqrt{3}B\tau_{xy} + (2A - B)\sigma_{xx} + (2A + B)\sigma_{yy} \tag{3.143}$$

$$U3 = u_c + u_e = -2\sqrt{3}B\tau_{xy} + (2A - B)\sigma_{xx} + (2A + B)\sigma_{yy} \tag{3.144}$$

Equations (3.142), (3.143) and (3.144) express the three measured displacements *U1*, *U2* and *U3* in terms of the three desired stresses σ_{xx}, σ_{yy}, and τ_{xy}. Solving these three equations leads to three equations for stresses

$$\sigma_{xx} = \frac{A(2U1 - U2 - U3) + B(U1 + U2 + U3)}{6AB} \tag{3.145}$$

$$\sigma_{yy} = \frac{A(2U1 - U2 - U3) + B(U1 + U2 + U3)}{6AB} \tag{3.146}$$

$$\tau_{xy} = \frac{U2 - U3}{2\sqrt{3}B} \tag{3.147}$$

Uniform In-situ Stress Equations in Terms of Principal Stresses and Direction

Equation (3.129) is applied to Test Configuration C to get measured displacements *U1*, *U2*, *U3*.

$$U1 = u_a + u_d = (A + B\cos(2\theta))\sigma_{max} + (A - B\cos(2\theta))\sigma_{min} \tag{3.148}$$

$$U2 = u_b + u_e = (2A - B\cos(2\theta) + \sqrt{3}B\sin(2\theta))\sigma_{max}$$
$$+ (2A + B\cos(2\theta) - \sqrt{3}B\sin(2\theta))\sigma_{min} \tag{3.149}$$

$$U3 = u_c + u_f = B\cos(\frac{4\pi}{3} - 2\theta)\ (\sigma_{max} - \sigma_{min})$$
$$+ B\cos(\frac{10\pi}{3} - 2\theta)\ (\sigma_{max} - \sigma_{min}) + 2A(\sigma_{max} - \sigma_{min}) \tag{3.150}$$

Equations (3.148), (3.149) and (3.150) express the three measured displacements $U1$, $U2$ and $U3$ in terms of the three desired stresses σ_{max}, σ_{min}, and direction θ. Solving these three equations leads to three equations for stresses

$$\sigma_{max} = \frac{U1+U2+U3}{6A} + \frac{2\sqrt{(U1^2+U2^2-U2\,U3+U3^2-U1(U2+U3))}}{6B} \tag{3.151}$$

$$\sigma_{min} = \frac{U1+U2+U3}{6A} - \frac{2\sqrt{(U1^2+U2^2-U2\,U3+U3^2-U1(U2+U3))}}{6B} \tag{3.152}$$

$$\theta = -ArcSec\left[\frac{2}{\sqrt{2 + \dfrac{2U1-U2-U3}{\sqrt{U1^2+U2^2-U2\,U3+U3^2-U1\,(U2+U3)}}}} \right] \tag{3.153}$$

3.6.2.3. Test Configuration E

Uniform In-situ Stress Equations in Terms of Cartesian Stress Components

As shown in Figure 3.13, three displacement measurements $U1$, $U2$, $U3$ are required for Test Configuration E. Equation (3.128) is applied to Test Configuration B to obtain three measured displacements $U1$, $U2$ and $U3$.

$$U1 = u_a + u_d = (A+B)\sigma_{xx} + (A-B)\sigma_{yy} \tag{3.154}$$

$$U2 = u_b + u_e = 2\sqrt{3}B\tau_{xy} + (2A-B)\sigma_{xx} + (2A+B)\sigma_{yy} \tag{3.155}$$

$$U3 = u_c + u_e = (A-B)\sigma_{xx} + (A+B)\sigma_{yy} \tag{3.156}$$

Equations (3.154), (3.155) and (3.156) express the three measured displacements $U1$, $U2$ and $U3$ in terms of the three desired stresses σ_{xx}, σ_{yy}, and τ_{xy}. Solving these three equations leads to three equations for stresses

$$\sigma_{xx} = \frac{A(U1-U3)+B(U1+U3)}{4AB} \tag{3.157}$$

$$\sigma_{yy} = \frac{A(-U1+U3)+B(U1+U3)}{4AB} \tag{3.158}$$

$$\tau_{xy} = \frac{U1-4U2+3U3}{4\sqrt{3}B} \tag{3.159}$$

48

Uniform In-situ Stress Equations in Terms of Principal Stresses and Direction

Equation (3.129) is applied to Test Configuration C to get measured displacements $U1$, $U2$, $U3$.

$$U1 = u_a + u_d = (A + B\cos(2\theta))\sigma_{max} + (A - B\cos(2\theta))\sigma_{min} \tag{3.160}$$

$$U2 = u_b + u_e = (2A - B\cos(2\theta) + \sqrt{3}B\sin(2\theta))\sigma_{max}$$
$$+ (2A + B\cos(2\theta) - \sqrt{3}B\sin(2\theta))\sigma_{min} \tag{3.161}$$

$$U3 = u_c + u_f = 2((A - B\cos(2\theta))\sigma_{max} + (A + B\cos(2\theta))\sigma_{min}) \tag{3.162}$$

Equations (3.160), (3.161) and (3.162) express the three measured displacements $U1$, $U2$ and $U3$ in terms of the three desired stresses σ_{max}, σ_{min}, and direction θ. Solving these three equations leads to three equations for stresses

$$\sigma_{max} = \frac{1}{12}\left(-\frac{2\sqrt{3}\sqrt{(U1 - U2)^2 + 3(U2 - U3)^2}}{B} + \frac{3(U1 + U3)}{A} \right) \tag{3.163}$$

$$\sigma_{min} = \frac{1}{12}\left(\frac{2\sqrt{3}\sqrt{(U1 - U2)^2 + 3(U2 - U3)^2}}{B} + \frac{3(U1 + U3)}{A} \right) \tag{3.164}$$

$$\theta = -\frac{1}{2}arc\sec\left[-\frac{\sqrt{(U1 - U2)^2 + 3(U2 - U3)^2}}{\sqrt{3}(U1 - U3)} \right] \tag{3.165}$$

3.6.3. Type III

There is only one Type III Test Configuration, Test Configuration F, as shown in Figure 3.12. As shown in the figure, measured displacements $U1$, $U2$, and $U3$ are taken between two points that do not intersect the hole. The measured displacements are calculated by Equation (3.84).

3.6.3.1. Test Configuration F

Uniform In-situ Stress Equations in Terms of Cartesian Stress Components

As shown in Figure 3.13, three displacement measurements $U1$, $U2$, $U3$ are required for Test Configuration F. Equation (3.84) is applied to Test Configuration F to obtain three measured displacements $U1$, $U2$ and $U3$.

49

$$U1 = \frac{1}{4}(6(-B+C)\tau_{xy} + \sqrt{3}(4A-B+C)\sigma_{xx}$$

$$+ \sqrt{3}(4A+B-C)\sigma_{yy}) \tag{3.166}$$

$$U2 = \frac{1}{4}(6(B-C)\tau_{xy} + \sqrt{3}(4A-B+C)\sigma_{xx} + \sqrt{3}(4A+B-C)\sigma_{yy}) \tag{3.167}$$

$$U3 = \frac{1}{2}\sqrt{3}((2A+B-C)\sigma_{xx} + (2A-B+C)\sigma_{yy}) \tag{3.168}$$

Equations (3.166), (3.167) and (3.168) express the three measured displacements $U1$, $U2$ and $U3$ in terms of the three desired stresses σ_{xx}, σ_{yy}, and τ_{xy}. Solving these three equations leads to three equations for stresses

$$\sigma_{xx} = \frac{-2A(U1+U2-2U3)+(B-C)\ (U1+U2+U3)}{3\sqrt{3}A(B-C)} \tag{3.169}$$

$$\sigma_{yy} = \frac{2A(U1+U2-2U3)+(B-C)\ (U1+U2+U3)}{3\sqrt{3}A(B-C)} \tag{3.170}$$

$$\tau_{xy} = -\frac{2(U1-U2)}{-3B+3C} \tag{3.171}$$

Uniform In-situ Stress Equations in Terms of Principal Stresses and Direction

Equation (3.84) is applied to Test Configuration F to obtain measured displacements $U1$, $U2$, $U3$.

$$U1 = \frac{1}{2}(C\sin(2\theta)(\sigma_{max} - \sigma_{min}) + C\sin(\frac{1}{3}(\pi + 6\theta)(\sigma_{max} - \sigma_{min})$$

$$+ \sqrt{3}((A - B\cos(2\theta))\sigma_{max} + (A + B\cos(2\theta))\sigma_{min}) \tag{3.172}$$

$$+ \sqrt{3}(B\cos(\frac{1}{3}(\pi + 6\theta)(\sigma_{max} - \sigma_{min}) + A(\sigma_{max} - \sigma_{min})))$$

$$U2 = \frac{1}{2}(C\sin(\frac{7\pi}{3} - 2\theta)(\sigma_{max} - \sigma_{min}) + 2C\cos(\theta)\sin(\theta)(-\sigma_{max} + \sigma_{min})$$

$$+ \sqrt{3}((A - B\cos(2\theta))\sigma_{max} + (A + B\cos(2\theta))\sigma_{min}) \tag{3.173}$$

$$+ \sqrt{3}(B\cos(\frac{7\pi}{3} - 2\theta)(\sigma_{max} - \sigma_{min}) + A(\sigma_{max} - \sigma_{min})))$$

$$U3 = \frac{1}{2}\sqrt{3}((2A + (B-C)\cos(2\theta))\sigma_{max}) + (2A + (-B+C)\cos(2\theta))\sigma_{min})$$ (3.174)

Equations (3.172), (3.173) and (3.174) express the three measured displacements $U1$, $U2$ and $U3$ in terms of the three desired stresses σ_{max}, σ_{min}, and direction θ. Solving these three equations leads to three equations for stresses

$$\sigma_{max} = \frac{1}{3\sqrt{3}A(B-C)}((B-C)(U1+U2+U3)$$
$$-4A\sqrt{U1^2 U2^2 - U2U3 + U3^2 - U1(U2+U3)})$$ (3.175)

$$\sigma_{min} = \frac{1}{3\sqrt{3}A(B-C)}((B-C)(U1+U2+U3)$$
$$+4A\sqrt{U1^2 U2^2 - U2U3 + U3^2 - U1(U2+U3)})$$ (3.176)

$$\theta = -arcsec\left[-\frac{2}{\sqrt{2 + \dfrac{2U1-U2-U3}{\sqrt{U1^2 + U2^2 - U2\,U3 + U3^2 - U1\,(U2+U3)}}}} \right]$$ (3.177)

3.6.4. Type IV

There are two Type IV Test Configurations G and H, as shown in Figure 3.13. This configuration Type is a combination Type II and Type III. The measured displacements are calculated by Equation (3.84).

3.6.4.1. Test Configuration G

Uniform In-situ Stress Equations in Terms of Cartesian Stress Components

As shown in Figure 3.13, three displacement measurements $U1$, $U2$, $U3$ are required for Test Configuration G. Equation (3.84) is applied to Test Configuration G to obtain three measured displacements $U1$, $U2$ and $U3$.

$$U1 = (A+B)\sigma_{xx} + (A-B)\sigma_{yy}$$ (3.178)

$$U2 = \sqrt{2}(2C\tau_{xy} + A\sigma_{xx} + B\sigma_{yy})$$ (3.179)

$$U3 = 2((A - B)\sigma_{xx} + (A + B)\sigma_{yy}) \tag{3.180}$$

Equations (3.178), (3.179) and (3.180) express the three measured displacements *U1*, *U2* and *U3* in terms of the three desired stresses σ_{xx}, σ_{yy}, and τ_{xy}. Solving these three equations leads to three equations for stresses

$$\sigma_{xx} = \frac{A(U1 - U3) + B\ (U1 + U3)}{4AB} \tag{3.181}$$

$$\sigma_{yy} = \frac{A(U1 - U3) + B\ (U1 + U3)}{4AB} \tag{3.182}$$

$$\tau_{xy} = -\frac{U1 - 2\sqrt{2}U2 + U3}{4C} \tag{3.183}$$

Uniform In-situ Stress Equations in Terms of Principal Stresses and Direction

Equation (3.84) is applied to the Test Configuration G to obtain measured displacements *U1*, *U2*, *U3*.

$$U1 = (A + B\cos(2\theta)\sigma_{max} + (A - B\cos(2\theta)\sigma_{min} \tag{3.184}$$

$$U2 = \sqrt{2}((A + C\sin(2\theta)\sigma_{max} + (A - C\sin(2\theta)\sigma_{min}) \tag{3.185}$$

$$U3 = 2((A - B\cos(2\theta)\sigma_{max} + (A + B\cos(2\theta)\sigma_{min}) \tag{3.186}$$

Equations (3.184), (3.185) and (3.186) express the three measured displacements *U1*, *U2* and *U3* in terms of the three desired stresses σ_{maxx}, σ_{min}, and direction θ. Solving these three equations leads to three equations for stresses

$$\sigma_{max} = \frac{1}{4}\left(\frac{U1 + U3}{A} + \frac{1}{BC}\left(\sqrt{C^2(U1 - U3)^2 + B^2\left(\begin{array}{l} U1^2 - 4\sqrt{2}\ U1U2 + \\ 8U2^2 + 2U1U3 - 4\sqrt{2}\ U2U3 + U3^2 \end{array} \right)} \right) \right) \tag{3.187}$$

52

$$\sigma_{min} = \frac{1}{4}\left(\frac{U1+U3}{A} - \frac{1}{BC}\left(\sqrt{\left(C^2(U1-U3)^2 + B^2\left(\begin{array}{l} U1^2 - 4\sqrt{2}\ U1U2 + \\ 8U2^2 + 2U1U3 - 4\sqrt{2}\ U2U3 + U3^2 \end{array} \right) \right)} \right) \right) \tag{3.188}$$

$$\theta = \frac{1}{2}\arccos\left[\frac{(C(U1-U3))}{\left(\sqrt{C^2(U1-U3)^2 + B^2\left(\begin{array}{l} U1^2 - 4\sqrt{2}U1U2 + 8U2^2 \\ +2U1U3 - 4\sqrt{2}\ U2U3 + U3^2 \end{array} \right)} \right)} \right] \tag{3.189}$$

3.6.4.2. Test Configuration H

Uniform In-situ Stress Equations in Terms of Cartesian Stress Components

As shown in Figure 3.13, three displacement measurements *U1, U2, U3* are required for Test Configuration H. Equation (3.84) is applied to Test Configuration H to obtain three measured displacements *U1, U2* and *U3*.

$$U1 = (A+C)\sigma_{xx} + (A-C)\sigma_{yy} \tag{3.190}$$

$$U2 = \sqrt{2}((A-C)\sigma_{xx} + (A+C)\sigma_{yy}) \tag{3.191}$$

$$U3 = \sqrt{2}(2C\tau_{xy} + A\sigma_{xx} + A\sigma_{yy}) \tag{3.192}$$

Equations (3.190), (3.191) and (3.192) express the three measured displacements *U1, U2* and *U3* in terms of the three desired stresses σ_{xx}, σ_{yy}, and τ_{xy}. Solving these three equations leads to three equations for stresses

$$\sigma_{xx} = \frac{A(U1-U2)+C(U1+U2)}{2\sqrt{2}AC} \tag{3.193}$$

$$\sigma_{yy} = \frac{A(-U1+U2)+C(U1+U2)}{2\sqrt{2}AC} \tag{3.194}$$

$$\tau_{xy} = -\frac{U1+U2-2U3}{2\sqrt{2}C} \tag{3.195}$$

53

Uniform In-situ Stress Equations in Terms of Principal Stresses and Direction

Equation (3.84) is applied to Test Configuration H to obtain measured displacements ($U1$, $U2$, $U3$).

$$U1 = (A - B\sin(2\theta))\sigma_{\max} + (A + B\sin(2\theta))\sigma_{\min} \tag{3.196}$$

$$U2 = \sqrt{2}((A + C\sin(2\theta))\sigma_{\max} + (A - C\sin(2\theta))\sigma_{\min}) \tag{3.197}$$

$$U3 = \sqrt{2}((A - C\cos(2\theta))\sigma_{\max} + (A + C\cos(2\theta))\sigma_{\min}) \tag{3.198}$$

Equations (3.196), (3.197) and (3.198) express the three measured displacements $U1$, $U2$ and $U3$ in terms of the three desired stresses σ_{max}, σ_{min}, and direction θ. Solving these three equations leads to three equations for stresses

$$\sigma_{\max} = \frac{\left(\sqrt{2}BC(U2-U3)(U2+U3)\sqrt{\begin{array}{l}B^2(U2-U3)^2+C^2\\\left(\begin{array}{l}2U1^2-2\sqrt{2}U1(U2+U3)\\+(U2+U3)^2\end{array}\right)\end{array}} \\ -A\sqrt{(U2-U3)^2}\left(\begin{array}{l}-4C^2U1(U2+U3)+\\\sqrt{2}\left(B^2(U2-U3)^2+\left(2U1^2+(U2+U3)^2\right)\right)\end{array}\right) \right)}{\left(4ABC\left(U2-\sqrt{\begin{array}{l}B^2(U2-U3)^2+C^2\\\left(2U1^2-2\sqrt{2}U1(U2+U3)+(U2+U3)^2\right)\end{array}}\right)\right)} \tag{3.199}$$

$$\sigma_{\min} = \frac{\left(\sqrt{2}BC(U2-U3)(U2+U3)\sqrt{\begin{array}{l}B^2(U2-U3)^2+C^2\\\left(\begin{array}{l}2U1^2-2\sqrt{2}U1(U2+U3)\\+(U2+U3)^2\end{array}\right)\end{array}} \\ +A\sqrt{(U2-U3)^2}\left(\begin{array}{l}-4C^2U1(U2+U3)+\\\sqrt{2}\left(B^2(U2-U3)^2+\left(2U1^2+(U2+U3)^2\right)\right)\end{array}\right) \right)}{\left(4ABC\left(U2-\sqrt{\begin{array}{l}B^2(U2-U3)^2+C^2\\\left(2U1^2-2\sqrt{2}U1(U2+U3)+(U2+U3)^2\right)\end{array}}\right)\right)} \tag{3.200}$$

54

$$\theta = -arcsec\left[-\cfrac{2}{\sqrt{2 + \cfrac{2U1 - U2 - U3}{\sqrt{U1^2 + U2^2 - U2\,U3 + U3^2 - U1\,(U2 + U3)}}}}\right]$$

(3.201)

3.7. DERIVATION OF LINEAR GRADIENT IN-SITU STRESS EQUATIONS

The linear gradient in-situ stress equations, applicable to the linear gradient stress state shown in Figure 3.5, are calculated here as a function measured displacements (U). The derivation procedure is similar to the derivation procedure for the uniform in-situ stress equations. The same Types of test configurations, except Type I and Type II are available for the linear gradient in-situ stress state. The main difference here is the definition of the relieved displacements. In the derivation of the linear gradient in-situ stress equations, the relieved displacement Equations (3.82) and (3.83) are substituted in to Equation (3.84) to get measured displacement.

The linear gradient in-situ stress equations are derived for the 5 Test Configurations shown in Figure 3.14. The equations calculate linear gradient stress state components σ_{xx}, σ_{yy}, τ_{xy}, Kx, Ky. Figure 3.14 shows the equation numbers of in-situ stress equations for each Test Configuration. This is done to help reader locate equations that are of particular interest. The derivations presented in the following are grouped by Type of Test Configuuration.

3.7.1. Type III

There are two Type III Test Configurations, L and M, as shown in Figure 3.14. Measured displacements are taken between the points as shown in Figure 3.14. Measured displacements in Type III shown with $U1$, $U2$, $U3$, $U3$ and $U5$ are taken between two points that does not intersect the hole. The measured displacements are calculated by Equation (3.84).

3.7.1.1. Test Configuration L

As shown in Figure 3.14, five displacement measurements $U1$, $U2$, $U3$, $U4$, and $U5$ are required for Test Configuration L. Equation (3.84) is applied to Test Configuration L to obtain five measured displacements $U1$, $U2$ $U3$, $U4$ and $U5$.

$$U1 = \frac{1}{\sqrt{2}}\left(-F(Kx + Ky) + (H + I + J)(Kx + Ky) - 4C\tau + 2A(\sigma_{xx} + \sigma_{yy})\right)$$

(3.202)

$$U2 = \frac{1}{\sqrt{2}}\left(F(Kx - Ky) - (H + I + J)(Kx - Ky) + 4C\tau + 2A(\sigma_{xx} + \sigma_{yy})\right) \quad (3.203)$$

$$U3 = \frac{1}{\sqrt{2}}\left(-F(Kx + Ky) + (H + I + J)(Kx + Ky) + 4C\tau - 2A(\sigma_{xx} + \sigma_{yy})\right) \quad (3.204)$$

$$U4 = \frac{1}{\sqrt{2}}\left((-F + H + I + J)(Kx - Ky) + 4C\tau + 2A(\sigma_{xx} + \sigma_{yy})\right) \quad (3.205)$$

$$U5 = \left((F + H - I + J)Kx + \sqrt{2}\left((A - C)\right)\sigma_{xx} + (A + C)\sigma_{yy}\right) \quad (3.206)$$

Equations (3.98), (3.99), (3.100), (3.205) and (3.206) express the five measured displacements $U1$, $U2$, $U3$, $U4$ and $U5$ in terms of the five desired stresses σ_{xx}, σ_{yy}, τ_{xy}, Kx and Ky. Solving these five equations leads to five equations for stresses

$$\sigma_{xx} = -\frac{\left(\begin{array}{l} \sqrt{2}\left((A + C)(U1 + U2 + U3 + U4) - 4AU5\right)(F - H - I - J) \\ -2A(U1 - U2 - U3 + U4)(F + H - I + J) \end{array}\right)}{\left(8AC(-F + H + I + J)\right)} \quad (3.207)$$

$$\sigma_{yy} = -\frac{\left(\begin{array}{l} \sqrt{2}\left(-(A + C)(U1 + U2 + U3 + U4) + 4AU5\right)(F - H - I - J) \\ +2A(U1 - U2 - U3 + U4)(F + H - I + J) \end{array}\right)}{\left(8AC(-F + H + I + J)\right)} \quad (3.208)$$

$$\tau_{xy} = \frac{-U1 + U2 - U3 + U4}{4\sqrt{2}C} \quad (3.209)$$

$$Kx = -\frac{-U1 + U2 + U3 - U4}{2\sqrt{2}(-F + H + I + J)} \quad (3.210)$$

$$Kx = -\frac{-U1 - U2 + U3 + U4}{2\sqrt{2}(-F + H + I + J)} \quad (3.211)$$

3.7.1.2. Test Configuration M

As shown in Figure 3.14, five displacement measurements $U1$, $U2$, $U3$, $U4$, and $U5$ are required for Test Configuration M. Equation (3.84) is applied to obtain five measured displacements $U1$, $U2$ $U3$, $U4$ and $U5$.

$$U1 = \left(-(F + H - I + J)Ky + \sqrt{2}\left((A + C)\right)\sigma_{xx} + (A - C)\sigma_{yy}\right) \quad (3.212)$$

56

$$U2 = \frac{1}{\sqrt{2}}\left(F(Kx-Ky)-(H+I+J)(Kx-Ky)+4C\tau+2A(\sigma_{xx}+\sigma_{yy})\right)$$ (3.213)

$$U3 = \frac{1}{\sqrt{2}}\left(-F(Kx+Ky)+(H+I+J)(Kx+Ky)+4C\tau-2A(\sigma_{xx}+\sigma_{yy})\right)$$ (3.214)

$$U4 = \left((F+H-I+J)Ky+\sqrt{2}\left((A+C)\right)\sigma_{xx}+(A-C)\sigma_{yy}\right)$$ (3.215)

$$U5 = \left(-(F+H-I+J)Kx+\sqrt{2}\left((A-C)\right)\sigma_{xx}+(A+C)\sigma_{yy}\right)$$ (3.216)

Equations (3.212), (3.213), (3.214), (3.215) and (3.216) express the five measured displacements *U1, U2, U3, U4* and *U5* in terms of the five desired stresses σ_{xx}, σ_{yy}, τ_{xy}, *Kx* and *Ky*. Solving these five equations leads to five equations for stresses

$$\sigma_{xx} = \frac{\left(\begin{array}{l}2(F+H-I+J)(C(U2+U3)+A(U1-U2-U3+U4))\\+\sqrt{2}(F-H-I-J)(A(U1+U4-2U5)+C(U1+U4+2U5))\end{array}\right)}{\left(4AC((2+\sqrt{2})F+\sqrt{2}(H-I+J)-2(H+I+J)\right)}$$ (3.217)

$$\sigma_{yy} = -\frac{\left(\begin{array}{l}2(F+H-I+J)(-C(U2+U3)+A(U1-U2-U3+U4))\\+\sqrt{2}(F-H-I-J)((A-C)(U1+U4)-2(A+C)U5)\end{array}\right)}{\left(4AC((2+\sqrt{2})F+\sqrt{2}(H-I+J)-2(H+I+J)\right)}$$ (3.218)

$$\tau_{xy} = \frac{\left(\begin{array}{l}I+J)U1-\sqrt{2}IU2+\sqrt{2}JU2+\sqrt{2}IU3-\sqrt{2}JU3+H(U1\\+\sqrt{2}(U2-U3)-U4)-IU4-JU4+F(-U1+\sqrt{2}(U2-U3)+U4)\end{array}\right)}{4C(F+H-I+J)}$$ (3.219)

$$Kx = -\frac{-U1-2U2-2U3+U4+2U5}{2[(F+H-I)+\sqrt{2}(F-H-I-J)+J]}$$ (3.220)

$$Kx = \frac{U4-U1}{2(F+H-I+J)}$$ (3.221)

3.7.2. Type IV

There are three Type IV Test Configurations, P, Q and R, as shown in Figure 3.14. Measured displacements shown with *U1, U2 U3, U4* and *U5* are taken between the points as shown in

57

Figure 3.14. This configuration type is combination of Type II and Type III. The measured displacements are calculated by Equation (3.84).

3.7.2.1. Test Configuration P

As shown in Figure 3.14, five displacement measurements *U1, U2, U3, U4,* and *U5* are required for Test Configuration P. Equation (3.84) is applied to Test Configuration P to obtain five measured displacements *U1, U2 U3, U4* and *U5*.

$$U1 = \frac{1}{\sqrt{2}}\left(-F(Kx + Ky) + (H + I + J)(Kx + Ky) - 4C\tau + 2A(\sigma_{xx} + \sigma_{yy})\right) \tag{3.222}$$

$$U2 = \frac{1}{\sqrt{2}}\left(F(Kx - Ky) - (H + I + J)(Kx - Ky) + 4C\tau + 2A(\sigma_{xx} + \sigma_{yy})\right) \tag{3.223}$$

$$U3 = \frac{1}{\sqrt{2}}\left(-F(Kx + Ky) + (H + I + J)(Kx + Ky) + 4C\tau - 2A(\sigma_{xx} + \sigma_{yy})\right) \tag{3.224}$$

$$U4 = \frac{1}{\sqrt{2}}\left((-F + H + I + J)(Kx - Ky) + 4C\tau + 2A(\sigma_{xx} + \sigma_{yy})\right) \tag{3.225}$$

$$U5 = 2\left((A + B)\sigma_{xx} + (A - B)\sigma_{yy}\right) \tag{3.226}$$

Equations (3.222), (3.223), (3.224), (3.225) and (3.226) express the five measured displacements *U1, U2, U3, U4* and *U5* in terms of the five desired stresses σ_{xx}, σ_{yy}, τ_{xy}, *Kx* and *Ky*. Solving these five equations leads to five equations for stresses

$$\sigma_{xx} = \frac{-\sqrt{2}(A - B)(U1 + U2 + U3 + U4) + 4AU5}{8AB} \tag{3.227}$$

$$\sigma_{yy} = \frac{\sqrt{2}(A + B)(U1 + U2 + U3 + U4) - 4AU5}{8AB} \tag{3.228}$$

$$\tau_{xy} = \frac{-U1 + U2 - U3 + U4}{4\sqrt{2}C} \tag{3.229}$$

$$Kx = -\frac{-U1 + U2 + U3 - U4}{2\sqrt{2}(-F + H + I + J)} \tag{3.230}$$

$$Ky = -\frac{-U1 - U2 + U3 + U4}{2\sqrt{2}(-F + H + I + J)} \tag{3.231}$$

3.7.2.2. Test Configuration Q

As shown in Figure 3.14, five displacement measurements $U1$, $U2$, $U3$, $U4$, and $U5$ are required for Test Configuration Q. Equation (3.84) is applied to Test Configuration Q to obtain five measured displacements $U1$, $U2$ $U3$, $U4$ and $U5$.

$$U1 = 2\left((A+B)\sigma_{xx} + (A-B)\sigma_{yy}\right) \tag{3.232}$$

$$U2 = Kx(F+H-I+J) + \sqrt{2}\left((A-C)\sigma_{xx} + (A+C)\sigma_{yy}\right) \tag{3.233}$$

$$U3 = -Kx(F+H-I+J) + \sqrt{2}\left((A-C)\sigma_{xx} + (A+C)\sigma_{yy}\right) \tag{3.234}$$

$$U4 = 2\left(A(\sigma_{xx} + \sigma_{yy}) + 2B\tau\right) \tag{3.235}$$

$$U5 = -Ky(F+H-I+J) + \sqrt{2}\left((A+C)\sigma_{xx} + (A-C)\sigma_{yy}\right) \tag{3.236}$$

Equations (3.232), (3.233), (3.234), (3.235) and (3.236) express the five measured displacements $U1$, $U2$, $U3$, $U4$ and $U5$ in terms of the five desired stresses σ_{xx}, σ_{yy}, τ_{xy}, Kx and Ky. Solving these five equations leads to five equations for stresses

$$\sigma_{xx} = \frac{\sqrt{2}(A+C)U1 - (A-B)(U2+U3)}{2\sqrt{2}A(B+C)} \tag{3.237}$$

$$\sigma_{yy} = \frac{-\sqrt{2}(A-C)U1 + (A+B)(U2+U3)}{2\sqrt{2}A(B+C)} \tag{3.238}$$

$$\tau_{xy} = \frac{-B\left(\sqrt{2}(U2+U3) - 2U4\right) + 2C(-U1+U4)}{4B(B+C)} \tag{3.239}$$

$$Kx = \frac{U2-U3}{2(F+H-I+J)} \tag{3.240}$$

$$Ky = \frac{C\left(2\sqrt{2}U1 - U2 - U3 - 2U5\right) + B(U2+U3-2U5)}{2(B+C)(F+H-I+J)} \tag{3.241}$$

3.7.2.3. Test Configuration R

As shown in Figure 3.14, five displacement measurements $U1$, $U2$, $U3$, $U4$, and $U5$ are required for Test Configuration R. Equation (3.84) is applied Test Configuration R to obtain five measured displacements $U1$, $U2$ $U3$, $U4$ and $U5$.

$$U1 = 2\left((A-B)\sigma_{xx} + (A+B)\sigma_{yy}\right) \tag{3.242}$$

$$U2 = Kx(F+H-I+J) + \sqrt{2}\left((A-C)\sigma_{xx} + (A+C)\sigma_{yy}\right) \tag{3.243}$$

$$U3 = -Kx(F+H-I+J) + \sqrt{2}\left((A-C)\sigma_{xx} + (A+C)\sigma_{yy}\right) \tag{3.244}$$

$$U4 = 2\left(A(\sigma_{xx} + \sigma_{yy}) + 2B\tau\right) \tag{3.245}$$

$$U5 = -Ky(F+H-I+J) + \sqrt{2}\left((A+C)\sigma_{xx} + (A-C)\sigma_{yy}\right) \tag{3.246}$$

Equations (3.242), (3.243), (3.244), (3.245) and (3.246) express the five measured displacements $U1$, $U2$, $U3$, $U4$ and $U5$ in terms of the five desired stresses σ_{xx}, σ_{yy}, τ_{xy}, Kx and Ky. Solving these five equations leads to five equations for stresses

$$\sigma_{xx} = \frac{-\sqrt{2}(A+C)U1 + (A+B)(U2+U3)}{2\sqrt{2}A(B-C)} \tag{3.247}$$

$$\sigma_{yy} = \frac{\sqrt{2}(A-C)U1 - (A-B)(U2+U3)}{2\sqrt{2}A(B-C)} \tag{3.248}$$

$$\tau_{xy} = \frac{-B\left(\sqrt{2}(U2+U3) - 2U4\right) + 2C(U1-U4)}{4B(B-C)} \tag{3.249}$$

$$Kx = \frac{U2-U3}{2(F+H-I+J)} \tag{3.250}$$

$$Ky = \frac{C\left(-2\sqrt{2}U1 + U2 + U3 + 2U5\right) + B(U2+U3-2U5)}{2(B-C)(F+H-I+J)} \tag{3.251}$$

60
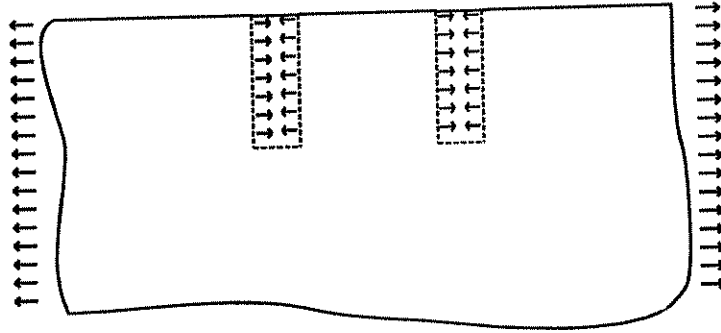
Figure 3.1 Existing in-situ stresses before core-hole is drilled in a structure. Cross-section of measurement area.
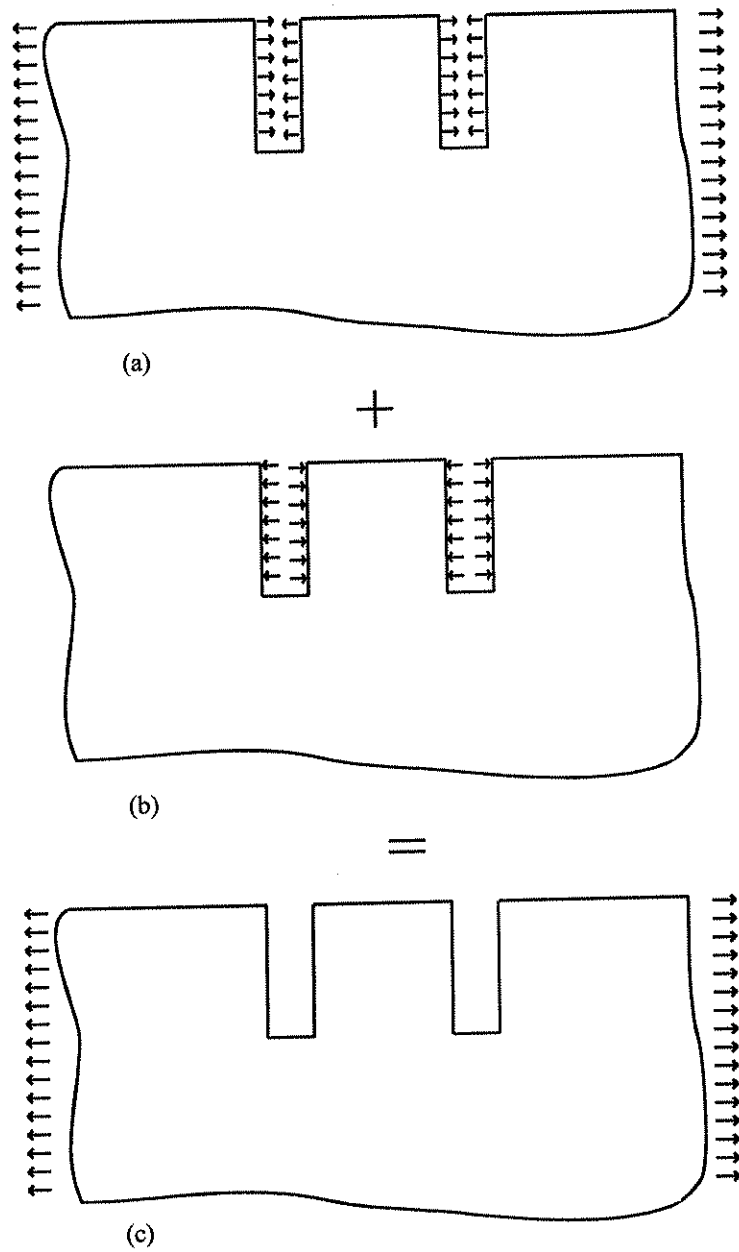
Figure 3.2 Superposition of loading to find relieved displacement caused by drilling a core-hole: (a) original stress; (b) stress change (relieved in-situ stresses); (c) final stress.
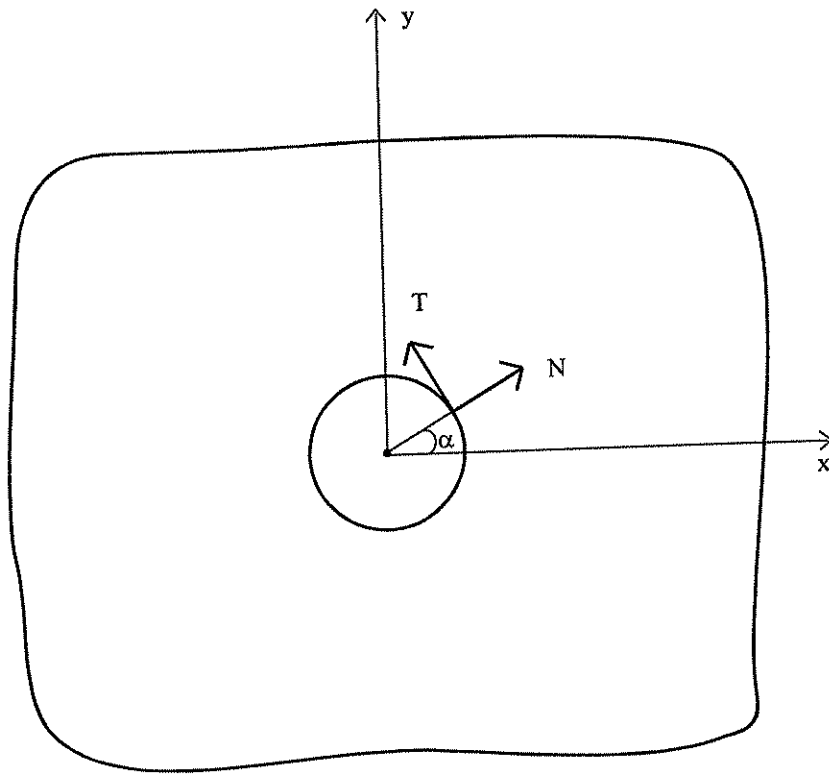
(a)
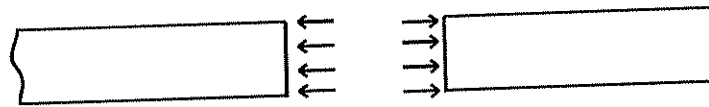
(b)

Figure 3.3 Schematic representation of the in-situ stress relaxation due to a through-hole drilling: (a) plan view; (b) cross-section.
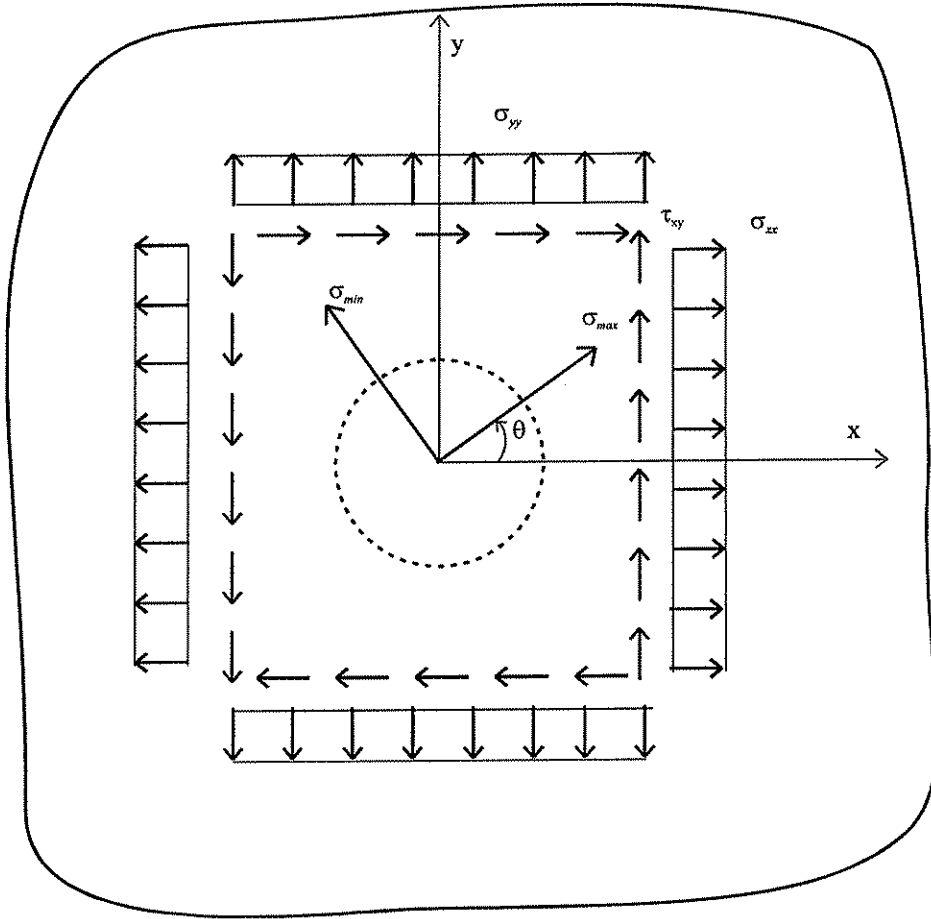
Figure 3.4 Schematic representation of the uniform stress state.
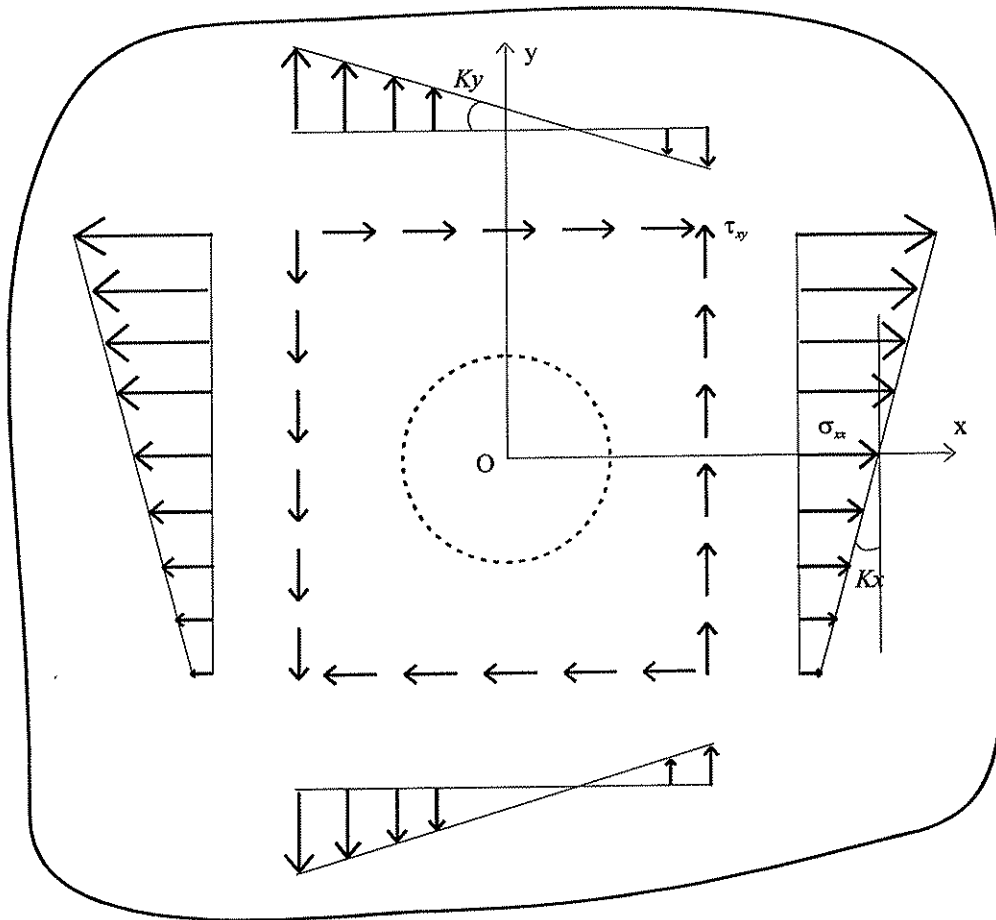
Figure 3.5 Schematic representation of the linear gradient stress state.
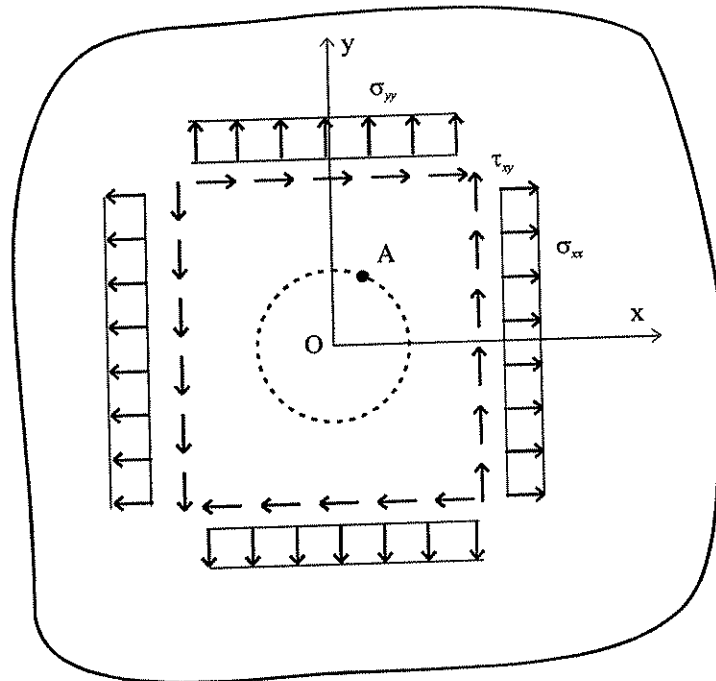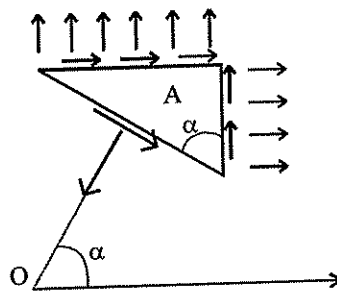
Figure 3.6 Calculation of relieved in-situ stresses due to hole drilling: (a) plan view; (b) cross-section; (c) stress distribution on infinitesimal element.
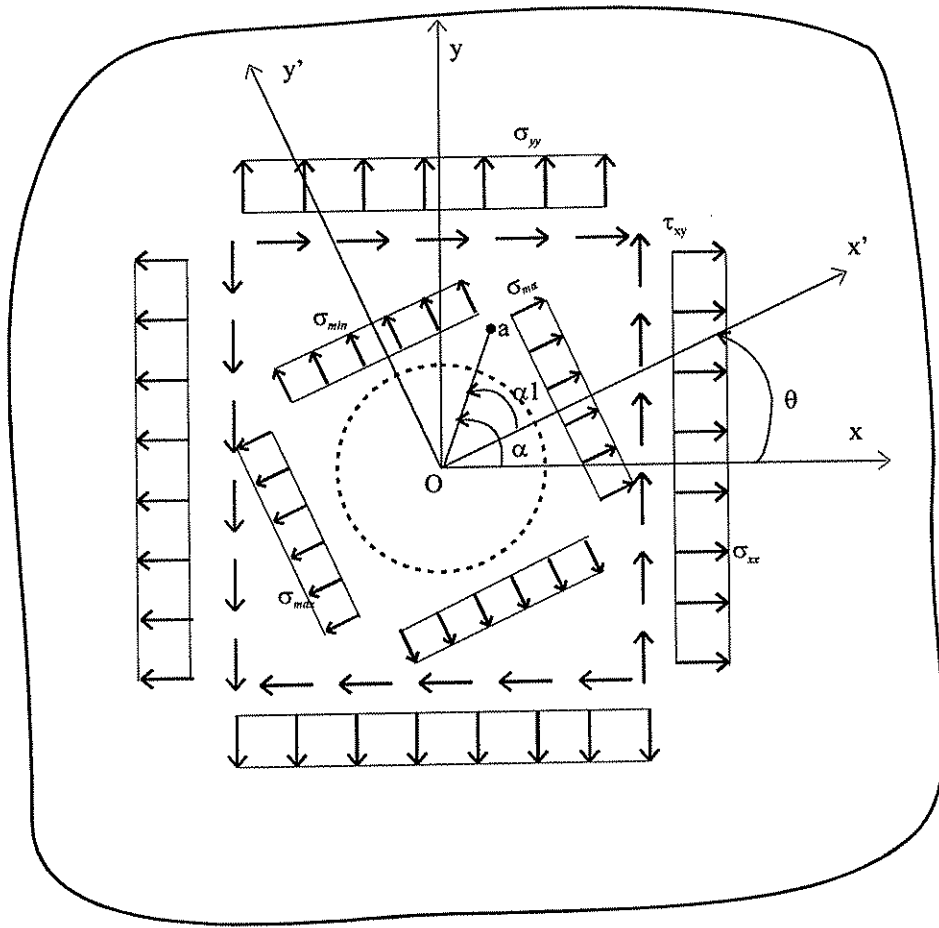
Figure 3.7 Schematic representation of uniform in-situ stress state in terms of both cartesian stress components and principal stresses.
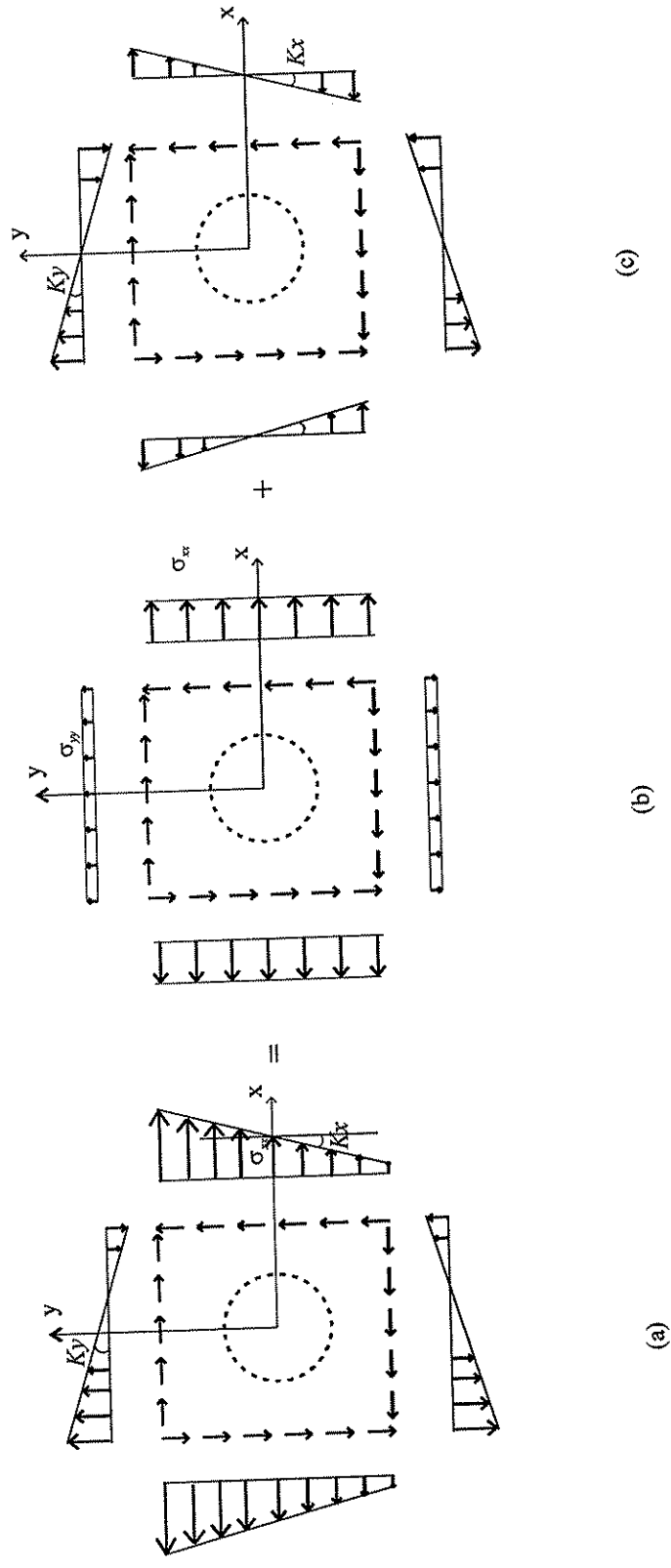
Figure 3.8 Schematic representation of linear gradient stress state as superposition of two different in-situ stress states: (a) linear gradient stress state; (b) uniform stress state; (c) concentric linear gradient normal stress.

68
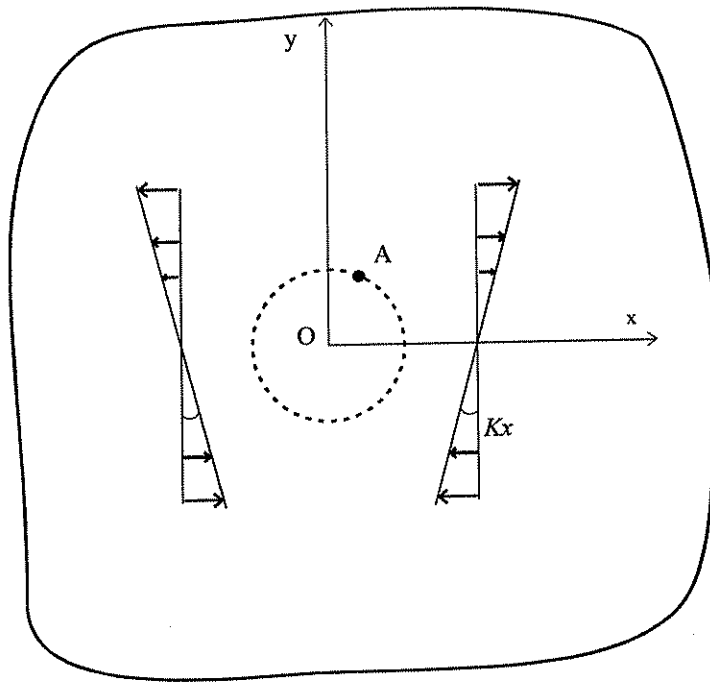
(a)
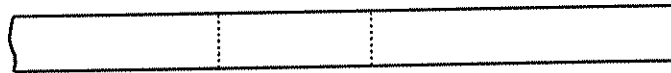
(b)
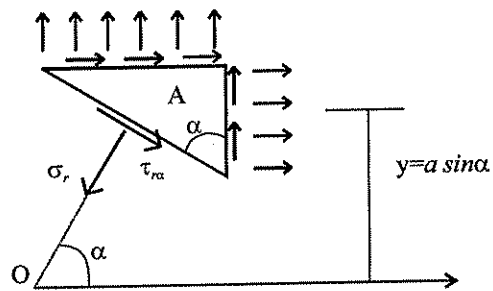
(c)

Figure 3.9 Calculation of relieved in-situ stresses due to hole drilling for uniaxial concentric linear gradient normal stress state: (a) plan view; (b) cross-section; (c) stress distribution on infinitesimal element.
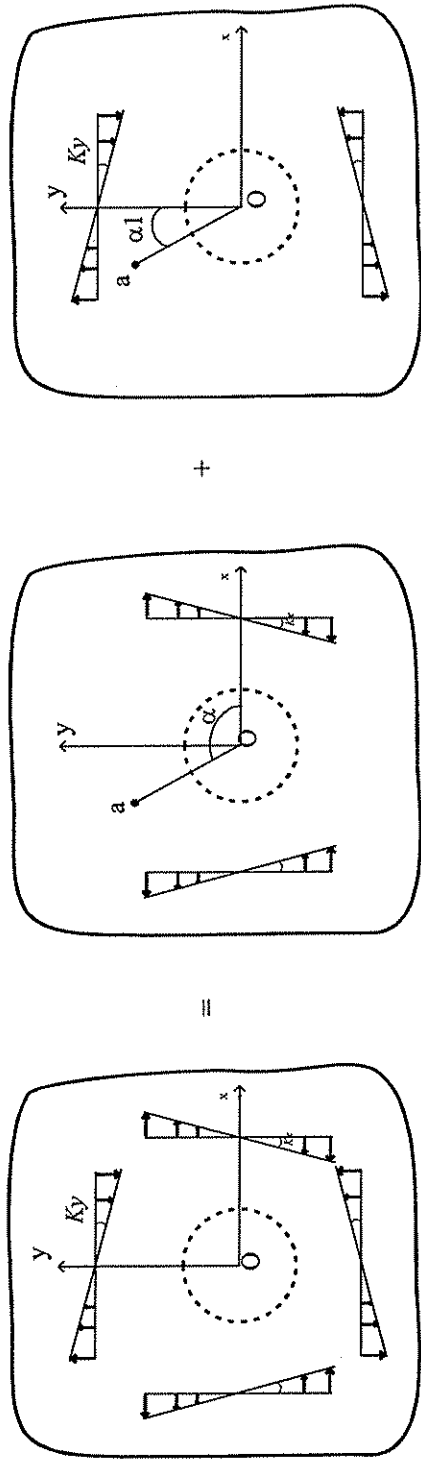
Figure 3.10 Superposition of uniaxial concentric linear gradient normal stress states to obtain biaxial concentric linear gradient normal stress state: (a) biaxial concentric linear gradient normal stress state; (b) uniaxial concentric linear gradient normal stress states in x direction; (c) uniaxial concentric linear gradient normal stress states in y direction.

70
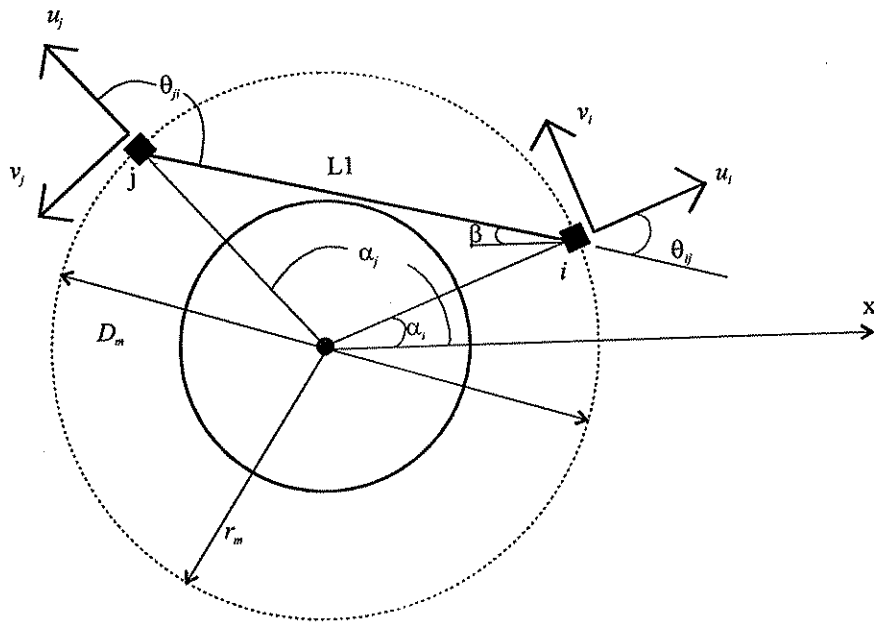
Figure 3.11 Representation of displacement measurement between two measurement points (measured displacement is U).
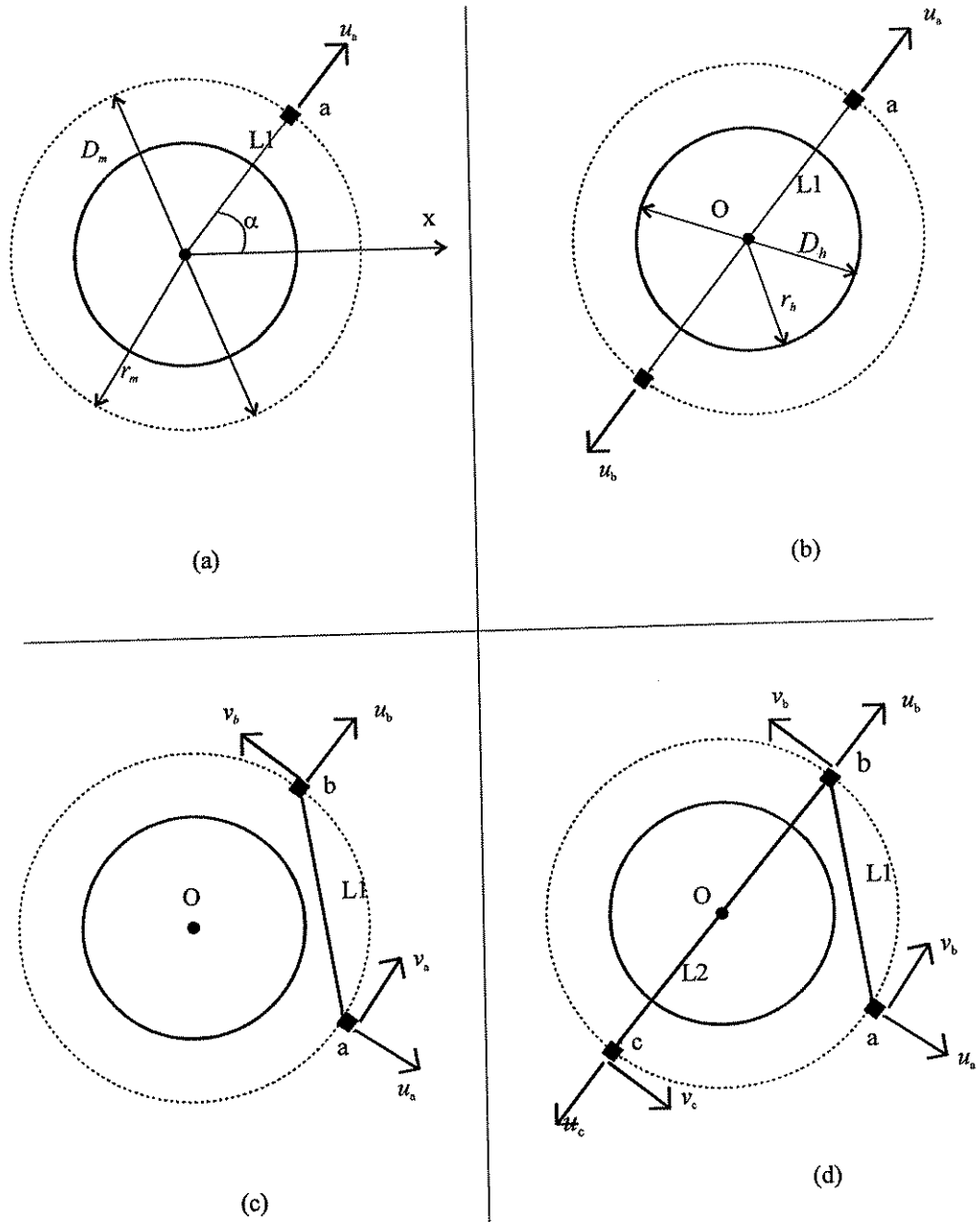
Figure 3.12 Four Types of Test Configurations: (a) Type I; (b) Type II; (c) Type III; (d) example of a Type IV.
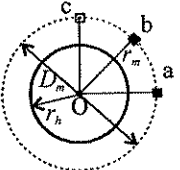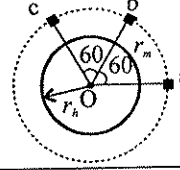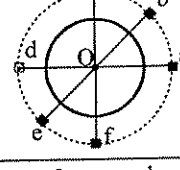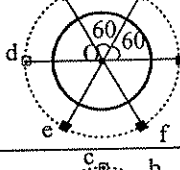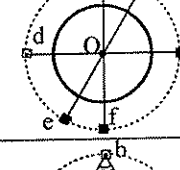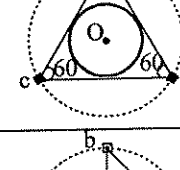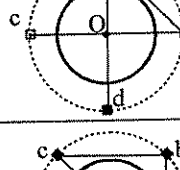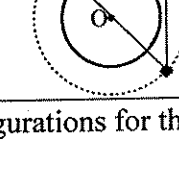
Measument Type	Test Configuration	Equation Numbers for Cartesian Stresses	Equation Numbers for Principal Stresses
I	A	(3.101) (3.102) (3.103)	(3.110) (3.111) (3.112)
	B	(3.116) (3.117) (3.118)	(3.122) (3.123) (3.124)
II	C	(3.133) (3.134) (3.134)	(3.139) (3.140) (3.141)
	D	(3.145) (3.146) (3.147)	(3.151) (3.152) (3.153)
	E	(3.157) (3.158) (3.159)	(3.163) (3.164) (3.165)
III	F	(3.169) (3.170) (3.171)	(3.175) (3.176) (3.177)
IV	G	(3.181) (3.182) (3.183)	(3.187) (3.188) (3.189)
	H	(3.193) (3.194) (3.195)	(3.199) (3.200) (3.201)

Figure 3.13 Test Configurations for the uniform stress state.

73
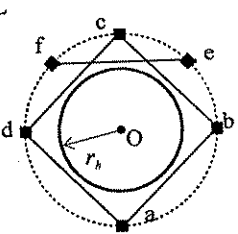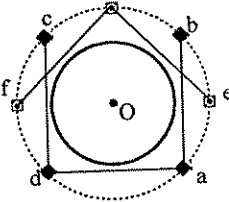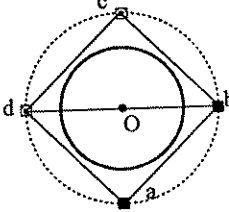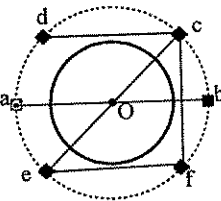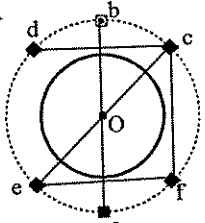
Measurment Type	Test Configuration	Equation Numbers
III	L	(3.207) (3.208) (3.209) (3.210) (3.211)
	M	(3.217) (3.218) (3.219) (3.220) (3.221)
IV	P	(3.227) (3.228) (3.229) (3.230) (3.231)
	Q	(3.237) (3.238) (3.239) (3.240) (3.241)
	R	(3.247) (3.248) (3.249) (3.250) (3.251)

Figure 3.14 Test Configurations for the linear gradient stress state.

74

Constants	Plane stress	Plane strain
A	$\dfrac{a^2(1+v)}{2Er}$	$\dfrac{a^2(1+v)}{2Er}$
B	$\dfrac{4a^2r^2-a^4(1+v)}{2Er^3}$	$\dfrac{a^2\left(4r^2(v-1)-a^2\right)(1+v)}{2Er^3}$
C	$\dfrac{2a^2r^2(v-1)-a^4(1+v)}{2Er^3}$	$\dfrac{a^2\left(2r^2(2v-1)-a^2\right)(1+v)}{2Er^3}$

Table 3.1 Definition of constants A, B and C for plane stress and plane strain.

Constants	Plane Stress	Plane Strain
F	$\dfrac{a^4(1+v)}{8Er^2}$	$\dfrac{a^4(1+v)}{8Er^2}$
H	$\dfrac{a^4\left[-2a^2(1+v)+r^2(5+v)\right]}{8Er^4}$	$\dfrac{a^4(1+v)\left[2a^2(1+v)+r^2(4v-5)\right]}{8Er^4}$
I	$-\dfrac{a^4(1+v)}{8Er^2}$	$-\dfrac{a^4(1+v)}{8Er^2}$
J	$\dfrac{a^4\left[r^2(1-3v)+2a^2(1+v)\right]}{8Er^4}$	$\dfrac{a^4\left[\left(r^2(1-4v)+2a^2\right)(1+v)\right]}{8Er^4}$

Table 3.2 Definition of constants $F,H,$ I and J for plane stress and plane strain.

	$U1+U3-2U2>0$	$U1+U3-2U2=0$	$U1+U3-2U2<0$
$U1-U3>0$	$0<\theta<\dfrac{\pi}{4}$	$\dfrac{\pi}{4}$	$\dfrac{\pi}{4}<\theta<0$
$U1-U3=0$	0		$\dfrac{\pi}{2}$
$U1-U3<0$	$-\dfrac{\pi}{4}<\theta<0$	$-\dfrac{\pi}{4}$	$-\dfrac{\pi}{2}<\theta<\dfrac{\pi}{4}$

Table 3.3 Angle of principal stress.

CHAPTER 4

VERIFICATION OF THEORETICAL FORMULATION

4.1. INTRODUCTION

In this chapter, the closed-form equations for relieved displacements and in-situ stresses that were derived in Chapter 3 are verified. The closed-form equations for relieved displacements are verified using finite element analyses. Once these equations are verified, they are then used to verify the closed-form equations for in-situ stresses.

The outline of this chapter is as follows. Section 4.2 presents general information about the finite element analyses that are performed to verify the closed-form equations for relieved displacements. Section 4.3 verifies the closed-form relieved displacement equations for the uniform stress state, and Section 4.4 verifies the closed-form relieved displacement equations for the linear gradient stress state. Section 4.5 verifies the uniform in-situ stress equations, and Section 4.6 verifies the linear gradient in-situ stress equations.

4.2. FINITE ELEMENT MODEL

This section describes general features of the finite element analyses that were performed to verify the closed-form equations for the relieved displacement that were derived in Chapter 3. Included in this section are descriptions how hole drilling was simulated, model geometry, element types and boundary conditions, material properties, a convergence study, information about the specific analysis software that was used, and a discussion of issues related to plane stress versus plane strain analysis.

4.2.1. Simulation of Hole Drilling

A finite element model was created to simulate stress relief and corresponding displacement relief resulting from drilling a through-hole in a linear elastic, isotropic infinite thin plate in which defined in-situ stresses are uniformly distributed through the plate thickness. The correlation between stress relief and displacement relief due to hole drilling was explained in Section 3.1 (Figure 3.2). It was shown that the stress redistribution and displacement relief created by hole drilling can be calculated by loading the surface of the hole by the in-situ stresses which are relaxed when the hole is drilled (Figure 3.3).

77

Linear elastic finite element analyses were carried out using ABAQUS, a commercial finite element analysis software package.

4.2.2. Modeling and Model Geometry

Based on the information above, the finite element model is created as follows. An infinite thin plate with a through-hole is modeled. The entire plate is modeled as shown in Figure 4.1 instead of using symmetric, asymmetric, or axisymmetric models, which require superposition to calculate the relieved displacements due to through-hole drilling. The full plate model gives flexibility to apply any kind of loading in one analysis without changing boundary conditions. Figure 4.1 shows the general geometry of the finite element model. The diameter of the through-hole is 150 mm. L, which is length and width of part of the model that is modeled with finite elements, is defined as 3000 mm, based on a convergence study.

4.2.3. Material Properties

The material properties of the model are as follows. Young's modulus E and Poisson's ratio are 30000 MPa (4340 ksi) and 0.2 respectively. This Young's modulus corresponds to a normal weight concrete with a a compressive strength of 40 MPa (5800 psi). The analyses assume that the material is linear elastic.

4.2.4. Load Condition

As explained earlier, loads are applied to the inner surface of the through-hole. These loads, which represent relieved stresses due to through-hole drilling, are calculated as a function of α for both the uniform stress state (Equations (3.5) and (3.6)) and the linear gradient stress state (Equations (3.48) and (3.49)) in Chapter 3. The loads found by these equations are applied to the nodes at the surface of the hole as concentrated forces in radial and in tangential directions.

4.2.5. Elements Types and Boundary Conditions

The area surrounding the hole is modeled by 8-node biquadratic plane stress elements (element type CPS8). Far-field conditions are modeled by infinite elements (element type CINPS5). Stress concentration effects require the region near the through-hole to be meshed with a finer mesh, while the far field region is more coarsely meshed.

No other boundary conditions are used other than infinite elements. Infinite elements work like boundary conditions, which provide required boundary conditions for an infinite medium.

Infinite elements are used in boundary value problems defined in unbounded domains or problems in which the region of interest is small in size compared to surrounding medium. The basis of the formulation of these elements for static analysis is that the far-field solution along each element edge that stretches to infinity is centered about an origin, called "pole". For example, the finite element model has its pole at the center of the hole. It is important to choose

the position of the nodes in the infinite direction appropriately with respect to the pole. The second node along each edge pointing in the infinite direction must be positioned so that it is twice as far from the pole as the node on the same edge at the boundary between the finite and the infinite elements. A more detailed description of the infinite element (CINPS5) can be found in the ABAQUS User's Manual.

4.2.6. Convergence Study

A preliminary convergence study was conducted to establish where the boundary conditions (infinite elements) should be placed with respect to the hole, and to assess the accuracy of results. Figure 4.1 shows the general geometry of the model. In this figure, L represents location of the boundary (infinite element) conditions. A mesh refinement convergence study was then conducted. Convergence was evaluated by examining relieved displacements at the surface of the through-hole.

Table 4.1 summarizes key values from the preliminary convergence study. The table shows the relieved displacement results for different length (L), number of elements, number of nodes and total number of variables. The relieved displacement u_r shown in the table is $r_m = a$ and $\alpha = 0$.

As shown in the first three rows of Table 4.1, L is varied as the number of elements and the diameter of the through-hole were held constant. L was defined as 3000 mm since the results were not improved any further when taking L greater. In the following rows of the table, results for increased number of elements are reported as L is kept constant. As shown in Table 4.1, the relieved displacements converge quickly. It is observed that mesh refinements do not improve the results any further beyond the model with 1312 elements. Thus, the finite element model shown in fourth row was chosen for the verification analyses.

The mesh of the finite element model in different views is shown in Figures 4.2 to 4.4. Figure 4.2 shows general view of the finite element mesh. Figures 4.3 and 4.4 show closer look of the mesh at the vicinity of the hole.

4.2.7. Plane Stress versus Plane Strain

The closed-form equations for relieved displacements and in-situ stresses are derived in a form that can be converted to plane stress as well as plane strain conditions. The verifications presented here treat only the plane stress condition. This is done because the relieved displacements measured at the surface are thought to be closer to the plane stress solution. This decision was made at the beginning of the verification analysis. After an evaluation of the applicability of the closed-form equations to three-dimensional objects (Chapter 5), it is seen that the results are in fact closer to the plane stress condition. Thus, verification for plane strain solutions is not done.

4.3. VERIFICATION OF THE CLOSED-FORM RELIEVED DISPLACEMENT EQUATIONS FOR THE UNIFORM STRESS STATE

In this section, the closed-form relieved displacement equations for the uniform stress state, derived in Chapter 3, are verified. The finite element model described in Section 4.2 is used to perform this verification.

The verification of the closed-form relieved displacement equations for the uniform stress state is done as follows. First, in-situ stress states prior to through-hole drilling are defined. Then the finite element model is used to calculate relieved displacements for these stress states. The relieved displacements obtained from the finite element analyses are compared with the relieved displacements obtained from the closed-form relieved displacement equations.

Three different Load Cases are treated as shown in Table 4.2. Load Case 1 applies uniaxial normal stress. Load Case 2 applies pure shear stress. Load Case 3 is the most general, and includes both biaxial normal stress and shear stress.

The comparisons of the relieved displacement results are shown from Figures 4.5 to 4.10 in terms of the relieved displacement (u_r, v_α) versus α/π for different Load Cases. α is the angle of a measurement point from the x-axis in the anti clock-wise direction. All relieved displacements are taken at the measurement circles which have dimensionless radii $k=r_m/a$ of 1, 2, and 3, where r_m is the radius of the measurement circle and a is the radius of the through-hole.

Figures 4.5 to 4.7 show relieved displacements in the radial direction (u_r) versus α/π for the measurement circles of radii $k = 1, 2,$ and 3. Figures 4.8 to 4.10 show relieved displacements in the tangential direction (v_α) versus α/π for the dimensionless measurement circles of radii $k = 1,$ 2, and 3. In these figures, the relieved displacements obtained at discrete points from the finite element analyses are shown with markers, and the relieved displacements obtained from the closed-form equations are shown with solid lines.

As seen from the figures, excellent agreement was obtained between the relieved displacement results obtained from the closed-form equations and the finite element analyses. These results confirm that the closed-form relieved displacement equations for the uniform stress state are correct under the assumptions made in the derivation.

4.4. VERIFICATION OF THE CLOSED-FORM RELIEVED DISPLACEMENT EQUATIONS FOR THE LINEAR GRADIENT STRESS STATE

Similar to the verification of the relieved displacement equations for the uniform stress state, the finite element model described in Section 4.2 is used to verify the relieved displacement equations for the linear gradient stress state.

Two different Load Cases are treated as shown in Table 4.3. Load Case 1 applies a uniaxial concentric linear gradient stress. Load Case 2 applies a biaxial concentric linear gradient stress.

The comparison of the relieved displacement results are shown from Figures 4.11 to 4.14 in terms of relieved displacement (u_r, v_α) versus α/π for different Load Cases. All relieved displacements are taken at the measurement circles which have dimensionless radii $k=r_m/a$ of 1, 2, and 3.

Figures 4.11 to 4.12 show relieved displacements in the radial direction (u_r) versus α/π for the measurement circles of radii k = 1, 2, and 3. Figures 4.13 to 4.14 show relieved displacements in the tangential direction (v_α) versus α/π for the measurement circles of radii k = 1, 2, and 3. In these figures, the relieved displacements obtained at discrete points from the finite element analyses are shown with markers, and the relieved displacements obtained from the closed-form equations are shown with solid lines.

As seen from the figures, excellent agreement was obtained between the relieved displacement results obtained from the closed-form equations and the finite element analyses. These results confirm that the closed-form relieved displacement equations for the linear gradient stress state are correct under the assumptions made in the derivation.

4.5. VERIFICATION OF THE CLOSED-FORM UNIFORM IN-SITU STRESS EQUATIONS

In this section, the closed-form uniform in-situ stress equations that were derived in Chapter 3 are verified. The closed-form uniform in-situ stress equations are derived for 8 different test configurations shown in Figure 3.13 (Test Configurations A through H). The in-situ stress equations are a function of measured displacements.

In order to verify the in-situ stress equations, the following steps are done. First, an infinite thin plate under a known in-situ stress state is considered. The relieved displacements at the measurement points are calculated for each of the test configurations. Then these relieved displacements are used to calculate the measured displacements for each of the test configurations. These measured displacements are then substituted in to the in-situ stress equations to calculate in-situ stresses. Finally, these calculated in-situ stresses are then compared with the in-situ stress states, which exist in the plate prior to the through-hole drilling.

The relieved displacements can also be calculated from the finite element model explained in Section 4.2. However, since the closed-form equations for relieved displacements have been proved correct in previous sections, the closed-form relieved displacement equations are used to generate the relieved displacements instead of the finite element analyses.

Three different Load Cases shown in Table 4.4 are used to calculate relieved displacements for the test configurations shown in Figure 3.13. Load Case 1 applies a uniaxial normal stress. Load Case 2 applies pure shear stress. Load Case 3 is the most general, and includes both biaxial normal stress and shear stress.

The results of the verification analyses for the closed-form uniform in-situ stress equations are tabulated in Tables 4.5 to 4.12 for each test configuration shown in Figure 3.13. These tables show calculated in-situ stresses for the three different in-situ stress states (Load Cases) used to

81

calculate the relieved displacements. For the uniform stress state, there are two sets of uniform in-situ stress equations for each test configuration. One set of equations calculates cartesian stress components $(\sigma_{xx}, \sigma_{yy}, \tau_{xy})$. The other set calculates principal stresses $(\sigma_{max}, \sigma_{min}, \theta)$ directly. The results for each set of equations for each test configuration are tabulated in the same table. As stated before Load Cases represent the in-situ stresses that exist before drilling the through-hole. Since Load Cases gives Cartesian stress components, it is easy to compare the calculated Cartesian components of in-situ stresses with the Load Cases. To compare the calculated principal in-situ stresses with the Load Cases, we need to calculate the exact principal stresses from the Cartesian stress components given in Load Cases. The exact principal stresses are given for the Load Cases as follows. Load Case 1: $\sigma_{max} = 10$ MPa, $\sigma_{min} = 0$, $\theta = 0$; Load Case 2: $\sigma_{max} = 10$ MPa, $\sigma_{min} = -10$ MPa, $\theta = 45°$; Load Case 3: $\sigma_{max} = 10.96291$ MPa, $\sigma_{min} = -15.96291$ MPa, $\theta = 10.9007$ degrees.

In these tables, the first column shows the Load Case, which indicates which in-situ stress state (Table 4.4) is used to calculate the relieved displacements (and thus measured displacements from the relieved displacements). The second column shows the radii of the measurement circles. The dimensionless radii $(k = r_m/a)$ of the measurement circles considered are k = 1.5, 2, 2.5, and 3. The columns labeled with lower case u with subscripted letters show the relieved displacements in the radial direction. The columns labeled with lower case v with subscripted letters show the relieved displacements in the tangential direction. The subscripted letters indicate the locations of the measurement points shown in the test configurations in Figure 3.13. The columns labeled with upper case U with numbers show measured displacements between two measurement points of the test configurations shown in Figure 3.13.

As seen from the results tabulated in Tables 4.5 to 4.12, the closed-form uniform in-situ stress equations give exact results. However, it is also observed that for Load Case 2, the uniform in-situ stress equation in terms of principal stresses for Test Configuration H cannot calculate principal stresses directly. When $\sigma_x = \sigma_y$ and τ_{xy} is not equal to zero, U2 and U3 became zero and that causes a zero value in denominator of the principal stress formulas. The zero value results in indeterminate results for principal stress equations. However, this problem can be overcome by defining the following additional equations.

When $U2 = U3 = 0$ & $U1 \neq 0$

$$\sigma_{max} = \frac{U1}{4B} \tag{4.1}$$

$$\sigma_{min} = -\frac{U1}{4B} \tag{4.2}$$

$$\theta = \frac{\pi}{4} \tag{4.3}$$

When $U2 = U3 \neq 0$ & $U1 \neq 0$

$$\sigma_{max} = \sigma_{min} = \frac{U1}{4A} \tag{4.4}$$

To evaluate to these additional equations, reconsider Load Case 2 for test configuration H. Since $U2 = U3 = 0$ and $U1 \neq 0$ as shown in Table 4.12, we need to use Equations (4.1), (4.2), and (4.3). Substituting U1 in to Equations (4.1), (4.2), and (4.3) we get

$$\sigma_{max} = -\sigma_{min} = 10 \text{ MPa}$$

$$\theta = 45^{\circ}$$

4.6. VERIFICATION OF THE CLOSED-FORM LINEAR GRADIENT IN-SITU STRESS EQUATIONS

In this section, the closed-form linear gradient in-situ stress equations derived for the 5 test configurations shown in Figure 3.14 in Chapter 3 are verified. Similar to the verification of the closed-form uniform in-situ stress equations, the closed-form relieved displacement equations for the linear gradient stress state are used to calculate relieved displacements. Then these relieved displacements are used to calculate measured displacements required for the test configurations shown in Figure 3.14. By substituting the measured displacements in to the closed-form linear gradient in-situ stress equations, in-situ stress states are calculated.

Three different Load Cases shown in Table 4.13 are used to calculate relieved displacements for the test configurations shown in Figure 3.14. Load Case 1 applies a uniaxial concentric linear gradient stress. Load Case 2 applies a biaxial concentric linear gradient stress. Load Case 3 is the most general stress state, having biaxial stress with linear gradient and pure shear stress.

The in-situ stresses calculated using the closed-form linear gradient in-situ stress equations derived in Chapter 3 are tabulated in Tables 4.14 to 4.18 for each test configuration shown in Figure 3.14. In these tables, the first column shows the Load Cases that are used to calculate the relieved displacements (and thus the measured displacements from the relieved displacements). The second column shows the radii of the measurement circles. The dimensionless radii ($k = r_m/a$) of the measurement circles considered are $k = 1.5, 2, 2.5$, and 3. The columns labeled with lower case u with subscripted letters show the relieved displacements in the radial direction. The columns labeled with lower case v with subscripted letters show the relieved displacements in the tangential direction. The subscripted letters indicate the locations of the measurement points shown in the test configurations in Figure 3.14. The columns labeled with upper case U with numbers show measured displacements between two measurement points as shown in Figure 3.14.

As seen from the results tabulated from Tables 4.14 to 4.18, the in-situ stress equations give exact results. It is concluded that the closed-form linear gradient in-situ stress equations give exact results under the assumptions made in the derivation of the equations.

83
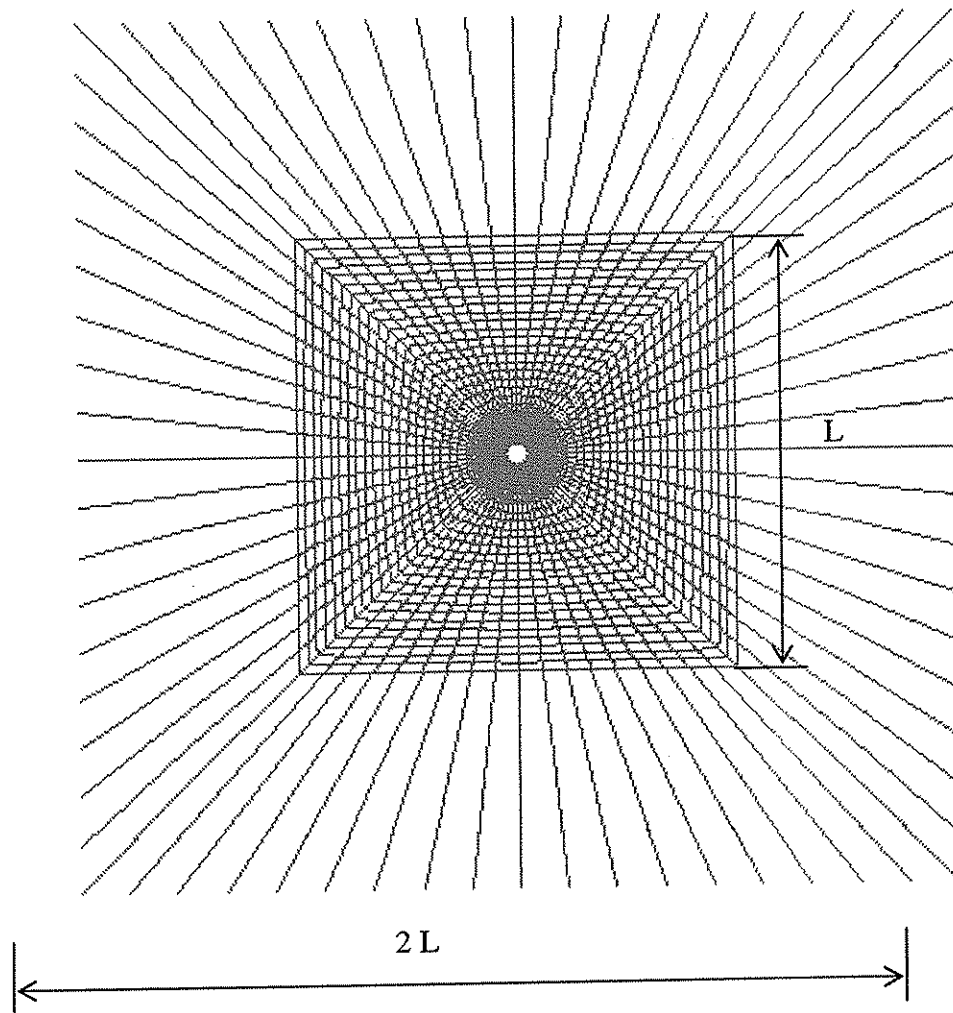
Figure 4.1 Geometry of the finite element model.
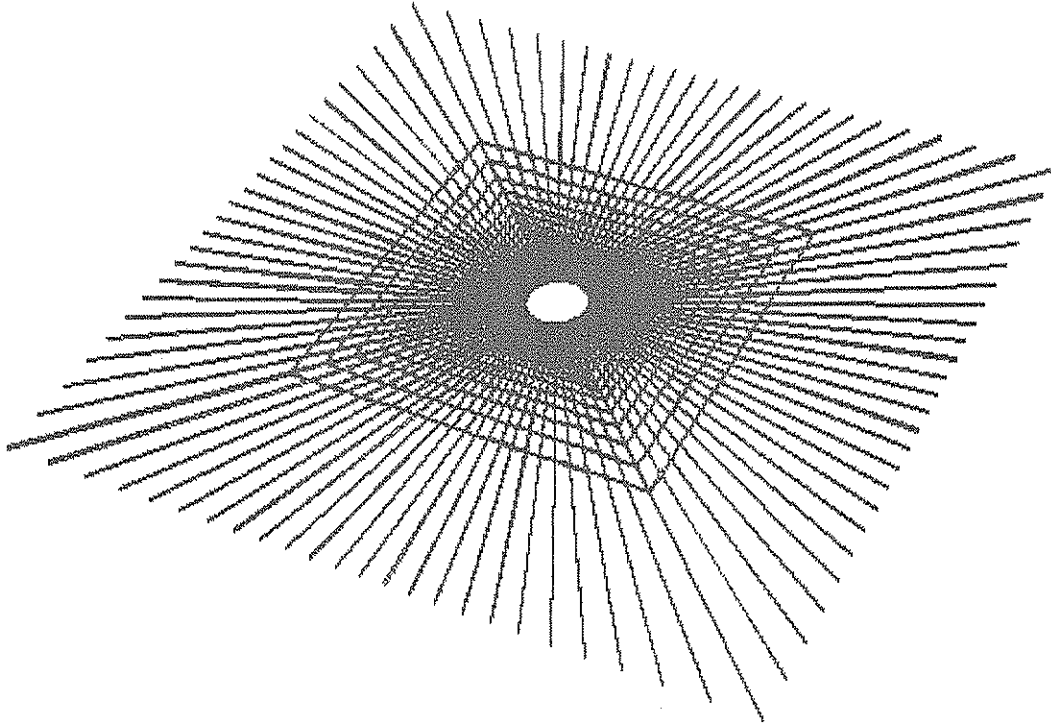
Figure 4.2 Finite element mesh used for the verification of the closed-form relieved displacement equations.
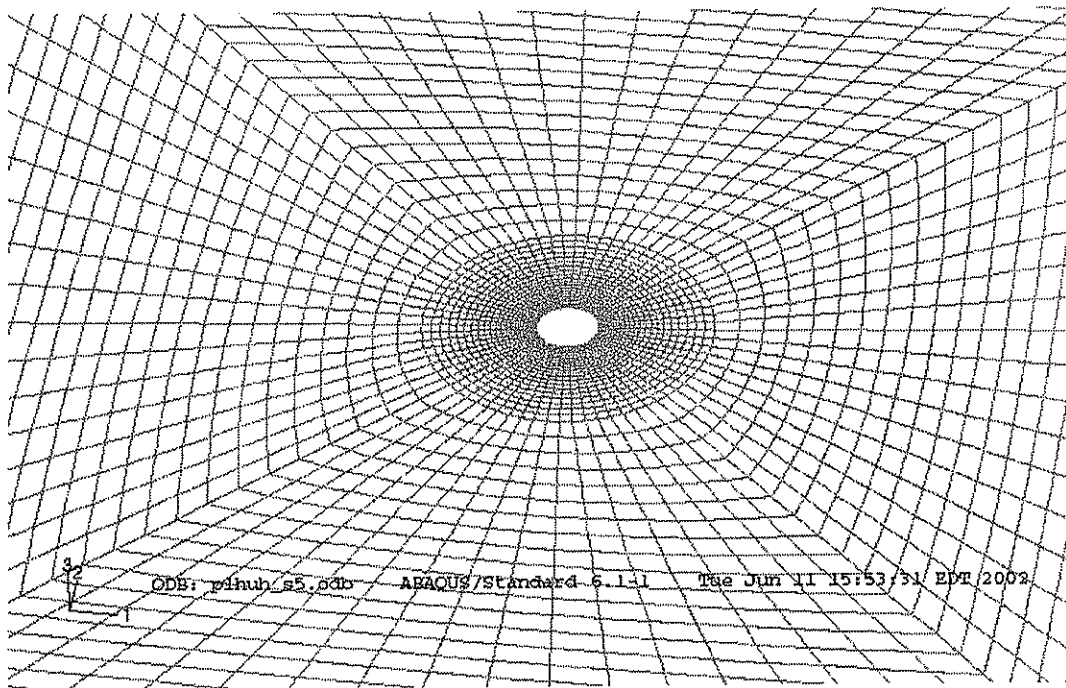
Figure 4.3 A general view of finite element mesh.
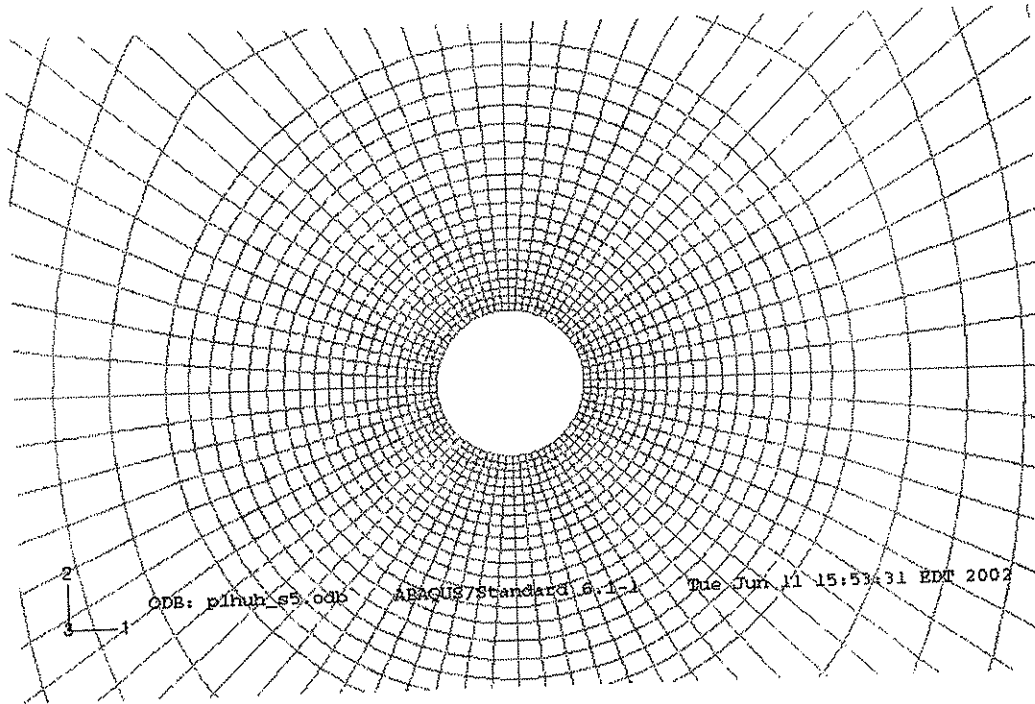
Figure 4.4 A general view of finite element mesh, zoomed in on the hole.
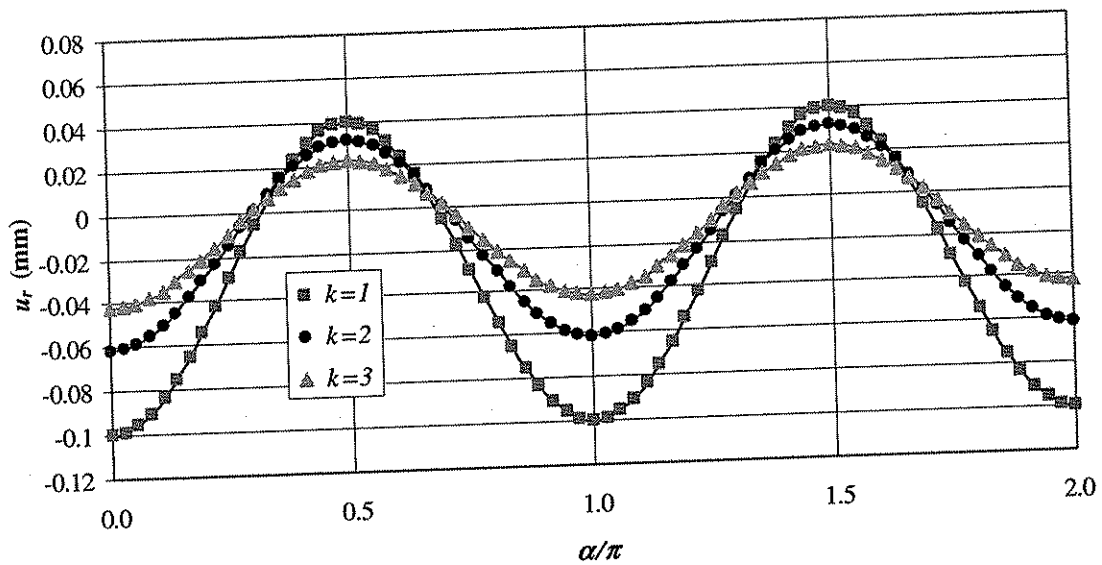
Figure 4.5 Verification of the closed-form relieved displacement equation in the radial direction (u_r) for the uniform stress state for Load Case 1 ($\sigma_{xx}= -20$, $\sigma_{yy}=\tau_{xy}=0$).
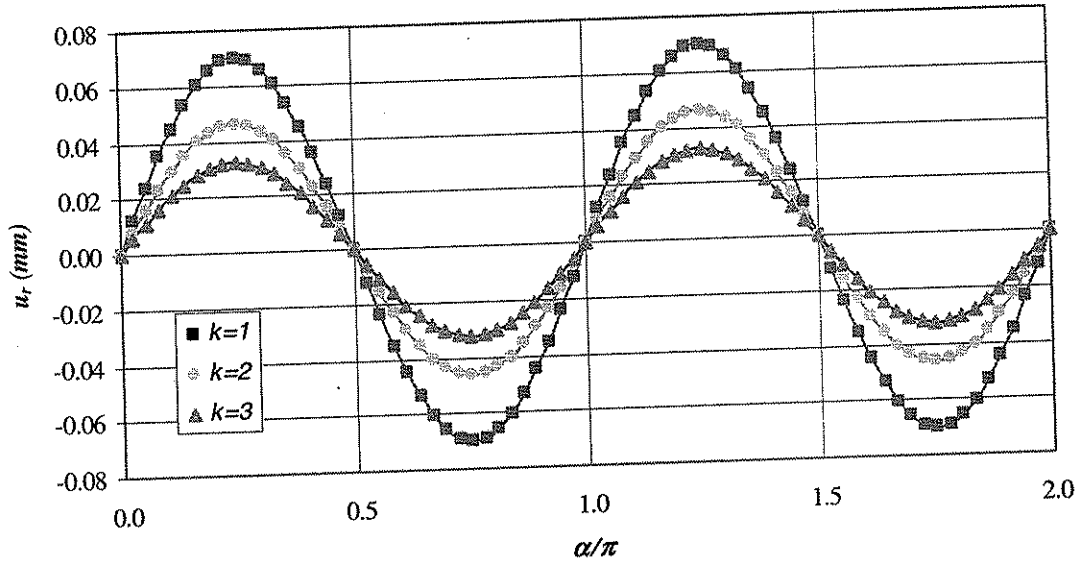
Figure 4.6 Verification of the closed-form relieved displacement equation in the radial direction (u_r) for the uniform stress state for Load Case 2 ($\sigma_{xx}=0$, $\sigma_{yy}=0$, $\tau_{xy}=10$).
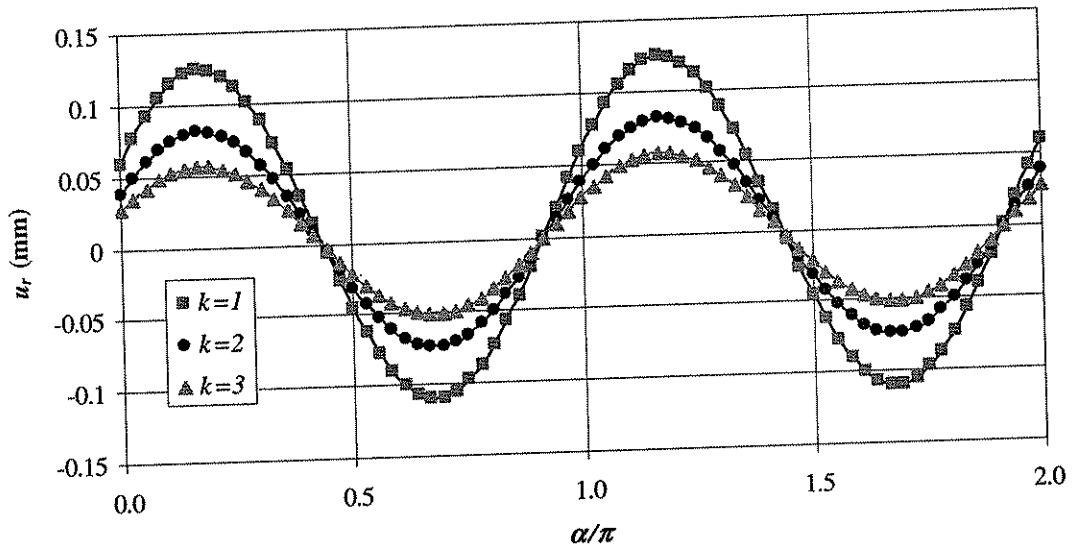
Figure 4.7 Verification of the closed-form relieved displacement equation in the radial direction (u_r) for the uniform stress state for Load Case 3 ($\sigma_{xx}=10$, $\sigma_{yy}=-5$, $\tau_{xy}=15$).
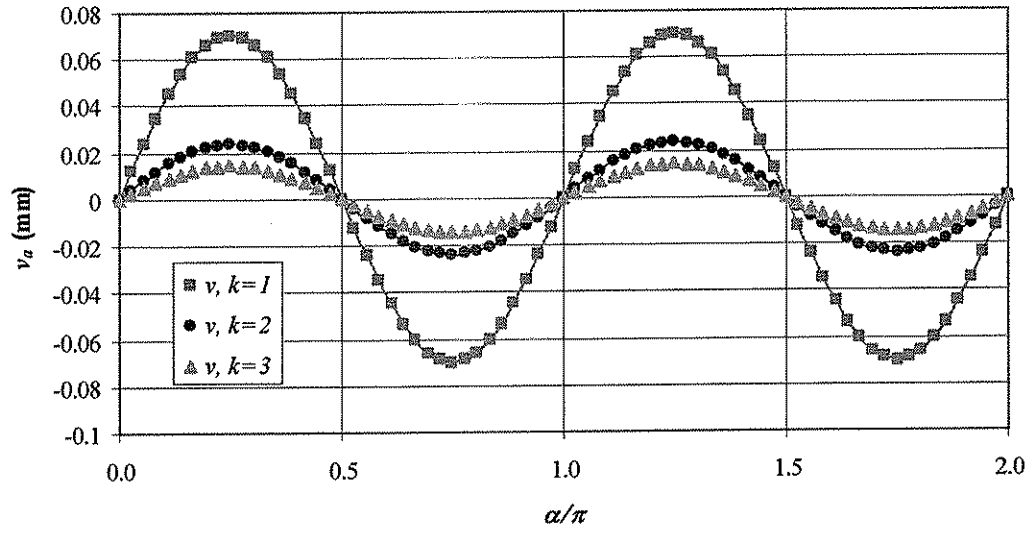
Figure 4.8 Verification of the closed-form relieved displacement equation in the tangential direction (v_α) for the uniform stress state for the Load Case 1 (σ_{xx}=-20, σ_{yy}=0, τ_{xy}=0).
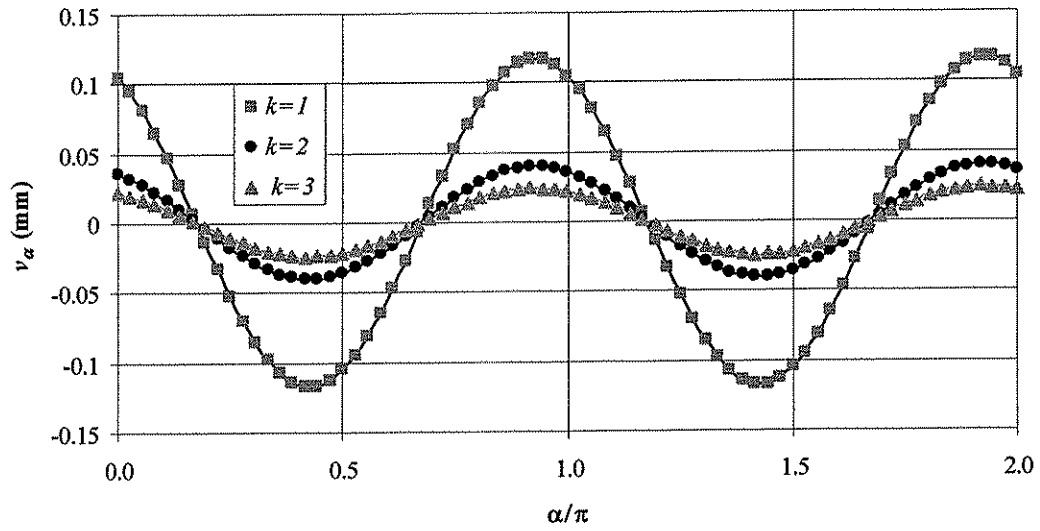
Figure 4.9 Verification of the closed-form relieved displacement equation in the tangential direction (v_α) for the uniform stress state for Load Case 2 (σ_{xx}=0, σ_{yy}=0, τ_{xy}=-10).

Figure 4.10 Verification of the closed-form relieved displacement equation in the tangential direction (v_α) for the uniform stress state for Load Case 3 (σ_{xx}=10, σ_{yy}=-5, τ_{xy}=15).

Figure 4.11 Verification of the closed-form relieved displacement equation in the radial direction (u_r) for the linear gradient stress state for Load Case 1 ($Kx=1$, $Ky=0$).
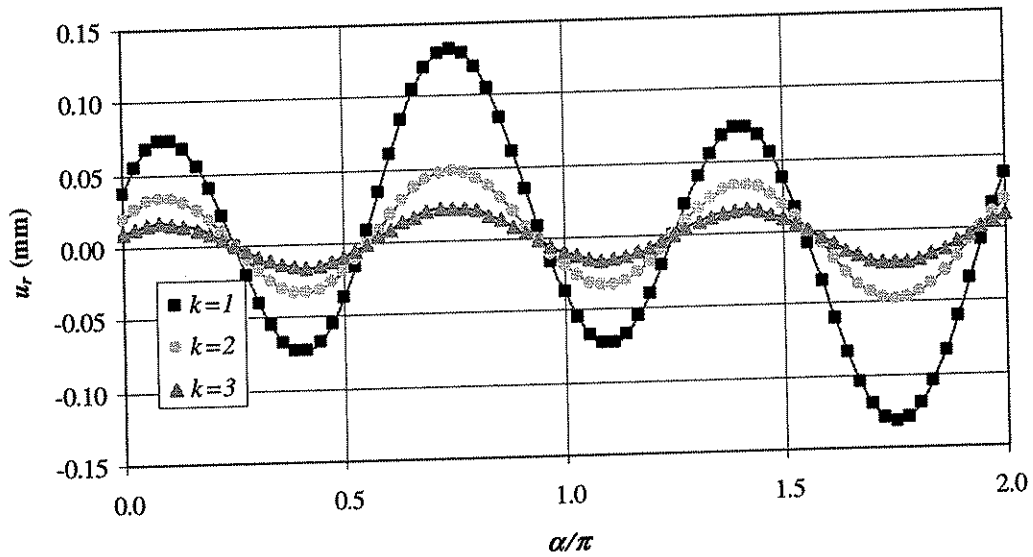
Figure 4.12 Verification of the closed-form relieved displacement equation in the radial direction (u_r) for the linear gradient stress state for Load Case 2 ($Kx=1$, $Ky=1$).
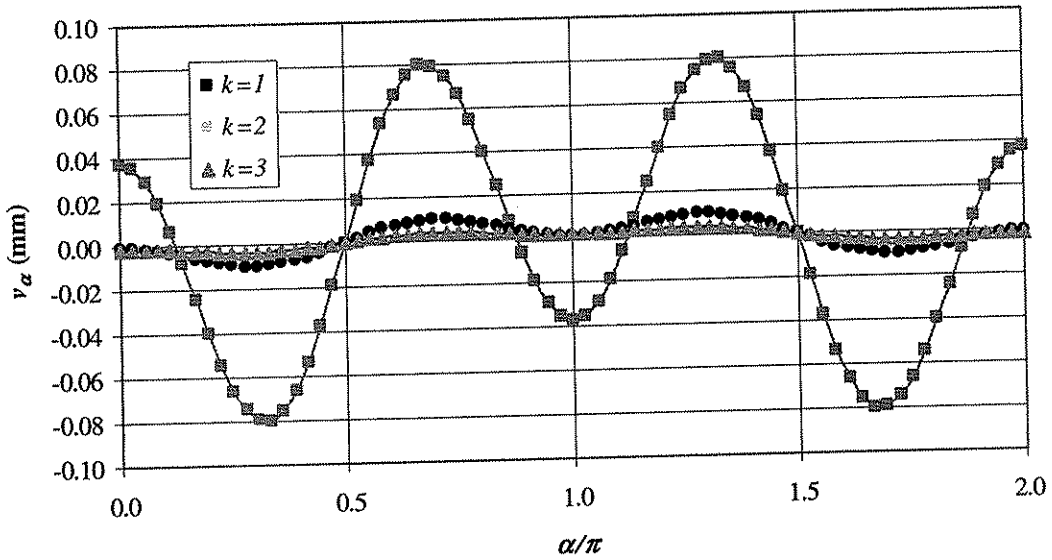
Figure 4.13 Verification of the closed-form relieved displacement equation in the tangential direction (v_α) for the linear gradient stress state for Load Case 1 ($Kx=1$, $Ky=0$).
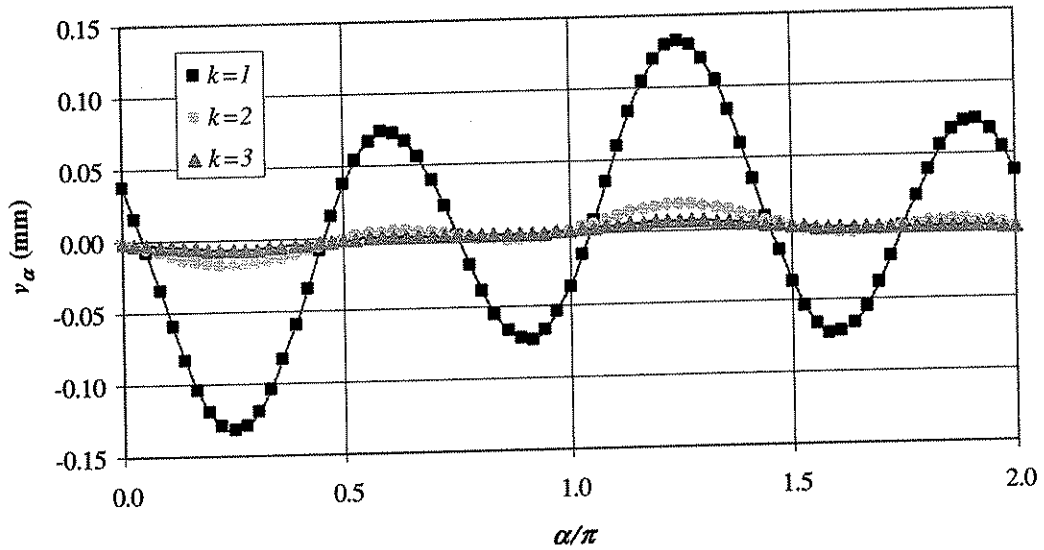
Figure 4.14 Verification of the closed-form relieved displacement equation in the tangential direction (v_α) for the linear gradient stress state for Load Case 2 ($Kx=1$, $Ky=1$).

L	Number of elements	Number of nodes	Total number of variables	u_r [mm]
1000	672	2100	4200	0.0285
2000	672	2100	4200	0.0284
3000	672	2100	4200	0.0284
3000	1312	4100	8200	0.0283
3000	2952	9020	18040	0.0283

Table 4.1 Convergence of the finite element models for verification analyses.

Load Case	In-situ Stresses (MPa)		
	σ_{xx}	σ_{yy}	τ_{xy}
1	-20	0	0
2	0	0	10
3	10	-5	15

Table 4.2 In-situ stress states used to verify the closed-form relieved displacement equations for the uniform stress state.

Load Case	In-situ Stresses (MPa/mm)	
	Kx	Ky
1	1	0
2	1	1

Table 4.3 In-situ stress states used to verify the closed-form relieved displacement equations for the linear gradient stress state.

Load Case	In-situ Stresses (MPa)		
	σ_x	σ_y	τ_{xy}
1	10	0	0
2	0	0	10
3	10	-15	5

Table 4.4 In-situ stress states used to verify the uniform in-situ stress equations.

Test Configuration A

Load Case	$k=r_m/a$	Relieved Displacements (mm)			Measured Displacements (mm)			Calculated In-situ Stresses (MPa)					
		u_a	u_b	u_c	$U1$	$U2$	$U3$	σ_{xx}	σ_{yy}	τ_{xy}	σ_{max}	σ_{min}	θ
1	1.5	0.0389	0.0100	-0.0189	0.0389	0.0100	-0.0189	10.0000	0.0000	0.0000	10.0000	0.0000	0.0000
	2	0.0306	0.0075	-0.0156	0.0306	0.0075	-0.0156	10.0000	0.0000	0.0000	10.0000	0.0000	0.0000
	2.5	0.0250	0.0060	-0.0130	0.0250	0.0060	-0.0130	10.0000	0.0000	0.0000	10.0000	0.0000	0.0000
	3	0.0211	0.0050	-0.0111	0.0211	0.0050	-0.0111	10.0000	0.0000	0.0000	10.0000	0.0000	0.0000
2	1.5	0.0000	0.0578	0.0000	0.0000	0.0578	0.0000	0.0000	0.0000	10.0000	10.0000	-10.0000	45.0000
	2	0.0000	0.0463	0.0000	0.0000	0.0463	0.0000	0.0000	0.0000	10.0000	10.0000	-10.0000	45.0000
	2.5	0.0000	0.0381	0.0000	0.0000	0.0381	0.0000	0.0000	0.0000	10.0000	10.0000	-10.0000	45.0000
	3	0.0000	0.0322	0.0000	0.0000	0.0322	0.0000	0.0000	0.0000	10.0000	10.0000	-10.0000	45.0000
3	1.5	0.0672	0.0239	-0.0772	0.0672	0.0239	-0.0772	10.0000	-15.0000	5.0000	10.9629	-15.9629	10.9007
	2	0.0541	0.0194	-0.0616	0.0541	0.0194	-0.0616	10.0000	-15.0000	5.0000	10.9629	-15.9629	10.9007
	2.5	0.0446	0.0160	-0.0506	0.0446	0.0160	-0.0506	10.0000	-15.0000	5.0000	10.9629	-15.9629	10.9007
	3	0.0378	0.0136	-0.0428	0.0378	0.0136	-0.0428	10.0000	-15.0000	5.0000	10.9629	-15.9629	10.9007

Table 4.5 Verification of uniform in-situ stress equations for Test Configuration A.

94

Test Configuration B

Load Case	$k=r_m/a$	Relieved Displacements (mm)			Measured Displacements (mm)			Calculated In-situ Stresses (MPa)					
		u_a	u_b	u_c	$U1$	$U2$	$U3$	σ_{xx}	σ_{yy}	τ_{xy}	σ_{max}	σ_{min}	θ
1	1.5	0.0389	-0.0044	-0.0044	0.0389	-0.0044	-0.0044	10.0000	0.0000	0.0000	10.0000	0.0000	0.0000
	2	0.0306	-0.0041	-0.0041	0.0306	-0.0041	-0.0041	10.0000	0.0000	0.0000	10.0000	0.0000	0.0000
	2.5	0.0250	-0.0035	-0.0035	0.0250	-0.0035	-0.0035	10.0000	0.0000	0.0000	10.0000	0.0000	0.0000
	3	0.0211	-0.0031	-0.0031	0.0211	-0.0031	-0.0031	10.0000	0.0000	0.0000	10.0000	0.0000	0.0000
2	1.5	0.0000	0.0500	-0.0500	0.0000	0.0500	-0.0500	0.0000	0.0000	10.0000	10.0000	-10.0000	45.0000
	2	0.0000	0.0401	-0.0401	0.0000	0.0401	-0.0401	0.0000	0.0000	10.0000	10.0000	-10.0000	45.0000
	2.5	0.0000	0.0330	-0.0330	0.0000	0.0330	-0.0330	0.0000	0.0000	10.0000	10.0000	-10.0000	45.0000
	3	0.0000	0.0279	-0.0279	0.0000	0.0279	-0.0279	0.0000	0.0000	10.0000	10.0000	-10.0000	45.0000
3	1.5	0.0672	-0.0161	-0.0661	0.0672	-0.0161	-0.0661	10.0000	-15.0000	5.0000	10.9629	-15.9629	10.9007
	2	0.0541	-0.0126	-0.0527	0.0541	-0.0126	-0.0527	10.0000	-15.0000	5.0000	10.9629	-15.9629	10.9007
	2.5	0.0446	-0.0103	-0.0433	0.0446	-0.0103	-0.0433	10.0000	-15.0000	5.0000	10.9629	-15.9629	10.9007
	3	0.0378	-0.0087	-0.0366	0.0378	-0.0087	-0.0366	10.0000	-15.0000	5.0000	10.9629	-15.9629	10.9007

Table 4.6 Verification of uniform in-situ stress equations for Test Configuration B.

Test Configuration C

Load Case	$k=r_m/a$	Relieved Displacements (mm)						Measured Displacements (mm)		
		u_a	u_b	u_c	u_d	u_e	u_f	U1	U2	U3
1	1.5	0.0389	0.0100	-0.0189	0.0389	0.0100	-0.0189	0.0778	0.0200	-0.0378
	2	0.0306	0.0075	-0.0156	0.0306	0.0075	-0.0156	0.0613	0.0150	-0.0313
	2.5	0.0250	0.0060	-0.0130	0.0250	0.0060	-0.0130	0.0501	0.0120	-0.0261
	3	0.0211	0.0050	-0.0111	0.0211	0.0050	-0.0111	0.0422	0.0100	-0.0222
2	1.5	0.0000	0.0578	0.0000	0.0000	0.0578	0.0000	0.0000	0.1156	0.0000
	2	0.0000	0.0463	0.0000	0.0000	0.0463	0.0000	0.0000	0.0925	0.0000
	2.5	0.0000	0.0381	0.0000	0.0000	0.0381	0.0000	0.0000	0.0762	0.0000
	3	0.0000	0.0322	0.0000	0.0000	0.0322	0.0000	0.0000	0.0644	0.0000
3	1.5	0.0672	0.0239	-0.0772	0.0672	0.0239	-0.0772	0.1344	0.0478	-0.1544
	2	0.0541	0.0194	-0.0616	0.0541	0.0194	-0.0616	0.1081	0.0388	-0.1231
	2.5	0.0446	0.0160	-0.0506	0.0446	0.0160	-0.0506	0.0892	0.0321	-0.1012
	3	0.0378	0.0136	-0.0428	0.0378	0.0136	-0.0428	0.0756	0.0272	-0.0856

Load Case	$k=r_m/a$	Calculated In-situ Stresses (MPa)					
		σ_{xx}	σ_{yy}	τ_{xy}	σ_{max}	σ_{min}	θ
1	1.5	10.0000	0.0000	0.0000	10.0000	0.0000	0.0000
	2	10.0000	0.0000	0.0000	10.0000	0.0000	0.0000
	2.5	10.0000	0.0000	0.0000	10.0000	0.0000	0.0000
	3	10.0000	0.0000	0.0000	10.0000	0.0000	0.0000
2	1.5	0.0000	0.0000	10.0000	10.0000	-10.0000	45.0000
	2	0.0000	0.0000	10.0000	10.0000	-10.0000	45.0000
	2.5	0.0000	0.0000	10.0000	10.0000	-10.0000	45.0000
	3	0.0000	0.0000	10.0000	10.0000	-10.0000	45.0000
3	1.5	10.0000	-15.0000	5.0000	10.9629	-15.9629	10.9007
	2	10.0000	-15.0000	5.0000	10.9629	-15.9629	10.9007
	2.5	10.0000	-15.0000	5.0000	10.9629	-15.9629	10.9007
	3	10.0000	-15.0000	5.0000	10.9629	-15.9629	10.9007

Table 4.7 Verification of uniform in-situ stress equations for Test Configuration C.

Test Configuration D

Load Case	$k=r_m/a$	Relieved Displacements (mm)						Measured Displacements (mm)		
		u_a	u_b	u_c	u_d	u_e	u_f	$U1$	$U2$	$U3$
1	1.5	0.0389	-0.0044	-0.0044	0.0389	-0.0044	-0.0044	0.0778	-0.0089	-0.0089
	2	0.0306	-0.0041	-0.0041	0.0306	-0.0041	-0.0041	0.0613	-0.0081	-0.0081
	2.5	0.0250	-0.0035	-0.0035	0.0250	-0.0035	-0.0035	0.0501	-0.0070	-0.0070
	3	0.0211	-0.0031	-0.0031	0.0211	-0.0031	-0.0031	0.0422	-0.0061	-0.0061
2	1.5	0.0000	0.0500	-0.0500	0.0000	0.0500	-0.0500	0.0000	0.1001	-0.1001
	2	0.0000	0.0401	-0.0401	0.0000	0.0401	-0.0401	0.0000	0.0801	-0.0801
	2.5	0.0000	0.0330	-0.0330	0.0000	0.0330	-0.0330	0.0000	0.0660	-0.0660
	3	0.0000	0.0279	-0.0279	0.0000	0.0279	-0.0279	0.0000	0.0558	-0.0558
3	1.5	0.0672	-0.0161	-0.0661	0.0672	-0.0161	-0.0661	0.1344	-0.0322	-0.1323
	2	0.0541	-0.0126	-0.0527	0.0541	-0.0126	-0.0527	0.1081	-0.0253	-0.1054
	2.5	0.0446	-0.0103	-0.0433	0.0446	-0.0103	-0.0433	0.0892	-0.0206	-0.0866
	3	0.0378	-0.0087	-0.0366	0.0378	-0.0087	-0.0366	0.0756	-0.0174	-0.0732

Load Case	$k=r_m/a$	Calculated In-situ Stresses (MPa)					
		σ_{xx}	σ_{yy}	τ_{xy}	σ_{max}	σ_{min}	θ
1	1.5	10.0000	0.0000	0.0000	10.0000	0.0000	0.0000
	2	10.0000	0.0000	0.0000	10.0000	0.0000	0.0000
	2.5	10.0000	0.0000	0.0000	10.0000	0.0000	0.0000
	3	10.0000	0.0000	0.0000	10.0000	0.0000	0.0000
2	1.5	0.0000	0.0000	10.0000	10.0000	-10.0000	45.0000
	2	0.0000	0.0000	10.0000	10.0000	-10.0000	45.0000
	2.5	0.0000	0.0000	10.0000	10.0000	-10.0000	45.0000
	3	0.0000	0.0000	10.0000	10.0000	-10.0000	45.0000
3	1.5	10.0000	-15.0000	5.0000	10.9629	-15.9629	10.9007
	2	10.0000	-15.0000	5.0000	10.9629	-15.9629	10.9007
	2.5	10.0000	-15.0000	5.0000	10.9629	-15.9629	10.9007
	3	10.0000	-15.0000	5.0000	10.9629	-15.9629	10.9007

Table 4.8 Verification of uniform in-situ stress equations for Test Configuration D.

Load Case	$k=r_m/a$	Relieved Displacement (mm)						Measured Displacements (mm)		
		u_a	u_b	u_c	u_d	u_e	u_f	$U1$	$U2$	$U3$
1	1.5	0.0389	-0.0044	-0.0189	0.0389	-0.0044	-0.0189	0.0778	-0.0089	-0.0378
	2	0.0306	-0.0041	-0.0156	0.0306	-0.0041	-0.0156	0.0613	-0.0081	-0.0313
	2.5	0.0250	-0.0035	-0.0130	0.0250	-0.0035	-0.0130	0.0501	-0.0070	-0.0261
	3	0.0211	-0.0031	-0.0111	0.0211	0.0279	-0.0111	0.0422	0.0248	-0.0222
2	1.5	0.0000	0.0500	0.0000	0.0000	0.0500	0.0000	0.0000	0.1001	0.0000
	2	0.0000	0.0401	0.0000	0.0000	0.0401	0.0000	0.0000	0.0801	0.0000
	2.5	0.0000	0.0330	0.0000	0.0000	0.0330	0.0000	0.0000	0.0660	0.0000
	3	0.0000	0.0279	0.0000	0.0000	0.0279	0.0000	0.0000	0.0558	0.0000
3	1.5	0.0672	-0.0161	-0.0772	0.0672	-0.0161	-0.0772	0.1344	-0.0322	-0.1544
	2	0.0541	-0.0126	-0.0616	0.0541	-0.0126	-0.0616	0.1081	-0.0253	-0.1231
	2.5	0.0446	-0.0103	-0.0506	0.0446	-0.0103	-0.0506	0.0892	-0.0206	-0.1012
	3	0.0378	-0.0087	-0.0428	0.0378	-0.0087	-0.0428	0.0756	-0.0174	-0.0856

Load Case	$k=r_m/a$	Calculated In-situ Stresses (MPa)					
		σ_{xx}	σ_{yy}	τ_{xy}	σ_{max}	σ_{min}	θ
1	1.5	10.0000	0.0000	0.0000	10.0000	0.0000	0.0000
	2	10.0000	0.0000	0.0000	10.0000	0.0000	0.0000
	2.5	10.0000	0.0000	0.0000	10.0000	0.0000	0.0000
	3	10.0000	0.0000	5.5475	10.0000	0.0000	0.0000
2	1.5	0.0000	0.0000	10.0000	10.0000	-10.0000	45.0000
	2	0.0000	0.0000	10.0000	10.0000	-10.0000	45.0000
	2.5	0.0000	0.0000	10.0000	10.0000	-10.0000	45.0000
	3	0.0000	0.0000	10.0000	10.0000	-10.0000	45.0000
3	1.5	10.0000	-15.0000	5.0000	10.9629	-15.9629	10.9007
	2	10.0000	-15.0000	5.0000	10.9629	-15.9629	10.9007
	2.5	10.0000	-15.0000	5.0000	10.9629	-15.9629	10.9007
	3	10.0000	-15.0000	5.0000	10.9629	-15.9629	10.9007

Table 4.9 Verification of uniform in-situ stress equations for Test Configuration E.

Test Configuration F

Load Case	$k = r_m/a$	Relieved Displacements (mm)						Measured Displacements (mm)		
		u_a	u_b	u_c	u_d	u_e	u_f	$U1$	$U2$	$U3$
1	1.5	0.0244	-0.0189	0.0244	0.0154	0.0000	-0.0154	-0.0029	-0.0029	0.0577
	2	0.0191	-0.0156	0.0191	0.0103	0.0000	-0.0103	-0.0022	-0.0022	0.0433
	2.5	0.0155	-0.0130	0.0155	0.0078	0.0000	-0.0078	-0.0017	-0.0017	0.0346
	3	0.0131	-0.0111	0.0131	0.0063	0.0000	-0.0063	-0.0014	-0.0014	0.0289
2	1.5	-0.0500	0.0000	0.0500	0.0178	-0.0356	0.0178	-0.0700	0.0700	0.0000
	2	-0.0401	0.0000	0.0401	0.0119	-0.0238	0.0119	-0.0525	0.0525	0.0000
	2.5	-0.0330	0.0000	0.0330	0.0090	-0.0179	0.0090	-0.0420	0.0420	0.0000
	3	-0.0279	0.0000	0.0279	0.0072	-0.0144	0.0072	-0.0350	0.0350	0.0000
3	1.5	0.0061	-0.0772	0.0561	0.0474	-0.0178	-0.0296	-0.0942	-0.0242	0.0924
	2	0.0051	-0.0616	0.0452	0.0316	-0.0119	-0.0198	-0.0706	-0.0181	0.0693
	2.5	0.0043	-0.0506	0.0373	0.0239	-0.0090	-0.0149	-0.0565	-0.0145	0.0554
	3	0.0037	-0.0428	0.0316	0.0192	-0.0072	-0.0120	-0.0471	-0.0121	0.0462

Load Case	$k = r_m/a$	Calculated In-situ Stresses (MPa)					
		σ_{xx}	σ_{yy}	τ_{xy}	σ_{max}	σ_{min}	θ
1	1.5	10.0000	0.0000	0.0000	10.0000	0.0000	0.0000
	2	10.0000	0.0000	0.0000	10.0000	0.0000	0.0000
	2.5	10.0000	0.0000	0.0000	10.0000	0.0000	0.0000
	3	10.0000	0.0000	0.0000	10.0000	0.0000	0.0000
2	1.5	0.0000	0.0000	10.0000	10.0000	-10.0000	45.0000
	2	0.0000	0.0000	10.0000	10.0000	-10.0000	45.0000
	2.5	0.0000	0.0000	10.0000	10.0000	-10.0000	45.0000
	3	0.0000	0.0000	10.0000	10.0000	-10.0000	45.0000
3	1.5	10.0000	-15.0000	5.0000	10.9629	-15.9629	10.9007
	2	10.0000	-15.0000	5.0000	10.9629	-15.9629	10.9007
	2.5	10.0000	-15.0000	5.0000	10.9629	-15.9629	10.9007
	3	10.0000	-15.0000	5.0000	10.9629	-15.9629	10.9007

Table 4.10 Verification of uniform in-situ stress equations for Test Configuration F.

Test Configuration G

Load Case	$k=r_m/a$	Relieved Displacements (mm)						Measured Displacements (mm)		
		u_a	u_b	u_c	u_d	u_e	u_f	$U1$	$U2$	$U3$
1	1.5	0.0389	-0.0189	0.0389	-0.0189	0.0000	0.0000	0.0778	0.0141	-0.0378
	2	0.0306	-0.0156	0.0306	-0.0156	0.0000	0.0000	0.0613	0.0106	-0.0313
	2.5	0.0250	-0.0130	0.0250	-0.0130	0.0000	0.0000	0.0501	0.0085	-0.0261
	3	0.0211	-0.0111	0.0211	-0.0111	0.0000	0.0000	0.0422	0.0071	-0.0222
2	1.5	0.0000	0.0000	0.0000	0.0000	0.0356	-0.0356	0.0000	-0.0503	0.0000
	2	0.0000	0.0000	0.0000	0.0000	0.0238	-0.0238	0.0000	-0.0336	0.0000
	2.5	0.0000	0.0000	0.0000	0.0000	0.0179	-0.0179	0.0000	-0.0253	0.0000
	3	0.0000	0.0000	0.0000	0.0000	0.0144	-0.0144	0.0000	-0.0204	0.0000
3	1.5	0.0672	-0.0772	0.0672	-0.0772	0.0178	-0.0178	0.1344	-0.0322	-0.1544
	2	0.0541	-0.0616	0.0541	-0.0616	0.0119	-0.0119	0.1081	-0.0221	-0.1231
	2.5	0.0446	-0.0506	0.0446	-0.0506	0.0090	-0.0090	0.0892	-0.0169	-0.1012
	3	0.0378	-0.0428	0.0378	-0.0428	0.0072	-0.0072	0.0756	-0.0137	-0.0856

Load Case	$k=r_m/a$	Calculated In-situ Stresses (MPa)					
		σ_{xx}	σ_{yy}	τ_{xy}	σ_{max}	σ_{min}	θ
1	1.5	10.0000	0.0000	0.0000	10.0000	0.0000	0.0000
	2	10.0000	0.0000	0.0000	10.0000	0.0000	0.0000
	2.5	10.0000	0.0000	0.0000	10.0000	0.0000	0.0000
	3	10.0000	0.0000	0.0000	10.0000	0.0000	0.0000
2	1.5	0.0000	0.0000	10.0000	10.0000	-10.0000	45.0000
	2	0.0000	0.0000	10.0000	10.0000	-10.0000	45.0000
	2.5	0.0000	0.0000	10.0000	10.0000	-10.0000	45.0000
	3	0.0000	0.0000	10.0000	10.0000	-10.0000	45.0000
3	1.5	10.0000	-15.0000	5.0000	10.9629	-15.9629	10.9007
	2	10.0000	-15.0000	5.0000	10.9629	-15.9629	10.9007
	2.5	10.0000	-15.0000	5.0000	10.9629	-15.9629	10.9007
	3	10.0000	-15.0000	5.0000	10.9629	-15.9629	10.9007

Table 4.11 Verification of uniform in-situ stress equations for Test Configuration G.

Test Configuration H

Load Case	$k=r_m/a$	Relieved Displacements (mm)						Measured Displacements (mm)		
		u_a	u_b	u_c	v_a	v_b	v_c	$U1$	$U2$	$U3$
1	1.5	0.0100	0.0100	0.0100	0.0178	-0.0178	0.0178	0.0200	-0.0110	0.0393
	2	0.0075	0.0075	0.0075	0.0119	-0.0119	0.0119	0.0150	-0.0062	0.0274
	2.5	0.0060	0.0060	0.0060	0.0090	-0.0090	0.0090	0.0120	-0.0042	0.0212
	3	0.0050	0.0050	0.0050	0.0072	-0.0072	0.0072	0.0100	-0.0031	0.0173
2	1.5	-0.0578	0.0578	-0.0578	0.0000	0.0000	0.0000	-0.1156	0.0000	0.0000
	2	-0.0463	0.0463	-0.0463	0.0000	0.0000	0.0000	-0.0925	0.0000	0.0000
	2.5	-0.0381	0.0381	-0.0381	0.0000	0.0000	0.0000	-0.0762	0.0000	0.0000
	3	-0.0322	0.0322	-0.0322	0.0000	0.0000	0.0000	-0.0644	0.0000	0.0000
3	1.5	-0.0339	0.0239	-0.0339	0.0444	-0.0444	0.0444	-0.0678	-0.0699	0.0558
	2	-0.0269	0.0194	-0.0269	0.0297	-0.0297	0.0297	-0.0538	-0.0473	0.0367
	2.5	-0.0220	0.0160	-0.0220	0.0224	-0.0224	0.0224	-0.0441	-0.0359	0.0274
	3	-0.0186	0.0136	-0.0186	0.0181	-0.0181	0.0181	-0.0372	-0.0291	0.0220

Load Case	$k=r_m/a$	Calculated In-situ Stresses (MPa)					
		σ_{xx}	σ_{yy}	τ_{xy}	σ_{max}	σ_{min}	θ
1	1.5	10.0000	0.0000	0.0000	10.0000	0.0000	0.0000
	2	10.0000	0.0000	0.0000	10.0000	0.0000	0.0000
	2.5	10.0000	0.0000	0.0000	10.0000	0.0000	0.0000
	3	10.0000	0.0000	0.0000	10.0000	0.0000	0.0000
2	1.5	0.0000	0.0000	10.0000	Ξ	Ξ	45.0000
	2	0.0000	0.0000	10.0000	Ξ	Ξ	45.0000
	2.5	0.0000	0.0000	10.0000	Ξ	Ξ	45.0000
	3	0.0000	0.0000	10.0000	Ξ	Ξ	45.0000
3	1.5	10.0000	-15.0000	5.0000	10.9629	-15.9629	10.9007
	2	10.0000	-15.0000	5.0000	10.9629	-15.9629	10.9007
	2.5	10.0000	-15.0000	5.0000	10.9629	-15.9629	10.9007
	3	10.0000	-15.0000	5.0000	10.9629	-15.9629	10.9007

Ξ = Indeterminate

Table 4.12 Verification of uniform in-situ stress equations for Test Configuration H.

101

Load Case	In-situ Stresses				
	σ_{xx} (MPa)	σ_{yy} (MPa)	τ_{xy} (MPa)	Kx (MPa/mm)	Ky (MPa/mm)
1	0	0	0	0.2	0
2	0	0	0	0.2	0.1
3	-10	10	15	-0.1	0.2

Table 4.13 In-situ stress states used to verify the linear gradient in-situ stress equations.

Table — Test Configuration L — Relieved Displacements (mm)

Load Case	$k=r_m/a$	u_a	u_b	u_c	u_d	u_e	u_f	v_a	v_b	v_c	v_d	v_e	v_f
1	1.5	0.00611	0.00000	-0.00611	0.00000	0.00786	0.00786	0.00000	0.00056	0.00000	-0.00056	-0.00393	0.00393
	2	0.00398	0.00000	-0.00398	0.00000	0.00481	0.00481	0.00000	-0.00023	0.00000	0.00023	-0.00182	0.00182
	2.5	0.00271	0.00000	-0.00271	0.00000	0.00319	0.00319	0.00000	-0.00031	0.00000	0.00031	-0.00105	0.00105
	3	0.00194	0.00000	-0.00194	0.00000	0.00226	0.00226	0.00000	-0.00028	0.00000	0.00028	-0.00069	0.00069
2	1.5	0.00611	0.00306	-0.00611	-0.00306	0.00393	0.01179	-0.00028	0.00056	0.00028	-0.00056	-0.00589	0.00196
	2	0.00398	0.00199	-0.00398	-0.00199	0.00240	0.00721	0.00012	-0.00023	-0.00012	0.00023	-0.00273	0.00091
	2.5	0.00271	0.00136	-0.00271	-0.00136	0.00160	0.00479	0.00016	-0.00031	-0.00016	0.00031	-0.00158	0.00053
	3	0.00194	0.00097	-0.00194	-0.00097	0.00113	0.00339	0.00014	-0.00028	-0.00014	0.00028	-0.00103	0.00034
3	1.5	0.05472	-0.05167	0.06083	-0.06389	0.07488	-0.08274	-0.05389	0.05306	-0.05278	0.05361	0.03359	-0.04145
	2	0.04426	-0.04227	0.04824	-0.05023	0.06217	-0.06697	-0.03539	0.03574	-0.03586	0.03551	0.02284	-0.02648
	2.5	0.03672	-0.03537	0.03944	-0.04079	0.05233	-0.05552	-0.02657	0.02704	-0.02719	0.02672	0.01739	-0.01950
	3	0.03125	-0.03028	0.03319	-0.03417	0.04495	-0.04720	-0.02139	0.02181	-0.02194	0.02153	0.01410	-0.01548

Measured Displacements (mm) and Calculated in-situ Stresses (MPa)

Load Case	$k=r_m/a$	U1	U2	U3	U4	U5	σ_{xx}	σ_{yy}	τ_{xy}	Kx	Ky
1	1.5	0.00471	-0.0047	-0.0047	0.00471	0.01667	0.00000	0.00000	0.00000	0.20000	0.00000
	2	0.00265	-0.0027	-0.0027	0.00265	0.00938	0.00000	0.00000	0.00000	0.20000	0.00000
	2.5	0.00170	-0.0017	-0.0017	0.00170	0.00600	0.00000	0.00000	0.00000	0.20000	0.00000
	3	0.00118	-0.0012	-0.0012	0.00118	0.00417	0.00000	0.00000	0.00000	0.20000	0.00000
2	1.5	0.00707	-0.0024	-0.0071	0.00236	0.01667	0.00000	0.00000	0.00000	0.20000	0.10000
	2	0.00398	-0.0013	-0.0040	0.00133	0.00938	0.00000	0.00000	0.00000	0.20000	0.10000
	2.5	0.00255	-0.0008	-0.0025	0.00085	0.00600	0.00000	0.00000	0.00000	0.20000	0.10000
	3	0.00177	-0.0006	-0.0018	0.00059	0.00417	0.00000	0.00000	0.00000	0.20000	0.10000
3	1.5	0.07778	-0.0684	0.07307	-0.0825	-0.0586	-10.000	10.0000	15.0000	-0.1000	0.20000
	2	0.05171	-0.0464	0.04906	-0.0544	-0.0383	-10.000	10.0000	15.0000	-0.1000	0.20000
	2.5	0.03886	-0.0355	0.03717	-0.0406	-0.0283	-10.000	10.0000	15.0000	-0.1000	0.20000
	3	0.03123	-0.0289	0.03005	-0.0324	-0.0225	-10.000	10.0000	15.0000	-0.1000	0.20000

Table 4.14 Verification of linear gradient in-situ stress equations for Test Configuration L.

103

Test Configuration M

Relieved Displacements (mm)

Load Case	$k=r_m/a$	u_a	u_b	u_c	u_d	u_e	u_f	u_g	v_a	v_b	v_c	v_d	v_e
1	1.5	-0.0079	0.0079	0.0000	-0.0061	0.0000	0.0079	-0.0079	-0.0039	-0.0039	0.0006	0.0000	-0.0006
	2	-0.0048	0.0048	0.0000	-0.0040	0.0000	0.0048	-0.0048	-0.0018	-0.0018	-0.0002	0.0000	0.0002
	2.5	-0.0032	0.0032	0.0000	-0.0027	0.0000	0.0032	-0.0032	-0.0011	-0.0011	-0.0003	0.0000	0.0003
	3	-0.0023	0.0023	0.0000	-0.0019	0.0000	0.0023	-0.0023	-0.0007	-0.0007	-0.0003	0.0000	0.0003
2	1.5	-0.0118	0.0039	0.0031	-0.0061	-0.0031	0.0118	-0.0039	-0.0020	-0.0059	0.0006	0.0003	-0.0006
	2	-0.0072	0.0024	0.0020	-0.0040	-0.0020	0.0072	-0.0024	-0.0009	-0.0027	-0.0002	-0.0001	0.0002
	2.5	-0.0048	0.0016	0.0014	-0.0027	-0.0014	0.0048	-0.0016	-0.0005	-0.0016	-0.0003	-0.0002	0.0003
	3	-0.0034	0.0011	0.0010	-0.0019	-0.0010	0.0034	-0.0011	-0.0003	-0.0010	-0.0003	-0.0001	0.0003
3	1.5	-0.0906	0.0749	-0.0517	0.0608	-0.0639	-0.0827	0.0985	-0.0297	0.0336	0.0531	-0.0528	0.0536
	2	-0.0718	0.0622	-0.0423	0.0482	-0.0502	-0.0670	0.0766	-0.0210	0.0228	0.0357	-0.0359	0.0355
	2.5	-0.0587	0.0523	-0.0354	0.0394	-0.0408	-0.0555	0.0619	-0.0163	0.0174	0.0270	-0.0272	0.0267
	3	-0.0495	0.0449	-0.0303	0.0332	-0.0342	-0.0472	0.0517	-0.0134	0.0141	0.0218	-0.0219	0.0215

Load Case	$k=r_m/a$	v_f	v_g	Measured Displacements (mm)					Calculated In-situ Stresses (Mpa)				
				$U1$	$U2$	$U3$	$U4$	$U5$	σ_{xx}	σ_{w}	τ_{xy}	Kx	Ky
1	1.5	0.0039	0.0039	0.0000	-0.0047	-0.0047	0.0000	-0.0167	0.0000	0.0000	0.0000	0.2000	0.0000
	2	0.0018	0.0018	0.0000	-0.0027	-0.0027	0.0000	-0.0094	0.0000	0.0000	0.0000	0.2000	0.0000
	2.5	0.0011	0.0011	0.0000	-0.0017	-0.0017	0.0000	-0.0060	0.0000	0.0000	0.0000	0.2000	0.0000
	3	0.0007	0.0007	0.0000	-0.0012	-0.0012	0.0000	-0.0042	0.0000	0.0000	0.0000	0.2000	0.0000
2	1.5	0.0020	0.0059	-0.0083	-0.0024	-0.0071	0.0083	-0.0167	0.0000	0.0000	0.0000	0.2000	0.1000
	2	0.0009	0.0027	-0.0047	-0.0013	-0.0040	0.0047	-0.0094	0.0000	0.0000	0.0000	0.2000	0.1000
	2.5	0.0005	0.0016	-0.0030	-0.0008	-0.0025	0.0030	-0.0060	0.0000	0.0000	0.0000	0.2000	0.1000
	3	0.0003	0.0010	-0.0021	-0.0006	-0.0018	0.0021	-0.0042	0.0000	0.0000	0.0000	0.2000	0.1000
3	1.5	-0.0414	0.0375	0.0336	-0.0684	0.0731	0.0669	-0.0419	-10.000	10.0000	15.0000	-0.1000	0.2000
	2	-0.0265	0.0247	0.0242	-0.0464	0.0491	0.0430	-0.0289	-10.000	10.0000	15.0000	-0.1000	0.2000
	2.5	-0.0195	0.0184	0.0193	-0.0355	0.0372	0.0313	-0.0223	-10.000	10.0000	15.0000	-0.1000	0.2000
	3	-0.0155	0.0148	0.0163	-0.0289	0.0301	0.0246	-0.0183	-10.000	10.0000	15.0000	-0.1000	0.2000

Table 4.15 Verification of linear gradient in-situ stress equations for Test Configuration M.

Test Configuration P

Load Case	$k=r_m/a$	Relieved Displacements (mm)							
		u_a	u_b	u_c	u_d	v_a	v_b	v_c	v_d
1	1.5	0.0061	0.0000	-0.0061	0.0000	0.0000	0.0006	0.0000	-0.0006
	2	0.0040	0.0000	-0.0040	0.0000	0.0000	-0.0002	0.0000	0.0002
	2.5	0.0027	0.0000	-0.0027	0.0000	0.0000	-0.0003	0.0000	0.0003
	3	0.0019	0.0000	-0.0019	0.0000	0.0000	-0.0003	0.0000	0.0003
2	1.5	0.0061	0.0031	-0.0061	-0.0031	-0.0003	0.0006	0.0003	-0.0006
	0	0.0040	0.0020	-0.0040	-0.0020	0.0001	-0.0002	-0.0001	0.0002
	0	0.0027	0.0014	-0.0027	-0.0014	0.0002	-0.0003	-0.0002	0.0003
	0	0.0019	0.0010	-0.0019	-0.0010	0.0001	-0.0003	-0.0001	0.0003
3	1.5	0.0547	-0.0517	0.0608	-0.0639	-0.0539	0.0531	-0.0528	0.0536
	2	0.0443	-0.0423	0.0482	-0.0502	-0.0354	0.0357	-0.0359	0.0355
	2.5	0.0367	-0.0354	0.0394	-0.0408	-0.0266	0.0270	-0.0272	0.0267
	3	0.0313	-0.0303	0.0332	-0.0342	-0.0214	0.0218	-0.0219	0.0215

Load Case	Measured Displacements (mm)					Calculated In-situ Stresses (MPa)				
	U1	U2	U3	U4	U5	σ_{xx}	σ_{yy}	τ_{xy}	K_x	K_y
1	0.0047	-0.0047	-0.0047	0.0047	0.0000	0.0000	0.0000	0.0000	0.2000	0.0000
	0.0027	-0.0027	-0.0027	0.0027	0.0000	0.0000	0.0000	0.0000	0.2000	0.0000
	0.0017	-0.0017	-0.0017	0.0017	0.0000	0.0000	0.0000	0.0000	0.2000	0.0000
	0.0012	-0.0012	-0.0012	0.0012	0.0000	0.0000	0.0000	0.0000	0.2000	0.0000
2	0.0071	-0.0024	-0.0071	0.0024	0.0000	0.0000	0.0000	0.0000	0.2000	0.1000
	0.0040	-0.0013	-0.0040	0.0013	0.0000	0.0000	0.0000	0.0000	0.2000	0.1000
	0.0025	-0.0008	-0.0025	0.0008	0.0000	0.0000	0.0000	0.0000	0.2000	0.1000
	0.0018	-0.0006	-0.0018	0.0006	0.0000	0.0000	0.0000	0.0000	0.2000	0.1000
3	0.0778	-0.0684	0.0731	-0.0825	-0.1156	-10.000	10.0000	15.0000	-0.1000	0.2000
	0.0517	-0.0464	0.0491	-0.0544	-0.0925	-10.000	10.0000	15.0000	-0.1000	0.2000
	0.0389	-0.0355	0.0372	-0.0406	-0.0762	-10.000	10.0000	15.0000	-0.1000	0.2000
	0.0312	-0.0289	0.0301	-0.0324	-0.0644	-10.000	10.0000	15.0000	-0.1000	0.2000

Table 4.16 Verification of linear gradient in-situ stress equations for Test Configuration P.

Test Configuration Q

Load Case	$k=r_m/a$	Relieved Displacements (mm)											
		u_a	u_b	u_c	u_d	u_e	u_f	v_a	v_b	v_c	v_d	v_e	v_f
1	1.5	0.0000	0.0000	0.0079	0.0079	-0.0079	-0.0079	-0.0006	0.0006	-0.0039	0.0039	0.0039	-0.0039
	2	0.0000	0.0000	0.0048	0.0048	-0.0048	-0.0048	0.0002	-0.0002	-0.0018	0.0018	0.0018	-0.0018
	2.5	0.0000	0.0000	0.0032	0.0032	-0.0032	-0.0032	0.0003	-0.0003	-0.0011	0.0011	0.0011	-0.0011
	3	0.0000	0.0000	0.0023	0.0023	-0.0023	-0.0023	0.0003	-0.0003	-0.0007	0.0007	0.0007	-0.0007
2	0	-0.0031	0.0031	0.0039	0.0118	-0.0039	-0.0118	-0.0006	0.0006	-0.0059	0.0020	0.0059	-0.0020
	0	-0.0020	0.0020	0.0024	0.0072	-0.0024	-0.0072	0.0002	-0.0002	-0.0027	0.0009	0.0027	-0.0009
	0	-0.0014	0.0014	0.0016	0.0048	-0.0016	-0.0048	0.0003	-0.0003	-0.0016	0.0005	0.0016	-0.0005
	0	-0.0010	0.0010	0.0011	0.0034	-0.0011	-0.0034	0.0003	-0.0003	-0.0010	0.0003	0.0010	-0.0003
3	1.5	-0.0639	-0.0517	0.0749	-0.0827	0.0985	-0.0906	0.0536	0.0531	0.0336	-0.0414	0.0375	-0.0297
	2	-0.0502	-0.0423	0.0622	-0.0670	0.0766	-0.0718	0.0355	0.0357	0.0228	-0.0265	0.0247	-0.0210
	2.5	-0.0408	-0.0354	0.0523	-0.0555	0.0619	-0.0587	0.0267	0.0270	0.0174	-0.0195	0.0184	-0.0163
	3	-0.0342	-0.0303	0.0449	-0.0472	0.0517	-0.0495	0.0215	0.0218	0.0141	-0.0155	0.0148	-0.0134

Load Case	$k=r_m/a$	Measured Displacements (mm)					Calculated In-situ Stresses (MPa)				
		U1	U2	U3	U4	U5	σ_{xx}	σ_{yy}	t_{xy}	K_x	K_y
1	1.5	0.0000	0.0167	-0.0167	0.0000	0.0000	0.0000	0.0000	0.0000	0.2000	0.0000
	2	0.0000	0.0094	-0.0094	0.0000	0.0000	0.0000	0.0000	0.0000	0.2000	0.0000
	2.5	0.0000	0.0060	-0.0060	0.0000	0.0000	0.0000	0.0000	0.0000	0.2000	0.0000
	3	0.0000	0.0042	-0.0042	0.0000	0.0000	0.0000	0.0000	0.0000	0.2000	0.0000
2	0	0.0000	0.0167	-0.0167	0.0000	-0.0083	0.0000	0.0000	0.0000	0.2000	0.1000
	0	0.0000	0.0094	-0.0094	0.0000	-0.0047	0.0000	0.0000	0.0000	0.2000	0.1000
	0	0.0000	0.0060	-0.0060	0.0000	-0.0030	0.0000	0.0000	0.0000	0.2000	0.1000
	0	0.0000	0.0042	-0.0042	0.0000	-0.0021	0.0000	0.0000	0.0000	0.2000	0.1000
3	1.5	-0.1156	-0.0586	-0.0419	0.1733	0.0336	-10.000	10.0000	15.0000	-0.1000	0.2000
	2	-0.0925	-0.0383	-0.0289	0.1388	0.0242	-10.000	10.0000	15.0000	-0.1000	0.2000
	2.5	-0.0762	-0.0283	-0.0223	0.1142	0.0193	-10.000	10.0000	15.0000	-0.1000	0.2000
	3	-0.0644	-0.0225	-0.0183	0.0967	0.0163	-10.000	10.0000	15.0000	-0.1000	0.2000

Table 4.17 Verification of linear gradient in-situ stress equations for Test Configuration Q

Relieved Displacements [mm] — Test Configuration R

Load Case	k=r_m/a	u_a	u_b	u_c	u_d	u_e	u_f	v_a	v_b	v_c	v_d	v_e	v_f
1	1.5	0.0061	-0.0061	0.0079	0.0079	-0.0079	-0.0079	0.0000	0.0000	-0.0039	0.0039	0.0039	-0.0039
	2	0.0040	-0.0040	0.0048	0.0048	-0.0048	-0.0048	0.0000	0.0000	-0.0018	0.0018	0.0018	-0.0018
	2.5	0.0027	-0.0027	0.0032	0.0032	-0.0032	-0.0032	0.0000	0.0000	-0.0011	0.0011	0.0011	-0.0011
	3	0.0019	-0.0019	0.0023	0.0023	-0.0023	-0.0023	0.0000	0.0000	-0.0007	0.0007	0.0007	-0.0007
2	1.5	0.0061	-0.0061	0.0039	0.0118	-0.0039	-0.0118	-0.0003	0.0003	-0.0059	0.0020	0.0059	-0.0020
	2	0.0040	-0.0040	0.0024	0.0072	-0.0024	-0.0072	0.0001	-0.0001	-0.0027	0.0009	0.0027	-0.0009
	2.5	0.0027	-0.0027	0.0016	0.0048	-0.0016	-0.0048	0.0002	-0.0002	-0.0016	0.0005	0.0016	-0.0005
	3	0.0019	-0.0019	0.0011	0.0034	-0.0011	-0.0034	0.0001	-0.0001	-0.0010	0.0003	0.0010	-0.0003
3	1.5	0.0547	0.0608	0.0749	-0.0827	0.0985	-0.0906	-0.0539	-0.0528	0.0336	-0.0414	0.0375	-0.0297
	2	0.0443	0.0482	0.0622	-0.0670	0.0766	-0.0718	-0.0354	-0.0359	0.0228	-0.0265	0.0247	-0.0210
	2.5	0.0367	0.0394	0.0523	-0.0555	0.0619	-0.0587	-0.0266	-0.0272	0.0174	-0.0195	0.0184	-0.0163
	3	0.0313	0.0332	0.0449	-0.0472	0.0517	-0.0495	-0.0214	-0.0219	0.0141	-0.0155	0.0148	-0.0134

Measured Displacements (mm)

Load Case	k=r_m/a	U1	U2	U3	U4	U5
1	1.5	0.0000	0.0167	-0.0167	0.0000	0.0000
	2	0.0000	0.0094	-0.0094	0.0000	0.0000
	2.5	0.0000	0.0060	-0.0060	0.0000	0.0000
	3	0.0000	0.0042	-0.0042	0.0000	0.0000
2	1.5	0.0000	0.0167	-0.0167	0.0000	-0.0083
	2	0.0000	0.0094	-0.0094	0.0000	-0.0047
	2.5	0.0000	0.0060	-0.0060	0.0000	-0.0030
	3	0.0000	0.0042	-0.0042	0.0000	-0.0021
3	1.5	0.1156	-0.0586	-0.0419	0.1733	0.0336
	2	0.0925	-0.0383	-0.0289	0.1388	0.0242
	2.5	0.0762	-0.0283	-0.0223	0.1142	0.0193
	3	0.0644	-0.0225	-0.0183	0.0967	0.0163

Calculated In-situ Stresses (Mpa)

σ_{xx}	σ_{yy}	τ_{xy}	Kx	Ky
0.0000	0.0000	0.0000	0.2000	0.0000
0.0000	0.0000	0.0000	0.2000	0.0000
0.0000	0.0000	0.0000	0.2000	0.0000
0.0000	0.0000	0.0000	0.2000	0.0000
0.0000	0.0000	0.0000	0.2000	0.1000
0.0000	0.0000	0.0000	0.2000	0.1000
0.0000	0.0000	0.0000	0.2000	0.1000
0.0000	0.0000	0.0000	0.2000	0.1000
-10.000	10.0000	15.0000	-0.1000	0.2000
-10.000	10.0000	15.0000	-0.1000	0.2000
-10.000	10.0000	15.0000	-0.1000	0.2000
-10.000	10.0000	15.0000	-0.1000	0.2000

Table 4.18 Verification of linear gradient in-situ stress equations for Test Configuration R

CHAPTER 5

APPLICATION OF THE THEORETICAL FORMULATIONS TO OBJECTS WITH FINITE DIMENSIONS

5.1. INTRODUCTION

Equations for relieved displacements and in-situ stresses were derived in Chapter 3 for an infinite plate with a through-hole. These equations were verified in Chapter 4. This chapter evaluates the applicability of the closed-form equations for relieved displacements and in-situ stresses to objects with finite dimensions. This is Task 6 in the research plan described in Chapter 1. The objective of this chapter is to determine the effect of the thickness of the object (T_p), depth of the core-hole (h), and width of the object (W_p) on the applicability of the equations as they are applied to bounded objects. A series of finite element analyses are performed in which the dimensions of an object are systematically varied to evaluate how the closed-form equations for relieved displacements and in-situ stresses are influenced by the object thickness, core-hole depth, and object width.

This chapter is organized as follows. Sections 5.2, 5.3, and 5.4 evaluate the influence of object thickness T_p, core-hole depth h, and object width W_p, respectively, on the applicability of the closed-form relieved displacement equations. Sections 5.5, 5.6, and 5.7 evaluate the influence of object thickness, core-hole depth, and object width, respectively, on the applicability of the closed-form in-situ stress equations.

5.2. INFLUENCE OF OBJECT THICKNESS ON APPLICABILITY OF CLOSED-FORM RELIEVED DISPLACEMENT EQUATIONS

In this section, the closed-form relieved displacement equations derived in Chapter 3 are studied to evaluate their applicability to objects of finite thickness. The evaluation analyses are performed by calculating relieved displacements as a function of the object thickness T_p. The finite element model explained in Section 5.2.1 is used to calculate the relieved displacements. The relieved displacements are taken at three measurement points a, b, and c that are on the same measurement circle and at angles of 0°, 45°, and 90° from the x-axis as shown in Figure 5.1. The measurement circle radius is made non-dimensional by the through-hole radius a as $k=r_m/a$. The dimensionless measurement circle radius k is taken as 1.5 for these analyses. The relieved displacements are compared with the relieved displacements calculated by the closed-form relieved displacement equations.

Both the uniform stress state and the linear gradient stress state are treated here in separate sections.

5.2.1. Finite Element Model

This section describes general features of the finite element analyses that were performed to evaluate the closed-form relieved displacement and the in-situ stresses equations to the object thickness T_p. Included in this section are a description of how drilling a through-hole is simulated, model geometry, element types, material properties, load conditions, and a mesh refinement convergence study.

5.2.1.1. Simulation of Hole Drilling

A series of finite element models were created to simulate drilling a through-hole in a three-dimensional object. These finite element models were used to calculate the relieved displacements of the measurement points for each of the Test Configurations shown in Figures 3.13 and 3.14. As explained in Section 3.1 and Section 4.2, the relieved displacements and stress redistribution due to drilling a hole can be calculated by applying the relieved in-situ stresses (N, T) to the hole surface.

5.2.1.2. Model Geometry, Element Type, and Load Condition

Two-dimensional linear elastic axisymmetric models were employed in these analyses. The use of axisymmetric model greatly reduced the modeling and analysis time compared to that of an equivalent three-dimensional model.

The basic geometry of the axisymmetric finite element model is shown in Figure 5.2. The through-hole diameter is 150 mm. The thickness of the model was varied from 10 mm to 3000 mm.

Since we assume that objects are infinite or large enough compared to the through-hole size, we can consider this problem as axisymmetric. However, the loads subjected to the through-hole surface are non-axisymmetric. The axisymmetric models with non-axisymmetric loadings were solved as follows.

The finite element analyses were carried out in the linear elastic range using ANSYS, commercial finite element analysis software. Axisymetric-harmonic 8-node elements (plane83) were employed. The elements are used for two-dimensional modeling of axisymmetric structures with non-axisymmetric loading. The element has three degrees of freedom per node: translations in the nodal x, y, and z directions (ANSYS 2000).

As explained earlier, the relieved displacements are calculated by applying the relieved in-situ stresses as loads. The relieved in-situ stresses (N, T), which are relaxed due to through-hole drilling, were found earlier in Equations (3.5) and (3.6), and Equations (3.48) and (3.49) for the uniform stress state and for the linear gradient stress states, respectively.

109

It is assumed that the in-situ stresses are acting in a plane parallel to the x-y surface of the object. In general, any arbitrary load can be represented by a Fourier series. For this problem, the loadings are given as a Fourier series as (Cook 1989).

$$N(r,z,\alpha) = \sum_{n=0}^{\infty} N_{cn}(r,z)\cos(n\alpha) + \sum_{n=0}^{\infty} N_{sn}(r,z)\sin(n\alpha) \tag{5.1}$$

$$T(r,z,\alpha) = \sum_{n=0}^{\infty} T_{cn}(r,z)\sin(n\alpha) + \sum_{n=0}^{\infty} T_{sn}(r,z)\cos(n\alpha) \tag{5.2}$$

where N_{cn}, N_{sn}, T_{cn}, and T_{sn} are amplitudes that depend on n (but not on α). Here n represents the harmonic number.

Like loads, the displacement fields can also be expanded in Fourier series (Cook 1989).

$$u_r(r,z,\alpha) = \sum_{n=0}^{\infty} u_{cn}(r,z)\cos(n\alpha) + \sum_{n=0}^{\infty} u_{sn}(r,z)\sin(n\alpha) \tag{5.3}$$

$$v(r,z,\alpha) = \sum_{n=0}^{\infty} v_{cn}(r,z)\sin(n\alpha) + \sum_{n=0}^{\infty} v_{sn}(r,z)\cos(n\alpha) \tag{5.4}$$

$$w(r,z,\alpha) = \sum_{n=0}^{\infty} u_{cn}(r,z)\cos(n\alpha) + \sum_{n=0}^{\infty} u_{sn}(r,z)\sin(n\alpha) \tag{5.5}$$

where, u, v, w are the radial, circumferential, and axial displacement distributions, respectively. u_{cn}, u_{sn}, v_{sn}, v_{cn}, w_{cn}, and w_{sn} are displacement field amplitudes that depend on r, z, and n but not α.

For the uniform stress state given in Equations (3.3) and (3.4), there are two Fourier components to consider, $n = 0$ and $n = 2$. For the linear gradient stress state given in Equations (3.47) and (3.48), there are two Fourier components to consider, $n = 1$ and $n = 3$. Due to the orthogonality of the harmonic functions, displacements can be calculated individually for each load component. The resulting displacements are the calculated by superposition.

5.2.1.3. Convergence Study

Since the closed-form relieved displacement equations were proved correct in Chapter 4, a finite element model that produce less than 0.3 error by comparison with the closed-form relieved displacement equation solutions is created. The same element distribution around the hole area of the finite element model was used for the other finite element models with different thickness.

The finite element mesh for the axisymmetric model is shown in Figure 5.2. It was designed with finer mesh in the immediate vicinity of the hole.

5.2.1.4. Material Properties

The Young's modulus E and Poisson's ratio ν of the model are 30000 MPa and 0.2 respectively. The analyses assume that the material is linear elastic. This Young's modulus corresponds to a normal weight concrete compressive strength of 40 MPa (5800 psi).

5.2.2. Influence of Object Thickness on Applicability of the Closed-Form Relieved Displacement Equations for the Uniform Stress State

In this section, the closed-form relieved displacement equations for the uniform stress state are applied to objects of finite thickness. The finite element models explained in Section 5.2.1 are used to perform the analyses described in this section. The models are run under same load conditions for varying thicknesses. The loading is a uniform uniaxial stress state of $\sigma_{xx}=10$ MPa, $\sigma_{yy}=0$, $\tau_{xy}=0$. This loading is the in-situ stress state that existed prior to drilling the hole.

Figure 5.3 to Figure 5.5 show the relieved displacements in the radial direction at measurement points a, b, and c, respectively, versus object thickness. The object thickness is shown in dimensionless form as T_p/D_h, where, D_h is the diameter of the through-hole. Figure 5.6 shows the relieved displacements in the tangential direction at measurement point b versus object thickness (T_p/D_h). These figures show the finite element solution as well as the closed-form solution for both plane stress and plane strain assumptions. The tangential displacements at measurement points a and b are zero.

As seen from the figures, the relieved displacements in the radial direction are not significantly affected by the object thickness variations. However, the effect of the object thickness on relieved displacement in the tangential direction is more significant. These figures also show that the relieved displacements in the radial direction as the object thickness varies are reasonably close to the plane stress solution. A maximum error in displacement of 3 % is observed when the ratio of the object thickness to through-hole diameter is equal to 1. Although the figure indicates that the relieved displacements in the tangential direction are closer to the plane strain solution as the object thickness increases, the plane strain solution produced more than 10 % an error as the object thickness increases.

The other observation from the figure is that the relieved displacement at measurement point b is not affected by the object thickness variations and is almost equal to both the plane stress and plane strain solutions. To explain why the relieved displacements at measurement point b behave differently than the relieved displacements at other measurement points, the closed-form relieved displacement Equation (3.41) is broken in to two parts. The first part of the equation corresponds to equibiaxial stresses $(\sigma_{xx}+\sigma_{yy})/2$ and it does not depend on α. It is seen that the first part of the equation does not depend on plane stress or plane stress assumptions. For both the plane stress and plane strain assumptions, the first part of the equation is same. The second part of the equation corresponds to shear stress components $(\sigma_{xx}-\sigma_{yy})/2 \cos(2\alpha)$ and is dependent on α. The second part of the relieved displacement equation will be zero when α is equal to 45°. This shows that the relieved displacement at measurement point b is caused by the equibiaxial stress

111

state. That means equibiaxial stresses produce relieved displacement that are equal to closed-form equation solution and are not affected by the object thickness.

5.2.3. Influence of Object Thickness on Applicability of the Closed-Form Relieved Displacement Equations for the Linear Gradient Stress State

In this section, the closed-form relieved displacement equations for the linear gradient stress state are applied to objects of finite thickness. The finite element models described in Section 5.2.1 are used to perform the analyses described in this section. The models are run under same load conditions for varying object thicknesses. The loading is a uniform uniaxial concentric linear gradient stress state of $Kx=0.2$ MPa/mm, $Ky=0$, $\sigma_{xx}=0$ MPa, $\sigma_{yy}=0$, $\tau_{xy}=0$. This loading is in-situ stress state that existed prior to drilling the hole.

The relieved displacements in the radial and in the tangential direction at measurement point b are plotted against the object thickness (T_p/D_h) in Figure 5.7, and Figure 5.8, respectively. The object thickness is shown in dimensionless form as T_p/D_h. These figures show the finite element solution as well as the closed-form solution for both plane stress and plane strain assumption.

As seen from the figures, the relieved displacements in the radial direction are not significantly affected by the object thickness variations. However, the effect of the thickness on relieved displacement in the tangential direction is more significant.

Figure 5.7 also shows that the relieved displacements in the radial direction as thickness varies are reasonably close to the plane stress solution. A maximum error in displacement of 3 % is observed when the ratio of the object thickness to through-hole diameter is equal to 1. Although Figure 5.8 indicates that the relieved displacements in the tangential direction are closer to the plane strain solution as the object thickness increases, more than 15% error is observed relative to the plane strain solution as the object thickness increases.

5.3. INFLUENCE OF CORE-HOLE DEPTH ON APPLICABILITY OF CLOSED-FORM RELIEVED DISPLACEMENT EQUATIONS

In this section, the closed-form relieved displacement equations derived in Chapter 3 are studied to evaluate their applicability to core-hole depth. The evaluation analyses are performed by calculating relieved displacements as a function of the core-hole-depth h. The finite element models explained in Section 5.3.1 are used to calculate the relieved displacements. The relieved displacements are taken at two measurement points, a and b, that are on the same measurement circle and at angles of $0°$, and $45°$ from the x-axis. The measurement circle radii are made non-dimensional by the through-hole radius a as $k=r_m/a$. The relieved displacements are compared with the relieved displacements calculated by the closed-form relieved displacement equations.

Both the uniform stress state and the linear gradient stress state are treated in separate sections below.

112

5.3.1. Finite Element Model

This section describes the general features of the finite element analyses that were performed to evaluate the closed-form equations for the relieved displacements and the in-situ stresses to the core-hole depth h.

The finite element model created here are very similar to the finite element models created in Section 5.2.1. The main difference between the finite element models is the geometry of the models. Thus, only the specimen geometry is explained below.

5.3.1.1. Models Geometry and Convergence Study

The length of the model (L) and the element distribution around the hole were defined based on the finite element models with a through-hole that produce less than 0.35% error by comparison with the relieved displacement solutions.

The basic geometry of axisymmetric finite element model is shown in Figure 5.9. The length of the model and diameter of the model are set equal to 3000 mm. The outer core-hole diameter and inner core-hole diameter are 150 mm and 144 mm, respectively.

It was designed with finer mesh in the immediate vicinity of the hole. A similar mesh to that used with through-hole case explained in Section 5.2.1 is used in the vicinity of the core-hole.

5.3.2. Influence of Core-Hole Depth on Applicability of the Closed-Form Relieved Displacement Equations for the Uniform Stress State

The finite element models with a core-hole described in Section 5.3.1 are used to perform the analyses described in this section. The models are run under same load conditions for the varying core-hole depths. The loading is a uniform uniaxial stress state of $\sigma_{xx}=10$ MPa, $\sigma_{yy}=0$, $\tau_{xy}=0$. This loading is in-situ stress state that existed prior to drilling the hole.

Figure 5.10 shows the relieved displacement at the measurement point a versus the core-hole depth h. This figure also shows the plane stress and the plane strain solutions obtained from the closed-form equations for relieved displacement. As seen from the figure, relieved displacements increase quickly as core-hole depth increases, and reach the maximum value. Relieved displacements obtained from finite element analysis are far beyond from the closed-form solutions at shallow core-hole depth, but get closer to closed-form solutions quickly as core-hole depth increases further and reach their maximum value between plane stress and plane strain solution. Although the relieved displacements get close to closed-form solutions at deep core-hole depth, it might not be practical to drill a core-hole that deep in to a structure.

The relieved displacements in the tangential direction are plotted against dimensionless core-hole depth in Figure 5.11. The closed-form solutions for plane stress and plane strain are also plotted in the figures. It is seen from the figures that the relieved displacements increase quickly, reach a maximum and then remain constant. These figures show that relieved displacements in the

113

tangential direction due to core-hole drilling are not the same as those obtained from closed-form solutions. Even at the core-hole depth at which the relieved displacement is reached maximum, the closed-form solution gives considerable error.

5.3.3. Influence of Core-Hole Depth on Applicability of the Closed-Form Relieved Displacement Equations for the Linear Gradient Stress State

The analysis is performed by calculating the relieved displacements as a function of core-hole depth by axisymmetric finite element models described in Section 5.3.1. The loading is a uniaxial concentric linear gradient stress state of $Kx=0.2$ MPa/mm, $Ky=0$, $\sigma_{xx}=0$, $\sigma_{yy}=0$, $\tau_{xy}=0$. This loading is in-situ stress state that existed prior to drilling the hole.

The relieved displacements in the radial and the tangential direction are plotted against core-hole depths in Figure 5.12 and Figure 5.13, respectively. The closed-form solutions for the plane stress and the plane strain are also plotted in these figures. These figures show that the relieved displacements obtained from the finite element analysis are far beyond from the closed-form solutions at shallow core-hole depth. These relieved displacements increase towards to closed-form solutions, reach a maximum and remain constant as core-hole depth increases. The relieved displacements in the radial direction are close to the closed-form solutions with small error at the core-hole depth where maximum relieved displacement is reached. However, the relieved displacements in the tangential direction have still considerably large error at the core-hole depth where relieved displacement is reached maximum. Although the relieved displacements in the radial direction are close to the closed-form solutions at deep core-hole depths, it might not be practical to drill a core-hole that deep in to a structure.

5.4. INFLUENCE OF OBJECT WIDTH ON APPLICABILITY OF CLOSED-FORM RELIEVED DISPLACEMENT EQUATIONS

In this section, the closed-form relieved displacement equations derived in Chapter 3 are studied to evaluate their applicability to objects of finite width. The evaluation analyses are performed by calculating relieved displacements as a function of the object width W_p. The finite element model explained in Section 5.4.1 is used to calculate the relieved displacements. The relieved displacements are taken at three measurement points a, b, and c that are on the same measurement circle and at angles of $0°$, $45°$, and $90°$ from the x-axis. The measurement circle radii are made non-dimensional by the through-hole radius a as $k=r_m/a$. The dimensionless measurement circle radius k is taken as 1.5 for these analyses. The relieved displacements are compared with the relieved displacements calculated by the closed-form relieved displacement equations.

The width of the object is made non-dimensional by measurement circle diameter D_h as W_p/D_h.

Both the uniform stress state and the linear gradient stress state are treated here in separate sections below.

114

5.4.1. Finite Element Model

This section describes the general features of the finite element analyses that were performed to evaluate the closed-form equations for the relieved displacements and the in-situ stresses to object width W_p. Included in this section are a description of how drilling a through-hole is simulated, model geometry, element types and, material properties, and a mesh refinement convergence study.

5.4.1.1. Simulation of Hole Drilling

The finite element models were created to simulate drilling a through-hole in a thin large object. As explained in Section 3.1 and Section 4.2, the relieved displacements and stress redistribution are calculated by applying the relieved in-situ stresses to the hole surface. The finite element analyses were carried out in linear elastic range using the ABAQUS, a commercial trademark finite element package.

5.4.1.2. Modeling, Model Geometry

Figure 5.14 shows general geometry of the finite element model. Based on the information above, the finite element models are created as follow. A number of objects with varying widths are modeled. The length L, through-hole diameter and thickness of the model are 2000 mm, 150 mm and 15 mm, respectively. In this instance, a full three-dimensional finite element model is preferred instead of symmetric or asymmetric models that require superposition. The full model provide the flexibility to apply any kind of loading in one analyses without changing boundary conditions.

A thin finite element model with a through-hole that produces less than 0.4 percent error by comparison with the relieved displacement equation solution was created. The same element distributions are used for the other finite element models. The ratio of the width (W_p) and length (L) of the model is unity at the beginning to produce ease of the modeling. The length, thickness, and the diameter of the model were set equal to 2000 mm, 15 mm, and 150 mm, respectively. Then the other models were created by changing the width of the model.

5.4.1.3. Material Properties

The modulus E and Poisson's ratio ν of the model are 30000 MPa and 0.2 respectively and the analysis assumes that the material is linear elastic.

5.4.1.4. Loads

As explained earlier, loads are applied to the inner surface of the hole. These loads, which represent relieved in-situ stresses due to through-hole drilling, are calculated as a function of in-situ state of stresses and α in Equations in Chapter 3. These loads, found in Equations (3.5) and (3.6), are applied to the nodes at the hole surface.

5.4.2. Influence of Object Width on Applicability of the Closed-Form Relieved Displacement Equations for the Uniform Stress State

The finite element models described in Section 5.4.1 are used to perform the analyses described in this section. The models are run under same load conditions for varying object widths (W_p). The loading is a uniform uniaxial stress of σ_{xx}=10 MPa, σ_{yy}=0, τ_{xy}=0. This loading is the in-situ stress state that existed prior to drilling the hole.

Figure 5.15, Figure 5.16, and Figure 5.17show the relieved displacements in the radial direction at the measurement points a, b, and c versus object width, respectively. Figure 5.18 shows relieved displacements in the tangential direction v_{a0} at the measurement point b versus object width. The relieved displacements are shown in dimensionless form as u_r/u_{ro} and v_α / v_{a0} where u_{ro}, and v_{a0} are the relieved displacement obtained where the ratio of the width and length of the specimen is unity. The widths of the models are also shown in dimensionless form as W_p/D_h. It is seen from the figures that errors on relieved displacements increase as object width to through-hole diameter ratio decreases. The error is very small in the region where the object width to the through-hole diameter ratio (W_p/D_h) is greater than 4, and become larger where ratio of the plate thickness to through-hole diameter is less than 4. The maximum percentage error occurred at the measurement point c.

5.4.3. Influence of Object Width on Applicability of the Closed-Form Relieved Displacement Equations for the Linear Gradient Stress State

The finite element model in Section 5.4.1 is used to perform the analyses described in this section. The models are run under same load conditions for varying object widths W_p. The loading is a uniform uniaxial concentric linear gradient stress state of Kx=0.2 MPa/mm, Ky=0, σ_{xx}=0 MPa, σ_{yy}=0, τ_{xy}=0. This loading is the in-situ stress state that existed prior to drilling the hole.

Figure 5.19 shows relieved displacement in the radial direction u_b/u_{bo} at the measurement point b versus dimensionless object width thickness W_p/D_h. It is seen from the figure that the errors on relieved displacements increase as object width to through-hole diameter ratio decreases. These error is very small in the region where the object width to the through-hole diameter ratio (W_p/D_h) is greater than 2, and become larger where ratio of the object width to through-hole diameter less than 3. Figure 5.20 shows relieved displacement in tangential direction v_b/v_{bo} at the measurement point b versus dimensionless object width thickness W_p/D_h. This figure shows that the relieved displacements in the tangential direction at measurement point b are not affected much by the object width.

5.5. INFLUENCE OF OBJECT THICKNESS ON APPLICABILITY OF CLOSED-FORM IN-SITU STRESS EQUATIONS

In this section, the closed-form in-situ stress equations that were derived in Chapter 3 are studied to evaluate their applicability objects of finite thickness. The analyses are performed by calculating in-situ stresses as a function of the object thickness T_p. The finite element model

explained in Section 5.2.1 is used to calculate the relieved displacements at the measurement points for each of the Test Configurations. Then these relieved displacements are used to calculate the measured displacements for each of the Test Configurations. In-situ stresses are then calculated using these measured displacements by the closed-form in-situ stress equations derived in Chapter 3. Finally, The calculated in-situ stresses are compared with the in-situ stresses that existed in the object prior to drilling the through-hole.

Both the uniform in-situ stress equations and the linear gradient in-situ stress equations are treated in separate sections.

5.5.1. Influence of Object Thickness on Applicability of the Closed-Form Uniform In-situ Stress Equations

Figure 5.21 to Figure 5.28 show the in-situ stress σ_{xx} versus object thickness for each of the Test Configurations shown in Figure 3.13. The object thickness is shown in dimensionless form as T_p/D_h. These figures show the calculated in-situ stress σ_{xx} for both the plane stress and the plane strain conditions. The calculated in-situ stresses (σ_{xx}, σ_{yy}, τ_{xy}) are tabulated in from Table 5.1 to Table 5.8. These tables include the calculated in-situ stresses for both the plane stress and the plane strain conditions, and percentage errors obtained between the calculated in-situ stresses and the in-situ stresses that existed prior to drilling the hole. As seen from the figures and tables, the effect of the thickness of the object on the closed-form in-situ stress equations for each of the Test Configurations are different. For most of the Test Configurations (except Test Configurations F and H,) the closed-form equations for the plane stress assumptions give reasonably good results and they are not affected much by the object thickness. A maximum error in displacement of about 1.5 % is observed when the ratio of the object thickness to through-hole diameter is equal to 1. However, the closed form uniform in-situ stress equations for Test Configurations F and H are affected by the object thickness and the equations cause some errors. Maximum errors in displacement of about 3.2 % and 6 % for the Test Configurations F and H, respectively, are observed from the plane strain assumptions. The reason why the closed form equations for Test Configurations F and H are affected more by the object thickness variation is that the closed-form in-situ stress equations for Test Configurations F and H consist of measurement displacements that are obtained from the tangential and radial relieved displacements. As investigated in Section 5.2.2, the relieved displacements in radial direction are affected by the object thickness.

5.5.2. Influence of Object Thickness on Applicability of the Closed-Form Linear Gradient In-situ Stress Equations

Figure 5.29 to Figure 5.33 show in-situ stress Kx versus the object thickness T_p/D_h for each of the test configurations shown in Figure 3.14. These figures show the calculated in-situ stresses Kx for both the plane stress and the plane strain assumptions. The all calculated in-situ stresses (σ_{xx}, σ_{yy}, τ_{xy}, Kx, Ky) are tabulated Table 5.9 to Table 5.13. These tables include the calculated in-situ stresses for both the plane stress and the plane strain assumptions, and percentage errors between the calculated in-situ stresses and the exact in-situ stresses that existed before the drilling the hole. As seen from the figures and tables, the effect of the thickness of the object on the closed-

117

form in-situ stress equations for each of the configurations are different. All test configurations are affected by the object thickness variations. When the object thickness is very small, the closed-form in-situ stress equations for plane stress equations produce very good results. However, as the object thickness increases, the in-situ stress (Kx) calculated by the closed-form linear gradient in-situ stress equations for both the plane stress and the plane strain assumptions increase or decrease quickly, reach a maximum, and then remain constant.

5.6. INFLUENCE OF CORE-HOLE DEPTH ON APPLICABILITY OF CLOSED-FORM IN-SITU STRESS EQUATIONS

In this section, the closed-form in-situ stress equations that were derived in Chapter 3 are studied to evaluate their applicability to core-hole depth. The analyses are performed by calculating the in-situ stresses as a function of the core-hole depth h. The finite element model described in Section 5.3.1 is used to calculate the relieved displacements at the measurement points for each of the Test Configurations. The relieved displacements are used to calculate the measured displacements for each of the test configurations. In-situ stresses are then calculated by the closed-form in-situ stress equations. Finally, the calculated in-situ stresses are compared with the in-situ stresses that existed in the object prior to drilling the through-hole.

Both the uniform in-situ stress equations and the linear gradient in-situ stress equations are treated in following sections, respectively.

5.6.1. Influence of Core-Hole Depth on Applicability of the Closed-form Uniform In-situ Stress Equations

Figure 5.34 to Figure 5.41 show the in-situ stress σ_{xx} versus the object depth h for each of the test configurations shown in Figure 3.13. These figures show the calculated in-situ stress σ_{xx} for the both plane stress and the plane strain conditions. The calculated in-situ stresses are tabulated in Table 5.14 to Table 5.21. These tables include the calculated in-situ stresses for the both plane stress and the plane strain conditions, and percentage errors obtained between the calculated in-situ stresses and the in-situ stresses that existed prior to drilling the hole.

These figures show that the calculated in-situ stress increases quickly as core-hole depth increases, and reach the maximum value. At the shallow core-hole depth, the closed-form uniform in-situ stress equations produce large errors. These errors decrease quickly as the core-hole depth increases. As seen from the results, neither the plane stress assumptions nor the plane strain assumptions give good results until the core-hole depth reaches a considerably high depth. Although the closed-form in-situ stress equations produce very small errors at deep core-hole depths, it might not be practical to drill a core-hole that deep in to a structure.

118

5.6.2. Influence of Core-Hole Depth on Applicability of the Closed-Form Linear Gradient In-situ Stress Equations

Figure 5.42 to Figure 5.46 show the calculated in-situ stress Kx versus core-hole depth h for each of the Test Configurations. These figures show the calculated in-situ stress Kx for both the plane stress and the plane strain assumptions. The calculated in-situ stresses are tabulated in Table 5.22 to Table 5.26. These tables include the calculated in-situ stresses for both the plane stress and the plane strain conditions, and percentage errors obtained between the calculated in-situ stress and the in-situ stress that existed before drilling the core-hole.

These figures show that the calculated in-situ stress increases quickly as core-hole depth increases, and reach the maximum value. At the shallow core-hole depth, the closed-form linear gradient in-situ stress equations produce large errors. These errors decrease quickly as the core-hole depth increases. As seen from the results, neither the plane stress assumptions nor the plane strain assumptions give good results until the core-hole depth reaches a considerably high depth. The closed-form equations for plane strain assumptions give better results than the closed-form equations for plane stress assumptions. Although the closed-form linear gradient in-situ stress equations for the plane strain assumptions produce small error at deep core-hole depths, it might not be practical to drill a core-hole that deep in to a structure.

5.7. INFLUENCE OF OBJECT WIDTH ON APPLICABILITY OF CLOSED-FORM IN-SITU STRESS EQUATIONS

In this section, the closed-form in-situ stress equations that were derived in Chapter 3 are studied to evaluate their applicability to objects of finite widths. The analyses are performed by calculating the in-situ stresses as a function of the object width W_p. The finite element model explained in Section 5.4.1 is used to calculate the relieved displacements at the measurement points for each of the Test Configurations. The relieved displacements are used to calculate the measured displacements for each of the Test Configurations. In-situ stresses are then calculated by the closed-form in-situ stress equations derived in Chapter 3. Finally, The calculated in-situ stresses are compared with the in-situ stresses that existed in the object prior to through-hole drilling.

Both the uniform in-situ stress equations and the linear gradient in-situ stress equations are treated in following sections.

5.7.1. Influence of Object Width on Applicability of the Closed-form Uniform In-situ Stress Equations

Figure 5.47 to Figure 5.54 show the calculated in-situ stress σ_{xx} versus the object width W_p/D_h for each of the Test Configurations shown in Figure 3.13. These figures show the calculated in-situ stress σ_{xx} for both the plane stress and the plane strain assumptions. The all calculated in-situ stresses are tabulated in Table 5.27 to Table 5.34. These tables include the calculated in-situ stresses for both the plane stress and the plane strain conditions, and percentage errors obtained between the calculated in-situ stress and the in-situ stress existed prior to drilling the hole. As

119

seen from the figures, plane stress assumptions give better results. This is because of modeling a thin finite element model described in Section 5.4.1. The closed-form uniform in-situ stress equations for both the plane stress and the plane strain assumptions show same characteristic behavior against the width to through-diameter ratio variations. The last columns of the tables show percentage change of the in-situ stress σ_{xx}. In this tables $\sigma_x(10)$ is the in-situ stress calculated where the specimen width to through-hole diameter ratio is equal to 10.

The figures and tables introduced above show that the uniform in-situ stress equations are not affected significantly by the object width variations. The uniform in-situ stress equations for both the plane stress and the plane strain assumptions show the same characteristic behavior for the width to through-hole diameter variations. It is seen that the object width has little effect on the closed-from uniform in-situ stress equations up to the width to through-hole diameter ratio equal to 3. Around a 3 % change of in-situ stress is observed for the all test configurations when the width to through-hole diameter ratio is equal to 3. This percentage change of the in-situ stress σ_{xx} for each of the Test Configurations are between 6 % and 10 % when the width to through-hole diameter ratio is equal to 2.

5.7.2. Influence of Object Width on Applicability of the Closed-Form Linear Gradient In-situ Stress Equations

Figure 5.55 to Figure 5.59 show the calculated in-situ stress σ_{xx} versus the object width for each of the test configurations. These figures show the calculated in-situ stress σ_{xx} for both the plane stress and the plane strain assumptions. The calculated in-situ stresses are tabulated in Table 5.35 to Table 5.39. These tables include the calculated in-situ stresses for both the plane stress and the plane strain assumptions, and percentage errors obtained between the calculated in-situ stresses and the in-situ stresses that existed before drilling the hole.

The figures and tables show that the linear gradient in-situ stress equations are not affected significantly by the object width variation. As seen from the figures, the plane stress assumptions give better results. This is because of modeling a thin finite element model described in Section 5.4.1. The linear gradient in-situ stress equations for both plane stress and plane strain assumptions show the same characteristic behavior to the width to through-diameter variations. The last columns of the tables show relative change of the in-situ stress Kx to in-situ stress $Kx(10)$, where $Kx(10)$ is the in-situ stress Kx when the specimen width to through-hole diameter ratio is equal to 10. It is seen that the object width has almost no effect on the closed-from linear gradient in-situ stress equations up to the width to through-hole diameter ratio equal to 3. When the width to through-hole diameter ratio reaches 2, a sudden dropt is observed on the relative change of the in-situ stress calculated. Even at the width to through-hole diameter ratio equal to 2, there are not significant change on the in-situ stress Kx calculated. Around a 4 % change is observed for all Test Configurations.

120
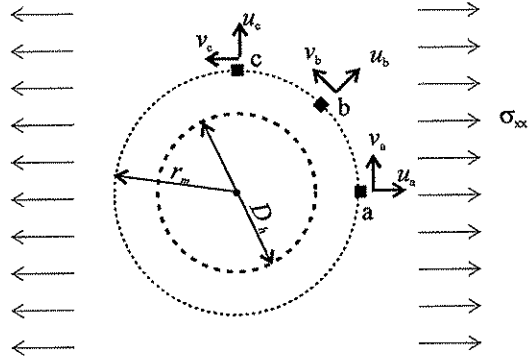
Figure 5.1 Measurement point locations used for the evaluation analyses.
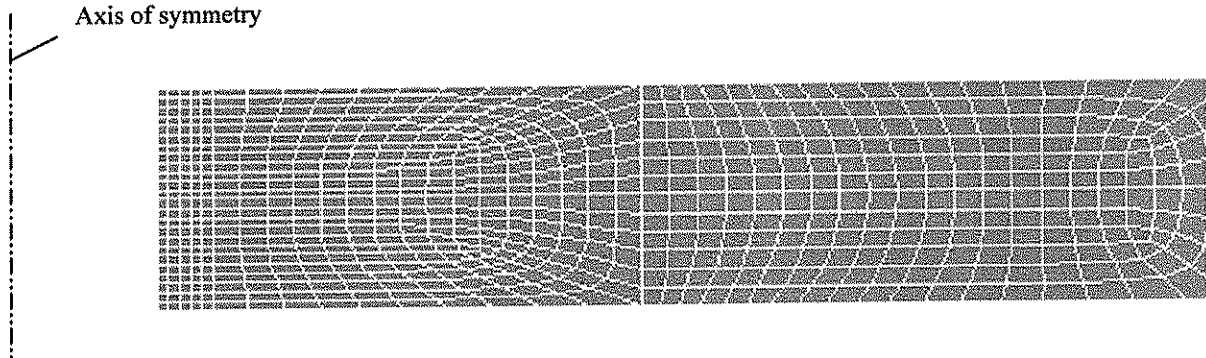
Figure 5.2 Basic geometry of axisymmetric finite element model with through-hole.
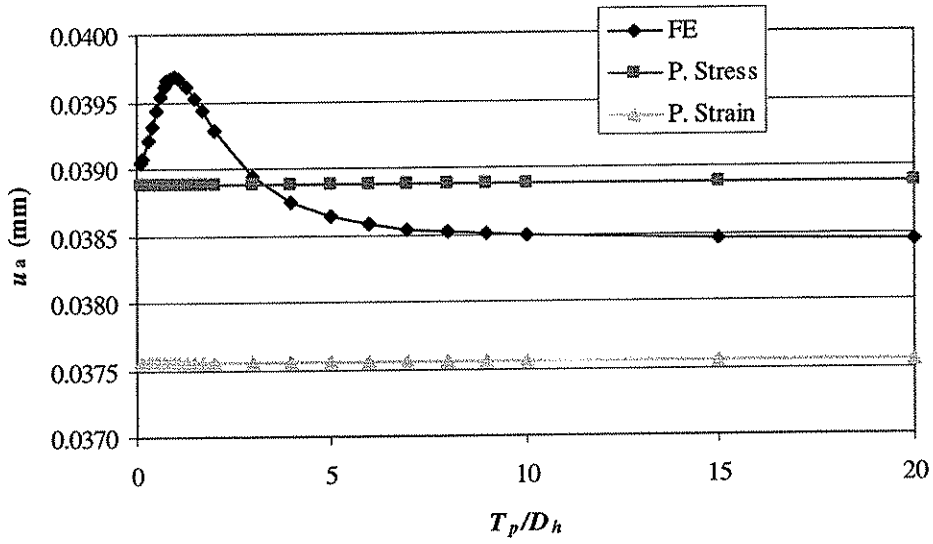
Figure 5.3 Relieved displacement in radial direction at measurement point a versus object thickness for the in-situ stress state of σ_{xx}=10 MPa, σ_{yy}= τ_{xy}=0.
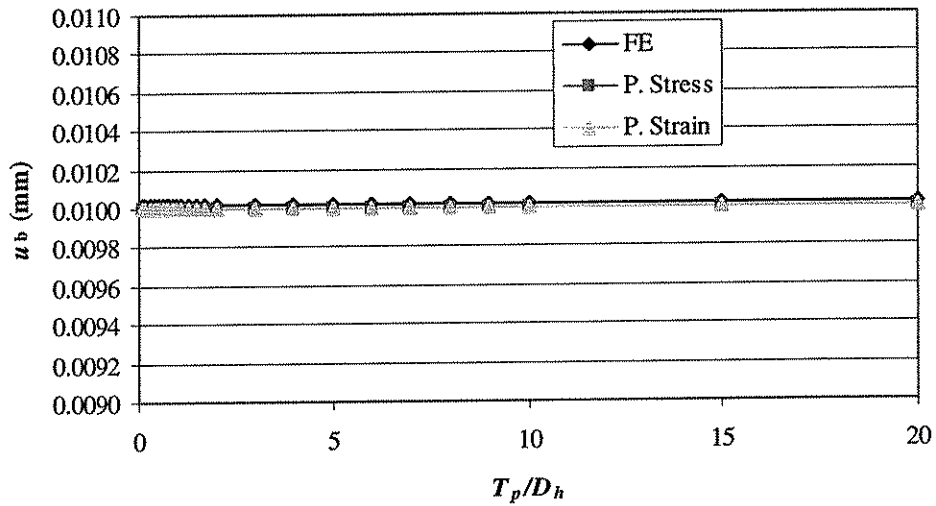
Figure 5.4 Relieved displacement in radial direction at measurement point b versus object thickness for the in-situ stress state of σ_{xx}=10 MPa, σ_{yy}= τ_{xy}=0.
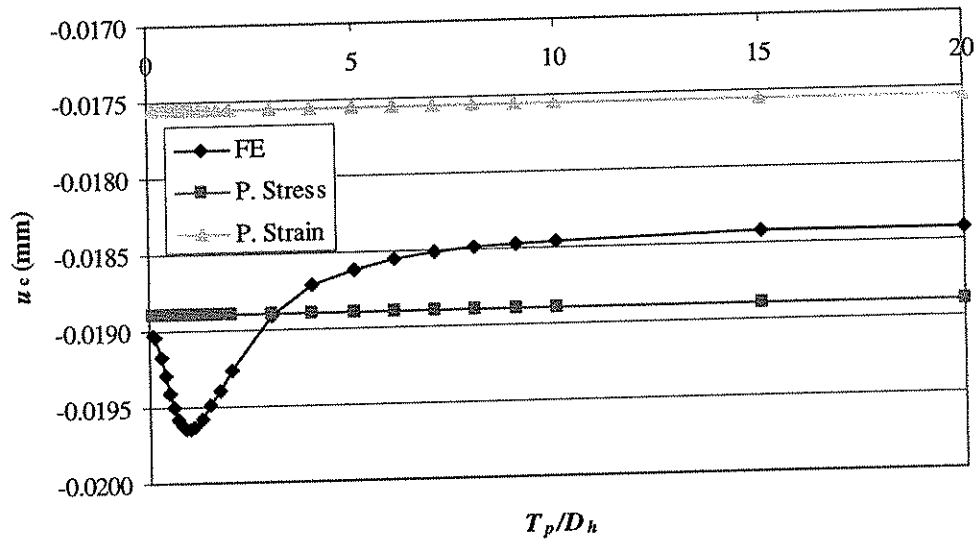
Figure 5.5 Relieved displacement in radial direction at measurement point c versus object thickness for the in-situ stress state of σ_{xx}=10 MPa, σ_{yy}= τ_{xy}=0.
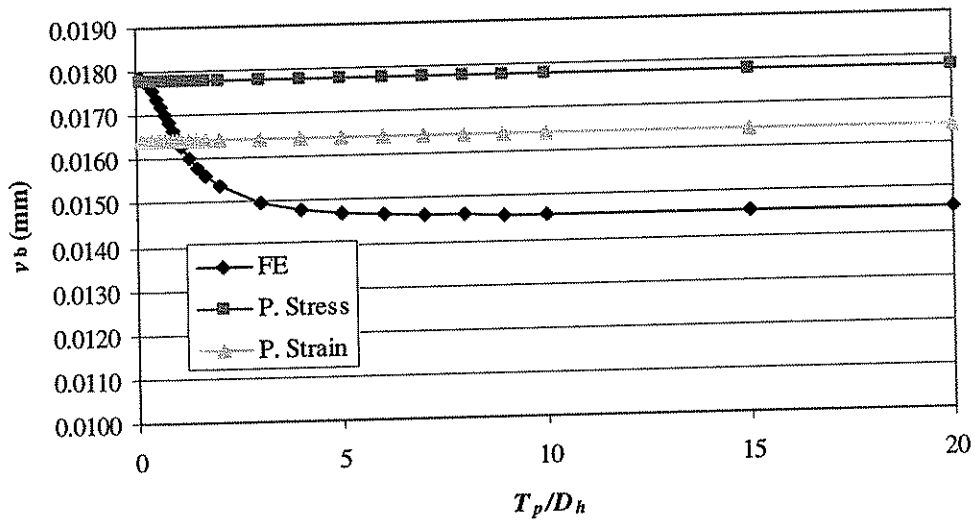
Figure 5.6 Relieved displacement in tangential direction at measurement point b versus object thickness for the in-situ stress state of σ_{xx}=10 MPa, σ_{yy}= τ_{xy}=0.
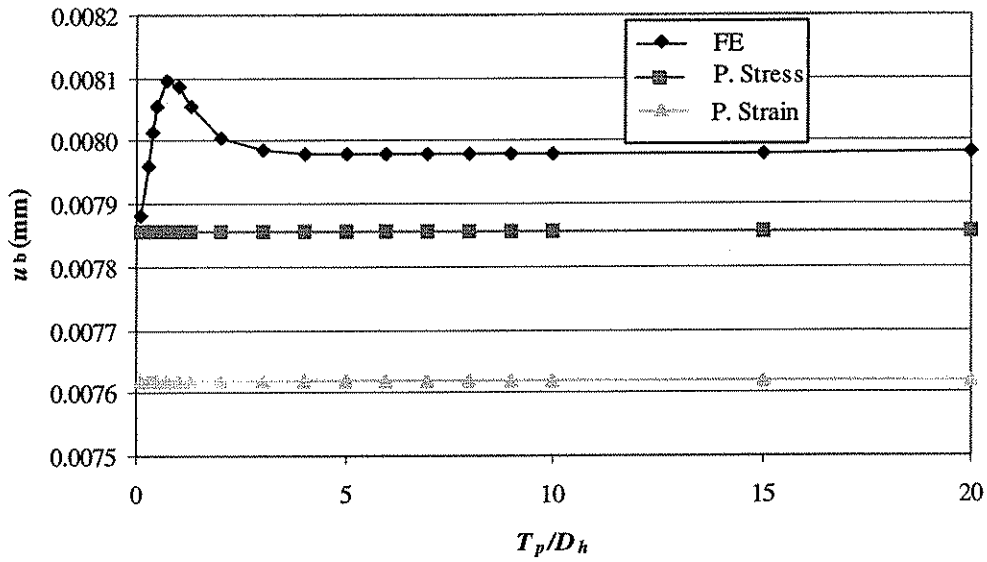
Figure 5.7 Relieved displacement in radial direction at measurement point b versus object thickness for the in-situ stress state of Kx=0.2 MPa/mm, Ky=0, σ_{xx}=0, σ_{yy}=τ_{xy}=0.
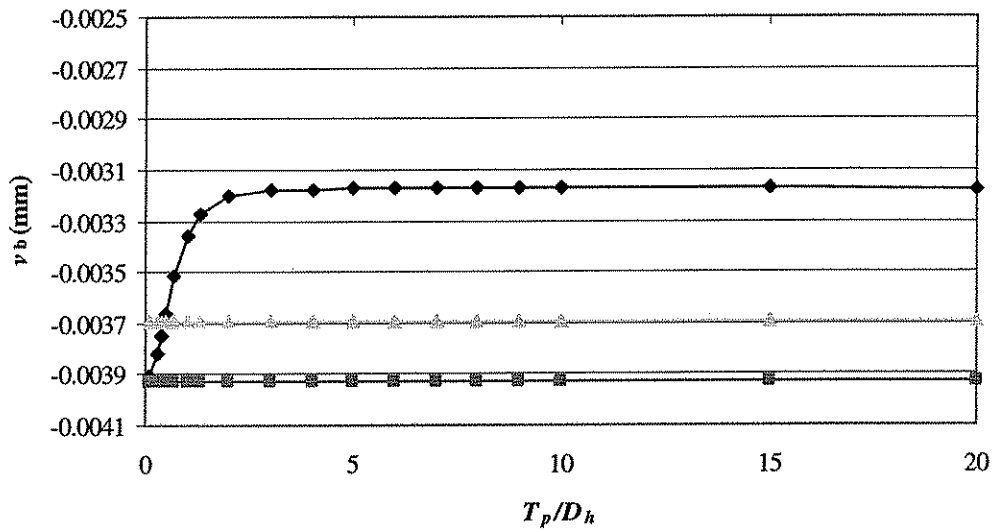
Figure 5.8 Relieved displacement in tangential direction at measurement point b versus the object thickness for the in-situ stress state of Kx=0.2 MPa/mm, Ky=0, σ_{xx}=0, σ_{yy}=τ_{xy}=0.
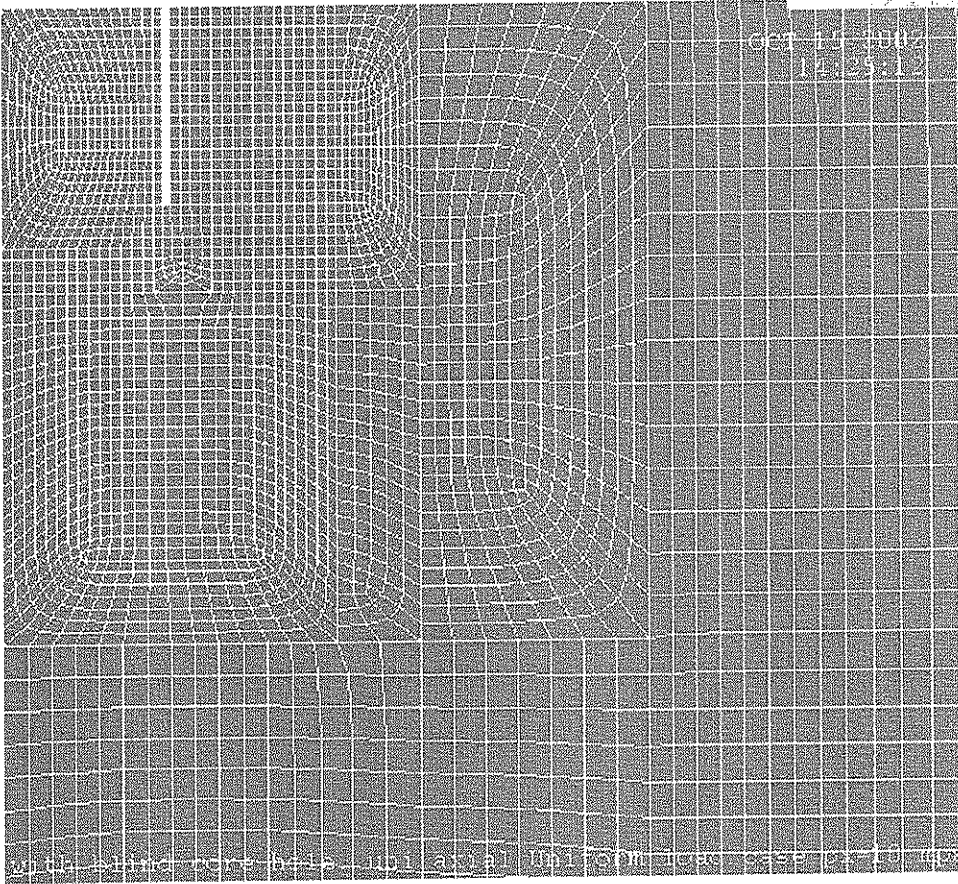
Figure 5.9 Basic geometry of axisymmetric finite element model with core-hole.
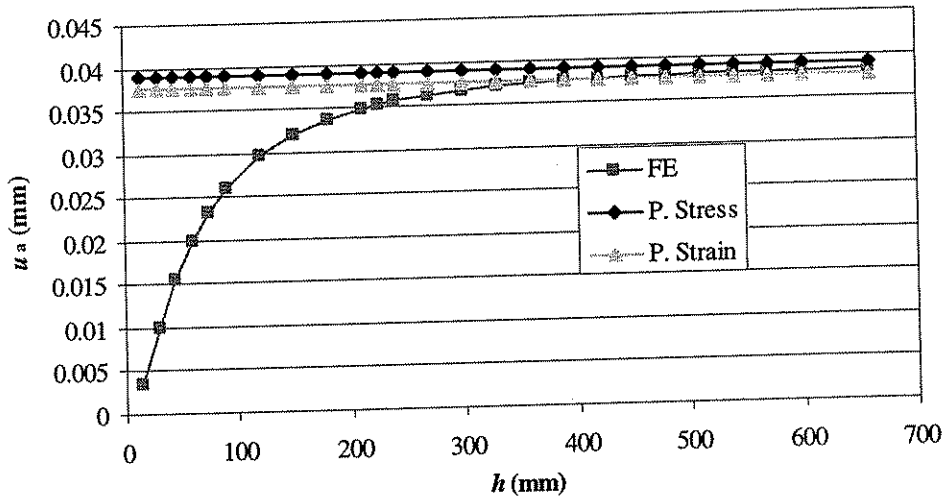
Figure 5.10 Relieved displacement in radial direction at measurement point a versus core-hole depth for the in-situ stress state of $\sigma_{xx}=10$ MPa, $\sigma_{yy}=\tau_{xy}=0$.
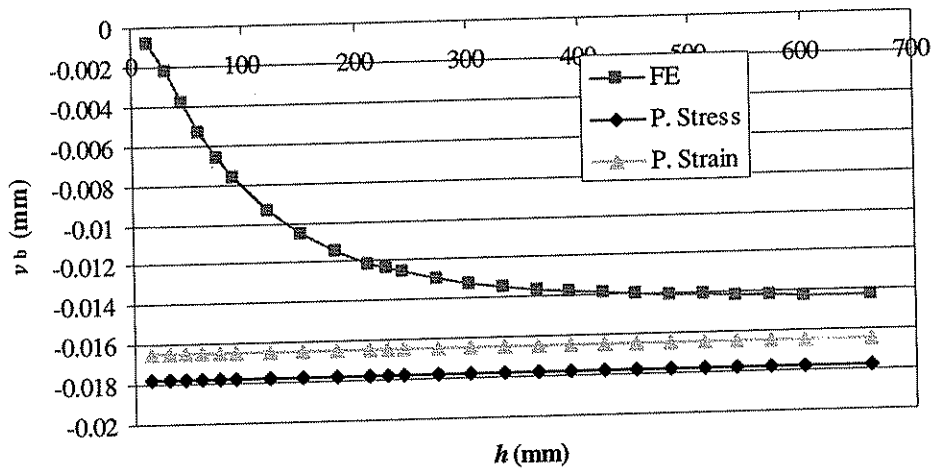
Figure 5.11 Relieved displacement in tangential direction at measurement point b versus the core-hole depth for the in-situ stress state of $\sigma_{xx}=10$ MPa, $\sigma_{yy}=\tau_{xy}=0$.

126
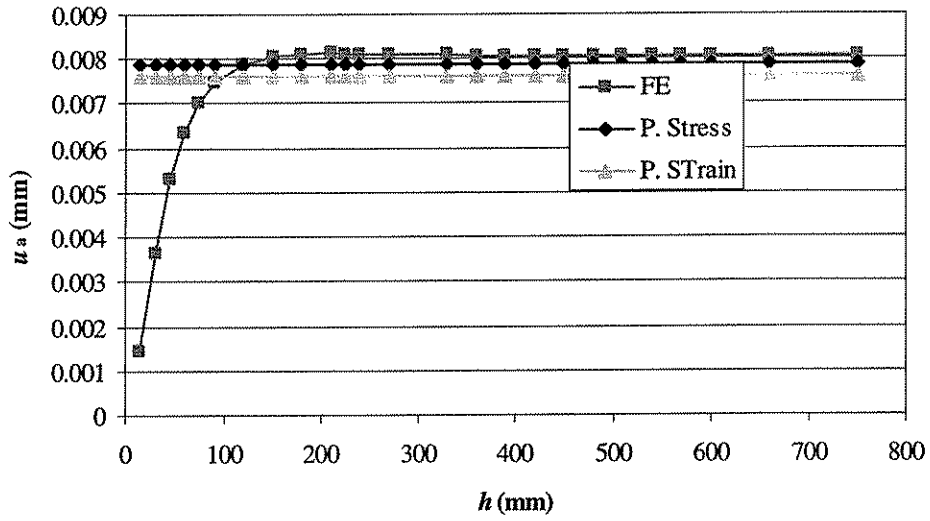
Figure 5.12 Relieved displacement in radial direction at measurement point b versus the core-hole depth for the in-situ stress state of Kx=0.2 MPa/mm, Ky=0, σ_{xx}=0, σ_{yy}= τ_{xy}=0.
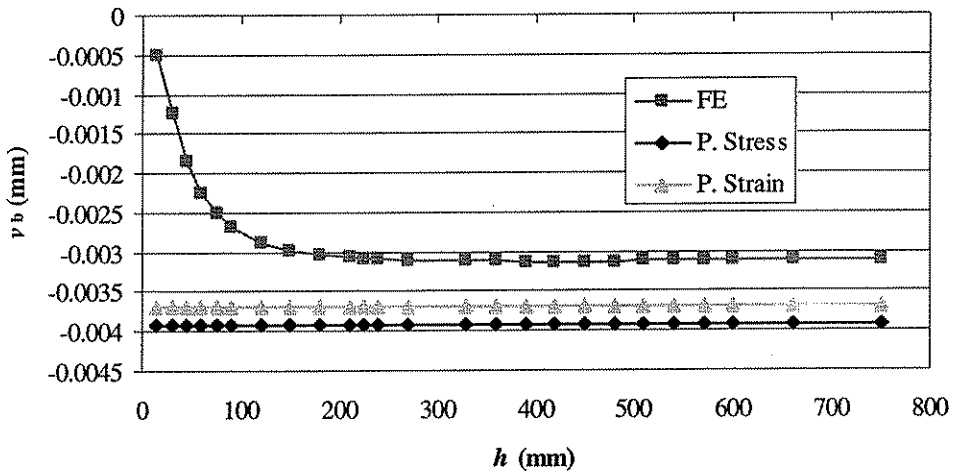
Figure 5.13 Relieved displacement in tangential direction at measurement point b versus the core-hole drilling for the in-situ stress state of Kx=0.2 MPa/mm, Ky=0, σ_{xx}=0, σ_{yy}= τ_{xy}=0.

127
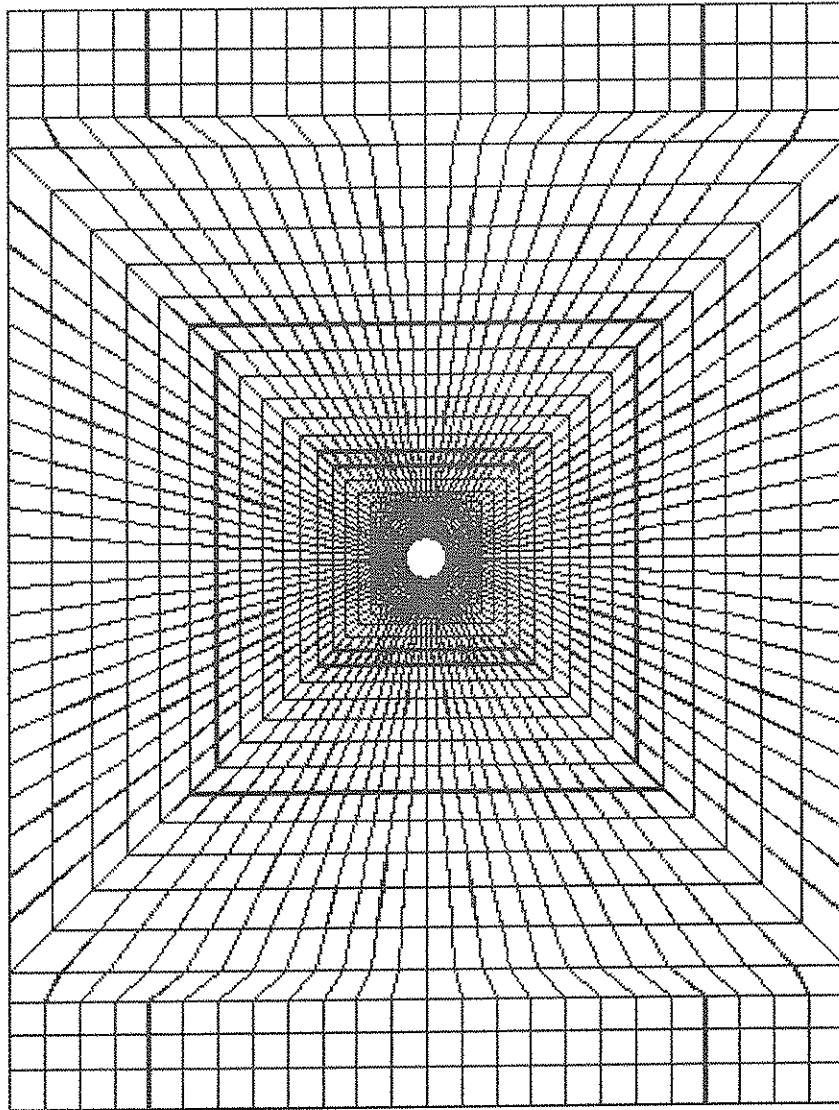
Figure 5.14 Finite element model used to evaluate object width.
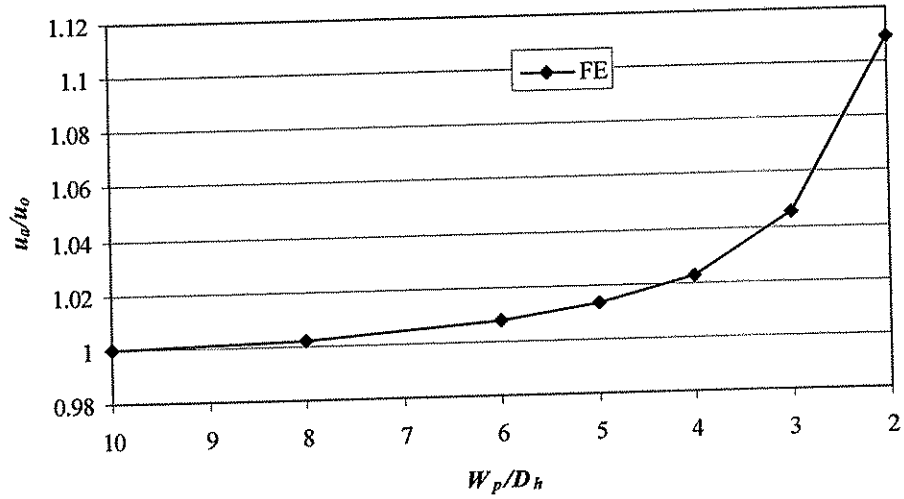
Figure 5.15 Relieved displacement in radial direction at measurement point a versus the object width for the in-situ stress state of σ_{xx}=10 MPa, σ_{yy}= τ_{xy}=0.
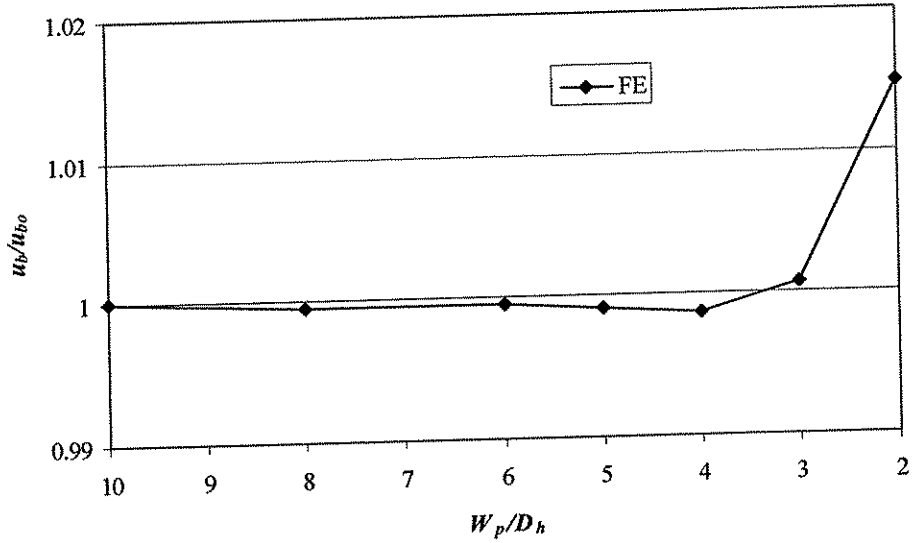
Figure 5.16 Relieved displacement in radial direction at measurement point b versus the object width for the in-situ stress state of σ_{xx}=10 MPa, σ_{yy}= τ_{xy}=0.
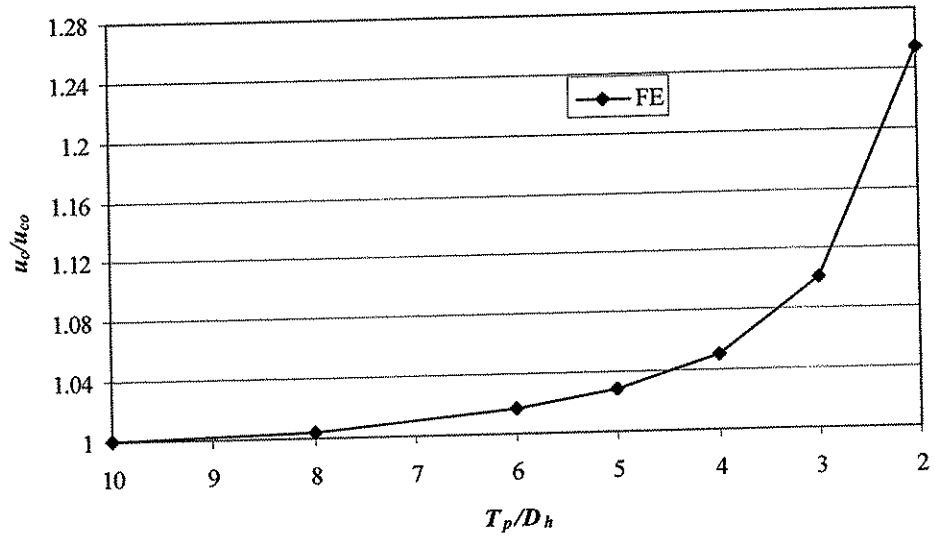
Figure 5.17 Relieved displacement in radial direction at measurement point c versus the object width for the in-situ stress state of σ_{xx}=10 MPa, σ_{yy}= τ_{xy}=0.
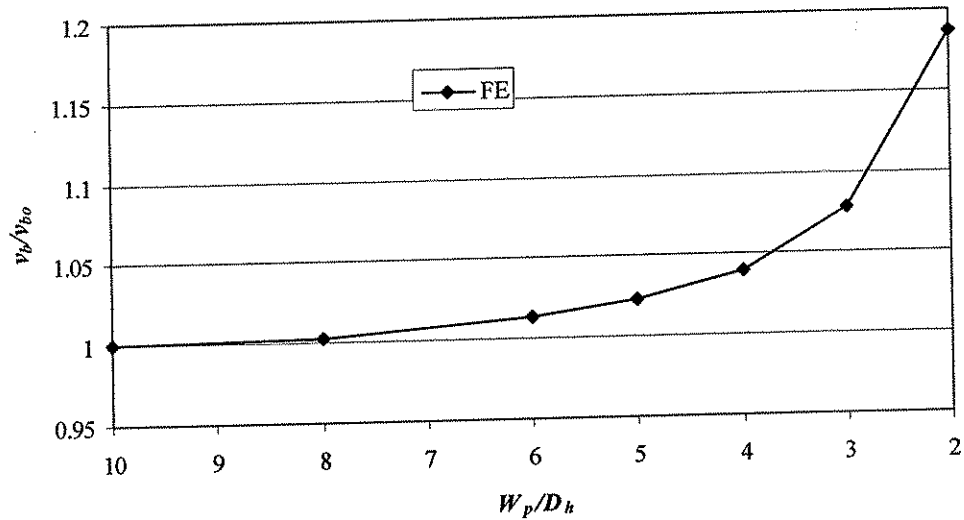
Figure 5.18 Relieved displacement in tangential direction at measurement point b versus the object width for the in-situ stress state of σ_{xx}=10 MPa, σ_{yy}= τ_{xy}=0.
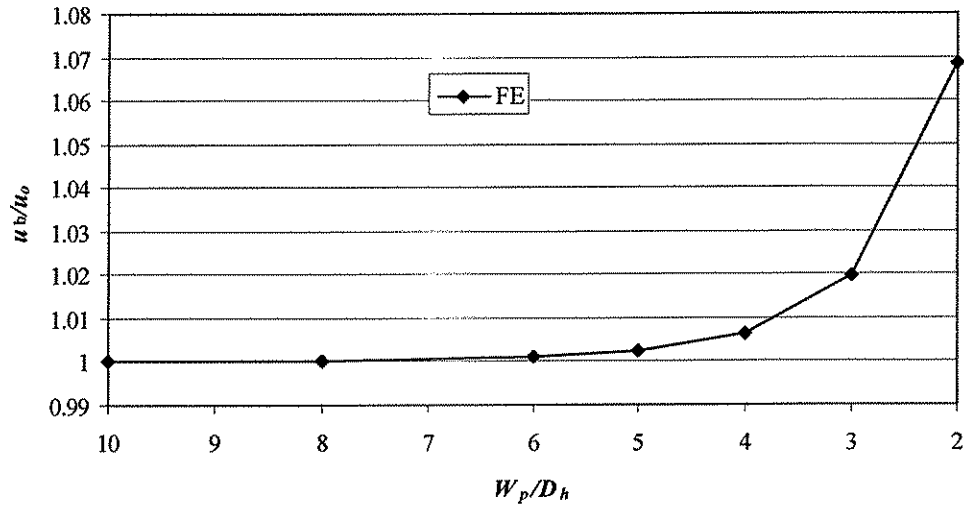
Figure 5.19 Relieved displacement in radial direction at measurement point b versus the object width for the in-situ stress state of Kx=0.2 MPa/mm, Ky=0.1 MPa/mm, σ_{xx}=0, $\sigma_{yy}= \tau_{xy}$=0.
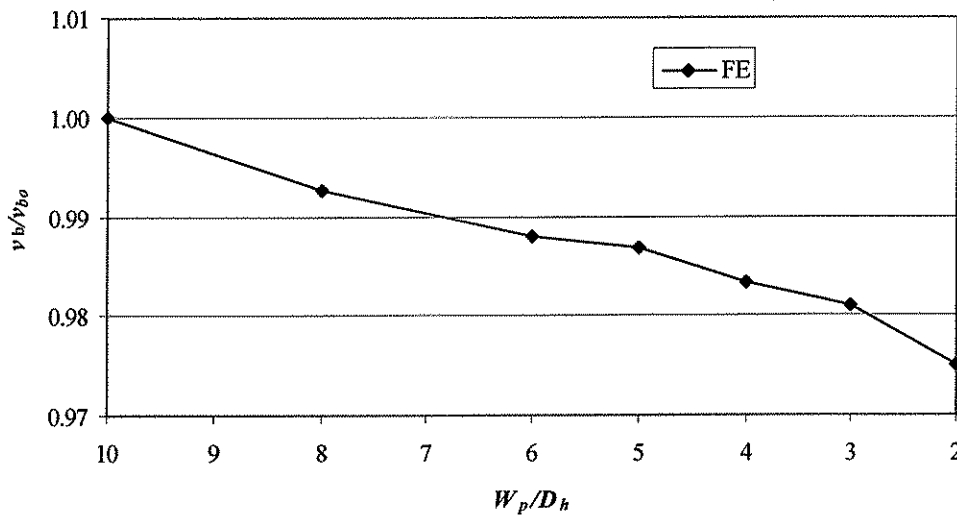
Figure 5.20 Relieved displacement in tangential direction at measurement point b versus the object width for the in-situ stress state of Kx=0.2 MPa/mm, Ky=0.1 MPa/mm, σ_{xx}=0, $\sigma_{yy}= \tau_{xy}$=0.
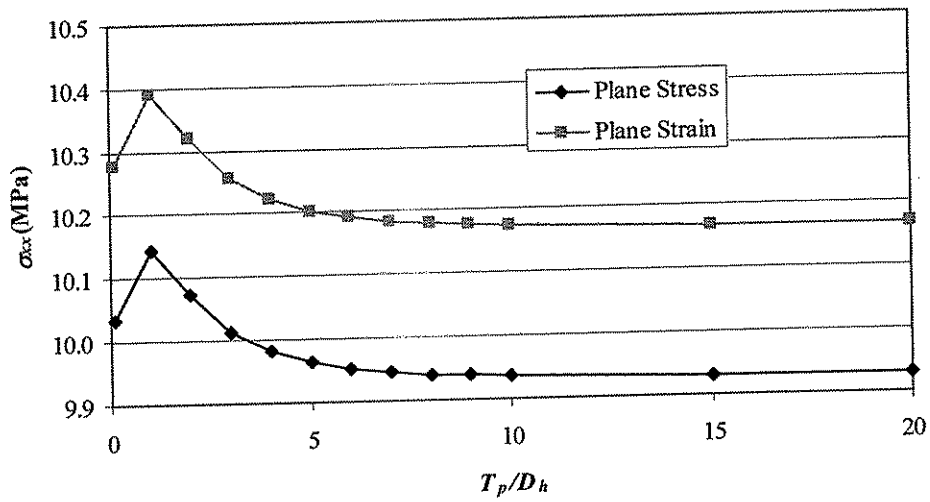
Figure 5.21 Calculated in-situ stress σ_{xx} versus the object thickness for Test Configuration A.
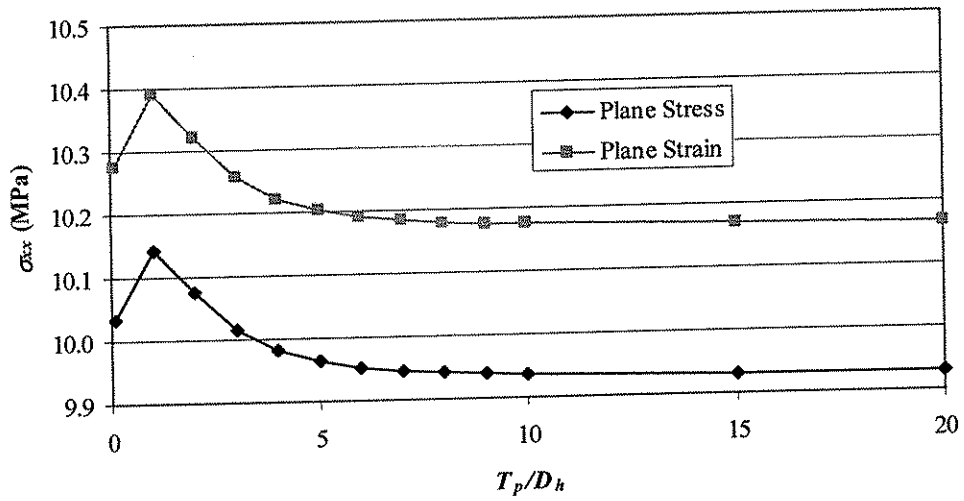
Figure 5.22 Calculated in-situ stress σ_{xx} versus the object thickness for Test Configuration B.

132
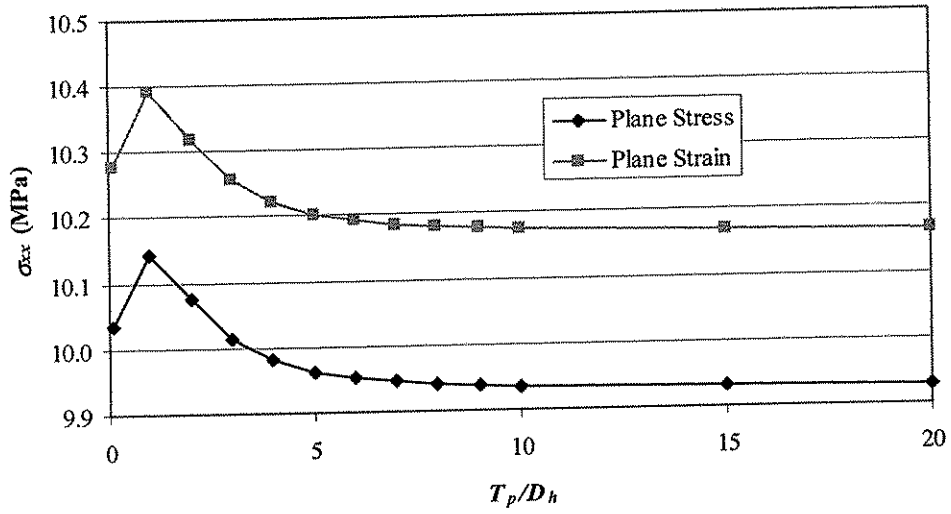
Figure 5.23 Calculated in-situ stress σ_{xx} versus the object thickness for Test Configuration C.
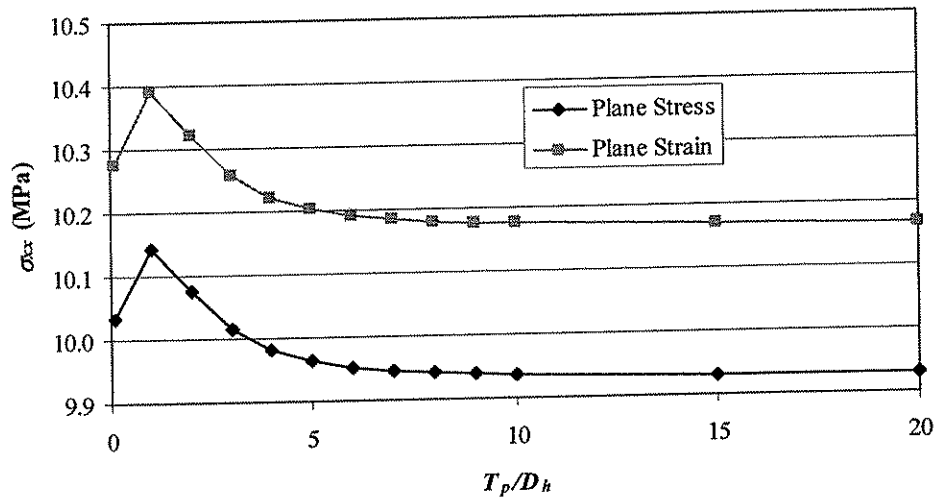
Figure 5.24 Calculated in-situ stress σ_{xx} versus the object thickness for Test Configuration D.
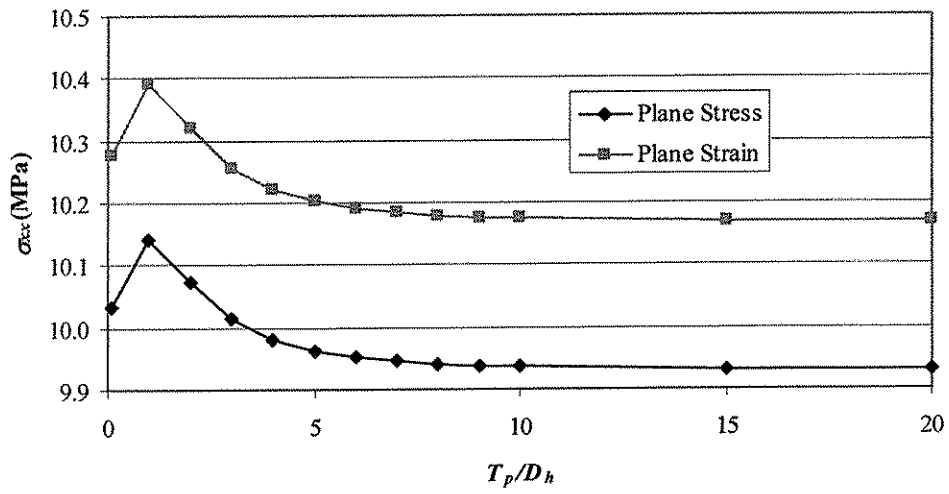
Figure 5.25 Calculated in-situ stress σ_{xx} versus the object thickness for Test Configuration E.
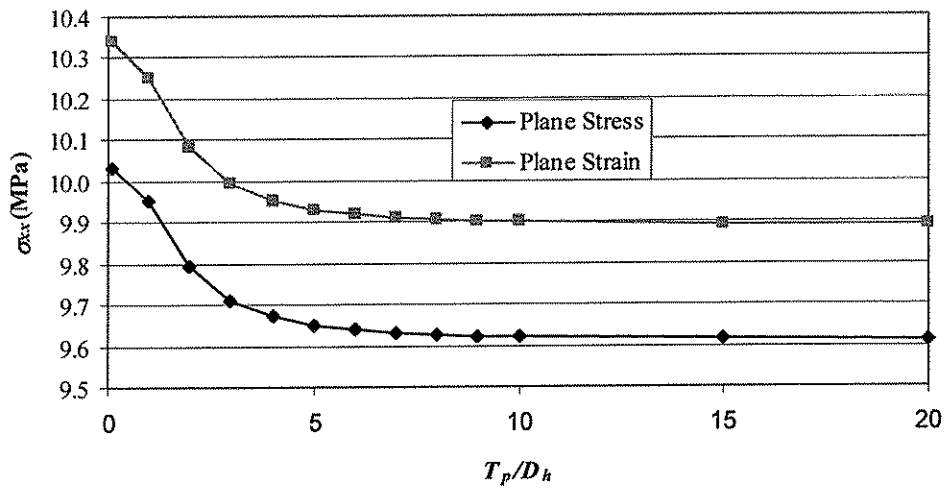
Figure 5.26 Calculated in-situ stress σ_{xx} versus the object thickness for Test Configuration F.
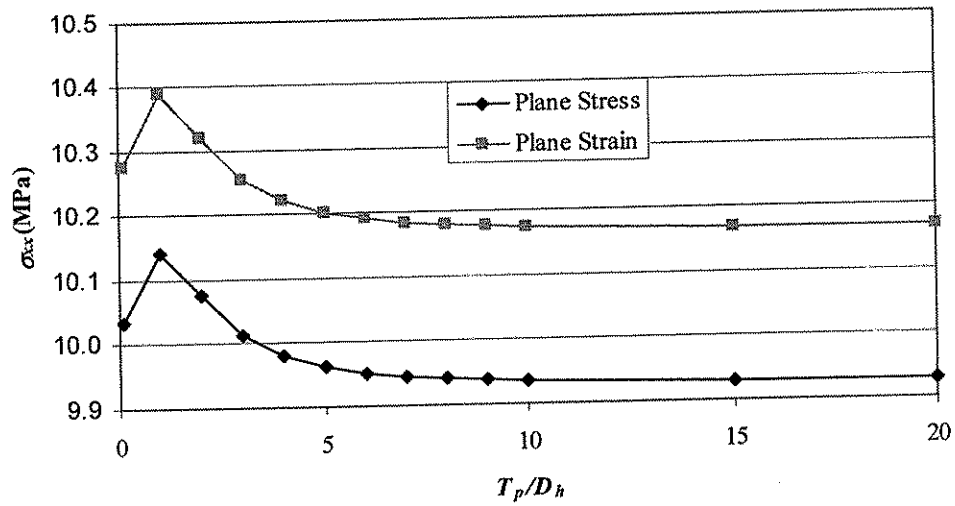
Figure 5.27 Calculated in-situ stress σ_{xx} versus the object thickness for Test Configuration G.
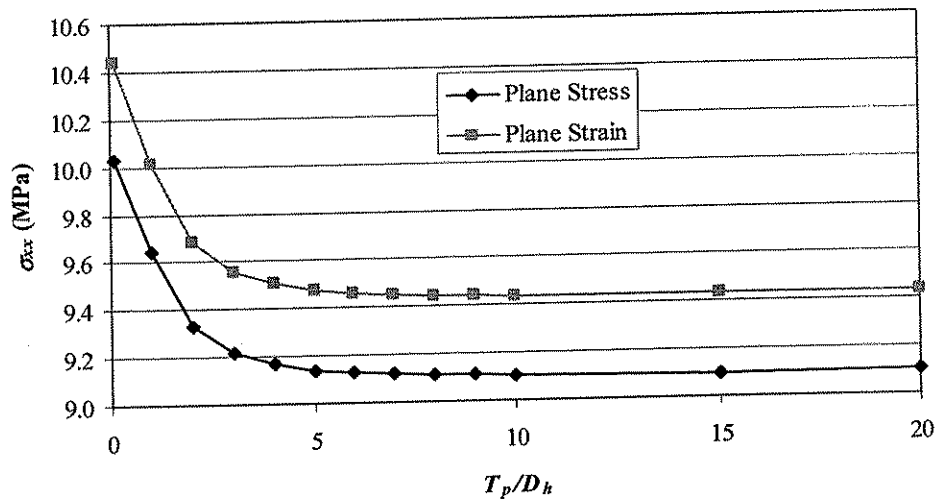
Figure 5.28 Calculated in-situ stress σ_{xx} versus the object thickness for Test Configuration H.
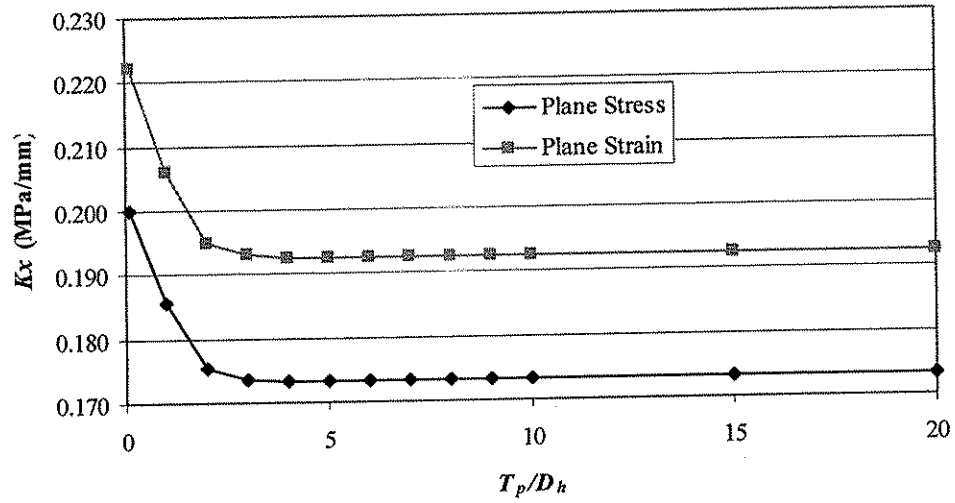
Figure 5.29 Calculated in-situ stress *Kx* versus the object thickness for Test Configuration L.
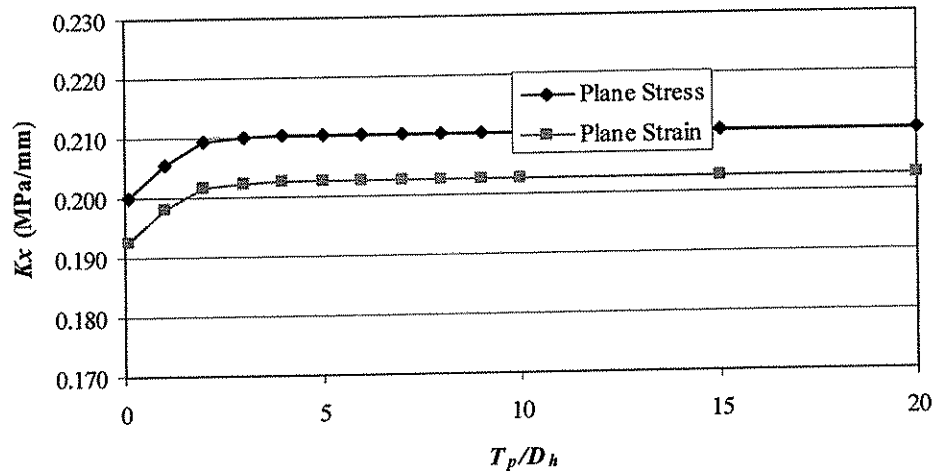
Figure 5.30 Calculated in-situ stress *Kx* versus the object thickness for Test Configuration M.
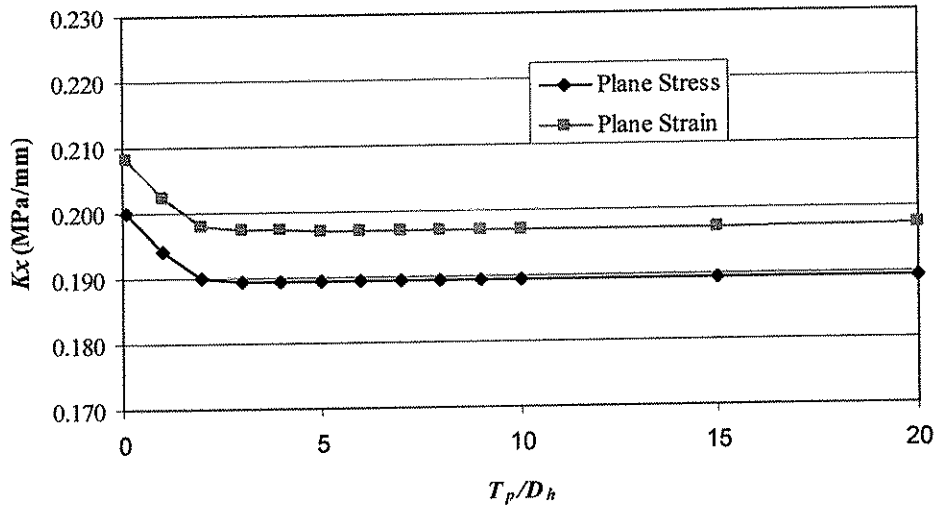
Figure 5.31 Calculated in-situ stress Kx versus the object thickness for Test Configuration P.
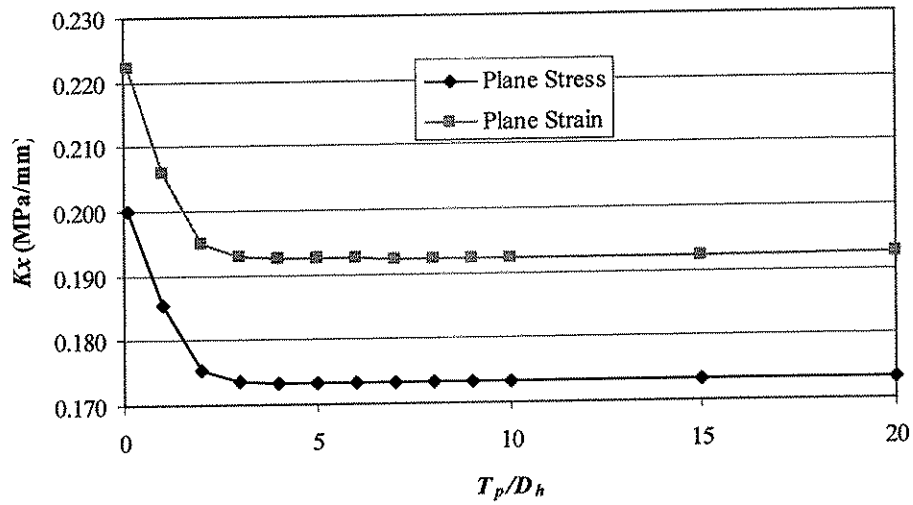
Figure 5.32 Calculated in-situ stress Kx versus the object thickness for Test Configuration Q.
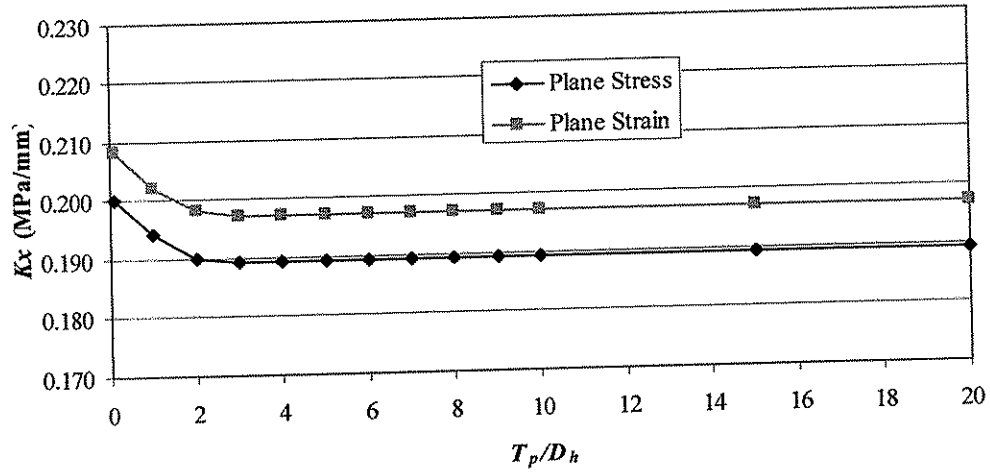
Figure 5.33 Calculated in-situ stress Kx versus the object thickness for Test Configuration R.
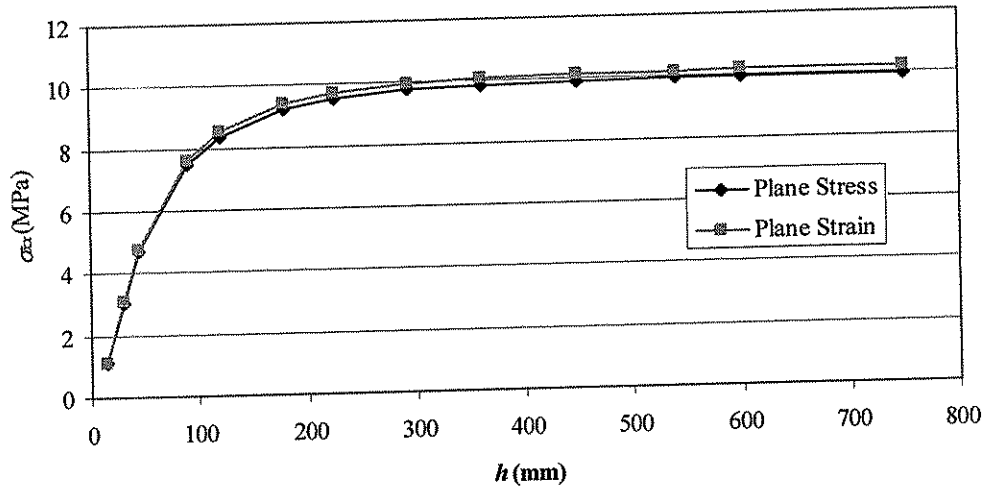
Figure 5.34 Calculated in-situ stress σ_{xx} versus the core-hole depth for Test Configuration A.
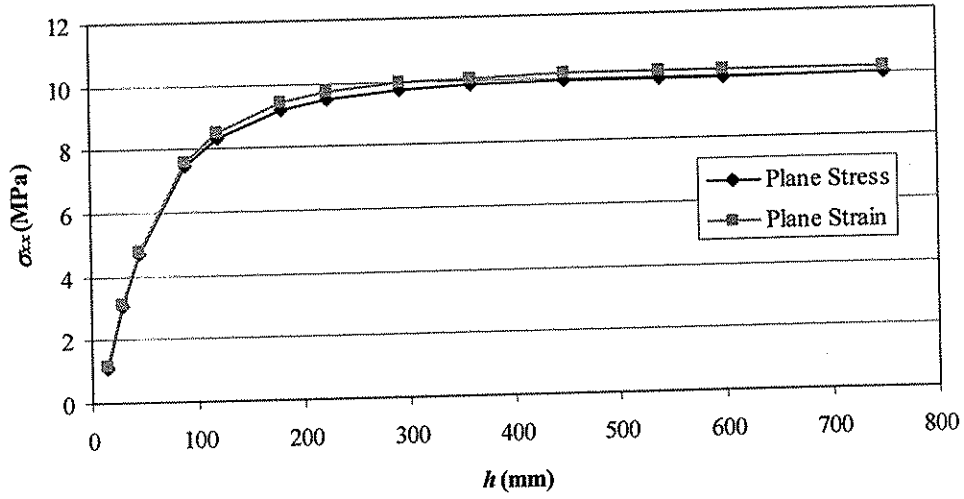
Figure 5.35 Calculated in-situ stress σ_{xx} versus the core-hole depth for Test Configuration B
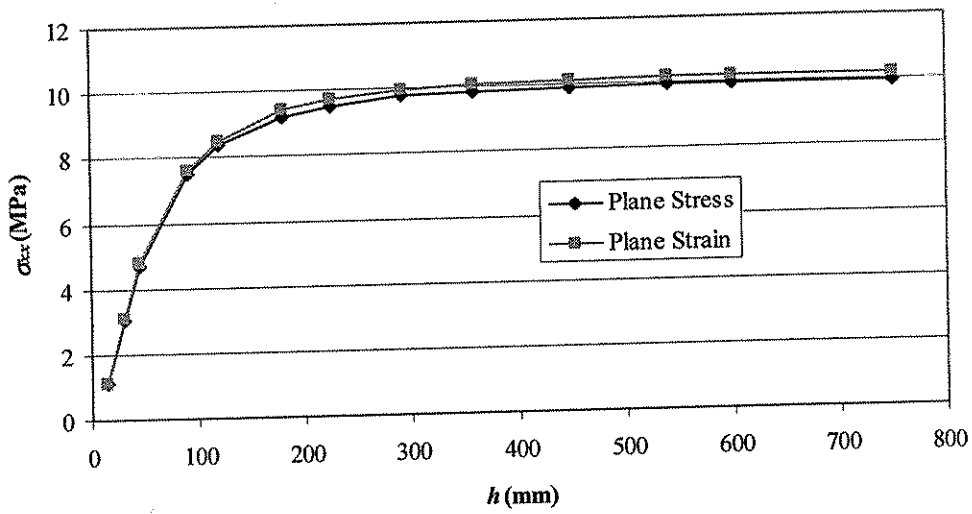
Figure 5.36 Calculated in-situ stress σ_{xx} versus the core-hole depth for Test Configuration C.
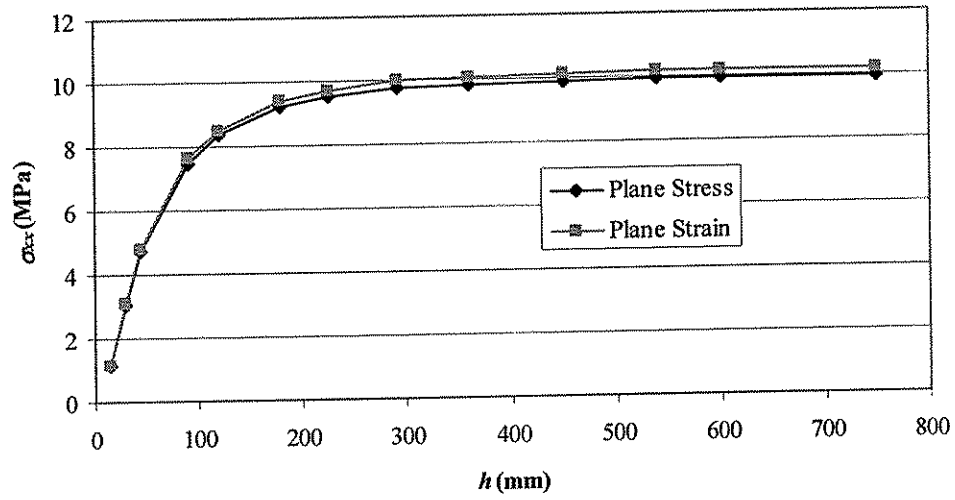
Figure 5.37 Calculated in-situ stress σ_{xx} versus the core-hole depth for Test Configuration D.
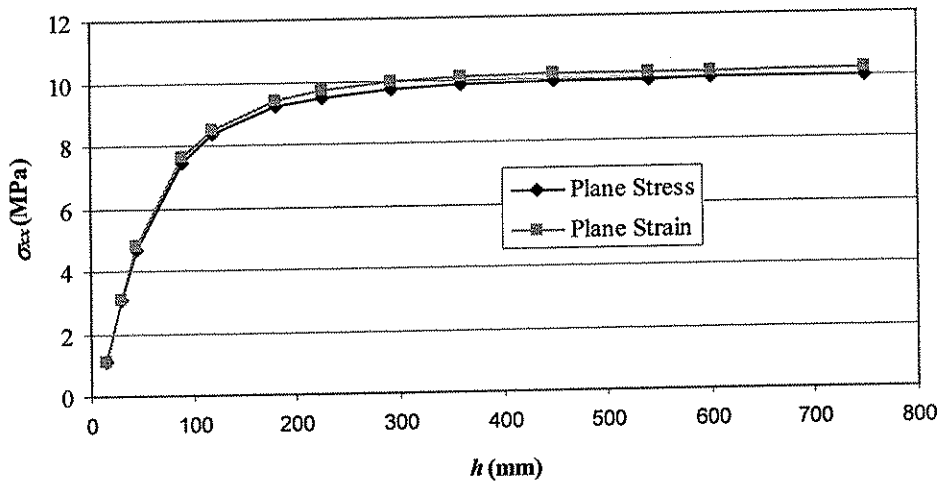
Figure 5.38 Calculated in-situ stress σ_{xx} versus the core-hole depth for Test Configuration E.
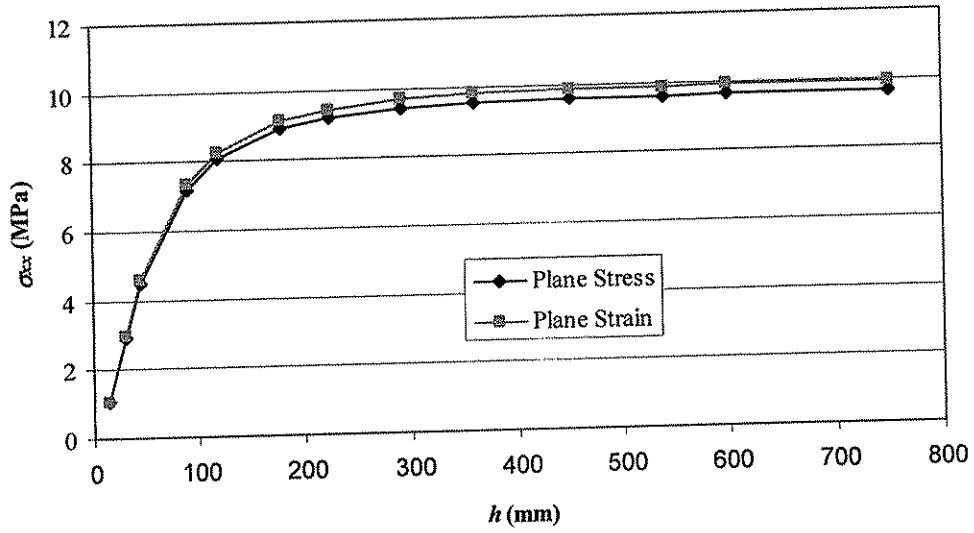
Figure 5.39 Calculated in-situ stress σ_{xx} versus the core-hole depth for Test Configuration F.
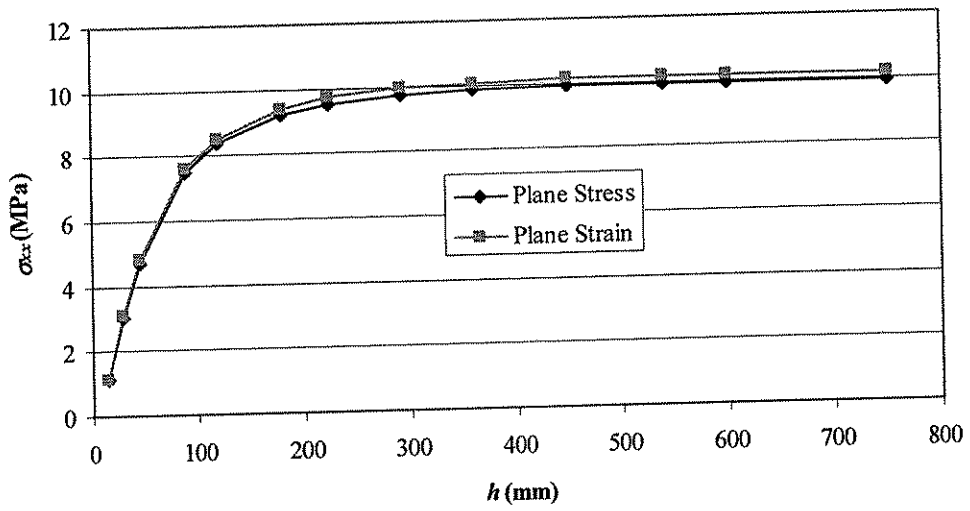
Figure 5.40 Calculated in-situ stress σ_{xx} versus the core-hole depth for Test Configuration G.
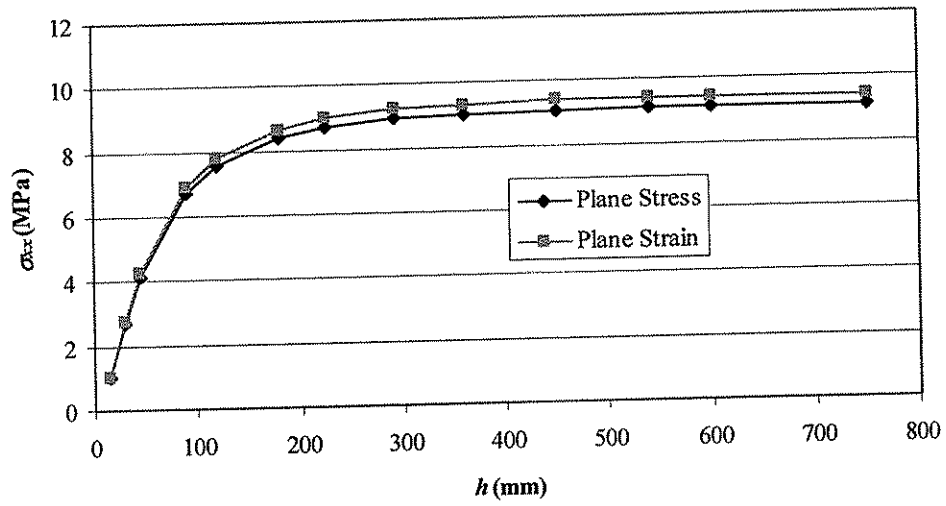
Figure 5.41 Calculated in-situ stress σ_{xx} versus the core-hole depth for Test Configuration H.
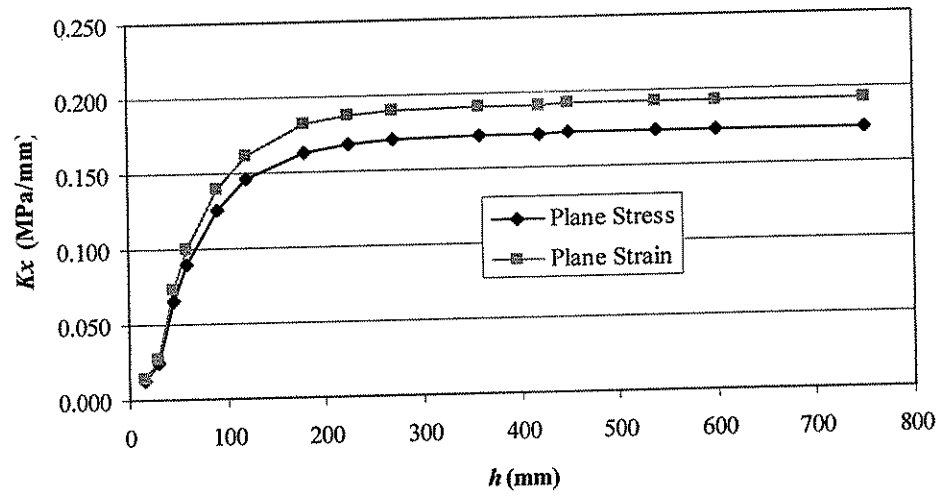
Figure 5.42 Calculated in-situ stress Kx versus the core-hole depth for Test Configuration L.
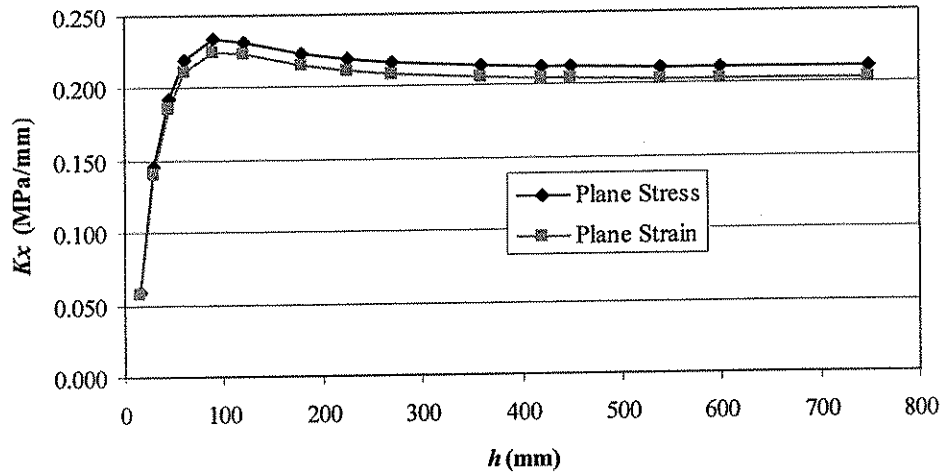
Figure 5.43 Calculated in-situ stress *Kx* versus the core-hole depth for Test Configuration M.
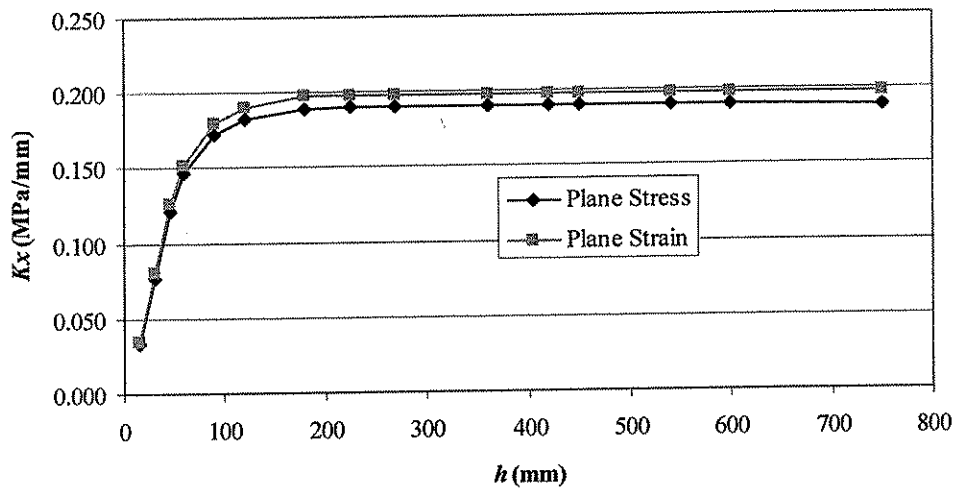
Figure 5.44 Calculated in-situ stress *Kx* versus the core-hole depth for Test Configuration P.
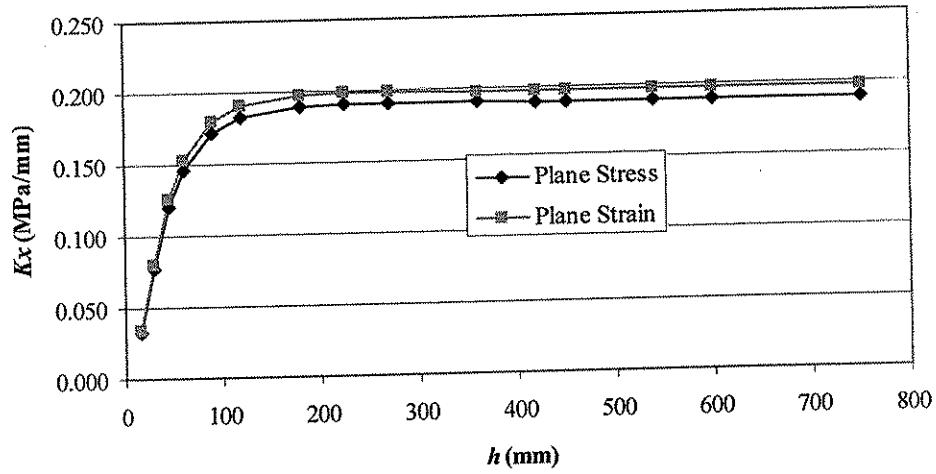
Figure 5.45 Calculated in-situ stress *Kx* versus the core-hole depth for Test Configuration Q.
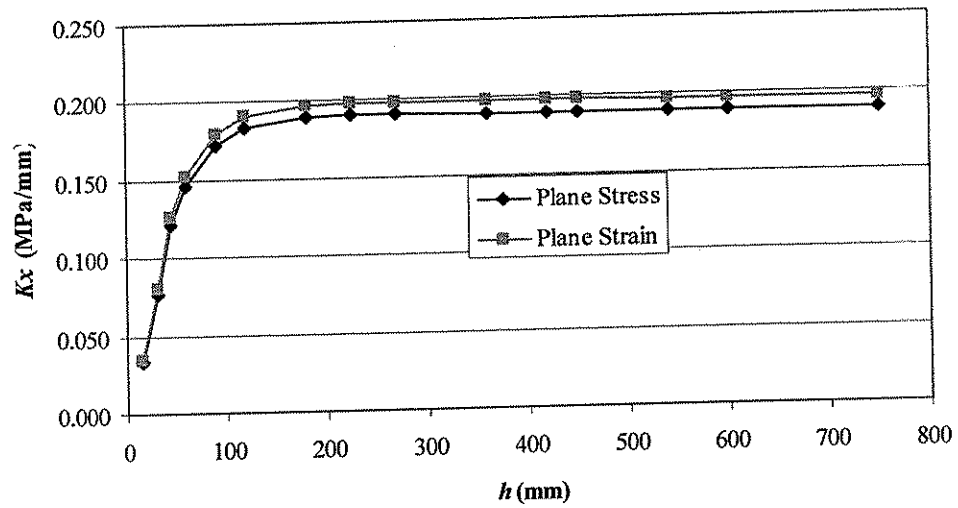
Figure 5.46 Calculated in-situ stress *Kx* versus the core-hole depth for Test Configuration R.
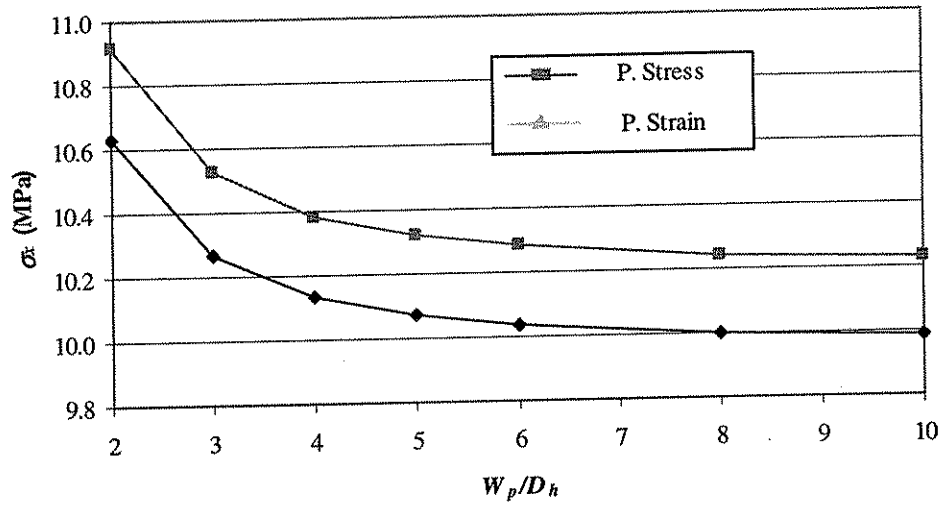
Figure 5.47 Calculated in-situ stress σ_{xx} versus the object width for Test Configuration A.
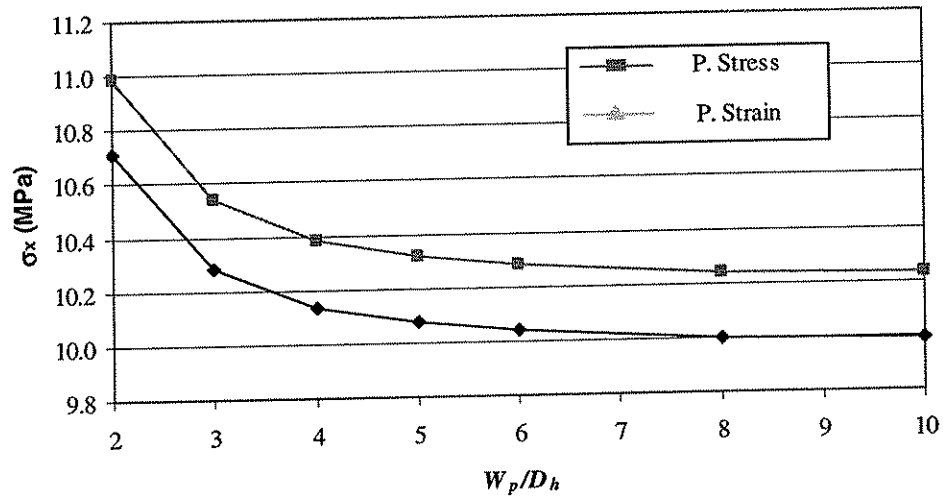
Figure 5.48 Calculated in-situ stress σ_{xx} versus the object width for Test Configuration B.
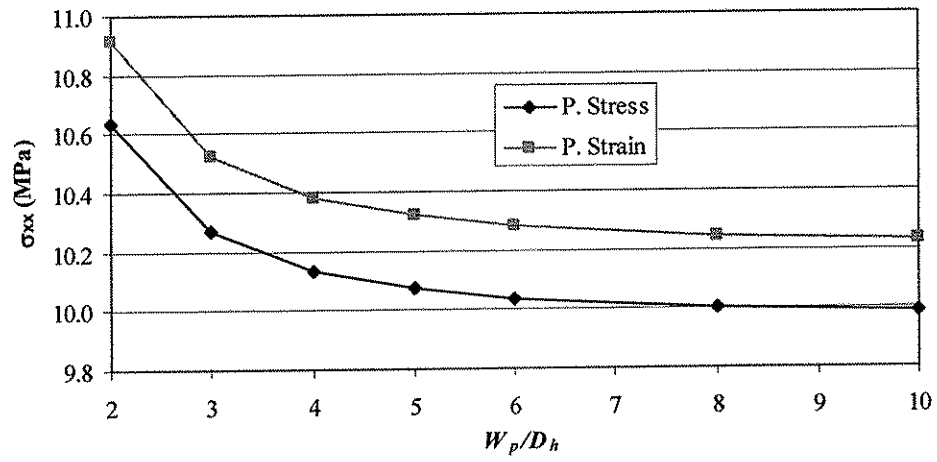
Figure 5.49 Calculated in-situ stress σ_{xx} versus the object width for Test Configuration C.
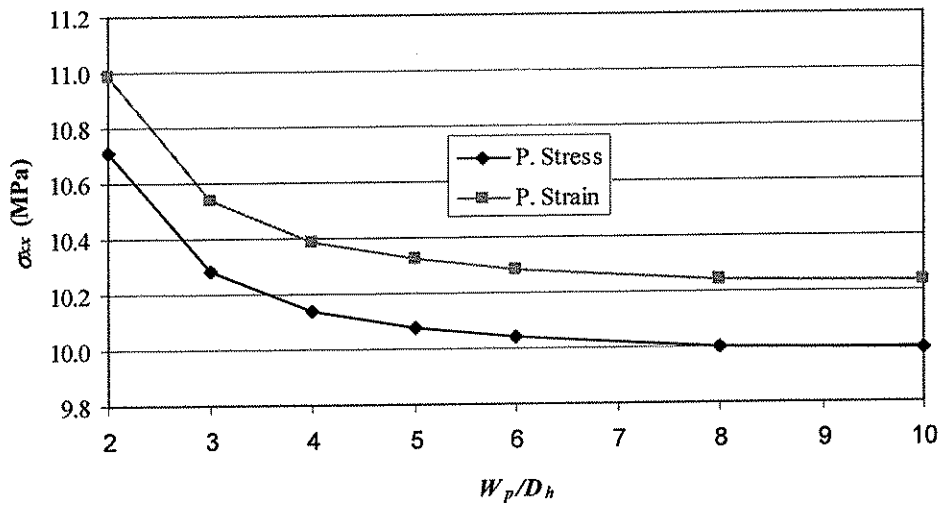
Figure 5.50 Calculated in-situ stress σ_{xx} versus the object width for Test Configuration D.

146
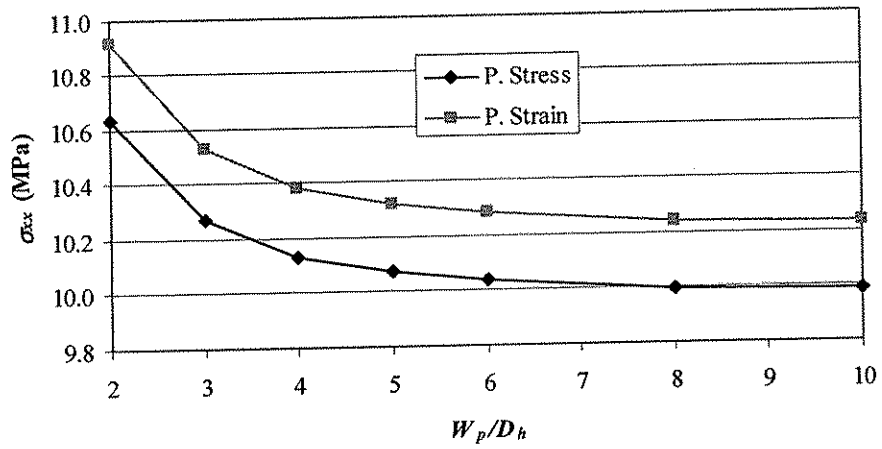
Figure 5.51 Calculated in-situ stress σ_{xx} versus the object width for Test Configuration E.
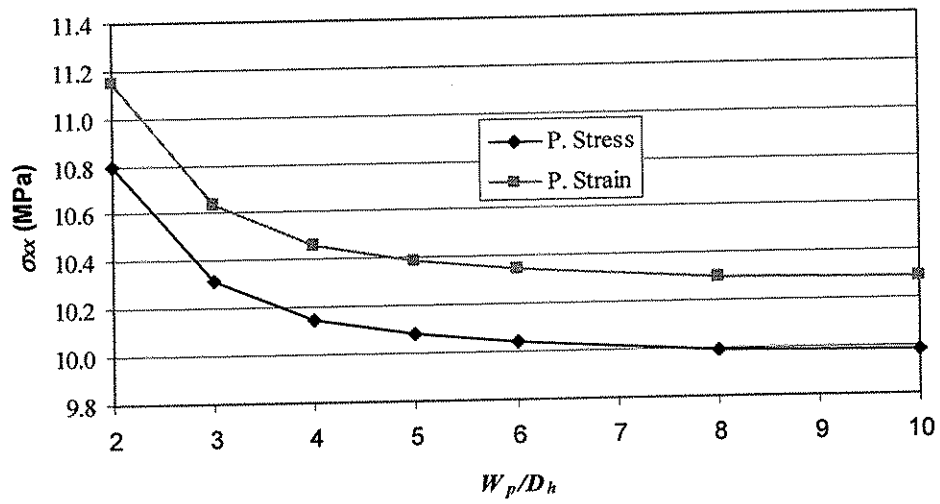
Figure 5.52 Calculated in-situ stress σ_{xx} versus the object width for Test Configuration F.
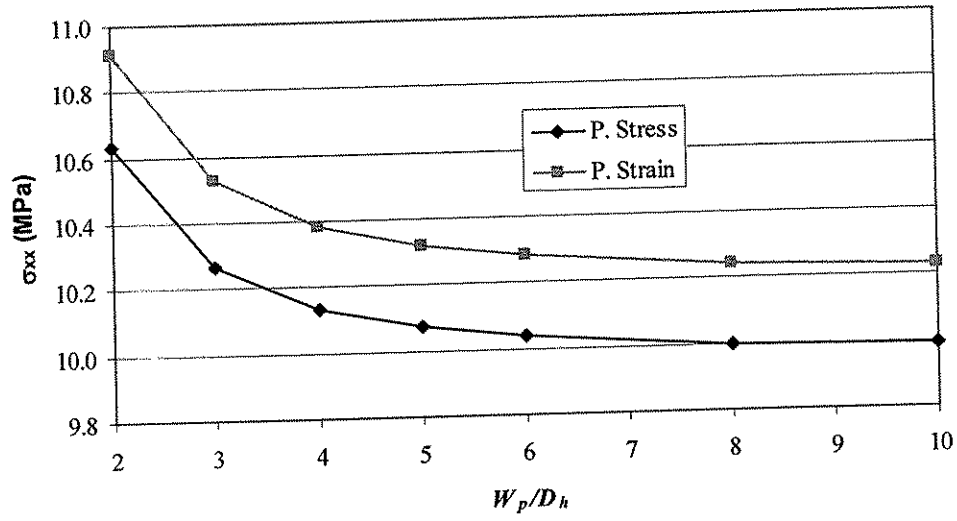
Figure 5.53 Calculated in-situ stress σ_{xx} versus the object width for Test Configuration G.
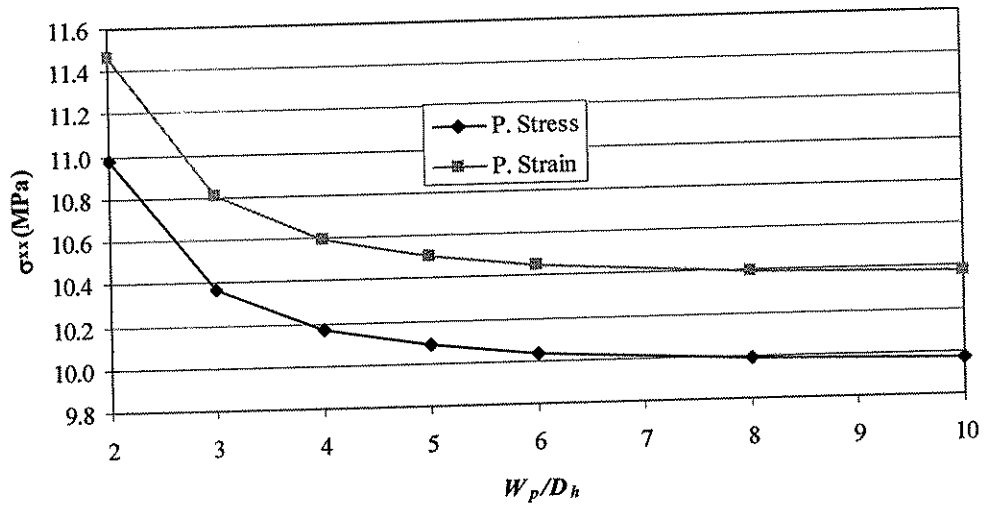
Figure 5.54 Calculated in-situ stress σ_{xx} versus the object width for Test Configuration H.
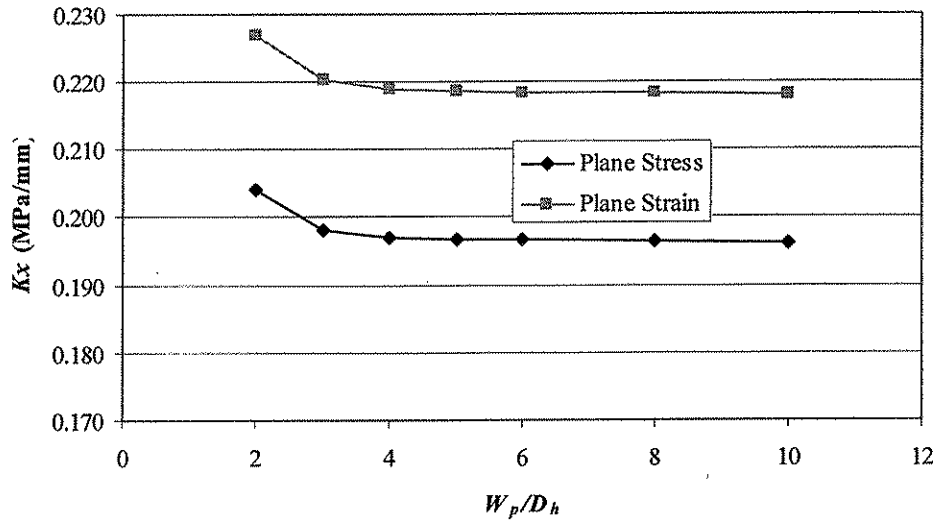
Figure 5.55 Calculated in-situ stress *Kx* versus the object width for Test Configuration L.
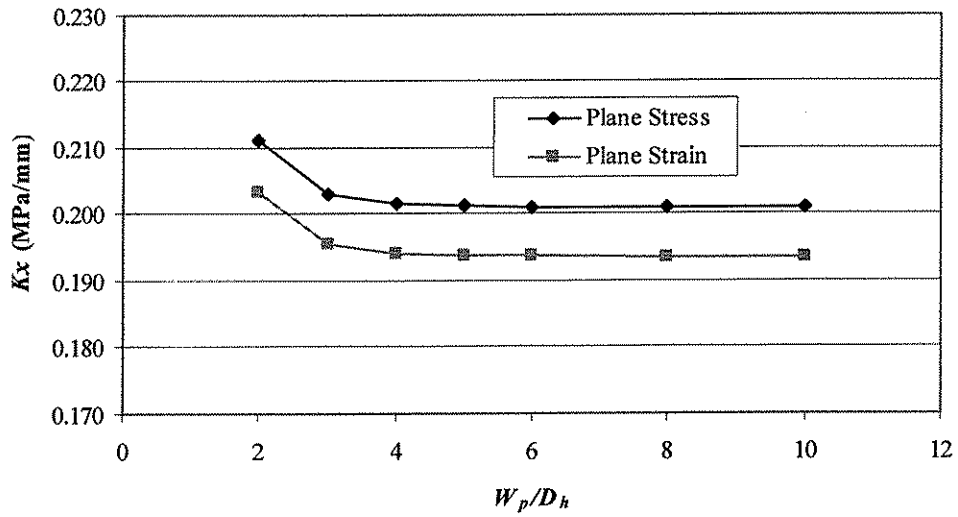
Figure 5.56 Calculated in-situ stress *Kx* versus the object width for Test Configuration M.
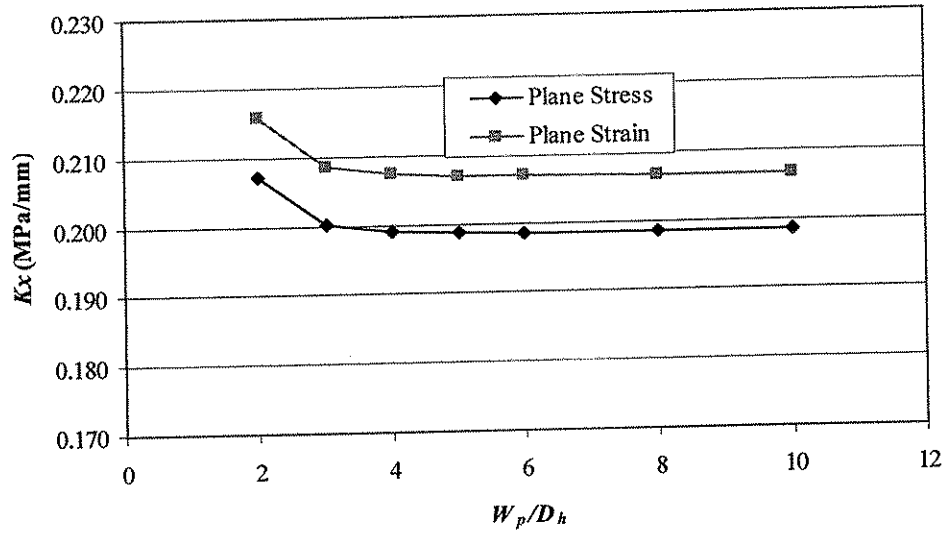
Figure 5.57 Calculated in-situ stress Kx versus the object width for Test Configuration Q.
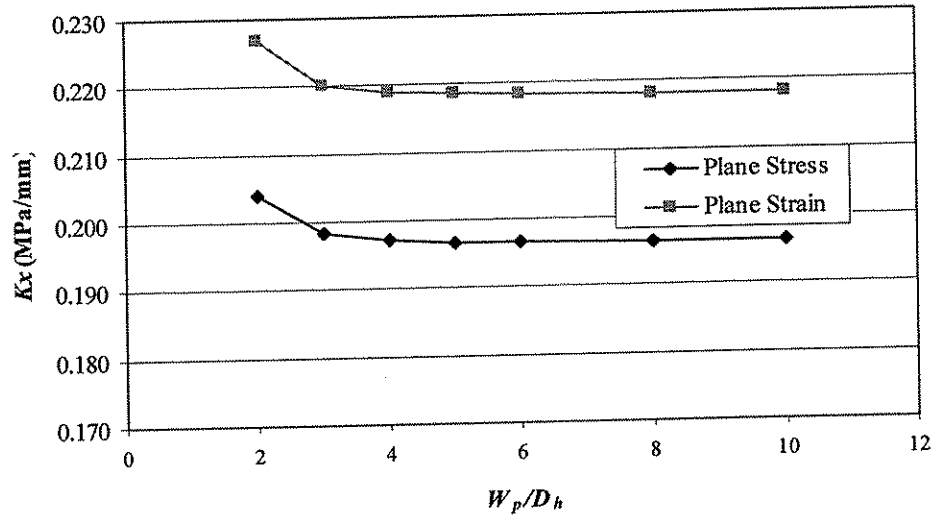
Figure 5.58 Calculated in-situ stress Kx versus the object width for Test Configuration P.
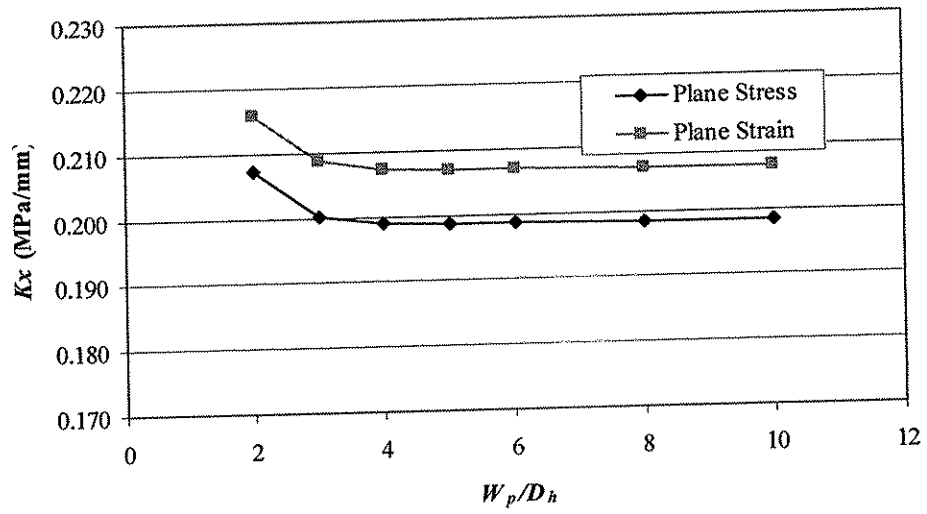
Figure 5.59 Calculated in-situ stress *Kx* versus the object width for Test Configuration R.

Configuration A								
T_p/D_h	Plane Stress (MPa)				Plane Strain (MPa)			
	σ_{xx}	σ_{yy}	τ_{xy}	$\%\sigma_{xx}$	σ_{xx}	σ_{yy}	τ_{xy}	$\%\sigma_{xx}$
0	10.0335	-0.0175	0.0000	-0.33	10.2766	-0.2606	0.0000	-2.77
1	10.1425	-0.1265	0.0000	-1.43	10.3909	-0.3749	0.0000	-3.91
2	10.0747	-0.0587	0.0000	-0.75	10.3198	-0.3038	0.0000	-3.20
3	10.0141	0.0019	0.0000	-0.14	10.2563	-0.2403	0.0000	-2.56
4	9.9810	0.0350	0.0000	0.19	10.2216	-0.2056	0.0000	-2.22
5	9.9628	0.0532	0.0000	0.37	10.2026	-0.1866	0.0000	-2.03
6	9.9521	0.0639	0.0000	0.48	10.1913	-0.1753	0.0000	-1.91
7	9.9455	0.0705	0.0000	0.54	10.1845	-0.1685	0.0000	-1.84
8	9.9410	0.0750	0.0000	0.59	10.1797	-0.1637	0.0000	-1.80
9	9.9381	0.0779	0.0000	0.62	10.1766	-0.1606	0.0000	-1.77
10	9.9358	0.0802	0.0000	0.64	10.1743	-0.1583	0.0000	-1.74
15	9.9308	0.0852	0.0000	0.69	10.1690	-0.1530	0.0000	-1.69
20	9.9294	0.0866	0.0000	0.71	10.1676	-0.1516	0.0000	-1.68

Table 5.1 Evaluation of uniform in-situ stress equations for Test Configuration A to the object thickness.

Configuration B								
T_p/D_h	Plane Stress (MPa)				Plane Strain (MPa)			
	σ_{xx}	σ_{yy}	τ_{xy}	$\%\sigma_{xx}$	σ_{xx}	σ_{yy}	τ_{xy}	$\%\sigma_{xx}$
0	10.0335	-0.0175	0.0000	-0.33	10.2766	-0.2606	0.0000	-2.77
1	10.1425	-0.1265	0.0000	-1.43	10.3909	-0.3749	0.0000	-3.91
2	10.0747	-0.0587	0.0000	-0.75	10.3198	-0.3038	0.0000	-3.20
3	10.0141	0.0019	0.0000	-0.14	10.2563	-0.2403	0.0000	-2.56
4	9.9810	0.0350	0.0000	0.19	10.2216	-0.2056	0.0000	-2.22
5	9.9628	0.0532	0.0000	0.37	10.2026	-0.1866	0.0000	-2.03
6	9.9521	0.0639	0.0000	0.48	10.1913	-0.1753	0.0000	-1.91
7	9.9455	0.0705	0.0000	0.54	10.1845	-0.1685	0.0000	-1.84
8	9.9410	0.0750	0.0000	0.59	10.1797	-0.1637	0.0000	-1.80
9	9.9381	0.0779	0.0000	0.62	10.1766	-0.1606	0.0000	-1.77
10	9.9358	0.0802	0.0000	0.64	10.1743	-0.1583	0.0000	-1.74
15	9.9308	0.0852	0.0000	0.69	10.1690	-0.1530	0.0000	-1.69
20	9.9294	0.0866	0.0000	0.71	10.1676	-0.1516	0.0000	-1.68

Table 5.2 Evaluation of uniform in-situ stress equations for Test Configuration B to the object thickness.

Configuration C								
	Plane Stress (MPa)				Plane Strain (MPa)			
T_p/D_h	σ_{xx}	σ_{yy}	τ_{xy}	$\%\sigma_{xx}$	σ_{xx}	σ_{yy}	τ_{xy}	$\%\sigma_{xx}$
0	10.0335	-0.0175	0.0000	-0.33	10.2766	-0.2606	0.0000	-2.77
1	10.1425	-0.1265	0.0000	-1.43	10.3909	-0.3749	0.0000	-3.91
2	10.0747	-0.0587	0.0000	-0.75	10.3198	-0.3038	0.0000	-3.20
3	10.0141	0.0019	0.0000	-0.14	10.2563	-0.2403	0.0000	-2.56
4	9.9810	0.0350	0.0000	0.19	10.2216	-0.2056	0.0000	-2.22
5	9.9628	0.0532	0.0000	0.37	10.2026	-0.1866	0.0000	-2.03
6	9.9521	0.0639	0.0000	0.48	10.1913	-0.1753	0.0000	-1.91
7	9.9455	0.0705	0.0000	0.54	10.1845	-0.1685	0.0000	-1.84
8	9.9410	0.0750	0.0000	0.59	10.1797	-0.1637	0.0000	-1.80
9	9.9381	0.0779	0.0000	0.62	10.1766	-0.1606	0.0000	-1.77
10	9.9358	0.0802	0.0000	0.64	10.1743	-0.1583	0.0000	-1.74
15	9.9308	0.0852	0.0000	0.69	10.1690	-0.1530	0.0000	-1.69
20	9.9294	0.0866	0.0000	0.71	10.1676	-0.1516	0.0000	-1.68

Table 5.3 Evaluation of uniform in-situ stress equations for Test Configuration C to the object thickness.

Configuration D								
	Plane Stress (MPa)				Plane Strain (MPa)			
T_p/D_h	σ_{xx}	σ_{yy}	τ_{xy}	$\%\sigma_{xx}$	σ_{xx}	σ_{yy}	τ_{xy}	$\%\sigma_{xx}$
0	10.0335	-0.0175	0.0000	-0.33	10.2766	-0.2606	0.0000	-2.77
1	10.1425	-0.1265	0.0000	-1.43	10.3909	-0.3749	0.0000	-3.91
2	10.0747	-0.0587	0.0000	-0.75	10.3198	-0.3038	0.0000	-3.20
3	10.0141	0.0019	0.0000	-0.14	10.2563	-0.2403	0.0000	-2.56
4	9.9810	0.0350	0.0000	0.19	10.2216	-0.2056	0.0000	-2.22
5	9.9628	0.0532	0.0000	0.37	10.2026	-0.1866	0.0000	-2.03
6	9.9521	0.0639	0.0000	0.48	10.1913	-0.1753	0.0000	-1.91
7	9.9455	0.0705	0.0000	0.54	10.1845	-0.1685	0.0000	-1.84
8	9.9410	0.0750	0.0000	0.59	10.1797	-0.1637	0.0000	-1.80
9	9.9381	0.0779	0.0000	0.62	10.1766	-0.1606	0.0000	-1.77
10	9.9358	0.0802	0.0000	0.64	10.1743	-0.1583	0.0000	-1.74
15	9.9308	0.0852	0.0000	0.69	10.1690	-0.1530	0.0000	-1.69
20	9.9294	0.0866	0.0000	0.71	10.1676	-0.1516	0.0000	-1.68

Table 5.4 Evaluation of uniform in-situ stress equations for Test Configuration D to the object thickness.

Configuration E								
T_p/D_h	Plane Stress (MPa)				Plane Strain (MPa)			
	σ_{xx}	σ_{yy}	τ_{xy}	$\%\sigma_{xx}$	σ_{xx}	σ_{yy}	τ_{xy}	$\%\sigma_{xx}$
0	10.0335	-0.0175	0.0000	-0.33	10.2766	-0.2606	0.0000	-2.77
1	10.1425	-0.1265	0.0000	-1.43	10.3909	-0.3749	0.0000	-3.91
2	10.0747	-0.0587	0.0000	-0.75	10.3198	-0.3038	0.0000	-3.20
3	10.0141	0.0019	0.0000	-0.14	10.2563	-0.2403	0.0000	-2.56
4	9.9810	0.0350	0.0000	0.19	10.2216	-0.2056	0.0000	-2.22
5	9.9628	0.0532	0.0000	0.37	10.2026	-0.1866	0.0000	-2.03
6	9.9521	0.0639	0.0000	0.48	10.1913	-0.1753	0.0000	-1.91
7	9.9455	0.0705	0.0000	0.54	10.1845	-0.1685	0.0000	-1.84
8	9.9410	0.0750	0.0000	0.59	10.1797	-0.1637	0.0000	-1.80
9	9.9381	0.0779	0.0000	0.62	10.1766	-0.1606	0.0000	-1.77
10	9.9358	0.0802	0.0000	0.64	10.1743	-0.1583	0.0000	-1.74
15	9.9308	0.0852	0.0000	0.69	10.1690	-0.1530	0.0000	-1.69
20	9.9294	0.0866	0.0000	0.71	10.1676	-0.1516	0.0000	-1.68

Table 5.5 Evaluation of uniform in-situ stress equations for Test Configuration E to the object thickness.

Configuration F								
T_p/D_h	Plane Stress (MPa)				Plane Strain (MPa)			
	σ_{xx}	σ_{yy}	τ_{xy}	$\%\sigma_{xx}$	σ_{xx}	σ_{yy}	τ_{xy}	$\%\sigma_{xx}$
0	10.0326	-0.0166	0.0000	-0.33	10.3371	-0.3211	0.0000	-3.37
1	9.9508	0.0652	0.0000	0.49	10.2504	-0.2344	0.0000	-2.50
2	9.7919	0.2241	0.0000	2.08	10.0819	-0.0659	0.0000	-0.82
3	9.7101	0.3059	0.0000	2.90	9.9950	0.0210	0.0000	0.05
4	9.6704	0.3456	0.0000	3.30	9.9530	0.0630	0.0000	0.47
5	9.6496	0.3664	0.0000	3.50	9.9310	0.0850	0.0000	0.69
6	9.6376	0.3784	0.0000	3.62	9.9182	0.0978	0.0000	0.82
7	9.6302	0.3857	0.0000	3.70	9.9104	0.1056	0.0000	0.90
8	9.6253	0.3907	0.0000	3.75	9.9052	0.1108	0.0000	0.95
9	9.6221	0.3939	0.0000	3.78	9.9017	0.1142	0.0000	0.98
10	9.6196	0.3964	0.0000	3.80	9.8991	0.1169	0.0000	1.01
15	9.6143	0.4017	0.0000	3.86	9.8935	0.1225	0.0000	1.07
20	9.6138	0.4022	0.0000	3.86	9.8929	0.1231	0.0000	1.07

Table 5.6 Evaluation of uniform in-situ stress equations for Test Configuration F to the object thickness.

154

Configuration G								
T_p/D_h	Plane Stress (MPa)				Plane Strain (MPa)			
	σ_{xx}	σ_{yy}	τ_{xy}	$\%\sigma_{xx}$	σ_{xx}	σ_{yy}	τ_{xy}	$\%\sigma_{xx}$
0	10.0335	-0.0175	0.0000	-0.33	10.2766	-0.2606	0.0000	-2.77
1	10.1425	-0.1265	0.0000	-1.43	10.3909	-0.3749	0.0000	-3.91
2	10.0747	-0.0587	0.0000	-0.75	10.3198	-0.3038	0.0000	-3.20
3	10.0141	0.0019	0.0000	-0.14	10.2563	-0.2403	0.0000	-2.56
4	9.9810	0.0350	0.0000	0.19	10.2216	-0.2056	0.0000	-2.22
5	9.9628	0.0532	0.0000	0.37	10.2026	-0.1866	0.0000	-2.03
6	9.9521	0.0639	0.0000	0.48	10.1913	-0.1753	0.0000	-1.91
7	9.9455	0.0705	0.0000	0.54	10.1845	-0.1685	0.0000	-1.84
8	9.9410	0.0750	0.0000	0.59	10.1797	-0.1637	0.0000	-1.80
9	9.9381	0.0779	0.0000	0.62	10.1766	-0.1606	0.0000	-1.77
10	9.9358	0.0802	0.0000	0.64	10.1743	-0.1583	0.0000	-1.74
15	9.9308	0.0852	0.0000	0.69	10.1690	-0.1530	0.0000	-1.69
20	9.9294	0.0866	0.0000	0.71	10.1676	-0.1516	0.0000	-1.68

Table 5.7 Evaluation of uniform in-situ stress equations for Test Configuration G to the object thickness.

Configuration H								
T_p/D_h	Plane Stress (MPa)				Plane Strain (MPa)			
	σ_{xx}	σ_{yy}	τ_{xy}	$\%\sigma_{xx}$	σ_{xx}	σ_{yy}	τ_{xy}	$\%\sigma_{xx}$
0	10.0311	-0.0151	0.0000	-0.31	10.4384	-0.4224	0.0000	-4.38
1	9.6393	0.3767	0.0000	3.61	10.0149	0.0011	0.0000	-0.15
2	9.3325	0.6835	0.0000	6.68	9.6831	0.3329	0.0000	3.17
3	9.2161	0.7999	0.0000	7.84	9.5573	0.4587	0.0000	4.43
4	9.1657	0.8503	0.0000	8.34	9.5028	0.5132	0.0000	4.97
5	9.1407	0.8753	0.0000	8.59	9.4758	0.5402	0.0000	5.24
6	9.1266	0.8894	0.0000	8.73	9.4606	0.5554	0.0000	5.39
7	9.1179	0.8981	0.0000	8.82	9.4511	0.5649	0.0000	5.49
8	9.1123	0.9037	0.0000	8.88	9.4451	0.5709	0.0000	5.55
9	9.1086	0.9074	0.0000	8.91	9.4411	0.5749	0.0000	5.59
10	9.1058	0.9102	0.0000	8.94	9.4381	0.5779	0.0000	5.62
15	9.0999	0.9161	0.0000	9.00	9.4317	0.5843	0.0000	5.68
20	9.1008	0.9152	0.0000	8.99	9.4326	0.5834	0.0000	5.67

Table 5.8 Evaluation of uniform in-situ stress equations for Test Configuration H to the object thickness.

155

Configuration L						
	Plane Stress					
T_p/D_h	**Kx (MPa/mm)**	**Ky (MPa/mm)**	σ_{xx} **(MPa)**	σ_{yy} **(MPa)**	τ_{xy} **(MPa)**	**%Kx**
0.1	0.2000	0.0000	0.0003	-0.0003	0.0000	-0.0035
1	0.1855	0.0000	0.1441	-0.1441	0.0000	7.2640
2	0.1754	0.0000	0.2449	-0.2449	0.0000	12.3175
3	0.1737	0.0000	0.2617	-0.2617	0.0000	13.1590
4	0.1733	0.0000	0.2652	-0.2652	0.0000	13.3345
5	0.1732	0.0000	0.2662	-0.2662	0.0000	13.3870
6	0.1732	0.0000	0.2667	-0.2667	0.0000	13.4080
7	0.1732	0.0000	0.2669	-0.2669	0.0000	13.4155
8	0.1732	0.0000	0.2670	-0.2670	0.0000	13.4200
9	0.1732	0.0000	0.2670	-0.2670	0.0000	13.4200
10	0.1732	0.0000	0.2670	-0.2670	0.0000	13.4200
15	0.1732	0.0000	0.2670	-0.2670	0.0000	13.4200
20	0.1733	0.0000	0.2665	-0.2665	0.0000	13.3495
	Plane Strain					
T_p/D_h	**Kx (MPa/mm)**	**Ky (MPa/mm)**	σ_{xx} **(MPa)**	σ_{yy} **(MPa)**	τ_{xy} **(MPa)**	**%Kx**
0.1	0.2222	0.0000	-0.2385	0.2385	0.0000	-11.1150
1	0.2061	0.0000	-0.0657	0.0657	0.0000	-3.0400
2	0.1949	0.0000	0.0553	-0.0553	0.0000	2.5750
3	0.1930	0.0000	0.0755	-0.0755	0.0000	3.5100
4	0.1926	0.0000	0.0797	-0.0797	0.0000	3.7050
5	0.1925	0.0000	0.0809	-0.0809	0.0000	3.7635
6	0.1924	0.0000	0.0815	-0.0815	0.0000	3.7865
7	0.1924	0.0000	0.0817	-0.0817	0.0000	3.7950
8	0.1924	0.0000	0.0818	-0.0818	0.0000	3.8000
9	0.1924	0.0000	0.0818	-0.0818	0.0000	3.8000
10	0.1924	0.0000	0.0818	-0.0818	0.0000	3.8000
15	0.1924	0.0000	0.0818	-0.0818	0.0000	3.8000
20	0.1926	0.0000	0.0811	-0.0811	0.0000	3.7215

Table 5.9 Evaluation of uniform in-situ stress equations for Test Configuration L to the object thickness.

Configuration M						
	Plane Stress					
T_p/D_h	Kx (MPa/mm)	Ky (MPa/mm)	σ_{xx} (MPa)	σ_{yy} (MPa)	τ_{xy} (MPa)	%Kx
0.1	0.2001	0.0000	0.0006	0.0002	0.0000	-0.0265
1	0.2055	0.0000	0.2608	0.0730	0.0000	-2.7490
2	0.2094	0.0000	0.4431	0.1241	0.0000	-4.6960
3	0.2100	0.0000	0.4735	0.1326	0.0000	-5.0230
4	0.2102	0.0000	0.4797	0.1343	0.0000	-5.0870
5	0.2102	0.0000	0.4816	0.1349	0.0000	-5.1070
6	0.2102	0.0000	0.4825	0.1351	0.0000	-5.1205
7	0.2102	0.0000	0.4828	0.1352	0.0000	-5.1235
8	0.2103	0.0000	0.4829	0.1352	0.0000	-5.1250
9	0.2103	0.0000	0.4829	0.1352	0.0000	-5.1250
10	0.2103	0.0000	0.4829	0.1352	0.0000	-5.1250
15	0.2103	0.0000	0.4829	0.1352	0.0000	-5.1250
20	0.2103	0.0000	0.4821	0.1350	0.0000	-5.1645
	Plane Strain					
T_p/D_h	Kx (MPa/mm)	Ky (MPa/mm)	σ_{xx} (MPa)	σ_{yy} (MPa)	τ_{xy} (MPa)	%Kx
0.1	0.1927	0.0000	-0.3561	-0.0868	0.0000	3.6495
1	0.1979	0.0000	-0.0981	-0.0239	0.0000	1.0265
2	0.2017	0.0000	0.0826	0.0201	0.0000	-0.8490
3	0.2023	0.0000	0.1127	0.0275	0.0000	-1.1635
4	0.2025	0.0000	0.1189	0.0290	0.0000	-1.2255
5	0.2025	0.0000	0.1208	0.0294	0.0000	-1.2445
6	0.2025	0.0000	0.1217	0.0297	0.0000	-1.2575
7	0.2025	0.0000	0.1219	0.0297	0.0000	-1.2605
8	0.2025	0.0000	0.1221	0.0298	0.0000	-1.2620
9	0.2025	0.0000	0.1221	0.0298	0.0000	-1.2620
10	0.2025	0.0000	0.1221	0.0298	0.0000	-1.2620
15	0.2025	0.0000	0.1221	0.0298	0.0000	-1.2620
20	0.2026	0.0000	0.1211	0.0295	0.0000	-1.3000

Table 5.10 Evaluation of uniform in-situ stress equations for Test Configuration M to the object thickness.

Configuration P						
	Plane Stress					
T_p/D_h	Kx (MPa/mm)	Ky (MPa/mm)	σ_{xx} (MPa)	σ_{yy} (MPa)	τ_{xy} (MPa)	$\%Kx$
0.1	0.2000	0.0000	0.0000	0.0000	0.0000	-0.0035
1	0.1855	0.0000	0.0000	0.0000	0.0000	7.2640
2	0.1754	0.0000	0.0000	0.0000	0.0000	12.3175
3	0.1737	0.0000	0.0000	0.0000	0.0000	13.1590
4	0.1733	0.0000	0.0000	0.0000	0.0000	13.3345
5	0.1732	0.0000	0.0000	0.0000	0.0000	13.3870
6	0.1732	0.0000	0.0000	0.0000	0.0000	13.4080
7	0.1732	0.0000	0.0000	0.0000	0.0000	13.4155
8	0.1732	0.0000	0.0000	0.0000	0.0000	13.4200
9	0.1732	0.0000	0.0000	0.0000	0.0000	13.4200
10	0.1732	0.0000	0.0000	0.0000	0.0000	13.4200
15	0.1732	0.0000	0.0000	0.0000	0.0000	13.4200
20	0.1733	0.0000	0.0000	0.0000	0.0000	13.3495
	Plane Strain					
T_p/D_h	Kx (MPa/mm)	Ky (MPa/mm)	σ_{xx} (MPa)	σ_{yy} (MPa)	τ_{xy} (MPa)	$\%Kx$
0.1	0.2222	0.0000	0.0000	0.0000	0.0000	-11.1150
1	0.2061	0.0000	0.0000	0.0000	0.0000	-3.0400
2	0.1949	0.0000	0.0000	0.0000	0.0000	2.5750
3	0.1930	0.0000	0.0000	0.0000	0.0000	3.5100
4	0.1926	0.0000	0.0000	0.0000	0.0000	3.7050
5	0.1925	0.0000	0.0000	0.0000	0.0000	3.7635
6	0.1924	0.0000	0.0000	0.0000	0.0000	3.7865
7	0.1924	0.0000	0.0000	0.0000	0.0000	3.7950
8	0.1924	0.0000	0.0000	0.0000	0.0000	3.8000
9	0.1924	0.0000	0.0000	0.0000	0.0000	3.8000
10	0.1924	0.0000	0.0000	0.0000	0.0000	3.8000
15	0.1924	0.0000	0.0000	0.0000	0.0000	3.8000
20	0.1926	0.0000	0.0000	0.0000	0.0000	3.7215

Table 5.11 Evaluation of uniform in-situ stress equations for Test Configuration P to the object thickness.

Configuration Q					
Plane Stress					
T_p/D_h	Kx (MPa/mm)	Ky (MPa/mm)	σ_{xx} (MPa)	σ_{yy} (MPa)	τ_{xy} (MPa)	%Kx
0.1	0.2000	0.0000	0.0000	0.0000	0.0000	-0.0135
1	0.1942	0.0000	0.0000	0.0000	0.0000	2.9150
2	0.1901	0.0000	0.0000	0.0000	0.0000	4.9280
3	0.1895	0.0000	0.0000	0.0000	0.0000	5.2625
4	0.1893	0.0000	0.0000	0.0000	0.0000	5.3340
5	0.1893	0.0000	0.0000	0.0000	0.0000	5.3550
6	0.1893	0.0000	0.0000	0.0000	0.0000	5.3610
7	0.1893	0.0000	0.0000	0.0000	0.0000	5.3640
8	0.1893	0.0000	0.0000	0.0000	0.0000	5.3655
9	0.1893	0.0000	0.0000	0.0000	0.0000	5.3655
10	0.1893	0.0000	0.0000	0.0000	0.0000	5.3655
15	0.1893	0.0000	0.0000	0.0000	0.0000	5.3655
20	0.1894	0.0000	0.0000	0.0000	0.0000	5.3085
Plane Strain					
T_p/D_h	Kx (MPa/mm)	Ky (MPa/mm)	σ_{xx} (MPa)	σ_{yy} (MPa)	τ_{xy} (MPa)	%Kx
0.1	0.2084	0.0000	0.0000	0.0000	0.0000	-4.1805
1	0.2023	0.0000	0.0000	0.0000	0.0000	-1.1300
2	0.1981	0.0000	0.0000	0.0000	0.0000	0.9670
3	0.1974	0.0000	0.0000	0.0000	0.0000	1.3150
4	0.1972	0.0000	0.0000	0.0000	0.0000	1.3895
5	0.1972	0.0000	0.0000	0.0000	0.0000	1.4110
6	0.1972	0.0000	0.0000	0.0000	0.0000	1.4175
7	0.1972	0.0000	0.0000	0.0000	0.0000	1.4205
8	0.1972	0.0000	0.0000	0.0000	0.0000	1.4225
9	0.1972	0.0000	0.0000	0.0000	0.0000	1.4225
10	0.1972	0.0000	0.0000	0.0000	0.0000	1.4225
15	0.1972	0.0000	0.0000	0.0000	0.0000	1.4225
20	0.1973	0.0000	0.0000	0.0000	0.0000	1.3630

Table 5.12 Evaluation of uniform in-situ stress equations for Test Configuration Q to the object thickness.

Configuration R						
	Plane Stress					
T_p/D_h	**Kx (MPa/mm)**	**Ky (MPa/mm)**	σ_{xx} (MPa)	σ_{yy} (MPa)	τ_{xy} (MPa)	**%Kx**
0.1	0.2000	0.0000	0.0000	0.0000	0.0000	-0.0135
1	0.1942	0.0000	0.0000	0.0000	0.0000	2.9150
2	0.1901	0.0000	0.0000	0.0000	0.0000	4.9280
3	0.1895	0.0000	0.0000	0.0000	0.0000	5.2625
4	0.1893	0.0000	0.0000	0.0000	0.0000	5.3340
5	0.1893	0.0000	0.0000	0.0000	0.0000	5.3550
6	0.1893	0.0000	0.0000	0.0000	0.0000	5.3610
7	0.1893	0.0000	0.0000	0.0000	0.0000	5.3640
8	0.1893	0.0000	0.0000	0.0000	0.0000	5.3655
9	0.1893	0.0000	0.0000	0.0000	0.0000	5.3655
10	0.1893	0.0000	0.0000	0.0000	0.0000	5.3655
15	0.1893	0.0000	0.0000	0.0000	0.0000	5.3655
20	0.1894	0.0000	0.0000	0.0000	0.0000	5.3085
	Plane Strain					
T_p/D_h	**Kx (MPa/mm)**	**Ky (MPa/mm)**	σ_{xx} (MPa)	σ_{yy} (MPa)	τ_{xy} (MPa)	**%Kx**
0.1	0.2084	0.0000	0.0000	0.0000	0.0000	-4.1805
1	0.2023	0.0000	0.0000	0.0000	0.0000	-1.1300
2	0.1981	0.0000	0.0000	0.0000	0.0000	0.9670
3	0.1974	0.0000	0.0000	0.0000	0.0000	1.3150
4	0.1972	0.0000	0.0000	0.0000	0.0000	1.3895
5	0.1972	0.0000	0.0000	0.0000	0.0000	1.4110
6	0.1972	0.0000	0.0000	0.0000	0.0000	1.4175
7	0.1972	0.0000	0.0000	0.0000	0.0000	1.4205
8	0.1972	0.0000	0.0000	0.0000	0.0000	1.4225
9	0.1972	0.0000	0.0000	0.0000	0.0000	1.4225
10	0.1972	0.0000	0.0000	0.0000	0.0000	1.4225
15	0.1972	0.0000	0.0000	0.0000	0.0000	1.4225
20	0.1973	0.0000	0.0000	0.0000	0.0000	1.3630

Table 5.13 Evaluation of uniform in-situ stress equations for Test Configuration R to the object thickness.

160

h (mm)	Plane Stress (MPa)				Plane Strain (MPa)			
	σ_{xx}	σ_{yy}	τ_{xy}	$\%\sigma_{xx}$	σ_{xc}	σ_{yy}	τ_{xy}	$\%\sigma_{xx}$
15	1.1217	0.4383	0.0000	88.8	1.1382	0.4218	0.0000	88.6
30	3.0578	1.0622	0.0000	69.4	3.1061	1.0139	0.0000	68.9
45	4.7052	1.4548	0.0000	52.9	4.7838	1.3762	0.0000	52.2
90	7.4739	1.6761	0.0000	25.3	7.6141	1.5359	0.0000	23.9
120	8.3470	1.5230	0.0000	16.5	8.5121	1.3579	0.0000	14.9
180	9.2085	1.1515	0.0000	7.9	9.4035	0.9565	0.0000	6.0
225	9.5077	0.9223	0.0000	4.9	9.7154	0.7146	0.0000	2.8
293	9.7521	0.6579	0.0000	2.5	9.9721	0.4379	0.0000	0.3
360	9.8413	0.5187	0.0000	1.6	10.0669	0.2931	0.0000	-0.7
450	9.9046	0.3854	0.0000	1.0	10.1349	0.1551	0.0000	-1.3
540	9.9334	0.3066	0.0000	0.7	10.1664	0.0736	0.0000	-1.7
600	9.9413	0.2687	0.0000	0.6	10.1753	0.0347	0.0000	-1.8
750	9.9502	0.2098	0.0000	0.5	10.1859	-0.0259	0.0000	-1.9

Table 5.14 Evaluation of uniform in-situ stress equations for Test Configuration A to the core-hole depth.

h (mm)	Plane Stress (MPa)				Plane Strain (MPa)			
	σ_{xx}	σ_{yy}	τ_{xy}	$\%\sigma_{xx}$	σ_{xc}	σ_{yy}	τ_{xy}	$\%\sigma_{xx}$
15	1.1217	0.4383	0.0000	88.8	1.1382	0.4218	0.0000	88.6
30	3.0578	1.0622	0.0000	69.4	3.1061	1.0139	0.0000	68.9
45	4.7052	1.4548	0.0000	52.9	4.7838	1.3762	0.0000	52.2
90	7.4739	1.6761	0.0000	25.3	7.6141	1.5359	0.0000	31.3
120	8.3470	1.5230	0.0000	16.5	8.5121	1.3579	0.0000	14.9
180	9.2085	1.1515	0.0000	7.9	9.4035	0.9565	0.0000	6.0
225	9.5077	0.9223	0.0000	4.9	9.7154	0.7146	0.0000	2.8
293	9.7521	0.6579	0.0000	2.5	9.9721	0.4379	0.0000	0.3
360	9.8413	0.5187	0.0000	1.6	10.0669	0.2931	0.0000	-0.7
450	9.9046	0.3854	0.0000	1.0	10.1349	0.1551	0.0000	-1.3
540	9.9334	0.3066	0.0000	0.7	10.1664	0.0736	0.0000	-1.7
600	9.9413	0.2687	0.0000	0.6	10.1753	0.0347	0.0000	-1.8
750	9.9502	0.2098	0.0000	0.5	10.1859	-0.0259	0.0000	-1.9

Table 5.15 Evaluation of uniform in-situ stress equations for Test Configuration B to the core-hole depth.

Configuration C								
h (mm)	Plane Stress (MPa)				Plane Strain (MPa)			
	σ_{xx}	σ_{yy}	τ_{xy}	%σ_{xx}	σ_{xc}	σ_{yy}	τ_{xy}	%σ_{xx}
15	1.1217	0.4383	0.0000	88.8	1.1382	0.4218	0.0000	88.6
30	3.0578	1.0622	0.0000	69.4	3.1061	1.0139	0.0000	68.9
45	4.7052	1.4548	0.0000	52.9	4.7838	1.3762	0.0000	52.2
90	7.4739	1.6761	0.0000	25.3	7.6141	1.5359	0.0000	23.9
120	8.3470	1.5230	0.0000	16.5	8.5121	1.3579	0.0000	14.9
180	9.2085	1.1515	0.0000	7.9	9.4035	0.9565	0.0000	6.0
225	9.5077	0.9223	0.0000	4.9	9.7154	0.7146	0.0000	2.8
293	9.7521	0.6579	0.0000	2.5	9.9721	0.4379	0.0000	0.3
360	9.8413	0.5187	0.0000	1.6	10.0669	0.2931	0.0000	-0.7
450	9.9046	0.3854	0.0000	1.0	10.1349	0.1551	0.0000	-1.3
540	9.9334	0.3066	0.0000	0.7	10.1664	0.0736	0.0000	-1.7
600	9.9413	0.2687	0.0000	0.6	10.1753	0.0347	0.0000	-1.8
750	9.9502	0.2098	0.0000	0.5	10.1859	-0.0259	0.0000	-1.9

Table 5.16 Evaluation of uniform in-situ stress equations for Test Configuration C to the core-hole depth.

Configuration D								
h (mm)	Plane Stress (MPa)				Plane Strain (MPa)			
	σ_{xx}	σ_{yy}	τ_{xy}	%σ_{xx}	σ_{xc}	σ_{yy}	τ_{xy}	%σ_{xx}
15	1.1217	0.4383	0.0000	88.8	1.1382	0.4218	0.0000	88.6
30	3.0578	1.0622	0.0000	69.4	3.1061	1.0139	0.0000	68.9
45	4.7052	1.4548	0.0000	52.9	4.7838	1.3762	0.0000	52.2
90	7.4739	1.6761	0.0000	25.3	7.6141	1.5359	0.0000	23.9
120	8.3470	1.5230	0.0000	16.5	8.5121	1.3579	0.0000	14.9
180	9.2085	1.1515	0.0000	7.9	9.4035	0.9565	0.0000	6.0
225	9.5077	0.9223	0.0000	4.9	9.7154	0.7146	0.0000	2.8
293	9.7521	0.6579	0.0000	2.5	9.9721	0.4379	0.0000	0.3
360	9.8413	0.5187	0.0000	1.6	10.0669	0.2931	0.0000	-0.7
450	9.9046	0.3854	0.0000	1.0	10.1349	0.1551	0.0000	-1.3
540	9.9334	0.3066	0.0000	0.7	10.1664	0.0736	0.0000	-1.7
600	9.9413	0.2687	0.0000	0.6	10.1753	0.0347	0.0000	-1.8
750	9.9502	0.2098	0.0000	0.5	10.1859	-0.0259	0.0000	-1.9

Table 5.17 Evaluation of uniform in-situ stress equations for Test Configuration D to the core-hole depth.

Configuration E								
	Plane Stress (MPa)				Plane Strain (MPa)			
h (mm)	σ_{xx}	σ_{yy}	τ_{xy}	%σ_{xx}	σ_{xc}	σ_{yy}	τ_{xy}	%σ_{xx}
15	1.1217	0.4383	0.0000	88.8	1.1382	0.4218	0.0000	88.6
30	3.0578	1.0622	0.0000	69.4	3.1061	1.0139	0.0000	68.9
45	4.7052	1.4548	0.0000	52.9	4.7838	1.3762	0.0000	52.2
90	7.4739	1.6761	0.0000	25.3	7.6141	1.5359	0.0000	23.9
120	8.3470	1.5230	0.0000	16.5	8.5121	1.3579	0.0000	14.9
180	9.2085	1.1515	0.0000	7.9	9.4035	0.9565	0.0000	6.0
225	9.5077	0.9223	0.0000	4.9	9.7154	0.7146	0.0000	2.8
293	9.7521	0.6579	0.0000	2.5	9.9721	0.4379	0.0000	0.3
360	9.8413	0.5187	0.0000	1.6	10.0669	0.2931	0.0000	-0.7
450	9.9046	0.3854	0.0000	1.0	10.1349	0.1551	0.0000	-1.3
540	9.9334	0.3066	0.0000	0.7	10.1664	0.0736	0.0000	-1.7
600	9.9413	0.2687	0.0000	0.6	10.1753	0.0347	0.0000	-1.8
750	9.9502	0.2098	0.0000	0.5	10.1859	-0.0259	0.0000	-1.9

Table 5.18 Evaluation of uniform in-situ stress equations for Test Configuration E to the core-hole depth.

Configuration F								
	Plane Stress (MPa)				Plane Strain (MPa)			
h (mm)	σ_{xx}	σ_{yy}	τ_{xy}	%σ_{xx}	σ_{xc}	σ_{yy}	τ_{xy}	%σ_{xx}
15	1.0742	0.4858	0.0000	89.3	1.0920	0.4680	0.0000	89.1
30	2.9194	1.2006	0.0000	70.8	2.9715	1.1485	0.0000	70.3
45	4.4999	1.6601	0.0000	55.0	4.5859	1.5741	0.0000	54.1
90	7.1926	1.9574	0.0000	28.1	7.3513	1.7988	0.0000	26.5
120	8.0510	1.8190	0.0000	19.5	8.2399	1.6301	0.0000	17.6
180	8.9021	1.4579	0.0000	11.0	9.1277	1.2323	0.0000	8.7
225	9.1978	1.2322	0.0000	8.0	9.4392	0.9908	0.0000	5.6
293	9.4386	0.9714	0.0000	5.6	9.6952	0.7148	0.0000	3.0
360	9.5261	0.8339	0.0000	4.7	9.7895	0.5705	0.0000	2.1
450	9.5878	0.7022	0.0000	4.1	9.8570	0.4330	0.0000	1.4
540	9.6159	0.6241	0.0000	3.8	9.8884	0.3516	0.0000	1.1
600	9.6235	0.5865	0.0000	3.8	9.8974	0.3126	0.0000	1.0
750	9.6324	0.5276	0.0000	3.7	9.9083	0.2517	0.0000	0.9

Table 5.19 Evaluation of uniform in-situ stress equations for Test Configuration F to the core-hole depth.

Configuration G								
_h_ (mm)	Plane Stress (MPa)				Plane Strain (MPa)			
	σ_{xx}	σ_{yy}	τ_{xy}	$\%\sigma_{xx}$	σ_{xc}	σ_{yy}	τ_{xy}	$\%\sigma_{xx}$
15	1.1217	0.4383	0.0000	88.8	1.1382	0.4218	0.0000	88.6
30	3.0578	1.0622	0.0000	69.4	3.1061	1.0139	0.0000	68.9
45	4.7052	1.4548	0.0000	52.9	4.7838	1.3762	0.0000	52.2
90	7.4739	1.6761	0.0000	25.3	7.6141	1.5359	0.0000	23.9
120	8.3470	1.5230	0.0000	16.5	8.5121	1.3579	0.0000	14.9
180	9.2085	1.1515	0.0000	7.9	9.4035	0.9565	0.0000	6.0
225	9.5077	0.9223	0.0000	4.9	9.7154	0.7146	0.0000	2.8
293	9.7521	0.6579	0.0000	2.5	9.9721	0.4379	0.0000	0.3
360	9.8413	0.5187	0.0000	1.6	10.0669	0.2931	0.0000	-0.7
450	9.9046	0.3854	0.0000	1.0	10.1349	0.1551	0.0000	-1.3
540	9.9334	0.3066	0.0000	0.7	10.1664	0.0736	0.0000	-1.7
600	9.9413	0.2687	0.0000	0.6	10.1753	0.0347	0.0000	-1.8
750	9.9502	0.2098	0.0000	0.5	10.1859	-0.0259	0.0000	-1.9

Table 5.20 Evaluation of uniform in-situ stress equations for Test Configuration G to the core-hole depth.

Configuration H								
_h_ (mm)	Plane Stress (MPa)				Plane Strain (MPa)			
	σ_{xx}	σ_{yy}	τ_{xy}	$\%\sigma_{xx}$	σ_{xc}	σ_{yy}	τ_{xy}	$\%\sigma_{xx}$
15	0.9971	0.5629	0.0000	90.0	1.0147	0.5453	0.0000	89.9
30	2.6945	1.4255	0.0000	73.1	2.7459	1.3741	0.0000	72.5
45	4.1662	1.9938	0.0000	58.3	4.2543	1.9057	0.0000	57.5
90	6.7356	2.4144	0.0000	32.6	6.9107	2.2393	0.0000	30.9
120	7.5700	2.3000	0.0000	24.3	7.7837	2.0863	0.0000	22.2
180	8.4043	1.9558	0.0000	16.0	8.6657	1.6943	0.0000	13.3
225	8.6943	1.7357	0.0000	13.1	8.9765	1.4535	0.0000	10.2
293	8.9293	1.4807	0.0000	10.7	9.2313	1.1787	0.0000	7.7
360	9.0140	1.3460	0.0000	9.9	9.3249	1.0351	0.0000	6.8
450	9.0729	1.2171	0.0000	9.3	9.3914	0.8986	0.0000	6.1
540	9.1000	1.1400	0.0000	9.0	9.4227	0.8173	0.0000	5.8
600	9.1072	1.1028	0.0000	8.9	9.4317	0.7783	0.0000	5.7
750	9.1159	1.0441	0.0000	8.8	9.4432	0.7168	0.0000	5.6

Table 5.21 Evaluation of uniform in-situ stress equations for Test Configuration H to the core-hole depth.

164

Configuration L						
	Plane Stress					
h (mm)	*Kx* (MPa/mm)	*Ky* (MPa/mm)	σ_{xx} (MPa)	σ_{yy} (MPa)	τ_{xy} (MPa)	*%Kx*
15	0.0131	0.0000	0.3312	-0.3312	0.0000	93.4540
30	0.0244	0.0000	0.8716	-0.8716	0.0000	87.7810
45	0.0659	0.0000	0.9121	-0.9121	0.0000	67.0495
60	0.0901	0.0000	0.9280	-0.9280	0.0000	54.9610
90	0.1252	0.0000	0.7785	-0.7785	0.0000	37.3855
120	0.1456	0.0000	0.6177	-0.6177	0.0000	27.1885
180	0.1633	0.0000	0.4297	-0.4297	0.0000	18.3460
225	0.1681	0.0000	0.3649	-0.3649	0.0000	15.9580
270	0.1703	0.0000	0.3302	-0.3302	0.0000	14.8690
360	0.1719	0.0000	0.2979	-0.2979	0.0000	14.0395
420	0.1724	0.0000	0.2877	-0.2877	0.0000	13.8220
450	0.1725	0.0000	0.2840	-0.2840	0.0000	13.7485
540	0.1728	0.0000	0.2772	-0.2772	0.0000	13.6180
600	0.1729	0.0000	0.2743	-0.2743	0.0000	13.5640
750	0.1730	0.0000	0.2706	-0.2706	0.0000	13.4950
	Plane Strain					
h (mm)	*Kx* (MPa/mm)	*Ky* (MPa/mm)	σ_{xx} (MPa)	σ_{yy} (MPa)	τ_{xy} (MPa)	*%Kx*
15	0.0145	0.0000	0.3424	-0.3424	0.0000	92.7267
30	0.0272	0.0000	0.9131	-0.9131	0.0000	86.4234
45	0.0732	0.0000	0.9073	-0.9073	0.0000	63.3884
60	0.1001	0.0000	0.8957	-0.8957	0.0000	49.9565
90	0.1391	0.0000	0.6921	-0.6921	0.0000	30.4285
120	0.1618	0.0000	0.4938	-0.4938	0.0000	19.0985
180	0.1815	0.0000	0.2695	-0.2695	0.0000	9.2735
225	0.1868	0.0000	0.1938	-0.1938	0.0000	6.6200
270	0.1892	0.0000	0.1536	-0.1536	0.0000	5.4100
360	0.1910	0.0000	0.1167	-0.1167	0.0000	4.4885
420	0.1915	0.0000	0.1051	-0.1051	0.0000	4.2465
450	0.1917	0.0000	0.1010	-0.1010	0.0000	4.1650
540	0.1920	0.0000	0.0933	-0.0933	0.0000	4.0200
600	0.1921	0.0000	0.0901	-0.0901	0.0000	3.9600
750	0.1922	0.0000	0.0859	-0.0859	0.0000	3.8835

Table 5.22 Evaluation of linear gradient in-situ stress equations for Test Configuration L to the core-hole depth.

Configuration M						
	Plane Stress					
h (mm)	*Kx* (MPa/mm)	*Ky* (MPa/mm)	σ_{xx} (MPa)	σ_{yy} (MPa)	τ_{xy} (MPa)	*%Kx*
15	0.0591	0.0000	0.5991	0.1677	0.0000	70.4495
30	0.1455	0.0000	1.5767	0.4415	0.0000	27.2345
45	0.1926	0.0000	1.6500	0.4620	0.0000	3.6895
60	0.2190	0.0000	1.6788	0.4701	0.0000	-9.5035
90	0.2334	0.0000	1.4084	0.3943	0.0000	-16.6965
120	0.2314	0.0000	1.1174	0.3129	0.0000	-15.7185
180	0.2230	0.0000	0.7773	0.2176	0.0000	-11.5025
225	0.2188	0.0000	0.6602	0.1848	0.0000	-9.3925
270	0.2161	0.0000	0.5972	0.1672	0.0000	-8.0650
360	0.2133	0.0000	0.5388	0.1509	0.0000	-6.6515
420	0.2123	0.0000	0.5204	0.1457	0.0000	-6.1600
450	0.2120	0.0000	0.5138	0.1439	0.0000	-5.9800
540	0.2113	0.0000	0.5014	0.1404	0.0000	-5.6345
600	0.2110	0.0000	0.4963	0.1390	0.0000	-5.4920
750	0.2106	0.0000	0.4895	0.1371	0.0000	-5.3030
	Plane Strain					
h (mm)	*Kx* (MPa/mm)	*Ky* (MPa/mm)	σ_{xx} (MPa)	σ_{yy} (MPa)	τ_{xy} (MPa)	*%Kx*
15	0.0569	0.0000	0.5112	0.1246	0.0000	71.5354
30	0.1402	0.0000	1.3632	0.3322	0.0000	29.9085
45	0.1855	0.0000	1.3547	0.3301	0.0000	7.2290
60	0.2110	0.0000	1.3372	0.3259	0.0000	-5.4795
90	0.2248	0.0000	1.0333	0.2518	0.0000	-12.4080
120	0.2229	0.0000	0.7373	0.1797	0.0000	-11.4660
180	0.2148	0.0000	0.4023	0.0980	0.0000	-7.4050
225	0.2107	0.0000	0.2893	0.0705	0.0000	-5.3725
270	0.2082	0.0000	0.2293	0.0559	0.0000	-4.0940
360	0.2055	0.0000	0.1742	0.0424	0.0000	-2.7325
420	0.2045	0.0000	0.1569	0.0382	0.0000	-2.2590
450	0.2042	0.0000	0.1508	0.0367	0.0000	-2.0855
540	0.2035	0.0000	0.1392	0.0339	0.0000	-1.7525
600	0.2032	0.0000	0.1345	0.0328	0.0000	-1.6155
750	0.2029	0.0000	0.1282	0.0313	0.0000	-1.4335

Table 5.23 Evaluation of linear gradient in-situ stress equations for Test Configuration M to the core-hole depth.

Configuration P						
	Plane Stress					
h (mm)	*Kx* (MPa/mm)	*Ky* (MPa/mm)	σ_{xx} (MPa)	σ_{yy} (MPa)	τ_{xy} (MPa)	%*Kx*
15	0.0131	0.0000	0.0000	0.0000	0.0000	93.4540
30	0.0244	0.0000	0.0000	0.0000	0.0000	87.7810
45	0.0659	0.0000	0.0000	0.0000	0.0000	67.0495
60	0.0901	0.0000	0.0000	0.0000	0.0000	54.9610
90	0.1252	0.0000	0.0000	0.0000	0.0000	37.3855
120	0.1456	0.0000	0.0000	0.0000	0.0000	27.1885
180	0.1633	0.0000	0.0000	0.0000	0.0000	18.3460
225	0.1681	0.0000	0.0000	0.0000	0.0000	15.9580
270	0.1703	0.0000	0.0000	0.0000	0.0000	14.8690
360	0.1719	0.0000	0.0000	0.0000	0.0000	14.0395
420	0.1724	0.0000	0.0000	0.0000	0.0000	13.8220
450	0.1725	0.0000	0.0000	0.0000	0.0000	13.7485
540	0.1728	0.0000	0.0000	0.0000	0.0000	13.6180
600	0.1729	0.0000	0.0000	0.0000	0.0000	13.5640
750	0.1730	0.0000	0.0000	0.0000	0.0000	13.4950
	Plane Strain					
h (mm)	*Kx* (MPa/mm)	*Ky* (MPa/mm)	σ_{xx} (MPa)	σ_{yy} (MPa)	τ_{xy} (MPa)	%*Kx*
15	0.0145	0.0000	0.0000	0.0000	0.0000	92.7267
30	0.0272	0.0000	0.0000	0.0000	0.0000	86.4234
45	0.0732	0.0000	0.0000	0.0000	0.0000	63.3884
60	0.1001	0.0000	0.0000	0.0000	0.0000	49.9565
90	0.1391	0.0000	0.0000	0.0000	0.0000	30.4285
120	0.1618	0.0000	0.0000	0.0000	0.0000	19.0985
180	0.1815	0.0000	0.0000	0.0000	0.0000	9.2735
225	0.1868	0.0000	0.0000	0.0000	0.0000	6.6200
270	0.1892	0.0000	0.0000	0.0000	0.0000	5.4100
360	0.1910	0.0000	0.0000	0.0000	0.0000	4.4885
420	0.1915	0.0000	0.0000	0.0000	0.0000	4.2465
450	0.1917	0.0000	0.0000	0.0000	0.0000	4.1650
540	0.1920	0.0000	0.0000	0.0000	0.0000	4.0200
600	0.1921	0.0000	0.0000	0.0000	0.0000	3.9600
750	0.1922	0.0000	0.0000	0.0000	0.0000	3.8835

Table 5.24 Evaluation of linear gradient in-situ stress equations for Test Configuration P to the core-hole depth.

Configuration Q						
	Plane Stress					
h (mm)	*Kx* (MPa/mm)	*Ky* (MPa/mm)	σ_{xx} (MPa)	σ_{yy} (MPa)	τ_{xy} (MPa)	*%Kx*
15	0.0331	0.0000	0.0000	0.0000	0.0000	83.4628
30	0.0770	0.0000	0.0000	0.0000	0.0000	61.4848
45	0.1209	0.0000	0.0000	0.0000	0.0000	39.5315
60	0.1461	0.0000	0.0000	0.0000	0.0000	26.9630
90	0.1722	0.0000	0.0000	0.0000	0.0000	13.8970
120	0.1829	0.0000	0.0000	0.0000	0.0000	8.5535
180	0.1892	0.0000	0.0000	0.0000	0.0000	5.3825
225	0.1901	0.0000	0.0000	0.0000	0.0000	4.9480
270	0.1902	0.0000	0.0000	0.0000	0.0000	4.9085
360	0.1899	0.0000	0.0000	0.0000	0.0000	5.0530
420	0.1897	0.0000	0.0000	0.0000	0.0000	5.1435
450	0.1896	0.0000	0.0000	0.0000	0.0000	5.1800
540	0.1895	0.0000	0.0000	0.0000	0.0000	5.2565
600	0.1894	0.0000	0.0000	0.0000	0.0000	5.2875
750	0.1893	0.0000	0.0000	0.0000	0.0000	5.3310
	Plane Strain					
h (mm)	*Kx* (MPa/mm)	*Ky* (MPa/mm)	σ_{xx} (MPa)	σ_{yy} (MPa)	τ_{xy} (MPa)	*%Kx*
15	0.0345	0.0000	0.0000	0.0000	0.0000	82.7738
30	0.0802	0.0000	0.0000	0.0000	0.0000	59.8800
45	0.1260	0.0000	0.0000	0.0000	0.0000	37.0120
60	0.1522	0.0000	0.0000	0.0000	0.0000	23.9200
90	0.1794	0.0000	0.0000	0.0000	0.0000	10.3095
120	0.1905	0.0000	0.0000	0.0000	0.0000	4.7430
180	0.1971	0.0000	0.0000	0.0000	0.0000	1.4400
225	0.1980	0.0000	0.0000	0.0000	0.0000	0.9875
270	0.1981	0.0000	0.0000	0.0000	0.0000	0.9465
360	0.1978	0.0000	0.0000	0.0000	0.0000	1.0970
420	0.1976	0.0000	0.0000	0.0000	0.0000	1.1915
450	0.1975	0.0000	0.0000	0.0000	0.0000	1.2295
540	0.1974	0.0000	0.0000	0.0000	0.0000	1.3085
600	0.1973	0.0000	0.0000	0.0000	0.0000	1.3410
750	0.1972	0.0000	0.0000	0.0000	0.0000	1.3860

Table 5.25 Evaluation of linear gradient in-situ stress equations for Test Configuration Q to the core-hole depth.

Configuration R						
Plane Stress						
h (mm)	*Kx* (MPa/mm)	*Ky* (MPa/mm)	σ_{xx} (MPa)	σ_{yy} (MPa)	τ_{xy} (MPa)	*%Kx*
15	0.0331	0.0000	0.0000	0.0000	0.0000	83.4628
30	0.0770	0.0000	0.0000	0.0000	0.0000	61.4848
45	0.1209	0.0000	0.0000	0.0000	0.0000	39.5315
60	0.1461	0.0000	0.0000	0.0000	0.0000	26.9630
90	0.1722	0.0000	0.0000	0.0000	0.0000	13.8970
120	0.1829	0.0000	0.0000	0.0000	0.0000	8.5535
180	0.1892	0.0000	0.0000	0.0000	0.0000	5.3825
225	0.1901	0.0000	0.0000	0.0000	0.0000	4.9480
270	0.1902	0.0000	0.0000	0.0000	0.0000	4.9085
360	0.1899	0.0000	0.0000	0.0000	0.0000	5.0530
420	0.1897	0.0000	0.0000	0.0000	0.0000	5.1435
450	0.1896	0.0000	0.0000	0.0000	0.0000	5.1800
540	0.1895	0.0000	0.0000	0.0000	0.0000	5.2565
600	0.1894	0.0000	0.0000	0.0000	0.0000	5.2875
750	0.1893	0.0000	0.0000	0.0000	0.0000	5.3310
Plane Strain						
h (mm)	*Kx* (MPa/mm)	*Ky* (MPa/mm)	σ_{xx} (MPa)	σ_{yy} (MPa)	τ_{xy} (MPa)	*%Kx*
15	0.0345	0.0000	0.0000	0.0000	0.0000	82.7738
30	0.0802	0.0000	0.0000	0.0000	0.0000	59.8800
45	0.1260	0.0000	0.0000	0.0000	0.0000	37.0120
60	0.1522	0.0000	0.0000	0.0000	0.0000	23.9200
90	0.1794	0.0000	0.0000	0.0000	0.0000	10.3095
120	0.1905	0.0000	0.0000	0.0000	0.0000	4.7430
180	0.1971	0.0000	0.0000	0.0000	0.0000	1.4400
225	0.1980	0.0000	0.0000	0.0000	0.0000	0.9875
270	0.1981	0.0000	0.0000	0.0000	0.0000	0.9465
360	0.1978	0.0000	0.0000	0.0000	0.0000	1.0970
420	0.1976	0.0000	0.0000	0.0000	0.0000	1.1915
450	0.1975	0.0000	0.0000	0.0000	0.0000	1.2295
540	0.1974	0.0000	0.0000	0.0000	0.0000	1.3085
600	0.1973	0.0000	0.0000	0.0000	0.0000	1.3410
750	0.1972	0.0000	0.0000	0.0000	0.0000	1.3860

Table 5.26 Evaluation of linear gradient in-situ stress equations for Test Configuration R to the core-hole depth.

Configuration A

W_p/D_h	Plane Stress (MPa)				
	σ_{xx}	σ_{yy}	τ_{xy}	$\%\sigma_{xx}$	$\sigma_{xx}/\sigma_{xx}(10)$
10	9.9900	-0.0200	0.0000	0.10	1.00
8	9.9997	-0.0352	0.0001	0.00	1.00
6	10.0375	-0.0765	0.0006	-0.37	1.00
5	10.0734	-0.1204	0.0014	-0.73	1.01
4	10.1313	-0.1993	0.0043	-1.31	1.01
3	10.2691	-0.3761	0.0146	-2.69	1.03
2	10.6321	-0.9481	0.0751	-6.32	1.06
W_p/D_h	Plane Strain (MPa)				
	σ_{xx}	σ_{yy}	τ_{xy}	$\%\sigma_{xx}$	$\sigma_{xx}/\sigma_{xx}(10)$
10	10.2322	-0.2622	0.0000	-2.32	1.00
8	10.2424	-0.2779	0.0001	-2.42	1.00
6	10.2822	-0.3212	0.0006	-2.82	1.00
5	10.3201	-0.3671	0.0015	-3.20	1.01
4	10.3812	-0.4492	0.0045	-3.81	1.01
3	10.5267	-0.6337	0.0153	-5.27	1.03
2	10.9123	-1.2283	0.0787	-9.12	1.07

Table 5.27 Evaluation of uniform in-situ stress equations for Test Configuration A to the object width.

Configuration B

W_p/D_h	Plane Stress (MPa)				
	σ_{xx}	σ_{yy}	τ_{xy}	$\%\sigma_{xx}$	$\sigma_{xx}/\sigma_{xx}(10)$
10	9.9901	-0.0200	0.0000	0.10	1.00
8	9.9998	-0.0350	0.0000	0.00	1.00
6	10.0382	-0.0750	0.0000	-0.38	1.00
5	10.0750	-0.1173	0.0000	-0.75	1.01
4	10.1355	-0.1907	0.0000	-1.36	1.01
3	10.2833	-0.3469	0.0000	-2.83	1.03
2	10.7063	-0.7953	0.0001	-7.06	1.07
W_p/D_h	Plane Strain (MPa)				
	σ_{xx}	σ_{yy}	τ_{xy}	$\%\sigma_{xx}$	$\sigma_{xx}/\sigma_{xx}(10)$
10	10.2322	-0.2622	0.0000	-2.32	1.00
8	10.2425	-0.2777	0.0000	-2.43	1.00
6	10.2829	-0.3197	0.0000	-2.83	1.00
5	10.3216	-0.3639	0.0000	-3.22	1.01
4	10.3853	-0.4405	0.0000	-3.85	1.01
3	10.5405	-0.6041	0.0000	-5.41	1.03
2	10.9846	-1.0736	0.0001	-9.85	1.07

Table 5.28 Evaluation of uniform in-situ stress equations for Test Configuration B to the object width.

Configuration C					
	Plane Stress (MPa)				
W_p/D_h	σ_{xx}	σ_{yy}	τ_{xy}	$\%\sigma_{xx}$	$\sigma_{xx}/\sigma_{xx}(10)$
10	9.9900	-0.0200	0.0000	0.10	1.00
8	9.9997	-0.0352	0.0001	0.00	1.00
6	10.0376	-0.0761	0.0007	-0.38	1.00
5	10.0739	-0.1194	0.0015	-0.74	1.01
4	10.1315	-0.1990	0.0043	-1.31	1.01
3	10.2689	-0.3766	0.0146	-2.69	1.03
2	10.6332	-0.9457	0.0753	-6.33	1.06
	Plane Strain (MPa)				
W_p/D_h	σ_{xx}	σ_{yy}	τ_{xy}	$\%\sigma_{xx}$	$\sigma_{xx}/\sigma_{xx}(10)$
10	10.2322	-0.2622	0.0000	-2.32	1.00
8	10.2424	-0.2779	0.0001	-2.42	1.00
6	10.2823	-0.3208	0.0007	-2.82	1.00
5	10.3205	-0.3660	0.0016	-3.21	1.01
4	10.3814	-0.4489	0.0045	-3.81	1.01
3	10.5264	-0.6342	0.0153	-5.26	1.03
2	10.9133	-1.2258	0.0789	-9.13	1.07

Table 5.29 Evaluation of uniform in-situ stress equations for Test Configuration C to the object width.

Configuration D					
	Plane Stress (MPa)				
W_p/D_h	σ_{xx}	σ_{yy}	τ_{xy}	$\%\sigma_{xx}$	$\sigma_{xx}/\sigma_{xx}(10)$
10	9.9901	-0.0199	0.0000	0.10	1.00
8	9.9998	-0.0349	0.0000	0.00	1.00
6	10.0384	-0.0745	0.0000	-0.38	1.00
5	10.0755	-0.1161	0.0000	-0.76	1.01
4	10.1357	-0.1903	0.0000	-1.36	1.01
3	10.2831	-0.3474	0.0000	-2.83	1.03
2	10.7076	-0.7925	0.0000	-7.08	1.07
	Plane Strain (MPa)				
W_p/D_h	σ_{xx}	σ_{yy}	τ_{xy}	$\%\sigma_{xx}$	$\sigma_{xx}/\sigma_{xx}(10)$
10	10.2323	-0.2621	-5.1837	-2.32	1.00
8	10.2425	-0.2777	-0.1192	-2.43	1.00
6	10.2831	-0.3192	20.1135	-2.83	1.00
5	10.3221	-0.3627	39.5655	-3.22	1.01
4	10.3855	-0.4401	71.0713	-3.86	1.01
3	10.5403	-0.6046	148.2895	-5.40	1.03
2	10.9858	-1.0707	370.6291	-9.86	1.07

Table 5.30 Evaluation of uniform in-situ stress equations for Test Configuration D to the object width.

Configuration E

W_p/D_h	Plane Stress (MPa)				
	σ_{xx}	σ_{yy}	τ_{xy}	$\%\sigma_{xx}$	$\sigma_{xx}/\sigma_{xx}(10)$
10	9.9900	-0.0200	0.0001	0.10	1.00
8	9.9997	-0.0352	0.0001	0.00	1.00
6	10.0376	-0.0761	0.0007	-0.38	1.00
5	10.0739	-0.1194	0.0015	-0.74	1.01
4	10.1315	-0.1990	0.0039	-1.31	1.01
3	10.2689	-0.3766	0.0130	-2.69	1.03
2	10.6332	-0.9457	0.0682	-6.33	1.06
W_p/D_h	Plane Strain (MPa)				
	σ_{xx}	σ_{yy}	τ_{xy}	$\%\sigma_{xx}$	$\sigma_{xx}/\sigma_{xx}(10)$
10	10.2322	-0.2622	0.0001	-2.32	1.00
8	10.2424	-0.2779	0.0001	-2.42	1.00
6	10.2823	-0.3208	0.0007	-2.82	1.00
5	10.3205	-0.3660	0.0015	-3.21	1.01
4	10.3814	-0.4489	0.0040	-3.81	1.01
3	10.5264	-0.6342	0.0137	-5.26	1.03
2	10.9133	-1.2258	0.0715	-9.13	1.07

Table 5.31 Evaluation of uniform in-situ stress equations for Test Configuration E to the object width.

Configuration F

W_p/D_h	Plane Stress (MPa)				
	σ_{xx}	σ_{yy}	τ_{xy}	$\%\sigma_{xx}$	$\sigma_{xx}/\sigma_{xx}(10)$
10	9.9844	-0.0144	0.0000	0.16	1.00
8	9.9954	-0.0304	0.0000	0.05	1.00
6	10.0374	-0.0744	0.0000	-0.37	1.01
5	10.0789	-0.1203	0.0000	-0.79	1.01
4	10.1469	-0.2022	0.0000	-1.47	1.02
3	10.3126	-0.3792	0.0001	-3.13	1.03
2	10.7944	-0.8984	-0.0001	-7.94	1.08
W_p/D_h	Plane Strain (MPa)				
	σ_{xx}	σ_{yy}	τ_{xy}	$\%\sigma_{xx}$	$\sigma_{xx}/\sigma_{xx}(10)$
10	10.2874	-0.3174	0.0000	-2.87	1.00
8	10.2992	-0.3342	0.0000	-2.99	1.00
6	10.3438	-0.3808	0.0000	-3.44	1.01
5	10.3880	-0.4293	0.0000	-3.88	1.01
4	10.4605	-0.5159	0.0000	-4.61	1.02
3	10.6365	-0.7032	0.0001	-6.37	1.03
2	11.1487	-1.2527	-0.0001	-11.49	1.08

Table 5.32 Evaluation of uniform in-situ stress equations for Test Configuration F to the object width.

Configuration G					
W_p/D_h	Plane Stress (MPa)				
	σ_{xx}	σ_{yy}	τ_{xy}	$\%\sigma_{xx}$	$\sigma_{xx}/\sigma_{xx}(10)$
10	9.9900	-0.0200	0.0000	0.10	1.00
8	9.9997	-0.0352	0.0001	0.00	1.00
6	10.0376	-0.0761	0.0007	-0.38	1.00
5	10.0739	-0.1194	0.0015	-0.74	1.01
4	10.1315	-0.1990	0.0043	-1.31	1.01
3	10.2689	-0.3766	0.0146	-2.69	1.03
2	10.6332	-0.9457	0.0753	-6.33	1.06
W_p/D_h	Plane Strain (MPa)				
	σ_{xx}	σ_{yy}	τ_{xy}	$\%\sigma_{xx}$	$\sigma_{xx}/\sigma_{xx}(10)$
10	10.2322	-0.2622	0.0000	-2.32	1.00
8	10.2424	-0.2779	0.0001	-2.42	1.00
6	10.2823	-0.3208	0.0007	-2.82	1.00
5	10.3205	-0.3660	0.0016	-3.21	1.01
4	10.3814	-0.4489	0.0045	-3.81	1.01
3	10.5264	-0.6342	0.0153	-5.26	1.03
2	10.9133	-1.2258	0.0789	-9.13	1.07

Table 5.33 Evaluation of uniform in-situ stress equations for Test Configuration G to the object width.

Configuration H					
W_p/D_h	Plane Stress (MPa)				
	σ_{xx}	σ_{yy}	τ_{xy}	$\%\sigma_{xx}$	$\sigma_{xx}/\sigma_{xx}(10)$
10	9.9752	-0.0052	0.0000	0.25	1.00
8	9.9879	-0.0229	0.0000	0.12	1.00
6	10.0371	-0.0717	0.0000	-0.37	1.01
5	10.0858	-0.1224	0.0000	-0.86	1.01
4	10.1678	-0.2105	0.0000	-1.68	1.02
3	10.3689	-0.3925	0.0000	-3.69	1.04
2	10.9828	-0.8603	0.0000	-9.83	1.10
W_p/D_h	Plane Strain (MPa)				
	σ_{xx}	σ_{yy}	τ_{xy}	$\%\sigma_{xx}$	$\sigma_{xx}/\sigma_{xx}(10)$
10	10.3798	-0.4098	0.0000	-3.80	1.00
8	10.3938	-0.4288	0.0000	-3.94	1.00
6	10.4469	-0.4815	0.0000	-4.47	1.01
5	10.4996	-0.5363	0.0000	-5.00	1.01
4	10.5886	-0.6313	0.0000	-5.89	1.02
3	10.8052	-0.8287	0.0000	-8.05	1.04
2	11.4630	-1.3405	0.0000	-14.63	1.10

Table 5.34 Evaluation of uniform in-situ stress equations for Test Configuration H to the object width.

Configuration L

W_p/D_h	Kx (MPa/mm)	Ky (MPa/mm)	σ_{xx} (MPa)	σ_{yy} (MPa)	τ_{xy} (MPa)	$\%Kx$	$Kx/K(10)$
Plane Stress							
10	0.1963	0.0000	0.0338	-0.0338	0.0000	1.8549	1.0000
8	0.1964	0.0000	0.0331	-0.0331	0.0000	1.8045	1.0005
6	0.1966	0.0000	0.0320	-0.0320	0.0000	1.7002	1.0016
5	0.1967	0.0000	0.0319	-0.0319	0.0000	1.6293	1.0023
4	0.1970	0.0000	0.0325	-0.0325	0.0000	1.4842	1.0038
3	0.1982	0.0000	0.0339	-0.0339	0.0000	0.9072	1.0097
2	0.2041	0.0000	0.0503	-0.0503	0.0000	-2.0510	1.0398
Plane Strain							
10	0.2181	0.0000	-0.1979	0.1979	0.0000	-9.05	1.00
8	0.2182	0.0000	-0.1988	0.1988	0.0000	-9.11	1.00
6	0.2184	0.0000	-0.2002	0.2002	0.0000	-9.22	1.00
5	0.2186	0.0000	-0.2005	0.2005	0.0000	-9.30	1.00
4	0.2189	0.0000	-0.2003	0.2003	0.0000	-9.46	1.00
3	0.2202	0.0000	-0.2000	0.2000	0.0000	-10.10	1.01
2	0.2268	0.0000	-0.1894	0.1894	0.0000	-13.39	1.04

Table 5.35 Evaluation of linear gradient in-situ stress equations for Test Configuration L to the object width.

Configuration M

W_p/D_h	Kx (MPa/mm)	Ky (MPa/mm)	σ_{xx} (MPa)	σ_{yy} (MPa)	τ_{xy} (MPa)	$\%Kx$	$Kx/K(10)$
Plane Stress							
10	0.2010	0.0000	0.0611	0.0171	0.0000	-0.4912	1.0000
8	0.2010	0.0000	0.0599	0.0168	0.0000	-0.4940	1.0000
6	0.2010	0.0000	0.0579	0.0162	0.0000	-0.5223	1.0003
5	0.2012	0.0000	0.0577	0.0161	0.0000	-0.5852	1.0009
4	0.2015	0.0000	0.0587	0.0164	0.0000	-0.7704	1.0028
3	0.2029	0.0000	0.0614	0.0172	0.0000	-1.4509	1.0095
2	0.2111	0.0000	0.0911	0.0255	0.0000	-5.5477	1.0503
Plane Strain							
10	0.1936	0.0000	-0.2955	-0.0720	0.0000	3.20	1.00
8	0.1936	0.0000	-0.2968	-0.0723	0.0000	3.20	1.00
6	0.1937	0.0000	-0.2990	-0.0729	0.0000	3.17	1.00
5	0.1938	0.0000	-0.2994	-0.0730	0.0000	3.11	1.00
4	0.1941	0.0000	-0.2990	-0.0729	0.0000	2.93	1.00
3	0.1954	0.0000	-0.2986	-0.0728	0.0000	2.28	1.01
2	0.2033	0.0000	-0.2827	-0.0689	0.0000	-1.67	1.05

Table 5.36 Evaluation of linear gradient in-situ stress equations for Test Configuration M to the object width.

Configuration P

W_p/D_h	Kx (MPa/mm)	Ky (MPa/mm)	σ_{xx} (MPa)	σ_{yy} (MPa)	τ_{xy} (MPa)	%Kx	Kx/K(10)
			Plane Stress				
10	0.1963	0.0000	0.0000	0.0000	0.0000	1.8549	1.0000
8	0.1964	0.0000	0.0000	0.0000	0.0000	1.8045	1.0005
6	0.1966	0.0000	0.0000	0.0000	0.0000	1.7002	1.0016
5	0.1967	0.0000	0.0000	0.0000	0.0000	1.6293	1.0023
4	0.1970	0.0000	0.0000	0.0000	0.0000	1.4842	1.0038
3	0.1982	0.0000	0.0000	0.0000	0.0000	0.9072	1.0097
2	0.2041	0.0000	0.0000	0.0000	0.0000	-2.0510	1.0398
			Plane Strain				
10	0.2181	0.0000	0.0000	0.0000	0.0000	-9.05	1.00
8	0.2182	0.0000	0.0000	0.0000	0.0000	-9.11	1.00
6	0.2184	0.0000	0.0000	0.0000	0.0000	-9.22	1.00
5	0.2186	0.0000	0.0000	0.0000	0.0000	-9.30	1.00
4	0.2189	0.0000	0.0000	0.0000	0.0000	-9.46	1.00
3	0.2202	0.0000	0.0000	0.0000	0.0000	-10.10	1.01
2	0.2268	0.0000	0.0000	0.0000	0.0000	-13.39	1.04

Table 5.37 Evaluation of linear gradient in-situ stress equations for Test Configuration P to the object width.

Configuration Q

W_p/D_h	Kx (MPa/mm)	Ky (MPa/mm)	σ_{xx} (MPa)	σ_{yy} (MPa)	τ_{xy} (MPa)	%Kx	Kx/K(10)
			Plane Stress				
10	0.1983	0.0000	0.0000	0.0000	0.0000	0.8359	1.0000
8	0.1984	0.0000	0.0000	0.0000	0.0000	0.8062	1.0003
6	0.1985	0.0000	0.0000	0.0000	0.0000	0.7349	1.0010
5	0.1987	0.0000	0.0000	0.0000	0.0000	0.6675	1.0017
4	0.1990	0.0000	0.0000	0.0000	0.0000	0.5050	1.0033
3	0.2002	0.0000	0.0000	0.0000	0.0000	-0.1170	1.0096
2	0.2071	0.0000	0.0000	0.0000	0.0000	-3.5696	1.0444
			Plane Strain				
10	0.2066	0.0000	0.0000	0.0000	0.0000	-3.30	1.00
8	0.2067	0.0000	0.0000	0.0000	0.0000	-3.33	1.00
6	0.2068	0.0000	0.0000	0.0000	0.0000	-3.40	1.00
5	0.2069	0.0000	0.0000	0.0000	0.0000	-3.47	1.00
4	0.2073	0.0000	0.0000	0.0000	0.0000	-3.64	1.00
3	0.2086	0.0000	0.0000	0.0000	0.0000	-4.29	1.01
2	0.2158	0.0000	0.0000	0.0000	0.0000	-7.89	1.04

Table 5.38 Evaluation of linear gradient in-situ stress equations for Test Configuration Q to the object width.

Configuration R							
Plane Stress							
W_p/D_h	Kx (MPa/mm)	Ky (MPa/mm)	σ_{xx} (MPa)	σ_{yy} (MPa)	τ_{xy} (MPa)	$\%Kx$	$Kx/K(10)$
10	0.1983	0.0000	0.0000	0.0000	0.0000	0.84	1.00
8	0.1984	0.0000	0.0000	0.0000	0.0000	0.81	1.00
6	0.1985	0.0000	0.0000	0.0000	0.0000	0.73	1.00
5	0.1987	0.0000	0.0000	0.0000	0.0000	0.67	1.00
4	0.1990	0.0000	0.0000	0.0000	0.0000	0.50	1.00
3	0.2002	0.0000	0.0000	0.0000	0.0000	-0.12	1.01
2	0.2071	0.0000	0.0000	0.0000	0.0000	-3.57	1.04
Plane Strain							
W_p/D_h	Kx (MPa/mm)	Ky (MPa/mm)	σ_{xx} (MPa)	σ_{yy} (MPa)	τ_{xy} (MPa)	$\%Kx$	$Kx/K(10)$
10	0.2066	0.0000	0.0000	0.0000	0.0000	-3.30	1.00
8	0.2067	0.0000	0.0000	0.0000	0.0000	-3.33	1.00
6	0.2068	0.0000	0.0000	0.0000	0.0000	-3.40	1.00
5	0.2069	0.0000	0.0000	0.0000	0.0000	-3.47	1.00
4	0.2073	0.0000	0.0000	0.0000	0.0000	-3.64	1.00
3	0.2086	0.0000	0.0000	0.0000	0.0000	-4.29	1.01
2	0.2158	0.0000	0.0000	0.0000	0.0000	-7.89	1.04

Table 5.39 Evaluation of linear gradient in-situ stress equations for Test Configuration Q to the object width.

CHAPTER 6

DEFINITION OF CALIBRATION CONSTANTS

6.1. INTRODUCTION

The theoretical background for the core-drilling method was developed in Chapter 3 for a through-hole in an infinite thin plate subjected to uniform plane stress through thickness. The closed-form equations were applied to objects with finite dimensions and to a core-hole in Chapter 5. It was observed that the closed-form in-situ stress equations might apply to an object of finite dimensions with a small through-hole compared with the length and width of the object. However, it was also observed that the closed-form equations will give some errors for a through-hole in a thick object. It was also seen that the closed-form equations might give considerable error for the core-hole case. In real applications, the structure requiring in-situ stress analysis might not be thin. Because of this, a core-hole might be required.

There are no closed-form solutions available from theory of elasticity for a through-hole or a core-hole in a thick object because of the complexity of the problems. However, because of the axisymmetric nature of the problems and the assumption of linear elastic behavior, these cases closely parallel the through-hole condition in the general nature of the stress distribution. Thus, the relieved displacements due to drilling the core-hole still vary sinusoidally along a circle concentric with the core-hole, in the manner described by the closed-form relieved displacement equations (u_r, v_α) derived in Chapter 3. These closed-form equations are formed with constants A, B, C, F, H, I and J which are defined algebraically in Tables 3.1 and 3.2 in Chapter 3. These constants apply only for the conditions assumed in the derivation: a through-hole, thin object, uniform stress throughout the object thickness, and object boundaries remote from the through-hole. It is assumed that the relieved displacement equation (u_r, v_α) also applies in the cases of a core-hole and through-hole in a thick object rather than a through-hole in thin object. However, the constants A, B, C, F, H, I and J for a core-hole and a thick object with a through-hole differ from the analytical definitions given in Tables (3.1) and (3.2). Since there is no closed-form solution available for core-hole or through-hole in a thick object, these constants are obtained through measurements with known stress fields by empirical means. This empirical analysis can be conducted by numerical analysis such as finite element analysis or by experimental test. This approach explained above to solve the problems is termed semi-analytical. These constants determined by empirical means are called calibration constants and are shown with A_c, B_c, C_c, F_c, H_c, I_c and J_c. In this research, only calibration constants A_c, B_c, C_c for the uniform stress state are defined and calculated. The calibration constants F_c, H_c, I_c and J_c for the linear gradient stress

state are not calculated in this work. The concepts of the definition and method of calculation of the calibration constants F_c, H_c, I_c and J_c are same as that for calibration constants A_c, B_c, C_c.

For the known stress state, the material and geometrical properties of these calibration constants can be calculated. This means that once the calibration constants are determined for a particular material and geometrical properties, these calibration constants will only be used for the same material and geometrical properties. One of the purposes here is to minimize the number of the variables of the calibration constants so that the calibration constants can be applied to broader applications. As seen from Table 3.1, constants A, B, and C are functions of through-hole radius (a), measurement circle radius (r_m), and material properties (E, v). Some simplification can also be achieved with the through-hole radius and measurement circle radius r_m dependencies. It is desirable to normalize the relieved displacement equations (given by Equations (3.37) and (3.38)) with respect to measurement circle radius, r_m as follows

$$uR = \frac{u_r}{r_m} = \frac{(\sigma_{xx} + \sigma_{yy})}{2} \frac{(1+v)}{E} \left(\frac{1}{k}\right)^2$$

$$+ \frac{(\sigma_{xx} - \sigma_{yy})}{2} \frac{(1+v)}{E} \left(\left(\frac{1}{k}\right)^2 + \left(\frac{1}{k}\right)^2 \frac{3-v}{1+v} - \left(\frac{1}{k}\right)^4 \right) \cos 2\alpha \qquad (6.1)$$

$$+ \tau_{xy} \frac{(1+v)}{E} \left(\left(\frac{1}{k}\right)^2 + \left(\frac{1}{k}\right)^2 \frac{3-v}{1+v} - \left(\frac{1}{k}\right)^4 \right) \sin 2\alpha$$

$$vR = \frac{v_\alpha}{r_m} = \frac{(\sigma_{xx} - \sigma_{yy})}{2} \frac{(1+v)}{E} \left(\left(\frac{1}{k}\right)^2 - \left(\frac{1}{k}\right)^2 \frac{3-v}{1+v} - \left(\frac{1}{k}\right)^4 \right) \sin 2\alpha$$

$$+ \tau_{xy} \frac{(1+v)}{E} \left(\left(\frac{1}{k}\right)^2 - \left(\frac{1}{k}\right)^2 \frac{3-v}{1+v} - \left(\frac{1}{k}\right)^4 \right) \cos 2\alpha \qquad (6.2)$$

where

$$k = \frac{r_m}{a} \qquad (6.3)$$

uR and vR are normalized relieved displacements in radial and tangential directions, respectively. As seen from Equations (6.1) and (6.2), when normalized in this way, the relieved displacement equations are functions of the dimensionless measurement circle radius, k.

To use same equations for relieved displacement and in-situ stress that were derived in Chapter 3, the constants are defined as follows

$$A = A_c \times r_m$$
$$B = B_c \times r_m \qquad (6.4)$$
$$C = C_c \times r_m$$

Substituting Equation (6.4) into the relieved displacement equation given by (3.38) and (3.39), the normalized relieved displacement equations are written for the general case as follows

$$uR = \frac{u_r}{r_m} = \frac{\left(\sigma_{xx} + \sigma_{yy}\right)}{2} A_c + \frac{\left(\sigma_{xx} - \sigma_{yy}\right)}{2} B_c \cos 2\alpha + \tau_{xy} B_c \sin 2\alpha \qquad (6.5)$$

$$vR = \frac{v_\alpha}{r_m} = \frac{\left(\sigma_{xx} - \sigma_{yy}\right)}{2} C_c \sin 2\alpha - \tau_{xy} C_c \cos 2\alpha \qquad (6.6)$$

The normalized relieved displacements given by Equations (6.5) and (6.6) above are called general relieved displacement equations because it is assumed that for known calibration constants these equations can be used for any type of problem such as a through-hole or core-hole. Definition and calculation of these calibration constants are different for different problem types. For a thin structure with through-hole, these calibration constants can be calculated analytically from Equations (6.4) for plane stress assumption as follows

$$A_c = \frac{(1+\nu)}{2E}\left(\frac{1}{k}\right)^2 \qquad (6.7)$$

$$B_c = \frac{(1+\nu)}{E}\left(\left(\frac{1}{k}\right)^2 + \left(\frac{1}{k}\right)^2 \frac{3-\nu}{1+\nu} - \left(\frac{1}{k}\right)^4\right) \qquad (6.8)$$

$$C_c = \left(\left(\frac{1}{k}\right)^2 - \left(\frac{1}{k}\right)^2 \frac{3-\nu}{1+\nu} - \left(\frac{1}{k}\right)^4\right) \qquad (6.9)$$

As seen from Equations (6.7) and (6.8), the calibration constants are a function of material properties and the measurement circle radius k for the structure with a through-hole. As explained earlier, the calibration constants for core-hole and through-hole in a thick object need to be calculated numerically. The calibration constants could have some additional variables for a core-hole and through-hole in a thick object.

In this chapter, the definition and calculation of the calibration constants are done for a core-hole and a through-hole in a thick object. Once the calibration constants are calculated numerically, the in-situ stress equations derived in Chapter 3 can be used directly.

The outline of this chapter is as follows. Section 6.2 defines calibration constant A_c, Section 6.3 defines calibration constant B_c, and Section 6.4 defines calibration constant C_c.

6.2. DEFINITION OF CALIBRATION CONSTANT A_c

As seen from the normalized relieved displacement given by Equation (6.5), the calibration constant A_c is associated with an equibiaxial stress state which is represented by a mean biaxial

stress $P=(\sigma_{xx}+\sigma_{yy})/2$. Therefore, in order to define the calibration constant A_c, we consider a known equibiaxial stress state of $\sigma_{xx}=\sigma_{yy}=\sigma_o$. The relieved displacement Equation (6.5) takes the following form.

$$uR = A_c \frac{(\sigma_{xx}+\sigma_{yy})}{2} = A_c\sigma_o \qquad (6.10)$$

The relieved displacement on the left side of Equation (6.10) is calculated for the known stress state by finite element analysis. Then the calibration constant A_c can be found as follows.

$$A_c = \frac{uR}{\sigma_o} \qquad (6.11)$$

The calibration constant A_c is found for the through-hole and core-hole cases in the following subsections.

6.2.1. Through-Hole

To understand the effect of object thickness on the calibration constant A_c, the relieved displacements are plotted against the object thickness (T_p/D_h) in Figure 6.1. u_r is the relieved displacement calculated by finite element analysis, and u_o is the theoretical solution of the relieved displacement for a thin object with a through-hole. D_h is the diameter of the hole.

The finite element model explained in Section 5.21 is used to calculate the relieved displacements. As seen from Figure 6.1, the relieved displacement under the assumed stress state is the same as the theoretical solution and is not affected by thickness variations. Thus, this shows us for the through-hole case, the calibration constant A_c is equal to the theoretical definition and can be calculated from the theoretical definition defined in Equation (6.1).

$$A_c = \frac{(1+\nu)}{2E}\left(\frac{1}{k}\right)^2 \qquad (6.12)$$

6.2.2. Core-Hole Case

To understand the effect of the core-hole depth h on the calibration constant A_c, the general variation of relieved displacement with core-hole depth h is illustrated in Figure 6.2. In this figure, the relieved displacements are normalized with respect to the theoretical solution of the relieved displacement, u_o and the core-hole depth is normalized with respect to measurement circle radius, r_m. The normalized relieved displacement plots for different measurement circle radii have similar shape and reach their maximum values at the same non-dimensional core-hole depth. This figure shows that relieved displacement increases quickly as the core-hole depth increases. The theoretical value of relieved displacement is approached at a large core-hole depth. It is obvious from Figure 6.2 that the analytical definition of the constant A cannot be used for the core-hole case.

180

Figure 6.3 shows the variation with core-hole depth of the non-dimensional relieved displacement for different core-hole radii, a. The ratio of the measurement circle radius to core-hole depth, $k=r_m/a$ in this plot is kept constant. This figure shows that when the relieved displacement is normalized with respect to the measurement circle radius (r_m), the dimensionless relieved displacement (u_r/r_m) will not change due to core-hole diameter change for constant k value. Figures 6.2 and 6.3 show that the radius of the core-hole influences the magnitude of the relieved displacement, whereas the measurement circle radius r_m influences the percentage of the displacement that is relieved. The percentage of the relieved displacement can be determined in terms of core-hole depth that is normalized with measurement circle radius r_m. As seen from the figure, when the core-hole depth reaches 0.6 times h/r_m, 80% of the relieved displacement is relieved. Compared to the analytical through-hole procedure, the calibration constant A_c for core-hole analysis involves one additional independent variable, namely, the dimensionless core-hole depth $\xi = h/r_m$. Thus, in a generalized functional form, the calibration constant A_c can be expressed as

$$A_c = f(E, v, k, \xi) \tag{6.13}$$

As seen from the generalized functional form above, for any given material properties E and v, the calibration constant A_c is simply geometric functions. This means that once the calibration constant has been determined for a particular dimensionless geometric property, the same calibration constant will apply when the core-hole diameter and depth are similarly scaled. In order to remove the material dependency from A_c leaving only the geometric dependency, the following function is introduced.

$$A_c = \frac{(a1_c + a2_c \, v)}{E} \tag{6.14}$$

Where, the constants $a1_c$ and $a2_c$ are dimensionless coefficients. Substituting Equation (6.14) into Equation (6.10) we get

$$uR = \frac{u}{r_m} = \frac{(a1_c + a2_c \, v)}{E} \sigma_o \tag{6.15}$$

For any core-hole depth $\xi = h/r_m$, the loading condition was imposed by applying a uniform pressure applied through the core-hole surfaces (from $\xi = 0$ to $\xi = 2$). In this analysis, there are 20 partial core-hole depths up to the maximum core-hole depth $\xi_{max} = 2$ considered. This analysis was repeated for six Poisson's ratios at each core-hole depth: $v = 0.1, 0.15, 0.2, 0.25, 0.30$, and 0.35. The corresponding values of the relieved displacements were calculated. The finite element model explained in Section 5.3.1 is used to calculate the relieved displacements on the left side of the Equation (6.15). The dimensionless coefficients $a1_c$ and $a2_c$ are the determined by least squares method.

Figure 6.4 and Figure 6.5 show the variation with core-hole depth of the dimensionless coefficients $a1_c$ and $a2_c$.

Now for the known geometric information, the dimensionless coefficients $a1_c$ and $a2_c$ can be found from Figure 6.4 and 6.5, and then calibration constant A_c can be calculated with material properties information. To estimate the accuracy of the coefficients, we will find the relative residual from the equation given below.

$$err(z) = \frac{E\ uR(z) - (a1_c + a2_c\ v)}{E\ uR(z)} * 100 \tag{6.16}$$

The relative residual is the relative difference between finite element and calculated relieved displacements.

Figure 6.6 shows relative residual versus Poisson's ratio for different core-hole depths. It can be observed that the maximum error is about 0.8 % at very shallow core-hole depth. These errors reduce quickly as the core-hole depth increases. It is also observed that errors are less than 0.04 % at large core-hole depths. These results confirm the validity of the definition of the calibration constant A_c.

In order to remove the core-hole depth dependency as well as material dependency, the following function is introduced.

$$A_c = \sum_{i=1}^{n} \frac{(a1_c(i) + a2_c(i)\ v)}{E} (\xi)^{i-1} \tag{6.17}$$

By substituting Equation (6.17) in to Equation (6.10), we get a linear algebraic equation having $a1_c(i)$ and $a2_c(i)$ as unknowns.

$$uR = \frac{u}{r_m} = A_c \sigma_o = \sum_{i=1}^{n} \frac{(a1_c(i) + a2_c(i)\ v)}{E} (\xi)^{i-1} \sigma_o \tag{6.18}$$

The number of equations is limited by the number of the relieved displacements calculated by the finite element analysis. The relieved displacements are calculated at 30 core-hole depths through the core-hole depth interval of ξ from 0 through 2 for six different Poisson's ratios. The number of unknowns ($a1_c(i)$'s and $a2_c(i)$'s) were considerably smaller than the number of equations (180). The least squares method is adopted for solving the linear system.

To estimate the accuracy of the coefficients, we will find the relative residual from the equation given below.

$$err(\xi) = \frac{E\ uR(\xi) - \sum_{i=1}^{n} (a1_c(i) + a2_c(i)\ v)(\xi)^{i-1}}{E\ uR(\xi)} * 100 \tag{6.19}$$

Figure 6.7 and 6.8 show the relative residual versus the core-hole depth ($\xi = h/r_m$) for n=4 and n=8. These figures also show the errors for the different Poisson's ratios at each core-hole depth.

It was observed that the number of terms $n = 8$ (16 coefficients) offered reasonable accuracy. It was also observed that the function A_c is well approximated (error less that 0.5 %) by means of an eight-order algebraic polynomial obtained by the least-squares method.

The dimensionless coefficients values $a_c(i)$'s of calibration constant A_c for core-hole are given in Table 6.1.

6.3. DEFINITION OF CALIBRATION CONSTANT B_c

As seen from the normalized relieved displacement given by Equation (6.5), the calibration constant B_c is associated with the shear stress state which is represented by $Q = (\sigma_{xx} - \sigma_{yy})/2$. Thus, in order define the calibration constant B_c, we consider a known stress state of $\sigma_{xx} = -\sigma_{yy} = \sigma_o$. The relieved displacement defined by Equation (6.5) take the form as follows

$$uR = \frac{u}{r_m} = B_c \frac{(\sigma_{xx} - \sigma_{yy})}{2} \cos 2\alpha = B_c \sigma_o \cos 2\alpha \tag{6.20}$$

The relieved displacement at $\alpha = 0$ under a known stress state is calculated by finite element analysis. Then the calibration constant B_c can be found as follows

$$B_c = \frac{uR}{\sigma_o} \tag{6.21}$$

The calibration constant B_c is found for the through-hole and core-hole cases in the following subsections.

6.3.1. Through-Hole

To understand the effect of the object thickness (T_p/D_h) on the calibration constant B_c, the relieved displacements are plotted against the object thickness in Figure 6.9. In this figure, u_r is the relieved displacement calculated by finite element analysis. The finite element model explained in Chapter 5.2.1 is used to calculate the relieved displacements. u_o is the theoretical solution of the relieved displacement for a thin object with a through-hole. As seen from the figure, the relieved displacements vary little as the object thickness changes. Although the constant B is not affected significantly by the thickness variation, a new function is introduced to get better approximation.

$$B_c = \frac{(b1_c + b2_c \nu)}{E} \tag{6.22}$$

where the constants $b1_c$ and $b2_c$ are dimensionless coefficients. Substituting Equation (6.22) into Equation (6.20) we get

$$uR = \frac{u}{r_m} = \frac{(b1_c + b2_c \ v)}{E} \sigma_o \qquad (6.23)$$

For any object thickness T_p, the loading condition was imposed by applying a uniform pressure applied to the through-hole surfaces (from $z=0$ to $z=T_p$). In this analysis, there are 20 partial thicknesses of the object up to the maximum thickness of the object $T_p/D_h = 2$ considered. This analysis was repeated for eleven Poisson's ratios at each object thickness: 0.1, 0.125, 0.15, 0.175, 0.2, 0.225, 0.25, 0.275, 0.30, 0.325, and 0.35. The corresponding values of the relieved displacements were calculated. The dimensionless coefficients $b1_c$ and $b2_c$ are determined by the least squares method. The finite element model explained in Section 5.2.1 is used to calculate the relieved displacements on the left side of Equation (6.23).

Figure 6.10 and 6.11 show the variation with core-hole depth of the dimensionless coefficients $b1_c$ and $b2_c$.

Now, for the known geometric information, the dimensionless coefficients $b1_c$ and $b2_c$ can be found from Figure 6.10 and 6.11, and then the calibration constant B_c can be calculated with material properties information. To estimate the accuracy of the coefficients, we will find the relative residuals from the equation given below.

$$err(\xi) = \frac{E \ uR(\xi) - (b1_c + b2_c \ v)\sigma_o}{E \ uR(\xi)} *100 \qquad (6.24)$$

Figure 6.12 shows the relative residuals versus Poisson's ratio for different core-hole depths. It is observed that the maximum error is about 0.015 %. These results confirm the validity of the definition of the calibration constant B_c. As seen from these figures, the new defined calibration constant B_c approximates well the relieved displacements due to core-hole drilling for different material properties.

As seen from Figure 6.10, the dimensionless coefficient $b1_c$ varies very little from 1.583 to 1.585 as the core-hole depth changes. For the sake of the further simplification, we set $b1_c$ equal to 1.584 and the calibration constant B_c is defined with only one dimensionless coefficient b as shown below.

$$B = \frac{(1.584 + b \ v)}{E} \qquad (6.25)$$

The dimensionless coefficient b is calculated as explained above. Figure 6.13 shows the variation with core-hole depth of the dimensionless coefficients b_c.

In order to remove the core-hole depth dependency as well as material dependency, the following approximation is introduced.

$$B_c = \sum_{i=1}^{n} \frac{(1.584 + b_c(i) \ v)}{E} \left(\frac{T_p}{a}\right)^{i-1} \qquad (6.26)$$

184

By substituting Equation (6.26) in to Equation (6.20), we obtain a linear algebraic equation having $b_c(i)$'s as unknowns.

$$uR = \frac{u}{r_m} = B_c \sigma_o = \sum_{i=1}^{n} \frac{(1.584 + b_c(i)\ v)}{E} \left(\frac{T_p}{a}\right)^{i-1} \sigma_o \qquad (6.27)$$

The number of equations is limited by the number of the relieved displacements calculated by finite element analysis. The relieved displacements are calculated for different object thicknesses and for eleven different Poisson's ratios. The number of unknowns ($b_c(i)$'s) are considerably smaller than the number of equations (220). The coefficients $b_c(i)$'s are calculated by least squares method.

Now for the known geometric information, the calibration constant B_c can be calculated by Equation (6.26) with these calculated dimensionless coefficients b_c. To estimate the accuracy of the coefficients, we will find the relative residual from the equation given below.

$$err(T_p / a) = \frac{E\ uR(T_p / a) - \sum_{i=1}^{n}(0.792 + b_c(i)\ v)\left(\frac{T_p}{a}\right)^{i-1} \sigma_o}{E\ uR(T_p / a)} \qquad (6.28)$$

Figure 6.14 and 6.15 show the relative residuals versus the object thickness (T_p/a) for $n=1$ and $n=5$. These figures also show the errors for the eleven different Poisson's ratio in the range between $v=0.1$ to $v=0.35$ at each core-hole depth. It is observed that the number of terms $n=5$ (5 coefficients) provided reasonable accuracy. It was observed that the function B_c is well approximated (error less that 0.2 %) by means of a five-order algebraic polynomial obtained by the least squares method.

The dimensionless coefficients values $b_c(i)$ s of calibration constant B_c for core-hole are given in Table 6.2.

6.3.2. Core-Hole Case

To understand the effect of the core-hole depth ($\xi = h/r_m$) on the calibration constant B_c, the general variation of relieved displacement with core-hole depth is illustrated in Figure 6.16. In this figure, relieved displacements are normalized with respect to the theoretical solution of the relieved displacement u_o, and core-hole depth is normalized with respect to the measurement circle radius r_m. The normalized relieved displacement plots for different displacement measurement radii have similar shapes and reach their maximum values at the same non-dimensional core-hole depth. This figure shows that relieved displacements increase quickly as the core-hole depth increases and reach maximum value. The theoretical value of relieved displacement is approached at large core-hole depths. Figure 6.17 shows the variation with core-hole depth of the non-dimensional relieved displacement for different core-hole radii, a. The ratio of the dimensionless measurement circle radius k is kept constant in this plot. This figure shows that when the relieved displacement is normalized with respect to the measurement circle

radius, the dimensionless relieved displacement (u_r/r_m) will not change due to core-hole diameter change for constant k value. Figure 6.16 and Figure 6.17 show that the radius of the core-hole, a influences the magnitude of the relieved displacement, whereas the measurement circle radius r_m influences the percentage of the relieved displacement. Compared to the analytical through-hole procedure, the calibration constant B_c for core-hole analysis involves one additional independent variable, namely, the dimensionless core-hole depth $\xi=h/r_m$. Thus, in a generalized functional form, the calibration constant B_c can be expressed as

$$B_c = f(E, v, k, h) \tag{6.29}$$

As seen from the generalized functional form above, for any given material properties E and v, the calibration constant B_c is simply geometric functions. This means that once the calibration constant has been determined for a particular dimensionless measurement circle radius $(k=r_m/a)$ and material, the same calibration constant will apply when the core-hole diameter and depth are similarly scaled. In order to remove the material dependency from B_c leaving only the geometric dependency, the following function is introduced.

$$B_c = \frac{(b1_c + b2_c\ v)}{E} \tag{6.30}$$

The coefficients $b1_c$ and $b2_c$ are dimensionless coefficients. Substituting Equation (6.30) into Equation (6.20) we get

$$uR = \frac{u}{r_m} = \frac{(b1_c + b2_c\ v)}{E} \sigma_o \tag{6.31}$$

For any core-hole depth h, the loading condition was imposed by applying a uniform pressure to core-hole surfaces (from $\xi = 0$ to $\xi = 2$). In this analysis, there are 20 partial core-hole depths up to the maximum core-hole depth $\xi_{max} = 2$ considered. This analysis was repeated for six Poisson's ratios at each core-hole depth: 0.1, 0.15, 0.2, 0.25, 0.30, and 0.35. The corresponding values of the relieved displacements were calculated. The dimensionless coefficients $b1_c$ and $b2_c$ are determined by least squares method. The finite element model explained in Section 5.3.1 is used to calculate the relieved displacements.

Figure 6.18 and 6.19 show the variation with core-hole depth of the dimensionless coefficients $b1_c$ and $b2_c$.

Now for known geometric information, the dimensionless coefficients $b1_c$ and $b2_c$ can be found from Figure 6.18 and Figure 6.19 and then calibration constant B_c can be calculated with material properties information. To estimate the accuracy of the coefficients, we will find the relative residual from the equation given below.

$$err(\xi) = \frac{E\ uR(\xi) - (b1_c + b2_c\ v)\sigma_o}{E\ uR(\xi)} * 100 \tag{6.32}$$

186

Figure 6.20 shows the relative residuals versus Poisson's ratio for different core-hole depths. It is observed that the maximum error is about 0.5 % at very shallow core-hole depths. These errors reduce quickly as core-hole depth increases. It is also observed that errors are less than 0.04 % at large core-hole depths. These results confirm the validity of the definition of the calibration constant B_c. As seen from these figures, the new defined calibration constant B_c approximates well the relieved displacement due to core-hole drilling for different material properties.

In order to remove the core-hole depth dependency as well as material dependency, the following approximation is introduced.

$$B_c = \sum_{i=1}^{n} \frac{(b1_c(i) + b2_c(i) \ v)}{E}(\xi)^{i-1} \tag{6.33}$$

By substituting Equation (6.33) in to Equation (6.20), we obtain a linear algebraic equation having $b1_c(i)$ and $b2_c(i)$ as unknowns.

$$uR = \frac{u}{r_m} = B_c\sigma_o = \sum_{i=1}^{n} \frac{(b1_c(i) + b2_c(i) \ v)}{E}(\xi)^{i-1}\sigma_o \cos 2\alpha \tag{6.34}$$

The number of equations is limited by the number of the relieved displacement at $\alpha=0$ calculated by finite element analysis. The relieved displacements are calculated at thirty partial core-hole depths through the core-hole depth ξ interval of 0 to 2 for six different Poisson's ratios. The number of unknowns ($b1_c(i)$'s and $b2_c(i)$'s) were considerably smaller than the number of equations (180). The least squares method is adopted for solving the linear system.

Now for known geometric information, the calibration constant B_c can be calculated by Equation (6.33) with these calculated dimensionless coefficients $b1_c$ and $b2_c$. To estimate the accuracy of this function, the relieved displacements were recalculated with these dimensionless coefficients. To estimate the accuracy of the coefficients a_{ij}, we find the relative residual from the equation given below.

$$err(\xi) = \frac{E \ uR(\xi) - \sum_{i=1}^{n}(b1_c(i) + b2_c(i) \ v)(\xi)^{i-1}\sigma_o}{E \ uR(\xi)} *100 \tag{6.35}$$

Figure 6.22 shows the relative residuals versus the core-hole depth ($\xi = h/r_m$) for n=5 and n=10. These figures also show the errors for the different Poisson's ratio at each core-hole depth. It is observed that number of terms $n = 10$ (20 coefficients) offered a reasonable compromise between accuracy and numerical stability. It was observed that the function B_c is well approximated.

6.4. DEFINITION OF CALIBRATION CONSTANT C_c

As seen from Equation (6.6), the calibration constant C_c relates to shear stress. Thus, in order define calibration constant C_c, we consider the known stress state of $\sigma_{xx} = -\sigma_{yy} = \sigma_o$. The relieved

displacement equations in the tangential direction defined by Equation (6.6) have the following form.

$$vR = \frac{v_\alpha}{r_m} = \frac{\left(\sigma_{xx} - \sigma_{yy}\right)}{2} C_c \sin 2\alpha \qquad (6.36)$$

The relieved displacement in radial direction at $\alpha=45°$ under a known stress state is calculated by finite element analysis. Then the calibration constant C_c can be found as follows

$$C_c = \frac{vR}{\sigma_o} \qquad (6.37)$$

The calibration constant C_c is found for the through-hole and core-hole cases in the following subsections.

6.4.1. Through-Hole

To understand the effect of the object thickness on the calibration constant C_c, the relieved displacements are plotted against the object thickness in Figure 6.23. v_α is the relieved displacement in radial direction calculated by finite element analysis. The finite element model explained in Section 5.2.1 is used to calculate the relieved displacements. v_o is the theoretical solution of the relieved displacement in tangential direction for a thin object with a through-hole. As seen from the figure, the relieved displacements vary as the object thickness changes. This means the calibration constant C_c is a function of object thickness T_p. A new function is introduced for the calibration constant C_c as follows

$$C_c = \frac{(c1_c + c2_c v)}{E} \qquad (6.38)$$

where the constants $c1_c$ and $c2_c$ are dimensionless coefficients. Substituting Equation (6.38) into Equation (6.36) we get

$$vR = \frac{v}{r_m} = \frac{(c1_c + c2_c\ v)}{E} \sigma_o \qquad (6.39)$$

For any object thickness T_p, the loading condition was imposed by applying a uniform pressure applied on the through-hole surfaces (from $z = 0$ to $z = T_p$). In this analysis, twenty partial object thicknesses up to the maximum object thickness $T_p/D_h = 20$ are considered. This analysis was repeated for eleven Poisson's ratios at each object thickness: 0.1, 0.125, 0.15, 0.175, 0.2, 0.225, 0.25, 0.275, 0.30, 0.325, and 0.35. The corresponding values of the relieved displacements were calculated. The finite element model explained in Section 5.2.1 is used to calculate the relieved displacements on the left side of Equation (6.39). The dimensionless coefficients $c1_c$ and $c2_c$ are determined by the least squares method.

188

Figure 6.24 and 6.25 show the variation with core-hole depth of the dimensionless coefficients $c1_c$ and $c2_c$.

Now for known geometric information, the dimensionless coefficients $c1_c$ and $c2_c$ can be found from Figure 6.24 and Figure 6.25 and then calibration constant C_c can be calculated with material properties information. To estimate the accuracy this function, the relieved displacements were recalculated with these dimensionless coefficients. To estimate the accuracy of the coefficients, we find the relative residuals from the equation given below.

$$err(\xi) = \frac{E\ vR(\xi) - (c1_c + c2_c\ v)\sigma_o}{E\ vR(\xi)} * 100 \qquad (6.40)$$

Figure 6.26 shows the relative residuals versus Poisson's ratio for different object thicknesses. It can be observed that the maximum error is less than 0.1 %. These results confirm the validity of the definition of the calibration constant C_c. As seen from these figures, the newly defined calibration constant C_c is well approximates the through-hole in a thick object.

As seen from Figure 6.24, the dimensionless coefficient $c1_c$ varies very little, from -1.088 to -1.096 as the core-hole depth changes. For the sake of the further simplification, $c1_c$ is set to -1.09 and the calibration constant C_c is defined with only one dimensionless coefficient c as shown below.

$$C_c = \frac{(-1.09 + c\ v)}{E} \qquad (6.41)$$

The dimensionless coefficient c is calculated as explained above. Figure 6.27 shows the variation with core-hole depth of the dimensionless coefficients c_c. The accuracy of the function defined by Equation (6.41) is estimated by Equation (6.40). Figure 6.28 shows the percentage error versus Poisson's ratio for different core-hole depths. It is observed that the maximum error is less than 0.3 %. These results confirm the validity of the definition of the calibration constant C_c.

In order to remove the core-hole depth dependency as well as material dependency, the following approximation is introduced.

$$C_c = \sum_{i=1}^{n} \frac{(-1.09 + c_c(i)\ v)}{E} \left(\frac{T_p}{a}\right)^{i-1} \qquad (6.42)$$

By substituting Equation (6.42) in to Equation (6.36), we obtain a linear algebraic equation having $c_c(i)$'s as unknowns.

$$vR = \frac{u}{r_m} = C_c\sigma_o = \sum_{i=1}^{n} \frac{(-1.09 + c_c(i)\ v)}{E} \left(\frac{T_p}{a}\right)^{i-1}\sigma_o \qquad (6.43)$$

The number of equations is limited by the number of the relieved displacements calculated by finite element analysis. The relieved displacements are calculated for different object thicknesses

189

and for eleven different Poisson's ratios. The number of unknowns ($c_c(i)$'s) are considerably smaller than the number of equations (220). The coefficients $c_c(i)$ are calculated by least squares method.

Now for the known geometric information, the calibration constant C_c can be calculated by Equation (6.42) with these calculated dimensionless coefficients c_c. To estimate the accuracy this function, the relieved displacement were recalculated with these dimensionless coefficients. To estimate the accuracy of the coefficients, we find the relative residual from the equation given below.

$$err(T_p / a) = \frac{E \, vR(T_p / a) - \sum_{i=1}^{n}(-1.09 + c_c(i) \, v)\left(\frac{T_p}{a}\right)^{i-1} \sigma_o}{E \, vR(T_p / a)} \tag{6.44}$$

Figure 6.29 and 6.30 show the relative residuals versus the object thickness (T_p/a) for n=1 and n=5. These figures also show the errors for the eleven different Poisson's ratio in the range between v=0.1 to v=0.35 at each core-hole depth. It is observed that number of terms n=5 (5 coefficients) provided a reasonable accuracy. It was also observed that the function C_c is well approximated (error less that 0.5 %) by means of a five-order algebraic polynomial obtained by the least squares method.

6.4.2. Core-Hole Case

To understand the effect of the core-hole depth ($\xi = h/r_m$) on the calibration constant C_c, the general variation of relieved displacement with core-hole depth is illustrated in Figure 6.31. In this figure, relieved displacements are normalized with respect to theoretical solution of the relieved displacement, v_o and core-hole depth is normalized with respect to measurement circle radius, r_m. The normalized the relieved displacement plots for different displacement measurement radii have similar shapes. The theoretical value of relieved displacement is approached at large core-hole depth. It is obvious that the analytical definition of the constant C cannot be used for a core-hole.

Figure 6.32 shows the variation with core-hole depth of the non-dimensional relieved displacements for different core-hole radii, a. The dimensionless measurement circle radius k in this plot is kept constant. This figure shows that when the relieved displacement is normalized with respect to the measured circle radius, dimensionless relieved displacement (v_a/r_m) will not change due to core-hole diameter change for constant k value. Figure 6.31 and Figure 6.32 show that the radius of the core-hole, a influences the magnitude of the relieved displacement, whereas the measurement circle radius r_m shows percentage relief of the relieved displacement. Compared to the analytical through-hole procedure, the calibration constant C_c for core-hole analysis involves one additional independent variable, namely, the dimensionless core-hole depth $\xi = h/r_m$. Thus, in a generalized functional form, the coefficients can be expressed as

$$C_c = f(E, v, k, \xi) \tag{6.45}$$

As seen from the generalized functional form above, for any given material properties E and v, the calibration constant C_c is simply geometric functions. This means that once the calibration constant has been determined for a particular dimensionless measurement circle radius ($k=r_m/a$) and material, same calibration constant will apply when the core-hole diameter and depth are similarly scaled. In order to remove the material dependency from C_c, leaving only the geometric dependency, the following function is introduced.

$$C_c = \frac{(c1_c + c2_c \; v)}{E}$$

(6.46)

The constants $c1_c$ and $c2_c$ are dimensionless coefficients. Substituting Equation (6.46) into Equation (6.36) we get

$$vR = \frac{v}{r_m} = \frac{(c1_c + c2_c \; v)}{E} \sigma_o$$

(6.47)

For any core-hole depth ξ, the loading condition was imposed by applying a uniform pressure applied to the core-hole surfaces (from $z = 0$ to $z = h$). In this analysis, twenty partial core-hole depths up to the maximum core-hole depth $\xi = 2$ were considered. This analysis was repeated for six Poisson's ratios at each core-hole depth: 0.1, 0.15, 0.2, 0.25, 0.30, and 0.35. The corresponding values of the relieved displacements were calculated. The finite element model explained in Section 5.3.1 is used to calculate the relieved displacements. The dimensionless coefficients $b1_c$ and $b2_c$ are determined by the least squares method.

Figure 6.33 and 6.34 show the variation with core-hole depth of the dimensionless coefficients $c1_c$ and $c2_c$.

Now for the known geometric information, the dimensionless coefficients $c1_c$ and $c2_c$ can be found from Figure 6.33 and Figure 6.34 and then calibration constant C_c can be calculated with material properties information. In order to estimate the error, relative residuals are calculated from the equation given below.

$$err(h) = \frac{E \; vR(h) - (c1_c + c2_c \; v)\sigma_o}{E \; vR(h)} * 100$$

(6.48)

Figure 6.35 shows the relative residuals versus Poisson's ratio for different core-hole depths. It is observed that the maximum error is about 0.5 % at very shallow core-hole depths. These errors reduce quickly as the core-hole depth increases. These results confirm the validity of the definition of the calibration constant C_c. As seen from these figures, the new defined calibration constant C_c approximates well the relieved displacement due to core-hole drilling for different material properties.

In order to remove the core-hole depth dependency as well as material dependency, the following approximation is introduced.

191

$$C_c = \sum_{i=1}^{n} \frac{(c1_c(i) + c2_c(i) \ v)}{E} (\xi)^{i-1} \qquad (6.49)$$

By substituting Equation (6.49) in to Equation (6.36), we obtain a linear algebraic equation having $c1_c(i)$ and $c2_c(i)$ as unknowns.

$$vR = \frac{v}{r_m} = C_c \sigma_o = \sum_{i=1}^{n} \frac{(c1_c(i) + c2_c(i) \ v)}{E} (\xi)^{i-1} \sigma_o \sin 2\alpha \qquad (6.50)$$

The number of equations is limited by the number of the relieved displacements calculated by finite element analysis at $\alpha=45°$. The relieved displacements are calculated at thirty partial core-hole depths through the core-hole depth interval of 0 to 2 times r_m for six different Poisson's ratios. The number of unknowns ($c1_c(i)$'s and $c2_c(i)$'s) were considerably smaller than the number of equations (180). The least squares method is adopted for solving the linear system.

Now for the known geometric information, the calibration constant C_c can be calculated by Equation (6.49) with these calculated dimensionless coefficients $c1_c$ and $c2_c$. To estimate the accuracy of this function, the relieved displacements were recalculated with these dimensionless coefficients. To estimate the accuracy of the coefficients, we find the relative residual from the equation given below.

$$err(\xi) = \frac{E \ vR(\xi) - \sum_{i=1}^{n}(c1_c(i) + c2_c(i) \ v)(\xi)^{i-1}\sigma_o}{E \ vR(\xi)} * 100 \qquad (6.51)$$

Figure 6.36 shows the relative residuals versus the core-hole depth (h/r_m) for n=4 and n=10. These figures also show the errors for the different Poisson's ratio at each core-hole depth. It is observed that the number of terms $n = 10$ (20 coefficients) offers a reasonable compromise between accuracy and numerical stability. It is also observed that the function C_c is well approximated (error less that 0.5 %).

6.5. EXAMPLE

In order to verify the core-drilling method for a core-hole, an example is solved below. A structure under a known in-situ state of stress before the core-hole is drilled is considered. The finite element model created in Chapter 5 is used to simulate the core-hole drilling. The measured displacements obtained from the finite element analysis are used in the procedure to calculate in-situ stresses which are assumed unknown prior to hole drilling.

In this example it is assumed that a core-hole is drilled to depth $h = 40$ mm in a structure that has uniaxial stress state of $\sigma_{xo} = 30$ MPa, $\sigma_{yo} = 0$. It is also assumed these stresses are uniformly distributed through the depth in the structure.

The material properties of the structure and geometric properties of the core-hole are given below as follows:

192

$E = 30000$ MPa, $a = 50$ mm, $k = 1.5$, $r_m = 50 * k = 75$ mm, $h = 40$ mm.

The measured displacements are calculated for Test Configuration C by finite element analysis as follows.

$U1 = 0.07992$ mm

$U2 = 0.03024$ mm

$U3 = -0.01944$ mm

Solution :

$$\left. \begin{array}{l} \xi = h/r_m = 40/75 = 0.533 \\ k = 1.5 \end{array} \right\} \rightarrow \left\{ \begin{array}{l} \text{From Figures} (6.4), \\ (6.5), (6.18) \,\&\, (6.19) \end{array} \right\} \rightarrow \boxed{ \begin{array}{l} a1_c = 0.36, a2_c = 0.176 \\ b1_c = 0.62, b2_c = 0.24 \end{array} }$$

Substituting the coefficients above into Equations (6.14) and (6.30) we get the calibration constants A_c an B_c for this particular core-hole geometry

$$A_c = \frac{a1_c + a2_c \, \nu}{E} = \frac{0.36 + 0.176 \times 0.2}{30000} = 1.31733 \times 10^{-5}$$

$$B_c = \frac{b1_c + b2_c \, \nu}{E} = \frac{0.62 + 0.24 \times 0.2}{30000} = 2.22667 \times 10^{-5}$$

From Equation (6.4), we get the constants A and B

$$A = A_c \, x \, r_m = 0.000988$$
$$B = B_c \, x \, r_m = 0.00167$$

The in-situ stress equations for Test Configuration C are given in Chapter 3 by Equations (3.132), (3.133) and (3.134). We get the in-situ stresses by substituting the measured displacements and A and B values in these equations as follows

$$\begin{aligned} \sigma_{xx} &= \frac{(U1+U3)}{4A} + \frac{(U1-U3)}{4B} \\ &= \frac{(0.07992+(-0.01944))}{4 \; 0.000988} + \frac{((0.07992-(-0.01944))}{4 \; 0.00167} = 30.178 \, \text{MPa} \end{aligned}$$

$$\begin{aligned} \sigma_{yy} &= \frac{(U1+U3)}{4A} - \frac{(U1-U3)}{4B} \\ &= \frac{(0.07992+(-0.01944))}{4 \; 0.000988} - \frac{((0.07992-(-0.01944))}{4 \; 0.00167} = 0.429 \, \text{MPa} \end{aligned}$$

$$\tau_{xy} = \frac{U1 - 2U2 + U3}{4B} = \frac{0.07992 - 2 \ x \ 0.03024 + (-0.01944)}{4 \ x \ 0.00167} = 0$$

If we use Equations (6.17) and (6.33) to calculate the calibration constants instead of using the figures, we get the results as follows

$A_c = 0.000013378$

$B_c = 0.0000220404$

$A = A_c \ x \ r_m = 0.00100335$

$B = B_c \ x \ r_m = 0.00165303$

$$\sigma_{xx} = \frac{(U1 + U3)}{4A} + \frac{(U1 - U3)}{4B} =$$

$$\frac{(0.07992 + (-0.01944))}{4 \ x \ 0.00100335} + \frac{((0.07992 - (-0.01944))}{4 \ x \ 0.00165303} = 30.096 \ MPa$$

$\sigma_{yy} = 0.042$

$\tau_{xy} = 0$
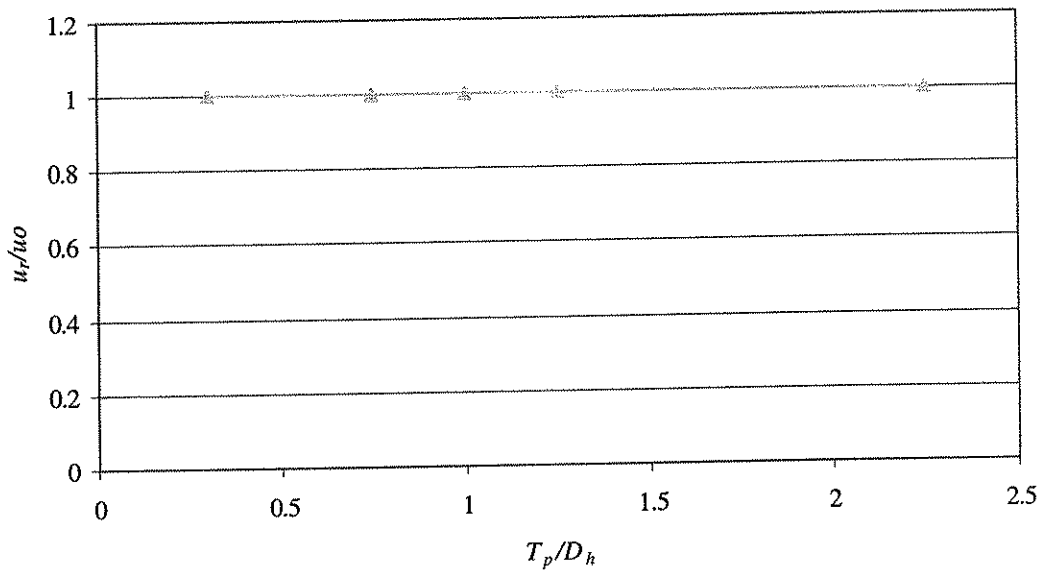
Figure 6.1 Variation with object thickness of the relieved displacement for the biaxial uniform stress state of $\sigma_{xx}=\sigma_{yy}=10$ MPa.
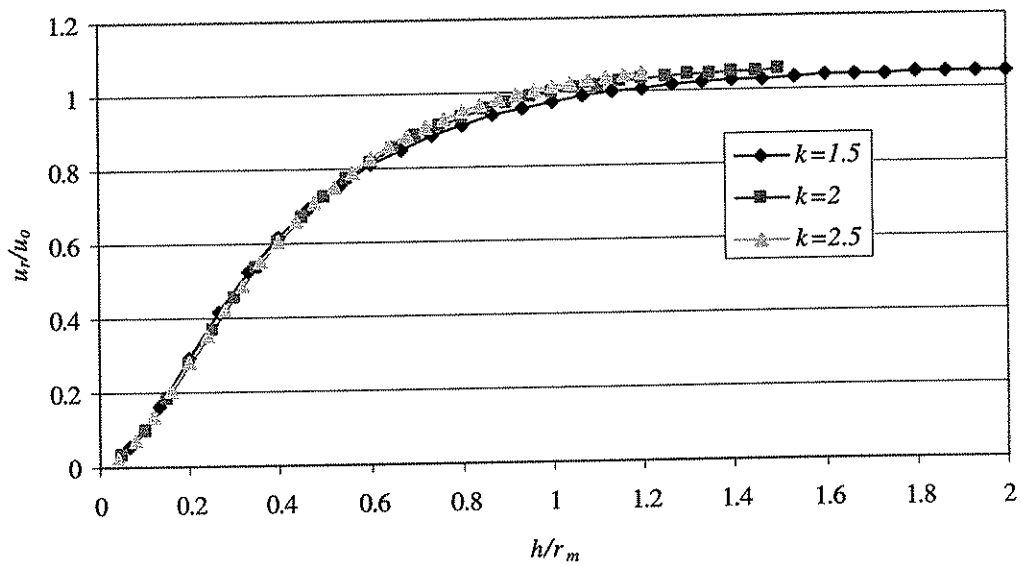
Figure 6.2 Variation with core-hole depth of the relieved displacement for the biaxial uniform stress state of $\sigma_{xx}=\sigma_{yy}=10$ MPa.
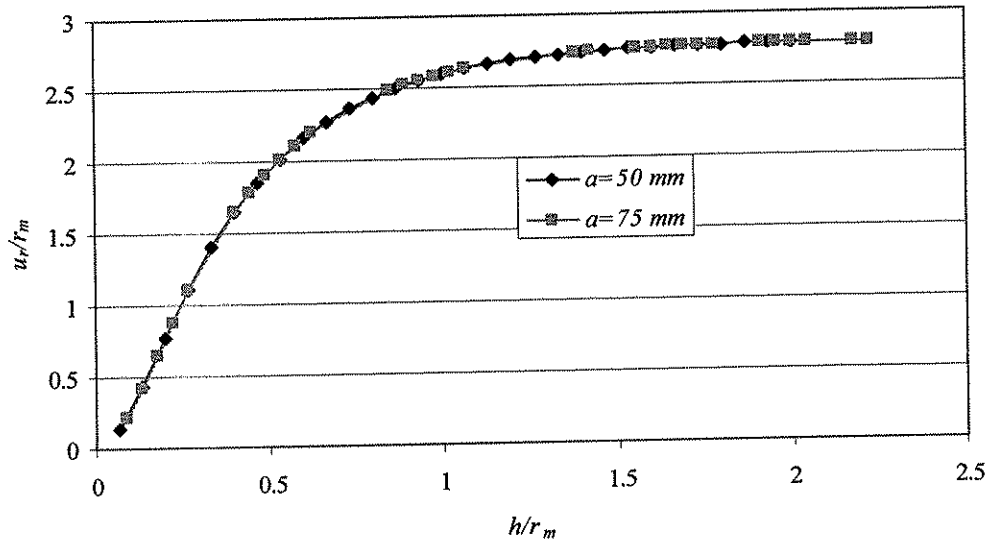
Figure 6.3 Variation with core-hole depth of the relieved displacement for different core-hole radii.
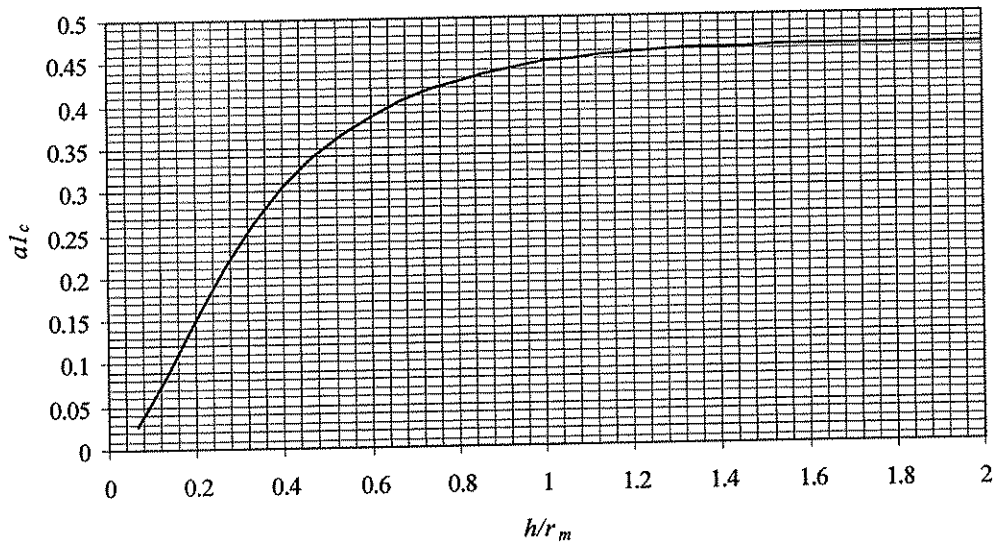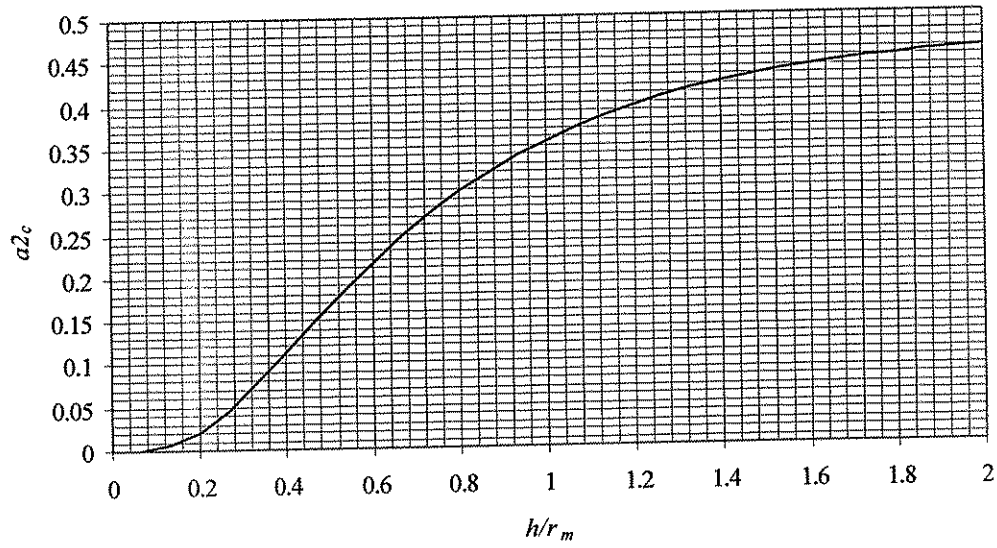

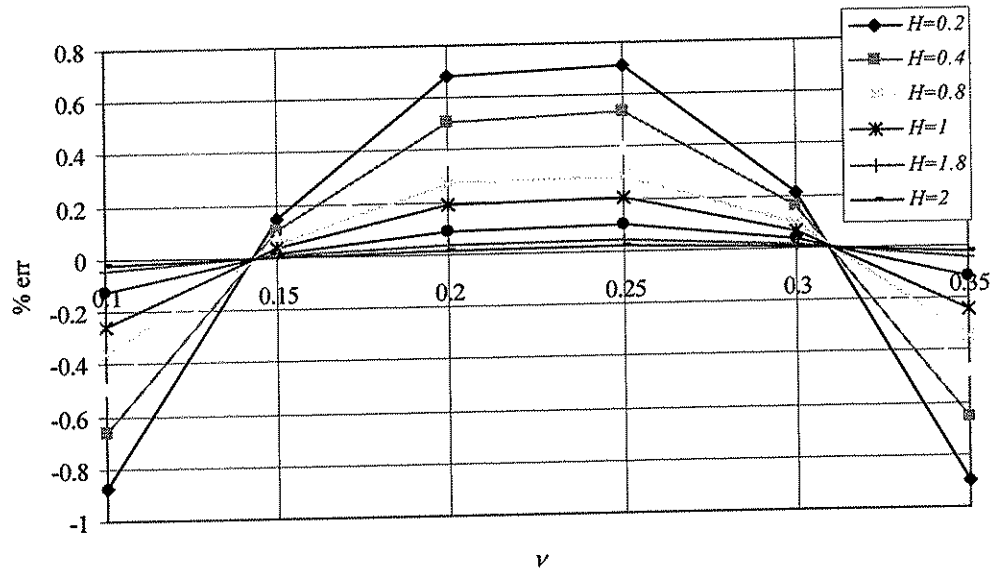Figure 6.4 Dimensionless coefficients $a1_c$ for k=1.5.

Figure 6.5 Dimensionless coefficients $a2_c$ for k=1.5.

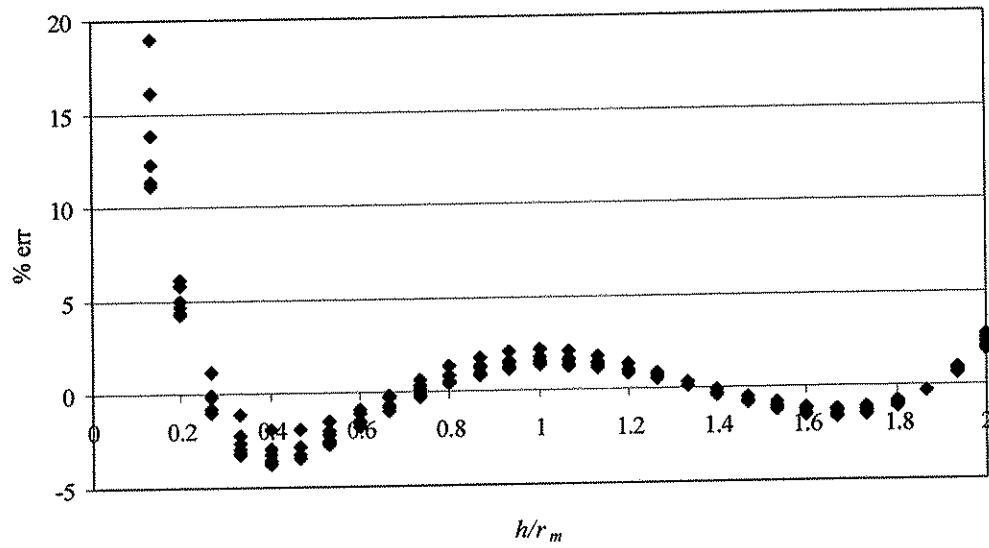Figure 6.6 Relative residual versus Poisson's ratio at different core-hole depths.

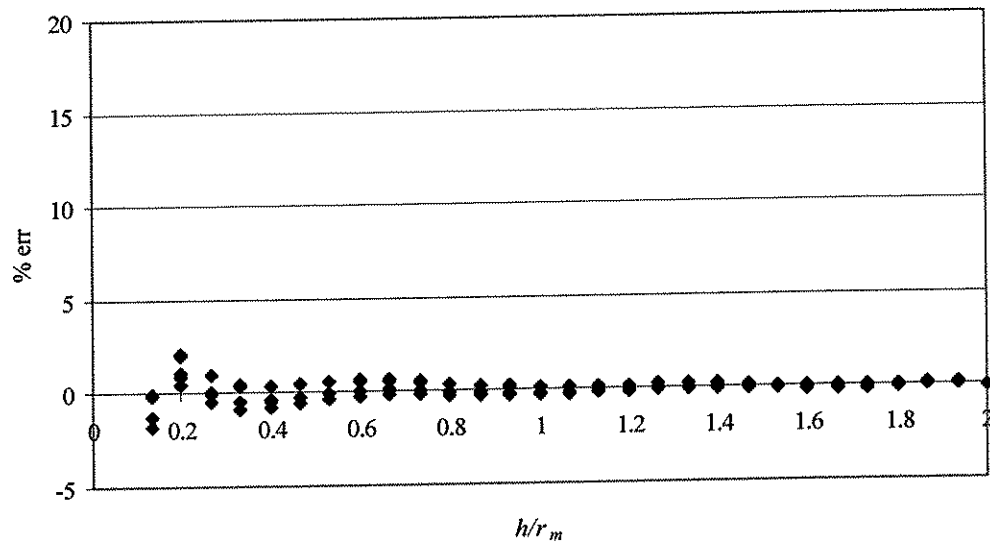Figure 6.7 Relative residual versus core-hole depth for n=4.

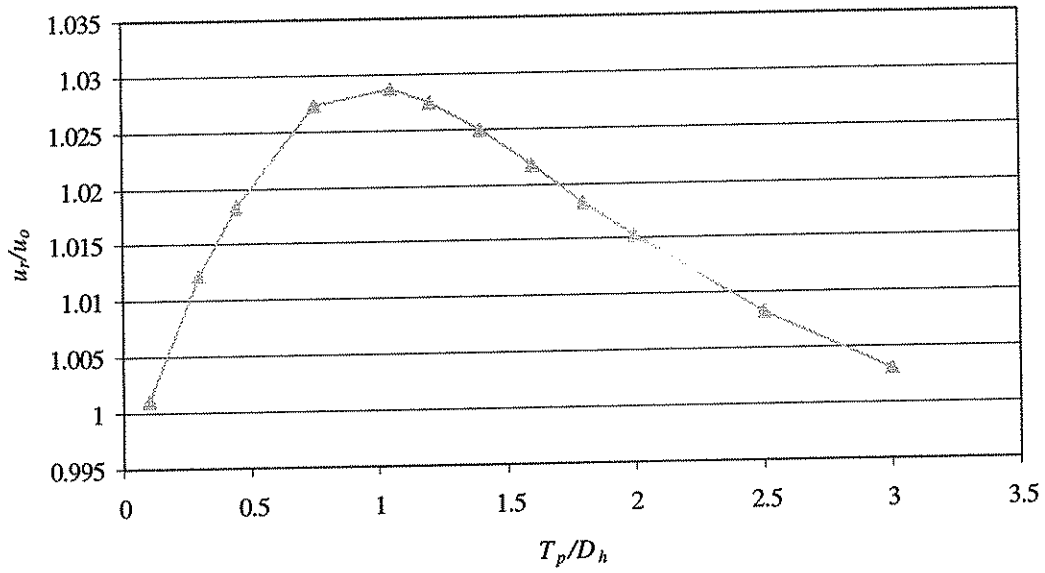Figure 6.8 Relative residual versus core-hole depth for n=8.

198

Figure 6.9 Variation with object thickness of the relieved displacement for the stress state of $\sigma_{xx}=-\sigma_{yy}=10$ MPa.
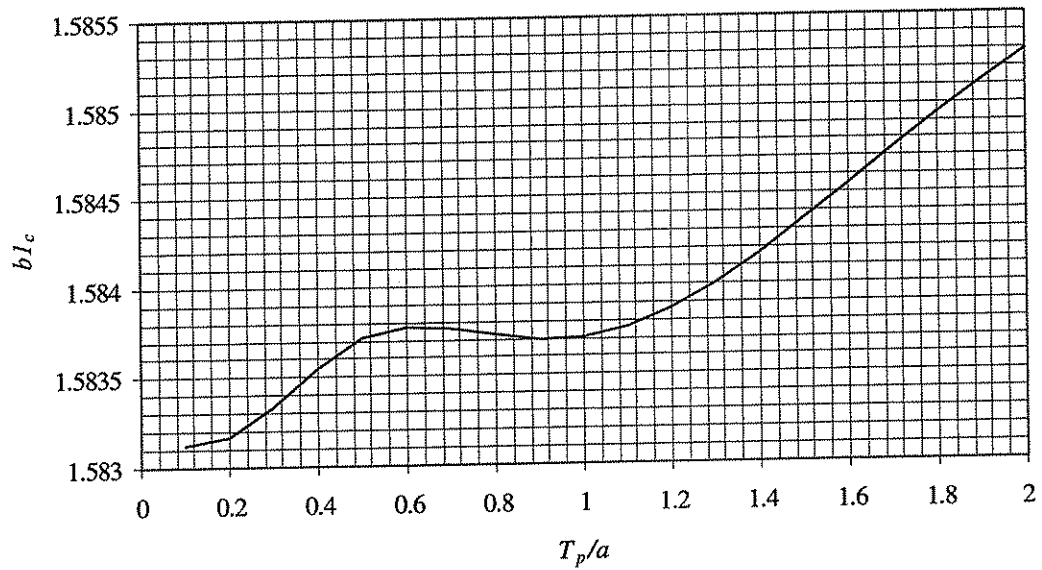
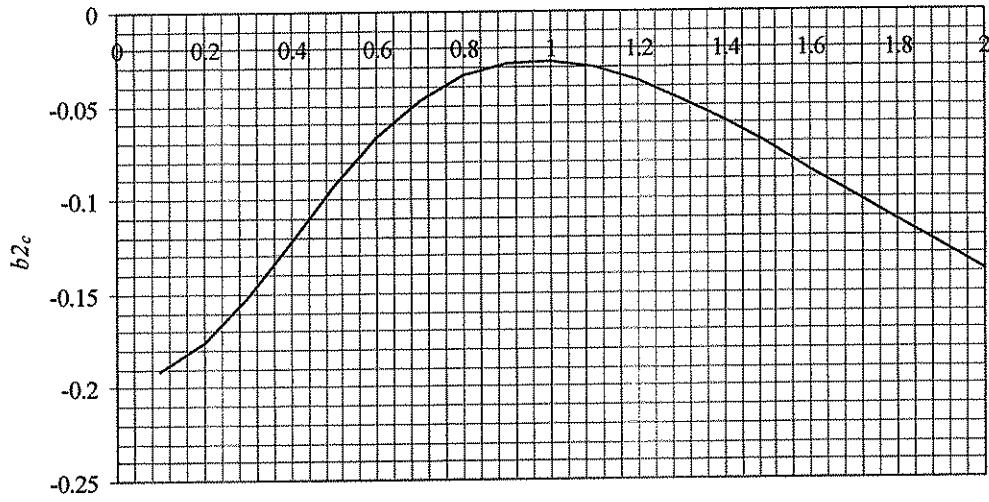

Figure 6.10 Dimensionless coefficient $b1_c$ for $k=1.5$.

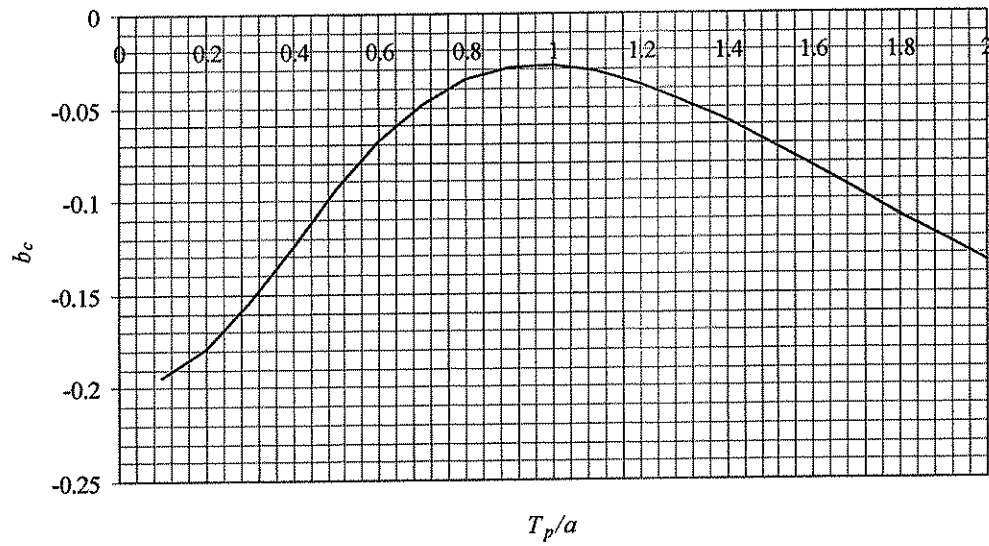Figure 6.11 Dimensionless coefficient $b2_c$ for $k=1.5$.

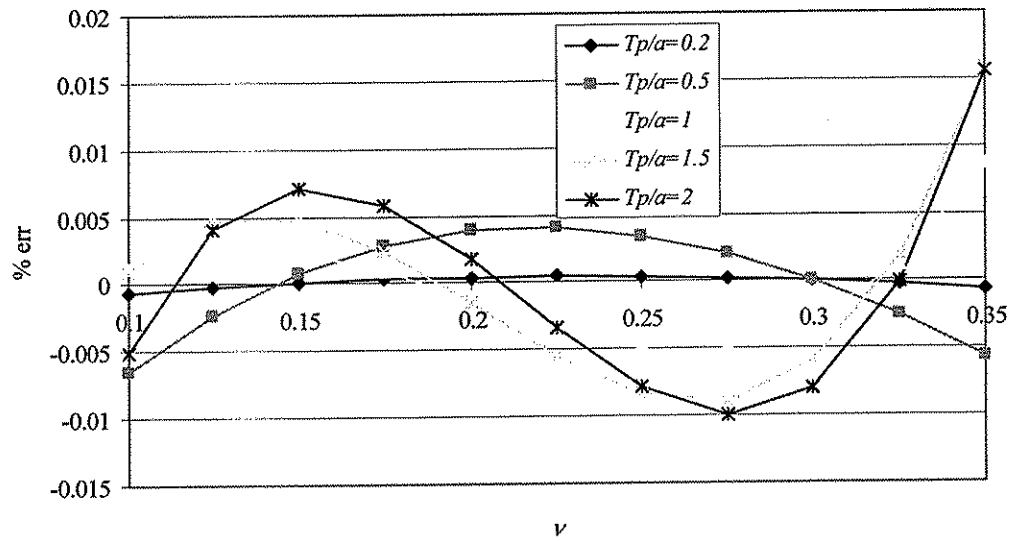Figure 6.12 Dimensionless coefficient b_c for $k=1.5$.

Figure 6.13 Relative residual versus Poisson's ratio for different core-hole depths.

Figure 6.14 Relative residual versus object thickness for n=1.

Figure 6.15 Relative residual versus object thickness for n=5.

Figure 6.16 Variation with core-hole depth of the relieved displacement for the stress state of $\sigma_{xx} = -\sigma_{yy} = 10$ MPa.

Figure 6.17 Variation with core-hole depth of the relieved displacement for different core-hole radii for stress state of $\sigma_{xx}=-\sigma_{yy}=10$ MPa.

Figure 6.18 Dimensionless coefficient $b1_c$ for $k=1.5$ and k=2.

Figure 6.19 Dimensionless coefficient $b2_c$ for k=1.5 and k=2.

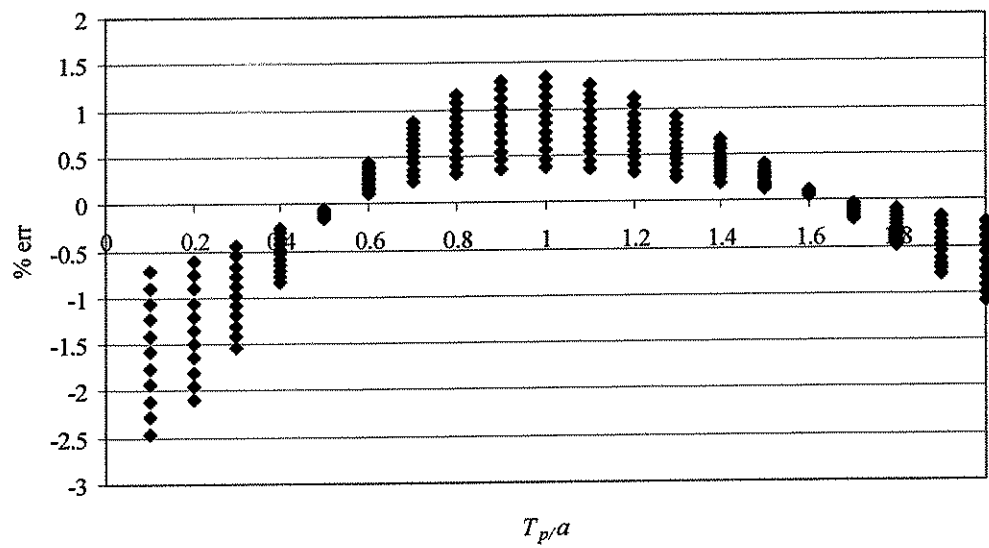Figure 6.20 Relative residual versus Poisson's ratio for different core-hole depths.

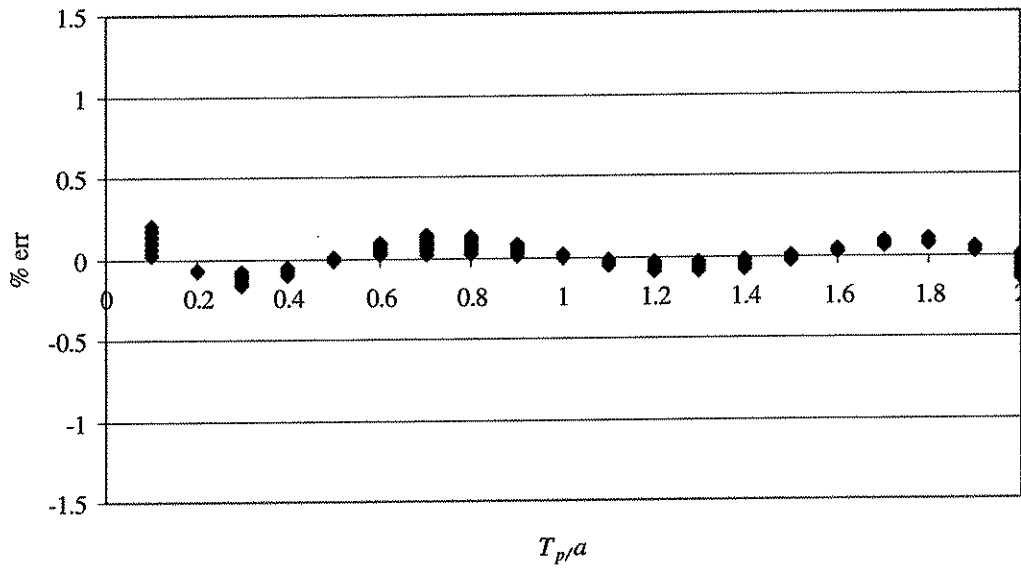Figure 6.21 Relative residual versus core-hole depth for n=3.

Figure 6.22 Relative residual versus core-hole depth for n=10.

205
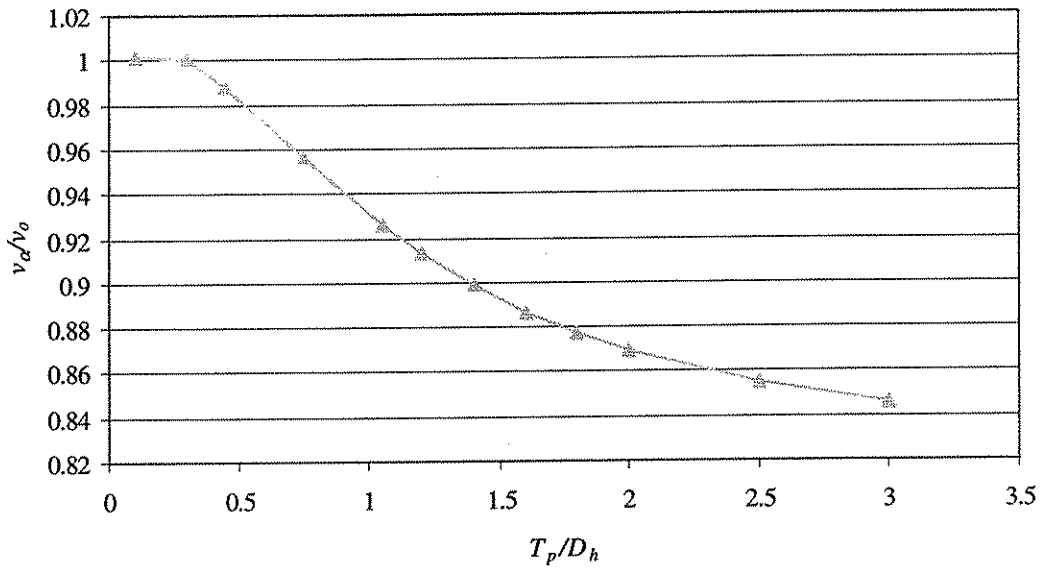
Figure 6.23 Variation with object thickness of the relieved displacement in radial direction for the stress state of $\sigma_{xx}=-\sigma_{yy}=10$ MPa.
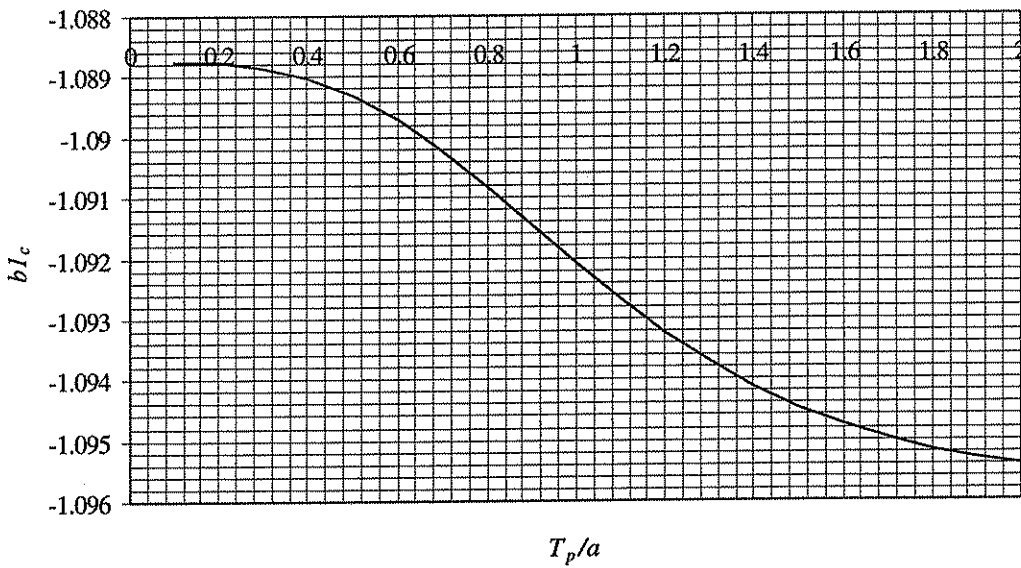
Figure 6.24 Dimensionless coefficient $c1_c$ for $k=1.5$.
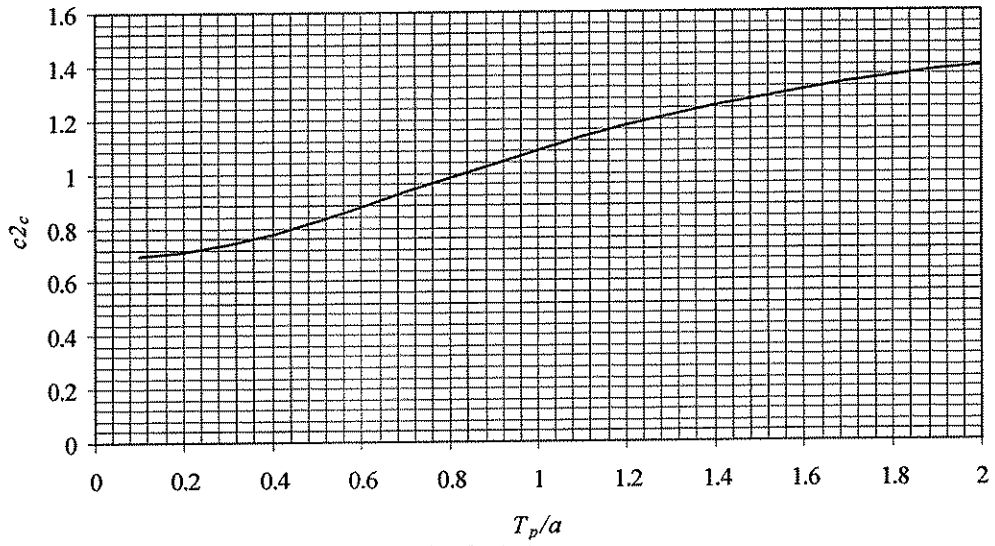
Figure 6.25 Dimensionless coefficient $c2_c$ for k=1.5.
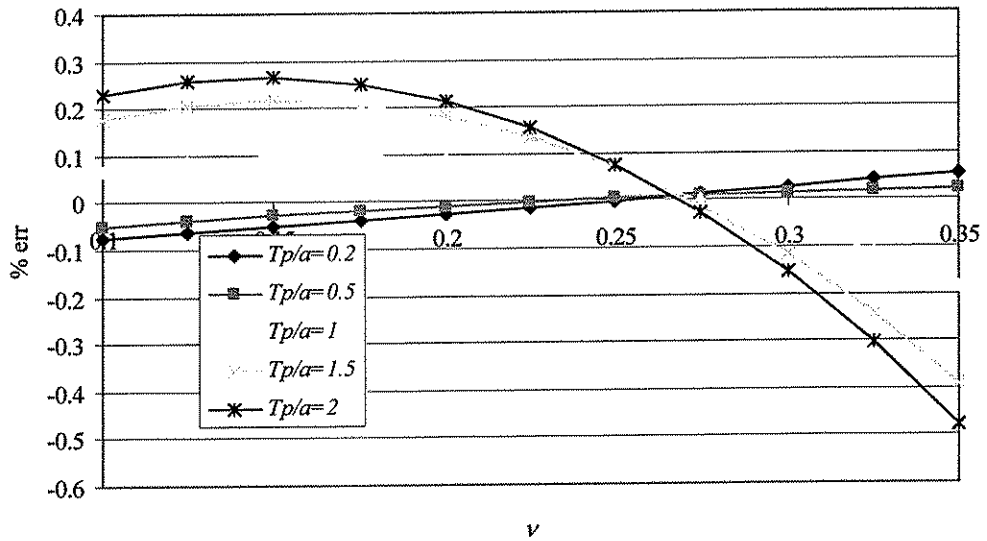
Figure 6.26 Relative residual versus Poisson's ratio for different core-hole depths.
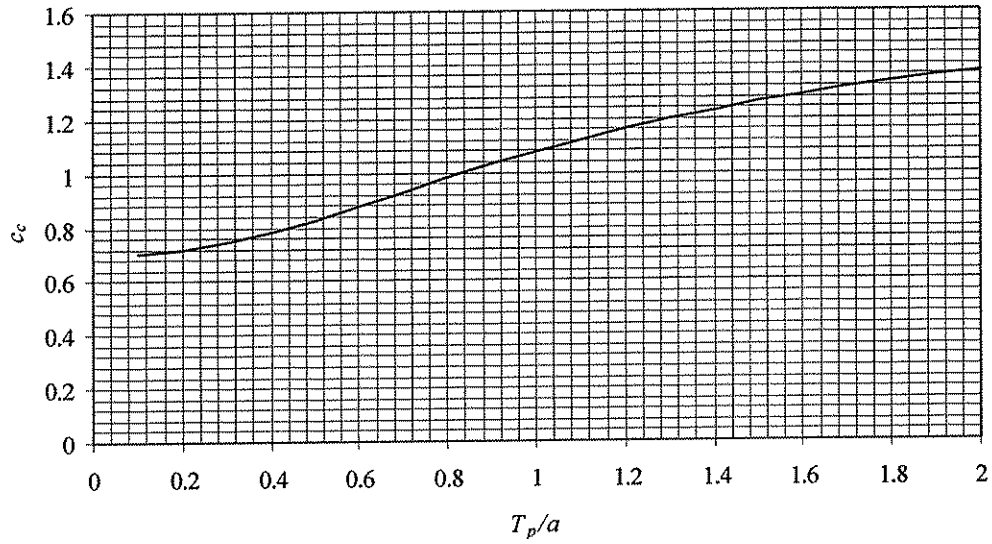
Figure 6.27 Dimensionless coefficient c_c for k=1.5.
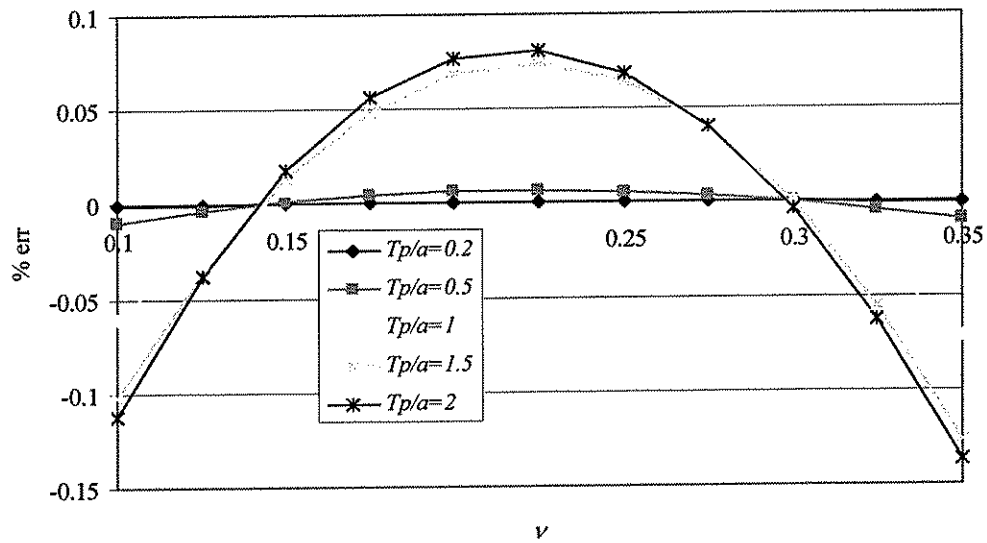
Figure 6.28 Relative residual versus Poisson's ratio for different core-hole depths.
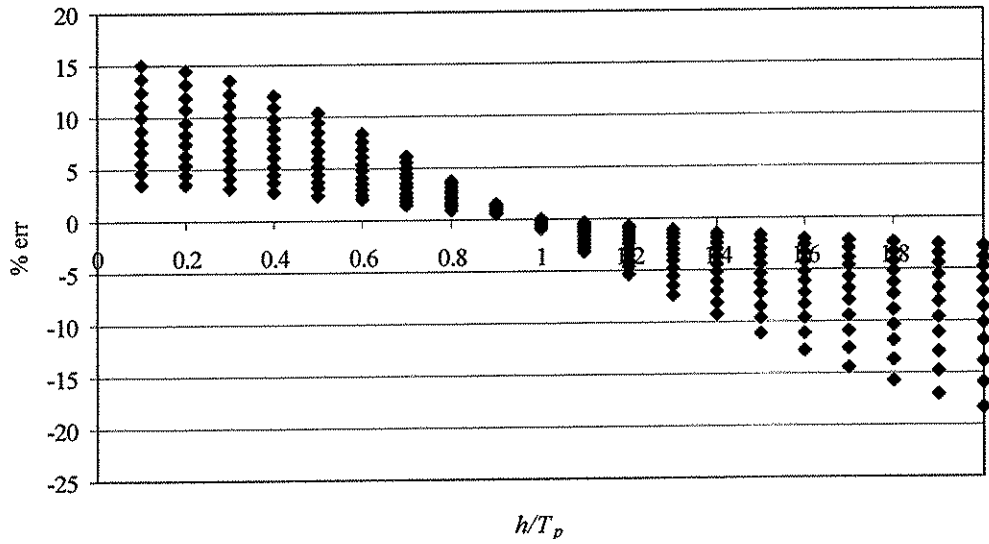
Figure 6.29 Relative residual versus core-hole depth for n=1.
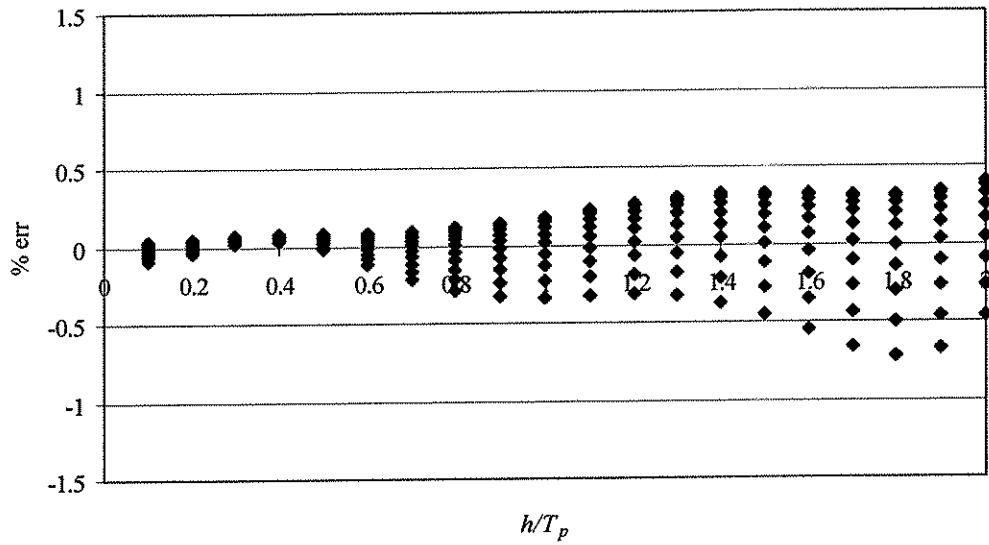
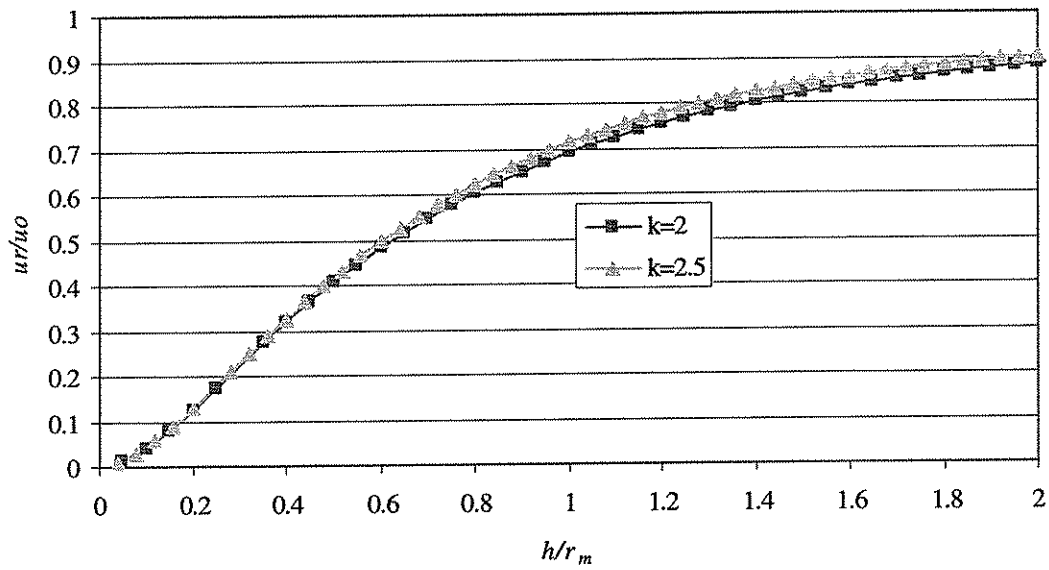Figure 6.30 Relative residual versus core-hole depth for n=5.
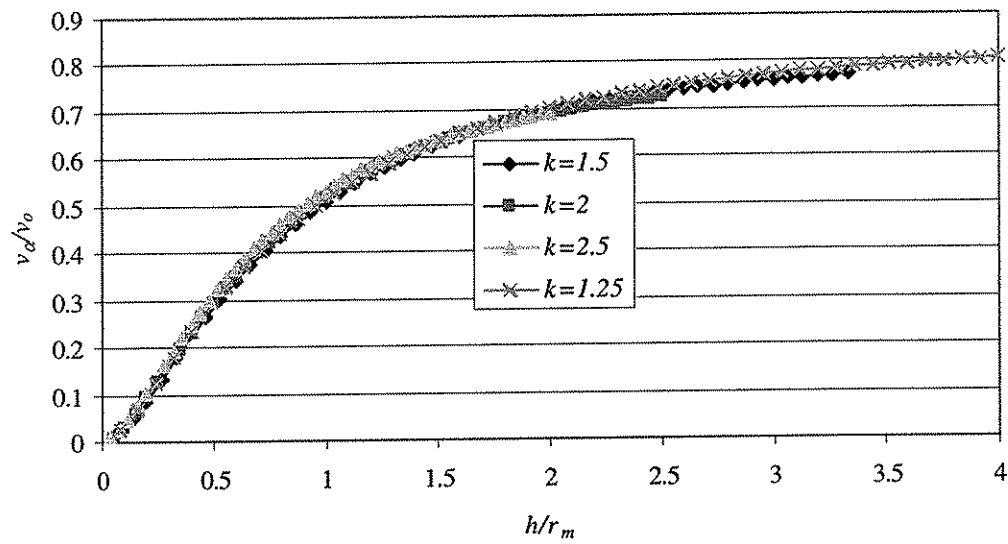
Figure 6.31 Variation with core-hole depth of the relieved displacement for the stress state of $\sigma_{xx}=-\sigma_{yy}=10$ MPa.
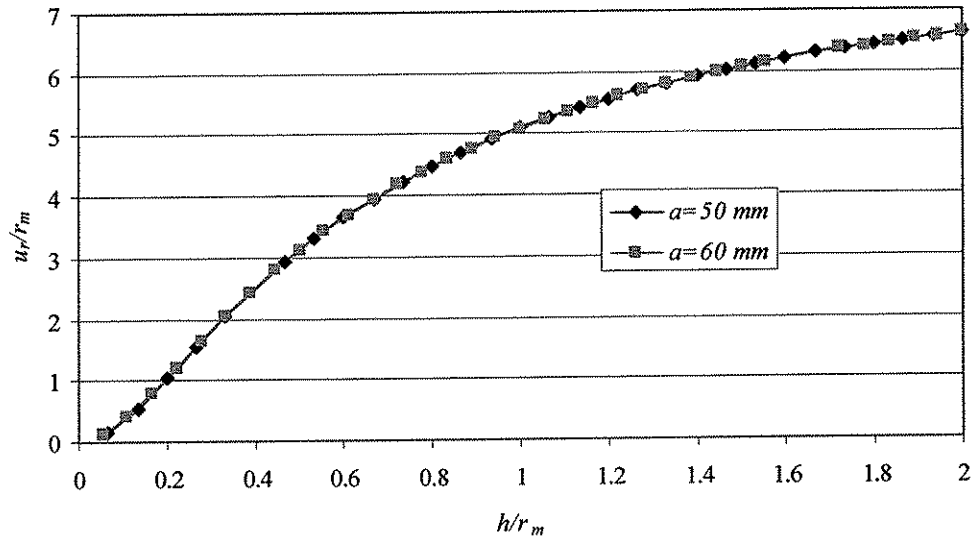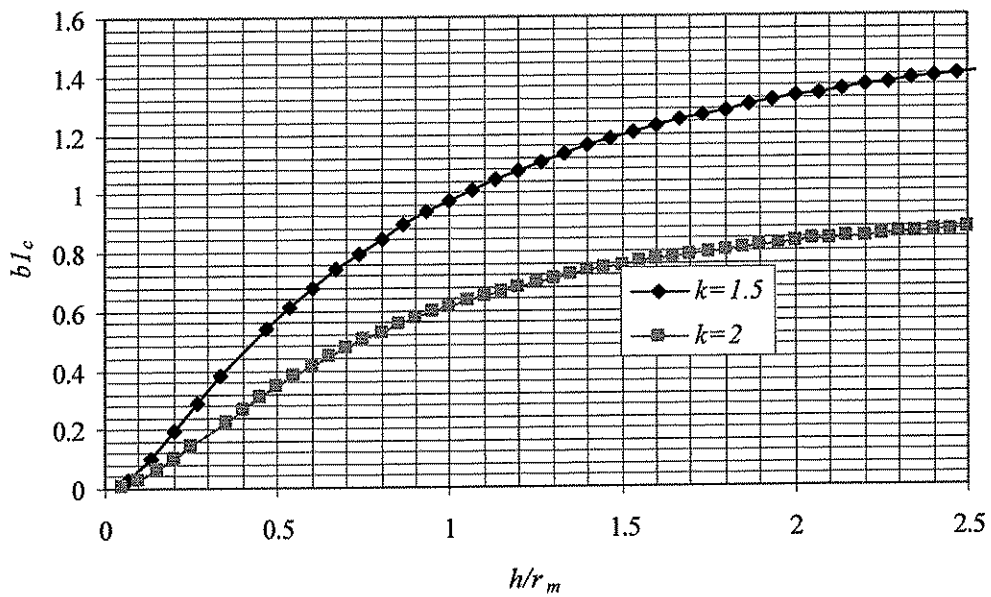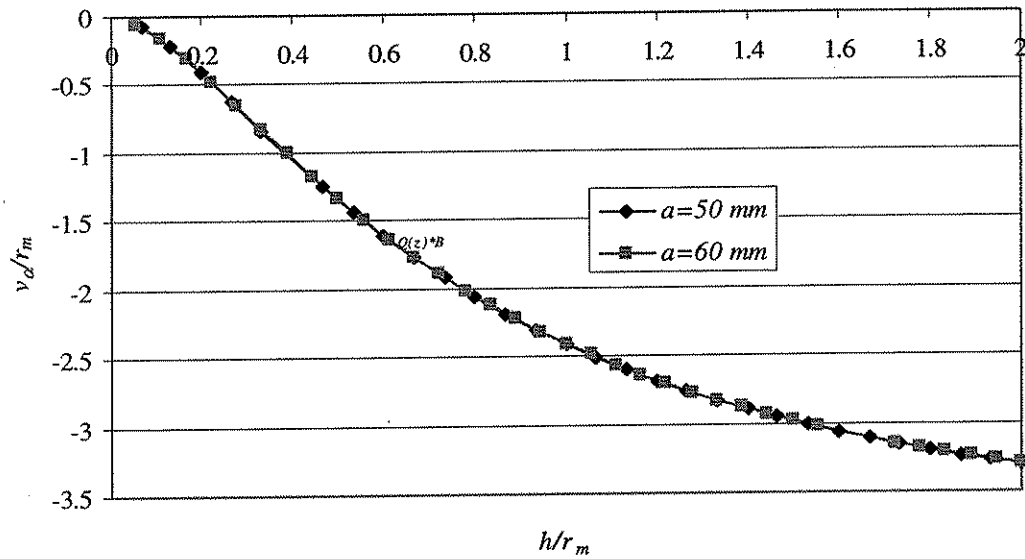

Figure 6.32 Variation with core-hole depth of the relieved displacement for different core-hole radii.
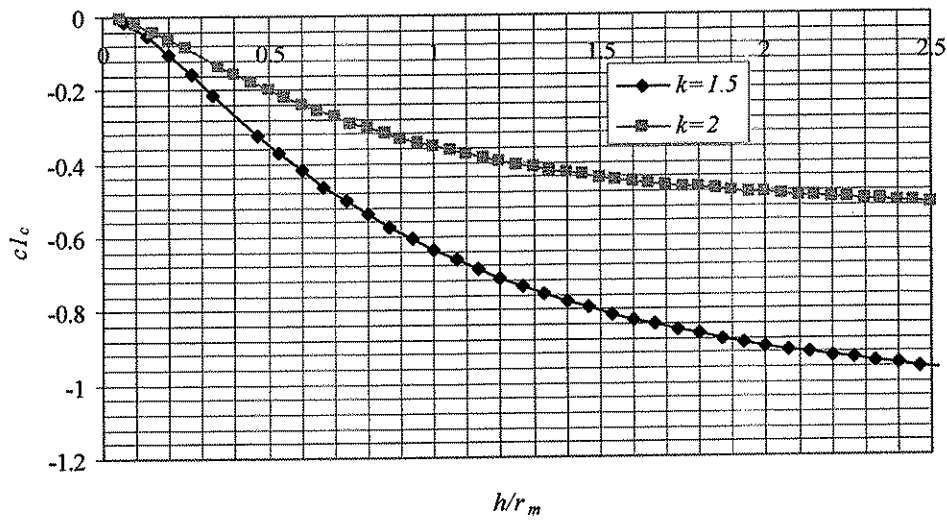
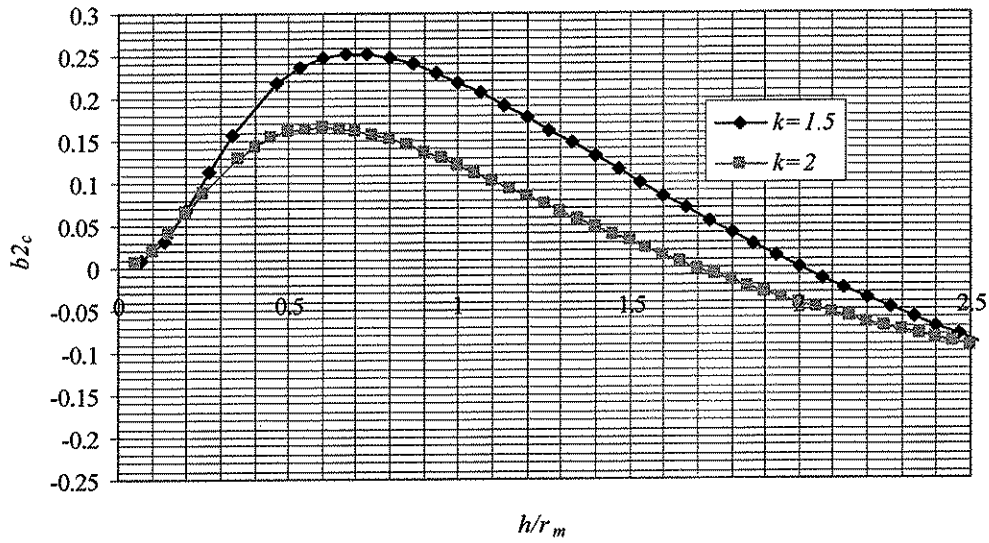Figure 6.33 Dimensionless coefficient $c1_c$ for k=1.5 and k=2.
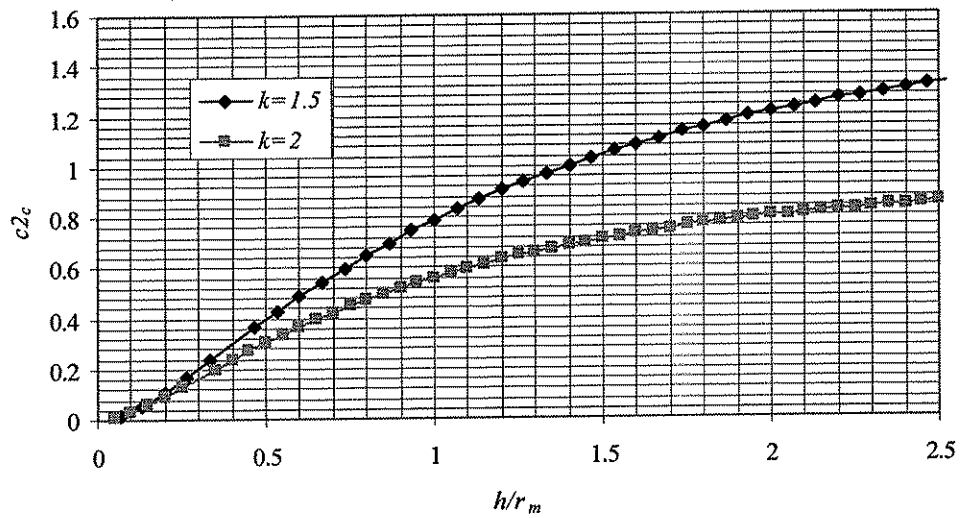
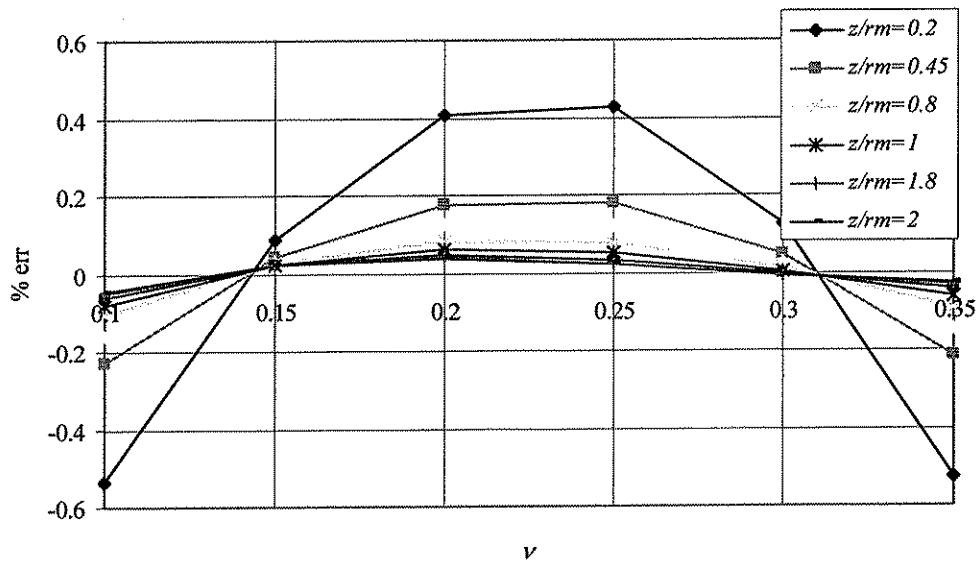Figure 6.34 Dimensionless coefficient $c2_c$ for k=1.5 and k=2.

211
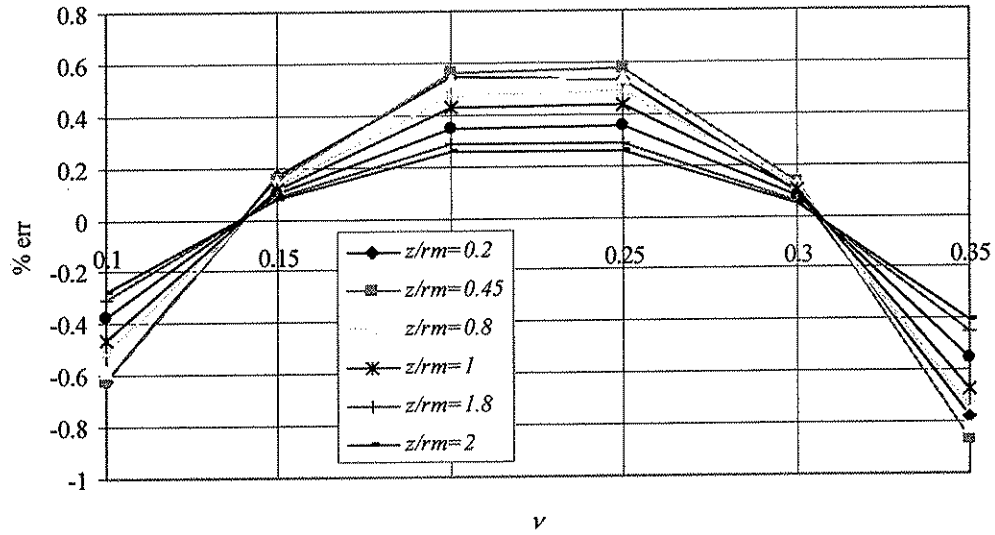
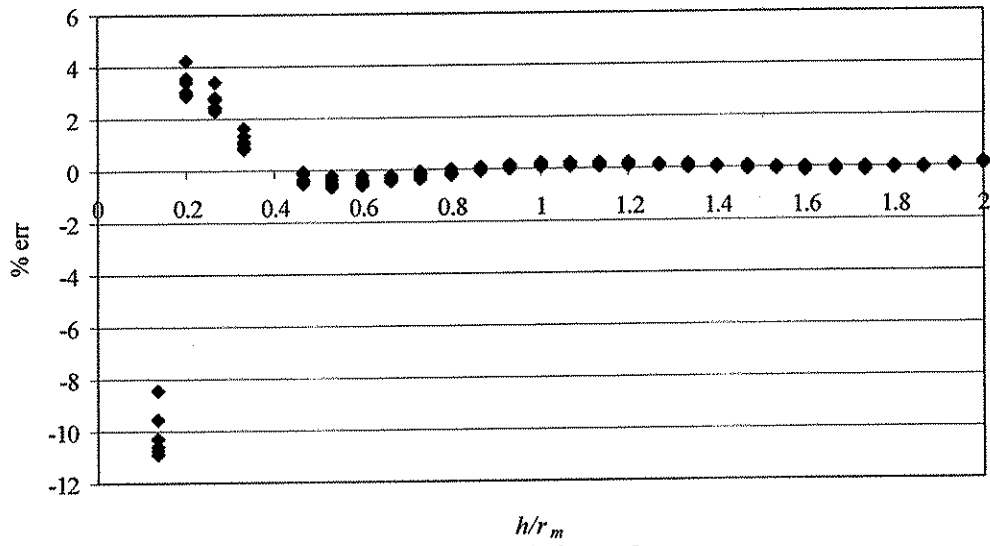Figure 6.35 Relative residual versus Poisson's ratio for different core-hole depths.
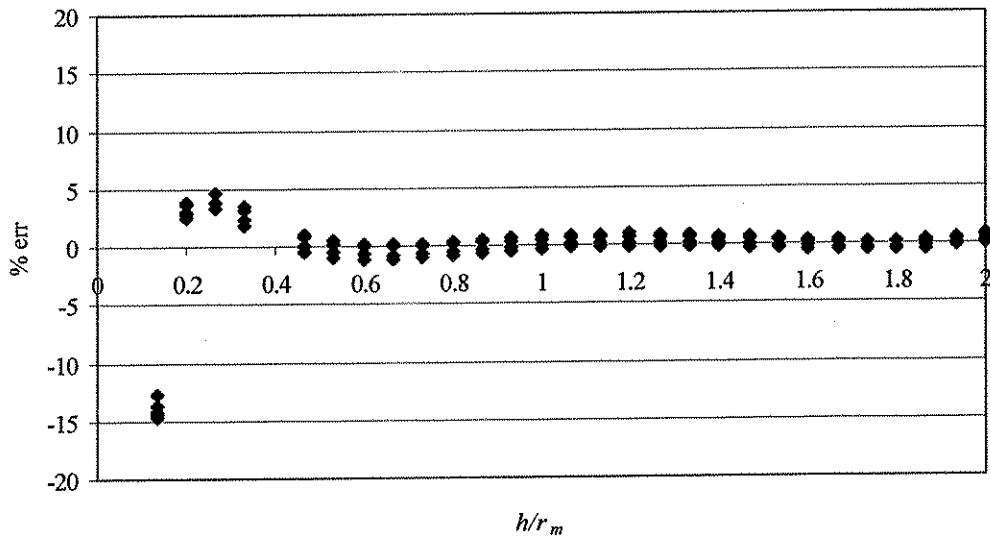
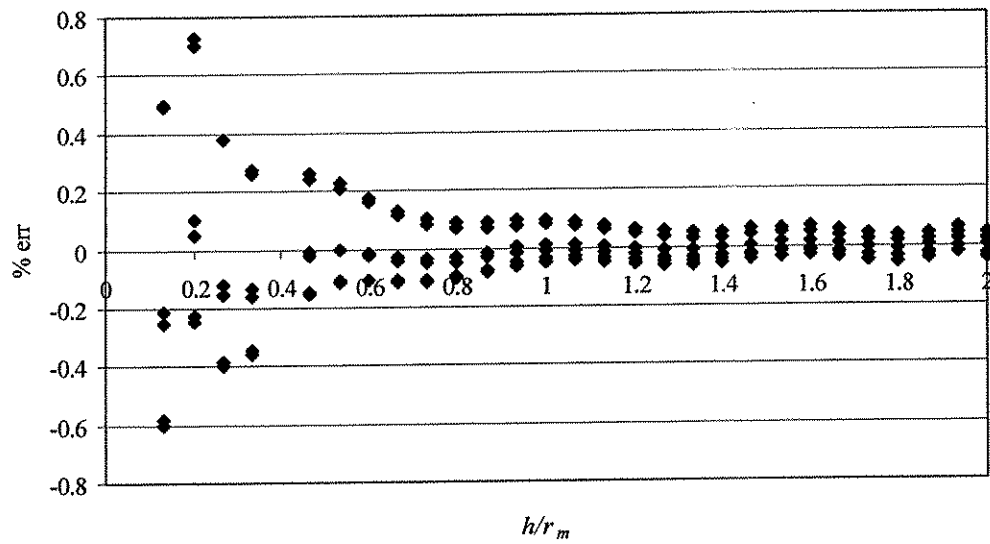Figure 6.36 Relative residual versus core-hole depth for n=4.
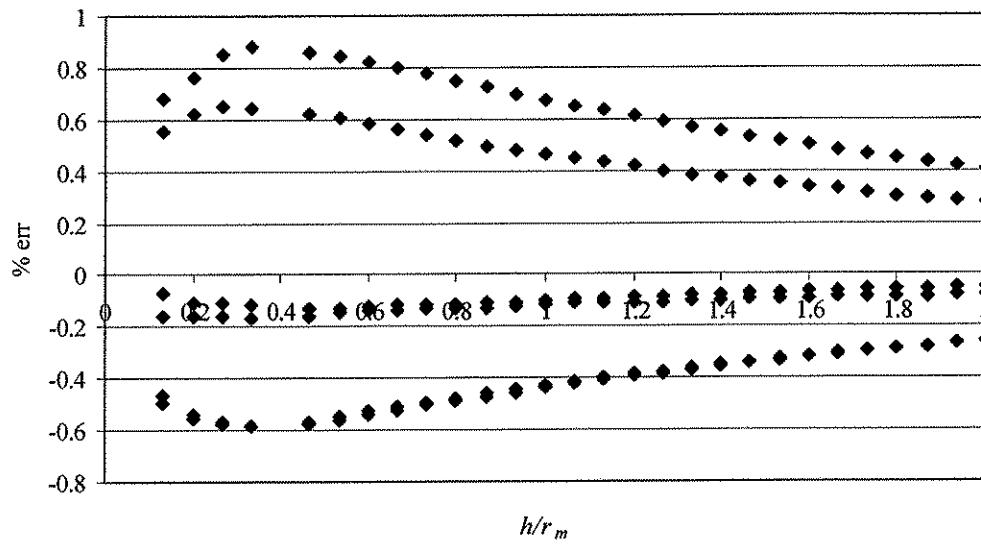
Figure 6.37 Relative residual versus core-hole depth for n=10.

i	$a1_c(i)$	$a2_c(i)$
1	-0.072834	0.044251
2	1.23465	-0.746918
3	-0.225292	4.28656
4	-2.40789	-6.97061
5	3.66435	5.98131
6	-2.43128	-2.92677
7	0.785519	0.771277
8	-0.100549	-0.084988

Table 6.1 Coefficients $a1_c(i)$ and $a2_c(i)$'s of calibration constant A_c for core-hole.

$b_c(1)$	$b_c(2)$	$b_c(3)$	$b_c(4)$	$b_c(5)$
-0.228525	0.243375	0.185763	-0.315128	0.086965

Table 6.2 Coefficients $b_c(i)$ of calibration constant B_c for through-hole.

i	$b1_c(i)$	$b2_c(i)$
1	-0.030346	-0.002529
2	0.487421	-0.081817
3	1.26614	2.23475
4	-3.22926	-5.43454
5	3.46104	5.91912
6	-1.99166	-3.42679
7	0.596501	1.02583
8	-0.072916	-0.124991

Table 6.3 Coefficients $b1_c(i)$ and $b2_c(i)$'s of calibration constant B_c for core-hole.

$c_c(1)$	$c_c(2)$	$c_c(3)$	$c_c(4)$	$c_c(5)$
0.689908	-0.063583	0.908608	-0.580321	0.113251

Table 6.4 Coefficients $c_c(i)$ of calibration constant C_c for through-hole.

i	$c1_c(i)$	$c2_c(i)$
1	0.010131	-0.014132
2	-0.207351	0.132517
3	-2.65581	3.32105
4	5.20287	-6.14804
5	-4.99857	5.87338
6	2.69098	-3.19519
7	-0.770175	0.927924
8	0.091102	-0.111366

Table 6.5 Coefficients $c1_c(i)$ and $c2_c(i)$'s of calibration constant C_c for core-hole.

CHAPTER 7

INCREMENTAL CORE-DRILLING METHOD

7.1. INTRODUCTION

The incremental core-drilling method is developed primarily for applications in which in-situ stresses are non-uniform through the drilling depth. In such cases, the procedure, analytical definition of the calibration constants, and the calibration constant values given in previous chapters are not applicable. However using the incremental core-drilling method, it is possible to obtain the in-situ stresses as a function of depth z measured from the specimen surface.

The experimental procedure in the incremental core-drilling method is similar to the procedure for the core-drilling method for uniform in-situ stress through the thickness. The incremental core-drilling method involves measuring displacements after successive increments of core-hole depth. Then these measured displacements are related to the in-situ stresses that vary through the depth.

The organization of the remainder of this chapter is as follows. Section 7.2 presents the theory of the formulation of the incremental core-drilling method. Section 7.3 explains the definition of the calibration constants for non-uniform stresses through the depth. Finally, Section 7.4 presents examples to illustrate the method.

7.2. THEORY

The incremental core-drilling method is similar to Integral Method (e.g. Flaman 1985; Niku-Lari 1985; Schajer 1981; 1988a; 1988b) and Influence Function Method (Beghini 1998; 2000) developed for measuring non-uniform residual stress in steel. Even though the main concept of the core-drilling method is similar to Integral Method, the calibration constants are defined with continuous influence functions, which do not need any interpolation.

In this method, the material is assumed linear elastic, isotropic and homogenous. Plane stress conditions are assumed. It is assumed that in-situ stresses perpendicular to the surface (in z direction) are zero or negligible. The in-situ stresses are described as a function of depth z from the surface.

There is no solution available in closed-form for non-uniform stress through depth. However, a similar approach as followed in Chapter 6, i.e. a so-called semi-analytical solution, is followed in this chapter to develop a solution procedure for non-uniform stress through depth. As mentioned earlier, in the semi-analytical solution procedure, the closed-form equations for relieved displacement and in-situ stresses that were derived in Chapter 3 are treated as the main form of the equations for the solution. However, the constants A, B, and C in these equations are treated as calibration constants and are calculated in numerical analysis.

Consider a structure having non-uniform in-situ stresses through its thickness as shown in Figure 7.1. If a core-hole is drilled to the core-hole depth h in three increments and then the stresses equivalent to the relieved in-situ stresses (stresses relieved due to core-hole drilling) are applied to the core-hole surface, the state of equilibrium remains unchanged as shown in Figure 7.2 (this figure shows half symmetry of the structure). As explained before, if the relieved in-situ stresses which are equivalent and opposite sign of the equilibrium stresses are applied to the hole surface, we get the relieved displacements due to the core-hole drilling to the depth h. This can be shown by superposition of the relieved in-situ stresses at each core-hole increment as shown in Figure 7.3. This shows that if a core-hole is drilled to the core-hole depth h in an incremental fashion, the relieved displacement measured at a core-hole depth h is partly due to the in-situ stresses released in the last increment, and partly due to the in-situ stresses relieved in previous core-hole increments.

As explained before, the relieved in-situ stresses due to drilling a hole in a structure under a uniform stress state are given by Equations (3.3) and (3.4). For the non-uniform stress state through the thickness, the in-situ stresses are a function of the depth H and are expressed as follows

$$N(H) = \frac{\sigma_{xx}(H) + \sigma_{yy}(H)}{2} + \frac{\sigma_{xx}(H) - \sigma_{yy}(H)}{2}\cos 2\alpha + \tau_{xy}(H)\sin 2\alpha \qquad (7.1)$$

$$T(H) = -\frac{\sigma_{xx}(H) - \sigma_{yy}(H)}{2}\sin 2\alpha + \tau_{xy}(H)\cos 2\alpha \qquad (7.2)$$

For convenience, all the geometric dimensions are normalized by the measurement circle radius r_m as follows

$H = z/r_m$ = non-dimensional depth from surface;

z = depth from surface;

$\xi = h/r_m$ = non-dimensional core-hole depth;

r_m = measurement circle radius;

h = core-hole depth.

217

As seen from the relieved in-situ stress equations, an arbitrary stress distribution can be decomposed into an equibiaxial and pure shear stress components. We can rearrange Equations (7.1), (7.2) as follows

$$N(H) = P(H) + Q(H)\cos 2\alpha + \tau_{xy}(H)\sin 2\alpha \tag{7.3}$$

$$T(H) = -Q(H)\sin 2\alpha + \tau_{xy}(H)\cos 2\alpha \tag{7.4}$$

where

$$P(H) = \frac{\sigma_{xx}(H) + \sigma_{yy}(H)}{2} \tag{7.5}$$

$$Q(H) = \frac{\sigma_{xx}(H) - \sigma_{yy}(H)}{2} \tag{7.6}$$

To ease calculation, the relieved in-situ stresses components $P(H)$, $Q(H)$, and $\tau(H)$ are considered separately. We first consider a core-hole under an equibiaxial loading distribution $P(H)$. To derive the equations for the relieved displacements, a unit load is applied to the core-hole surface at arbitrary point H when the core-hole depth is ξ as shown in Figure 7.4. If a unit concentrated load is applied in plane at an arbitrary point H when the core-hole depth is ξ (Figure 7.4), assume that the relieved displacement at the surface is

$$uR(\xi, H) = \frac{1}{Er_m} G_A(\xi, H) \tag{7.7}$$

The function $G_A(\xi, H)$, represents the relieved displacement due to a unit equibiaxial stress P applied at H when the core-hole depth is ξ. This function is known as the influence function. The influence functions depend on the geometric properties of the core-hole ξ, k and material property ν.

As a core-hole is drilled to a certain depth ξ, the in-situ stresses released at every intermediate depth H, between the surface and the depth ξ, contribute to the relieved displacements. As explained above (see Figure 7.3), the relieved displacements when the core-hole is drilled to depth h are the superposition of the relieved displacements due to the relieved in-situ stresses at each core-hole increment. By superposition, the relieved displacement $uR(\xi)$ due to a loading distribution $P(H)$ is given by

$$uR(\xi) = \frac{1}{E} \int_0^\xi G_A(\xi, H) P(H) dH \tag{7.8}$$

Similarly, if we consider pure shear stress case, we can write the relieved displacement equations caused by $Q(H)$ and $\tau(H)$ separately as follows

218

$$uR(\xi) = \frac{1}{E} \int_0^\xi G_B(\xi, H) Q(H) \cos(2\alpha) dH \qquad (7.9)$$

$$vR(\xi) = \frac{1}{E} \int_0^\xi G_C(\xi, H) Q(H) \sin(2\alpha) dH \qquad (7.10)$$

$$uR(\xi) = \frac{1}{E} \int_0^\xi G_B(\xi, H) \tau(H) \sin(2\alpha) dH \qquad (7.11)$$

$$vR(\xi) = \frac{1}{E} \int_0^\xi -G_C(\xi, H) \tau(H) \cos(2\alpha) dH \qquad (7.12)$$

By superposition, the relieved displacement equations can be written as follows

$$uR(\xi) = \frac{u_r(\xi)}{r_m} = \frac{1}{E} \int_0^\xi G_A(\xi, H) P(H) dH + \frac{1}{E} \int_0^\xi G_B(\xi, H) Q(H) dH \cos 2\alpha$$
$$+ \frac{1}{E} \int_0^\xi G_B(\xi, H) \tau_{xy}(H) dH \sin 2\alpha \qquad (7.13)$$

$$vR(\xi) = \frac{1}{E} \int_0^\xi G_C(\xi, H) Q(H) \sin(2\alpha) dH + \frac{1}{E} \int_0^\xi -G_C(\xi, H) \tau(H) \cos(2\alpha) dH \qquad (7.14)$$

where, $G_B(\xi, H)$ and $G_C(\xi, H)$ are the influence functions that represent the relieved displacements in radial and tangential directions, respectively, due to unit pure shear stress (Q) applied at a depth H when core-hole depth is ξ.

Now we deal with integral equation of first type (Tricomi 1985) because the stress profile is unknown inside the integral. Since Equations (7.13) and (7.14) cannot be solved in closed-form, these equations are solved numerically by expanding influence functions in double-power series. For the known influence functions and measured displacements, we can find stress variations through the core-hole depth by Equations (7.13), (7.14).

To solve Equations (7.13), (7.14), first the influence functions $G_A(\xi, H)$, $G_B(\xi, H)$ and $G_C(\xi, H)$ need to be calculated. These influence functions are represented by double-power expansion as follows

$$G_A(\xi, H) = \sum_{j=1}^n \sum_{i=1}^n a_{ij} \xi^{i-1} H^{j-1} \qquad (7.15)$$

$$G_B(\xi, H) = \sum_{j=1}^n \sum_{i=1}^n b_{ij} \xi^{i-1} H^{j-1} \qquad (7.16)$$

$$G_C(\xi, H) = \sum_{j=1}^n \sum_{i=1}^n c_{ij} \xi^{i-1} H^{j-1} \qquad (7.17)$$

219

If we substitute Equations (7.15), (7.16), and (7.17) in to Equation (7.13), we get

$$uR(\xi) = \frac{1}{E} \int_0^\xi \sum_{j=1}^n \sum_{i=1}^n a_{ij} \xi^{i-1} H^{j-1} P(H) dH$$

$$+ \frac{1}{E} \int_0^\xi \sum_{j=1}^n \sum_{i=1}^n b_{ij} \xi^{i-1} H^{j-1} Q(H) dH \cos 2\alpha \qquad (7.18)$$

$$+ \frac{1}{E} \int_0^\xi \sum_{j=1}^n \sum_{i=1}^n b_{ij} \xi^{i-1} H^{j-1} \tau_{xy}(H) dH \sin 2\alpha$$

where the coefficients a_{ij}, b_{ij} and c_{ij} depend on the geometric properties of the core-hole, k, and v. These coefficients are calculated by finite element analysis.

7.2.1. Calculation of Coefficients a_{ij}, b_{ij} and c_{ij}

The coefficients a_{ij}, b_{ij} and c_{ij} are calculated by finite element analysis. In these analyses, the incremental core-hole drilling process is simulated by removing subsequent layers of elements in the fine element model as explained in Chapter 5. A separate finite element analysis is performed for each coefficient. The coefficient a_{ij} is related equibiaxial stress acting through thickness. The coefficients b_{ij} and c_{ij} are related to pure shear stress. The coefficient a_{ij} is required to consider axisymmetrical part to which is applied ax symmetrical load. However, the coefficients b_{ij} and c_{ij}, corresponding pure shear stress, are required to consider non-axisymmetric loading.

The coefficient a_{ij} is associated with mean biaxial stress P. Therefore, in order define coefficient a_{ij}, we consider a known equibiaxial stress state of $\sigma_{xx} = \sigma_{yy} = \sigma_o$. If we integrate Equation (7.18) from 0 to H in a core-hole having depth ξ we get

$$uR(\xi, H) = \frac{1}{E} \int_0^H \sum_{i=1}^n \sum_{j=1}^n a_{ij} H^{j-1} \xi^{i-1} P(H) dH \qquad (7.19)$$

Considering $P(H)$ to be a constant, this yields

$$uR(\xi, H) = \frac{1}{E} \sum_{j=1}^n \sum_{i=1}^n \frac{a_{ij}}{j} \xi^{i-1} H^j P \qquad (7.20)$$

Equation (7.20) is the relieved displacement due to a loading of uniform stress from the surface to the depth H, when the core hole depth is ξ.

Equation (7.20) can be written as follows

$$\frac{1}{E} \sum_{j=1}^n \sum_{i=1}^n \frac{a_{ij}}{j} \xi_k^{i-1} \xi_l^j P = uR_{kl} \qquad (7.21)$$

A series of loading conditions are applied as shown in Figure 7.5 by applying a unit pressure to the core-hole surface in the interval depths H for any partial core-hole depth ξ. The relieved displacements under the described loading conditions are found by finite element calculations.

Similarly, the coefficients b_{ij} and c_{ij} are calculated by considering a pure shear stress state. To calculate the coefficient b_{ij}, the relieved displacement equations in the radial direction due to a uniform pressure from a surface to a depth H when a core-hole is ξ is considered as follows

$$\frac{1}{E}\sum_{j=1}^{n}\sum_{i=1}^{n}\frac{b_{ij}}{j}\xi_k^{i-1}\xi_l^j Q = uR_{kl} \tag{7.22}$$

In order to calculate the coefficients c_{ij}, we consider the relieved displacement equation in the radial direction

$$\frac{1}{E}\sum_{j=1}^{n}\sum_{i=1}^{n}\frac{c_{ij}}{j}\xi_k^{i-1}\xi_l^j Q = vR_{kl} \tag{7.23}$$

In this analysis, there are N=50 partial core-hole depths up to a maximum core-hole depth $\xi_{max} = 2$ considered. For any partial core-hole depth $\xi_k = \xi_{max} \times k/N$ ($k = 1,2,...,N$), a series of loading is subjected by applying a uniform pressure from 0 to $\xi_l = \xi_k \times l/k$ ($l = 1,...,k$). From this series of loading, 1275 relieved displacements are obtained for different loading depths H and core-hole depths ξ from the finite element analyses. The least squares method is employed to calculate the coefficients a_{ij}, b_{ij}, and c_{ij}. It is observed that $n = 10$ in Equation (7.20) give a reasonable compromise between accuracy and numerical stability.

Now for the known geometric information and the dimensionless coefficients a_{ij}, the relieved displacement under the known equibiaxial stress can be calculated by Equation (7.19). To estimate the accuracy of the coefficients, we find the relative residual from the equation given below.

$$err(\xi) = \frac{uR(\xi) - \frac{1}{E}\sum_{j=1}^{n}\sum_{i=1}^{n}\frac{a_{ij}}{j}\xi^{i-1}H^j P}{uR(\xi)} \tag{7.24}$$

Relative residual means the relative difference between finite element and calculated relieved displacements.

Figure 7.6 to Figure 7.8 show the relative residual for coefficients a_{ij}, b_{ij}, and c_{ij}, respectively versus core-hole depths. It is observed that the maximum error is about 0.5 % at a very shallow core-hole depth. The errors reduce quickly as the core-hole depth increases. It is also observed that errors are less than 0.1 % when $\xi > 0.25$. These results confirm the validity of the coefficients.

The values of the coefficients a_{ij}, b_{ij}, and c_{ij} are tabulated in   Table 7.1 to Table.

7.3. DEFINITION OF CONSTANTS A, B AND C FOR NON-UNIFORM STRESS THROUGH DEPTH

Compared to the procedure for the case of a uniform stress through depth procedure, the calibration constants A_c, B_c and C_c for core-hole analysis for non-uniform stress through the depth involves one additional independent variable, namely, the dimensionless depth H and core-hole depth $\xi = h/r_m$. Thus, in a generalized functional form, the calibration constant A_c can be expressed as

$$
\begin{aligned}
A_c, B_c, C_c = & f_A(E, v, k, h, H), \\
& f_B(E, v, k, h, H), \\
& f_C(E, v, k, h, H)
\end{aligned}
\tag{7.25}
$$

The calibration constant definitions for non-uniform stress through depth are different from those for uniform stress through depth. As will shown below, the calibration constants for non-uniform stress through thickness require some matrix calculations. There is very simple relationship between the constants A, B and C and the calibration constants A_c, B_c and C_c as given in Equation (6.4). In order to increase magnitude of the numbers in the matrix calculations and reduce the number of calculations, the calculations of the constants A, B and C are directly given below.

7.3.1. Constant A

Recall that in the relieved displacement equation given in Equation (3.42), the constant A is associated with equibiaxial stress P. Therefore, in order to define the calibration constant A_c for non-uniform stress through depth, we consider a known equibiaxial stress state of $\sigma_{xx} = \sigma_{yy} = \sigma_o$. The relieved displacement Equation (7.13) takes the following form

$$
uR(\xi) = \frac{1}{E} \int_0^\xi G_A(\xi, H) P(H) dH
\tag{7.26}
$$

After substituting Equation (7.15) in to Equation (7.26) we get

$$
uR(\xi) = \frac{1}{E} \int_0^\xi \sum_{i=1}^n \sum_{j=1}^n a_{kl} H^{j-1} \xi^{i-1} P(H) dH
\tag{7.27}
$$

Assume that the equibiaxial stress $P(H)$ is expressed as follows

$$
P(H) = \sum_{c=1}^C cp_c \phi_c(H)
\tag{7.28}
$$

where $\phi_c(H)$ are polynomials of degree c, and cp_c are coefficients to be found. If we substitute Equation (7.28) in to Equation (7.27) we get

222

$$uR(\xi) = \frac{1}{E} \int_0^\xi \sum_{i=1}^n \sum_{j=1}^n a_{kl} H^{j-1} \xi^{i-1} \sum_{c=1}^C cp_c \phi_c(H) dH \qquad (7.29)$$

Assume that $\phi_c(H)$ is given by the following power law

$$\phi_c = H^{c-1} \qquad (7.30)$$

If we substitute Equation (7.30) in to Equation (7.29), we get

$$uR(\xi) = \frac{1}{E} \int_0^\xi \sum_{i=1}^n \sum_{j=1}^n a_{kl} H^{j-1} \xi^{i-1} \sum_{c=1}^C cp_c H^{c-1} dH \qquad (7.31)$$

$$uR(\xi) = \frac{1}{E} \sum_{c=1}^C cp_c \sum_{i=1}^n \sum_{j=1}^n \frac{a_{kl}}{j+c-1} \xi^{i+j+c-2} \qquad (7.32)$$

$$u_r(\xi) = \frac{1}{E} \sum_{c=1}^C cp_c \sum_{i=1}^n \sum_{j=1}^n \frac{a_{kl}}{j+c-1} \xi^{i+j+c-2} r_m \qquad (7.33)$$

We can write the above Equation (7.32) in matrix form as follows

$$[M_A]\{C_P\} = \{UR\} \qquad (7.34)$$

where

$$[M_A] = \begin{pmatrix} mA_{11} & \cdots & mA_{1C} \\ \vdots & \ddots & \vdots \\ mA_{m1} & \cdots & mA_{mC} \end{pmatrix} \qquad (7.35)$$

$$mA_{rc} = \frac{1}{E} \sum_{i=1}^n \sum_{j=1}^n \frac{a_{ij}}{j+c-1} \xi_r^{i+j+c-2} r_m \qquad (7.36)$$

$$\{C_P\} = \begin{Bmatrix} cp_1 \\ cp_2 \\ \vdots \\ cp_C \end{Bmatrix} \qquad (7.37)$$

$$\{UR\} = \begin{Bmatrix} u_{r1} \\ u_{r2} \\ \vdots \\ u_{rm} \end{Bmatrix} \qquad (7.38)$$

223

In Equation (7.34), UR is the relieved displacement readings vector, and C_P is the vector of the unknowns that are the coefficients of the assumed in-situ stress function in Equation (7.28). This is an over determined linear system ($m>C$) (number of unknowns less than number of equations). Thus the linear system is solved by the normal equation method to get least-squares solution as follows

$$\{C_A\} = \left([M_A]^T [M_A]\right)^{-1} [M_A]^T \{UR\}$$

(7.39)

From the similarity of the relieved displacement equations under equibiaxial stress state, we can conclude that calibration constant A is

$$\frac{1}{A} = \left([M_A]^T [M_A]\right)^{-1} [M_A]^T$$

(7.40)

7.3.2. Constant B

In order to define constant B, we consider the known shear stress state of $\sigma_{xx} = -\sigma_{yy} = \sigma_o$. Similar to constant A, the relieved displacement equations due to drilling a core-hole to depth ξ are given below

$$uR(\xi) = \frac{1}{E} \int_0^\xi G_B(\xi, H) Q(H) \cos(2\alpha) dH$$

(7.41)

$$uR(\xi) = \frac{1}{E} \int_0^\xi \sum_{i=1}^n \sum_{j=1}^n b_{ij} H^{j-1} \xi^{i-1} Q(H) \cos(2\alpha) dH$$

(7.42)

Let the in-situ stress state be expressed as a function of H as follows

$$Q(H) = \sum_{c=1}^C cq_c \ \phi_c(H)$$

(7.43)

where $\phi_c(H)$ are polynomials of degree c, and cq_c are coefficients to be found.

$$uR(\xi) = \frac{1}{E} \int_0^\xi \sum_{i=1}^n \sum_{j=1}^n b_{ij} H^{j-1} \xi^{i-1} \sum_{c=1}^C cq_c \ \phi_c(H) \cos(2\alpha) dH$$

(7.44)

Assume that $\phi_c(H)$ is given by the following power law

$$\phi_c = H^{c-1}$$

(7.45)

From (7.42) it follows that

$$uR(\xi) = \frac{1}{E} \int_0^\xi \sum_{i=1}^n \sum_{j=1}^n b_{ij} H^{j-1} \xi^{i-1} \sum_{c=1}^C cq_c H^{c-1} \cos(2\alpha) dH \tag{7.46}$$

$$uR(\xi) = \frac{1}{E} \sum_{c=1}^C cq_c \sum_{i=1}^n \sum_{j=1}^n \frac{b_{ij}}{j+c-1} \xi^{i+j+c-2} \cos(2\alpha) \tag{7.47}$$

$$u_r(\xi) = \frac{1}{E} \sum_{c=1}^C cq_c \sum_{i=1}^n \sum_{j=1}^n \frac{b_{ij}}{j+c-1} \xi^{i+j+c-2} r_m \cos(2\alpha) \tag{7.48}$$

We can write the above equation in matrix form as follows

$$[M_B] \{C_Q\} = \{UR\} \tag{7.49}$$

where

$$[M_B] = \begin{pmatrix} mB_{11} & \cdots & mB_{1C} \\ \vdots & \ddots & \vdots \\ mB_{m1} & \cdots & mB_{mC} \end{pmatrix} \tag{7.50}$$

$$mB_{rc} = \frac{1}{E} \sum_{i=1}^n \sum_{j=1}^n \frac{b_{ij}}{j+c-1} \xi_r^{i+j+c-2} r_m \cos(2\alpha) \tag{7.51}$$

$$\{C_Q\} = \begin{Bmatrix} cq_1 \\ cq_2 \\ \vdots \\ cq_n \end{Bmatrix} \tag{7.52}$$

$$\{UR\} = \begin{Bmatrix} u_{r1} \\ u_{r2} \\ \vdots \\ u_{rm} \end{Bmatrix} \tag{7.53}$$

In Equation (7.50), UR represents the relieved displacement readings vector, and C_Q represents the vector of the unknowns that are the coefficients of the assumed in-situ stress function in Equation (7.28). This is again an over determined linear system ($m > C$). Thus, the linear system is solved by the normal equation method to get least squares solution.

$$\{C_Q\} = \left([M_B]^T [M_B] \right)^{-1} [M_B]^T \{UR\} \tag{7.54}$$

225

From the similarity of the relieved displacement equations under shear stress state, we can conclude that the calibration constant B is

$$\frac{1}{B} = \left(\left[M_B\right]^T \left[M_B\right]\right)^{-1} \left[M_B\right]^T \tag{7.55}$$

7.3.3. Constant C

In order to define constant C, we consider the known shear stress state of $\sigma_{xx}=-\sigma_{yy}=\sigma_o$. Similar to constant B, the tangential relieved displacement equations due to drilling a core-hole to depth ξ is given below

$$vR(\xi) = \frac{1}{E} \int_0^\xi G_C(\xi, H)Q(H)\sin(2\alpha)dH \tag{7.56}$$

$$vR(\xi) = \frac{1}{E} \int_0^\xi \sum_{i=1}^n \sum_{j=1}^n c_{ij} H^{j-1} \xi^{i-1} Q(H)\sin(2\alpha)dH \tag{7.57}$$

Let the in-situ stress state be expressed as a function of H as follows

$$Q(H) = \sum_{c=1}^C cq_c \; \phi_c(H) \tag{7.58}$$

where $\phi_c(H)$ are polynomials of degree c, and cq_c are coefficients to be found.

$$vR(\xi) = \frac{1}{E} \int_0^\xi \sum_{i=1}^n \sum_{j=1}^n c_{ij} H^{j-1} \xi^{i-1} \sum_{c=1}^C cq_c \; \phi_c(H)\sin(2\alpha)dH \tag{7.59}$$

Assume that $\phi_c(H)$ is given by the following power law

$$\phi_c = H^{c-1} \tag{7.60}$$

From (7.42) it follows that

$$vR(\xi) = \frac{1}{E} \int_0^\xi \sum_{i=1}^n \sum_{j=1}^n c_{ij} H^{j-1} \xi^{i-1} \sum_{c=1}^C cq_c H^{c-1} \sin(2\alpha)dH \tag{7.61}$$

$$vR(\xi) = \frac{1}{E} \sum_{c=1}^C cq_c \sum_{i=1}^n \sum_{j=1}^n \frac{c_{ij}}{j+c-1} \xi^{i+j+c-2} \sin(2\alpha) \tag{7.62}$$

$$v_\alpha(\xi) = \frac{1}{E} \sum_{c=1}^C cq_c \sum_{i=1}^n \sum_{j=1}^n \frac{c_{ij}}{j+c-1} \xi^{i+j+c-2} r_m \sin(2\alpha) \tag{7.63}$$

226

We can write the above equation in matrix form as follows

$$[M_C]\{C_Q\} = \{V\} \tag{7.64}$$

where

$$[M_C] = \begin{pmatrix} mC_{11} & \cdots & mC_{1C} \\ \vdots & \ddots & \vdots \\ mC_{m1} & \cdots & mC_{mC} \end{pmatrix} \tag{7.65}$$

$$mC_{rc} = \frac{1}{E}\sum_{i=1}^{n}\sum_{j=1}^{n}\frac{c_{ij}}{j+c-1}\xi_r^{i+j+c-2}r_m\sin(2\alpha) \tag{7.66}$$

$$\{C_Q\} = \begin{Bmatrix} cq_1 \\ cq_2 \\ \vdots \\ cq_C \end{Bmatrix} \tag{7.67}$$

$$\{V\} = \begin{Bmatrix} v_{\alpha 1} \\ v_{\alpha 2} \\ \vdots \\ v_{\alpha m} \end{Bmatrix} \tag{7.68}$$

In Equation (7.50), V represents the relieved displacement readings vector, and C_Q represents the vectors of the unknowns, which are the coefficient of the assumed in-situ stress function in Equation (7.28). This is again an over determined linear system (m>n). Thus, the linear system is solved by the normal equation method to get least squares solution.

$$\{C_Q\} = \left([M_C]^T[M_C]\right)^{-1}[M_C]^T\{V\} \tag{7.69}$$

From the similarity of the tangential relieved displacement equations under shear stress state, we can conclude that the constant C is

$$\frac{1}{C} = \left([M_C]^T[M_C]\right)^{-1}[M_C]^T \tag{7.70}$$

7.4. EXAMPLES

In order to verify the incremental core-drilling procedure, two examples are solved below. In each example, a structure under with in-situ stresses before the core-hole is drilled is considered. It is assumed that a core-hole is drilled in this structure in increments. The finite element model

created in Chapter 5 is used to simulate the core-hole drilling. The measured displacements (obtained from the finite element analysis) are recorded at each core-hole increment. Then these measured displacements are used in the procedure to calculate in-situ stresses that are assumed unknown prior to hole drilling as explained above. The in-situ stresses are presented as follows

$$\sigma_{xx}(z) = \sigma_{xo}(z) + \beta_{x1}z + \beta_{x2}z^2$$

$$\sigma_{yy}(z) = \sigma_{yo}(z) + \beta_{y1}z + \beta_{y2}z^2$$

$$\tau_{xy}(z) = \tau_{xyo}(z) + \beta_{xy1}z + \beta_{xy2}z^2$$

7.4.1. Example 1

In this example it is assumed that a core-hole is drilled in a structure that has a uniaxial stress state of σ_{xo} = 30 MPa, σ_{yo} = 0. It is also assumed that these in-situ stresses do not vary through the depth, $\tau_{xyo} = \beta_{x1} = \beta_{y1} = \beta_{xy1} = 0$.

The material properties of the structure and geometric properties of the core-hole are given as

E = 30000 MPa; a= 50 mm; k=1.5; r_m = 50 * k= 75 mm.

The measured displacements are calculated at four partial core-hole depths up to the maximum core-hole depth h = 40 mm for Test Configuration C by finite element analysis as follows.

$U1$={0.01456 mm, 0.03992 mm, 0.06242 mm, 0.07992 mm}

$U2$={0.0064 mm, 0.01658 mm, 0.02464 mm, 0.03024 mm}

$U3$ = {-0.00176 mm, -0.00676 mm, -0.01314 mm, -0.01944 mm}

Since we don't know how the in-situ stresses vary through depth, we need to estimate how the stresses vary through the depth. Let us assume that the in-situ stresses are linearly varying (C = 2) through the thickness. The matrices M_A, M_B are calculated by Equations (7.40) and (7.55) as follows

$$M_A = \begin{bmatrix} 2.1377x10^{-4} & 1.19161x10^{-5} \\ 5.52578x10^{-4} & 5.81755x10^{-5} \\ 8.21692x10^{-4} & 1.21717x10^{-4} \\ 1.00783x10^{-3} & 1.85896x10^{-4} \end{bmatrix}$$

$$
M_B = \begin{bmatrix} 2.1377x10^{-4} & 1.55871x10^{-5} \\ 7.78147x10^{-4} & 8.53626x10^{-5} \\ 1.2597x10^{-3} & 1.98861x10^{-4} \\ 1.65613x10^{-3} & 3.35164x10^{-4} \end{bmatrix}
$$

The constants A and B are calculated by Equations (7.40) and (7.55) as follows

$$
\frac{1}{A} = \left([M_A]^T [M_A] \right)^{-1} [M_A]^T
$$

$$
= \begin{bmatrix} 1739.83 & 2444.15 & 993.602 & -1526.98 \\ -10367.2 & -13780.8 & -3748.33 & 12810.8 \end{bmatrix}
$$

$$
\frac{1}{B} = \left([M_B]^T [M_B] \right)^{-1} [M_B]^T
$$

$$
= \begin{bmatrix} 968.098 & 1603.61 & 864.82 & -966.563 \\ -5223.68 & -8279.26 & -3506.27 & 7415.54 \end{bmatrix}
$$

The in-situ stress equations for Test Configuration C are given in Chapter 3 by Equations (3.132), (3.133) and (3.134). We obtain the in-situ stresses by substituting the measured displacements and A and B values in these equations as follows

$$
\sigma_{xx}(z) = \frac{1}{4}\frac{1}{A}(U1+U3) + \frac{1}{4}\frac{1}{B}(U1-U3) =
$$

$$
\frac{1}{4}\begin{bmatrix} 1739.83 & 2444.15 & 993.602 & -1526.98 \\ -10367.2 & -13780.8 & -3748.33 & 12810.8 \end{bmatrix} \cdot \begin{Bmatrix} 0.0128 \\ 0.03316 \\ 0.04928 \\ 0.06048 \end{Bmatrix}
$$

$$
+\frac{1}{4}\begin{bmatrix} 968.098 & 1603.61 & 864.82 & -966.563 \\ -5223.68 & -8279.26 & -3506.27 & 7415.54 \end{bmatrix} \cdot \begin{Bmatrix} 0.01632 \\ 0.04668 \\ 0.07556 \\ 0.09936 \end{Bmatrix}
$$

$$
= \begin{Bmatrix} 29.974\ \text{MPa} \\ 0.0018\ \text{MPa/mm} \end{Bmatrix}
$$

$$\sigma_{yy}(z) = \frac{1}{4}\frac{1}{A}(U1+U3) - \frac{1}{4}\frac{1}{B}(U1-U3) =$$

$$\frac{1}{4}\begin{bmatrix} 1739.83 & 2444.15 & 993.602 & -1526.98 \\ -10367.2 & -13780.8 & -3748.33 & 12810.8 \end{bmatrix} \cdot \begin{Bmatrix} 0.0128 \\ 0.03316 \\ 0.04928 \\ 0.06048 \end{Bmatrix}$$

$$-\frac{1}{4}\begin{bmatrix} 968.098 & 1603.61 & 864.82 & -966.563 \\ -5223.68 & -8279.26 & -3506.27 & 7415.54 \end{bmatrix} \cdot \begin{Bmatrix} 0.01632 \\ 0.04668 \\ 0.07556 \\ 0.09936 \end{Bmatrix}$$

$$= \begin{Bmatrix} -0.0083 \text{ MPa} \\ 0.0009 \text{ MPa/mm} \end{Bmatrix}$$

$$\tau_{xy} = \frac{U1-2U2+U3}{4B} =$$

$$\begin{bmatrix} 968.098 & 1603.61 & 864.82 & -966.563 \\ -5223.68 & -8279.26 & -3506.27 & 7415.54 \end{bmatrix} \begin{Bmatrix} 0 \\ 0 \\ 0 \\ 0 \end{Bmatrix}$$

$$= \begin{Bmatrix} 0 \text{ MPa} \\ 0 \text{ MPa/mm} \end{Bmatrix}$$

Let us approximate the in-situ stresses constant (C=1, uniform stress case). The matrices M_A, M_B are calculated by Equations (7.40) and (7.55) as follows

$$M_A = \begin{Bmatrix} 2.1377x10^{-4} \\ 5.52578x10^{-4} \\ 8.21692x10^{-4} \\ 1.00783x10^{-3} \end{Bmatrix}, \quad M_B = \begin{Bmatrix} 2.72177x10^{-4} \\ 7.78147x10^{-4} \\ 1.2597x10^{-3} \\ 1.65613x10^{-3} \end{Bmatrix}$$

The calibration constants are calculated as follows

$$\frac{1}{A} = \left([M_A]^T [M_A]\right)^{-1} [M_A]^T = \begin{bmatrix} 104.69 & 270.614 & 402.407 & 493.565 \end{bmatrix}$$

$$\frac{1}{B} = \left([M_B]^T [M_B]\right)^{-1} [M_B]^T = \begin{bmatrix} 54.3351 & 155.343 & 251.477 & 330.617 \end{bmatrix}$$

If we substitute the constants A and B and the measured displacements into the in-situ stress equations given by Equations (3.132), (3.133) and (3.134), we get in-situ stresses as follows

$$\sigma_{xx}(z) = \frac{1}{4}\frac{1}{A}(U1+U3) + \frac{1}{4}\frac{1}{B}(U1-U3) =$$

$$\frac{1}{4}[104.69 \quad 270.614 \quad 402.407 \quad 493.565] \cdot \begin{Bmatrix} 0.0128 \\ 0.03316 \\ 0.04928 \\ 0.06048 \end{Bmatrix}$$

$$+\frac{1}{4}[54.3351 \quad 155.343 \quad 251.477 \quad 330.617] \cdot \begin{Bmatrix} 0.01632 \\ 0.04668 \\ 0.07556 \\ 0.09936 \end{Bmatrix}$$

$$=29.9962 \text{ MPa}$$

$$\sigma_{yy}(z) = \frac{1}{4}\frac{1}{A}(U1+U3) - \frac{1}{4}\frac{1}{B}(U1-U3) =$$

$$\frac{1}{4}[104.69 \quad 270.614 \quad 402.407 \quad 493.565] \cdot \begin{Bmatrix} 0.0128 \\ 0.03316 \\ 0.04928 \\ 0.06048 \end{Bmatrix}$$

$$-\frac{1}{4}[54.3351 \quad 155.343 \quad 251.477 \quad 330.617] \cdot \begin{Bmatrix} 0.01632 \\ 0.04668 \\ 0.07556 \\ 0.09936 \end{Bmatrix}$$

$$=0.0013 \text{ MPa}$$

The last part of this example, assuming that the stresses are distributed uniformly through the depth, is same as the example given in Chapter 6. This result shows that incremental core-drilling formulations can be considered as the most general formulations for the calculations of the in-situ stresses.

7.4.2. Example 2

In this example it is assumed that a core-hole is drilled in a structure that has a uniaxial stress state of $\sigma_{xo} = 30$ MPa, $\beta_{xl} = 2$, $\sigma_{yo} = \tau_{xyo} = \beta_{yl} = \beta_{xyl} = 0$

The material properties of the structure and geometric properties of the core-hole are given as

$E = 30000$ Mpa; $a = 50$ mm; $k = 1.5$, $r_m = 50 * k = 75$ mm.

231

The measured displacements are calculated at five equal partial core-hole depth up to the maximum core-hole depth $h = 150$ mm for Test Configuration C by finite element analysis as follows.

$U1$={0.01438 mm, -0.03446 mm, -0.09238 mm, -0.1484 mm, -0.1839 mm}

$U2$={0.0064 mm, -0.00706 mm, -0.001718 mm, -0.02184 mm, -0.023 mm}

$U3$ = {-0.00158 mm, 0.02034 mm, 0.05802 mm, 0.09916 mm, 0.1379 mm}

Since we don't know how the in-situ stresses vary through depth, we need estimate how the stress vary through the depth. Let us assume that the in-situ stresses are uniformly distributed through depth ($C = 1$). The matrices M_A, M_B are calculated by Equations (7.40) and (7.55) as follows

$$M_A = \begin{Bmatrix} 8.21692x10^{-4} \\ 1.21866x10^{-4} \\ 1.3422x10^{-3} \\ 1.39031x10^{-3} \end{Bmatrix}, \; M_B = \begin{Bmatrix} 1.2597x10^{-3} \\ 2.223872x10^{-3} \\ 2.78255x10^{-3} \\ 3.30908x10^{-3} \end{Bmatrix}$$

The constants A and B are calculated as

$$\frac{1}{A} = \left([M_A]^T [M_A] \right)^{-1} [M_A]^T = [105.337 \quad 156.226 \quad 172.062 \quad 176.975 \quad 178.232]$$

$$\frac{1}{B} = \left([M_B]^T [M_B] \right)^{-1} [M_B]^T = [36.0538 \quad 64.074 \quad 79.6389 \quad 88.901 \quad 94.7087]$$

Substituting the constants A and B and the measured displacements into the in-situ stress equations for Test Configuration C, Equations (3.132), (3.133) and (3.134), we get in-situ stresses as follows

$$\sigma_{xx}(z) = \frac{1}{4} \frac{1}{A} (U1 + U3) + \frac{1}{4} \frac{1}{B} (U1 - U3) = 22.4 \text{ MPa}$$

$$\sigma_{yy}(z) = \frac{1}{4} \frac{1}{A} (U1 + U3) - \frac{1}{4} \frac{1}{B} (U1 - U3) = 11.05 \text{ MPa}$$

As seen from the results above, the uniform stress assumption of uniform stress through the depth produce large error in the estimate of in-situ stresses since the stresses vary significantly with depth.

Now lets approximate the in-situ stress with a third order polynomial ($C = 3$). The matrices M_A, M_B are calculated by Equations (7.40) and (7.55) as follows

$$
M_A = \begin{bmatrix}
8.21692x10^{-4} & 1.21717x10^{-4} & 2.66233x10^{-5} \\
1.21866x10^{-3} & 2.9078x10^{-4} & 1.11393x10^{-4} \\
1.3422x10^{-3} & 3.82997x10^{-4} & 1.8975x10^{-4} \\
1.38051x10^{-3} & 4.21796x10^{-4} & 2.35583x10^{-4} \\
1.39031x10^{-3} & 4.31717x10^{-4} & 2.4889x10^{-4}
\end{bmatrix},
$$

$$
M_B = \begin{bmatrix}
1.2597x10^{-3} & 1.98861x10^{-4} & 4.51918x10^{-5} \\
2.23872x10^{-3} & 6.303x10^{-4} & 2.685x10^{-4} \\
2.78255x10^{-3} & 1.05783x10^{-3} & 6.41465x10^{-4} \\
3.10616x10^{-3} & 1.42792x10^{-3} & 1.10089x10^{-3} \\
3.30908x10^{-3} & 1.7347x10^{-3} & 1.59735x10^{-3}
\end{bmatrix}
$$

The constants A and B are calculated as

$$
\frac{1}{A} = \left([M_A]^T [M_A] \right)^{-1} [M_A]^T = \begin{bmatrix}
4341.48 & -2356.54 & -1957.76 & 562.955 & 1550.01 \\
-25893.1 & 22432.1 & 15639.7 & -5695.5 & -13802.5 \\
20903.3 & -26439.6 & -15713.1 & 8527.24 & 17532.3
\end{bmatrix}
$$

$$
\frac{1}{B} = \left([M_B]^T [M_B] \right)^{-1} [M_B]^T = \begin{bmatrix}
1476.44 & 348.07 & -603.083 & -521.57 & 501.372 \\
-6377.64 & -392.087 & 3980.43 & 2798.41 & -3280.78 \\
3491.36 & -370.229 & -3137.66 & -1796.94 & 3075.23
\end{bmatrix}
$$

If we substitute the constants A and B and the measured displacements into the in-situ stress equations given by Equations (3.132), (3.133) and (3.134), we get the following in-situ stresses

$$
\sigma_{xx}(z) = \frac{1}{4}\frac{1}{A}(U1+U3) + \frac{1}{4}\frac{1}{B}(U1-U3) = \left\{ \begin{array}{c} 30.073 \text{ MPa} \\ 2.007 \text{ MPa/mm} \\ 0.00011 \text{ MPa/mm}^2 \end{array} \right\}
$$

$$
\sigma_{yy}(z) = \frac{1}{4}\frac{1}{A}(U1+U3) - \frac{1}{4}\frac{1}{B}(U1-U3) = \left\{ \begin{array}{c} 0.037 \text{ MPa} \\ -0.0048 \text{ MPa/mm} \\ 0.00008 \text{ MPa/mm}^2 \end{array} \right\}
$$

$$
\tau_{xy} = \frac{U1-2U2+U3}{4B} = \left\{ \begin{array}{c} 0.0000 \text{ MPa} \\ 0.0000 \text{ MPa/mm} \\ 0.0000 \text{ MPa/mm}^2 \end{array} \right\}
$$

233
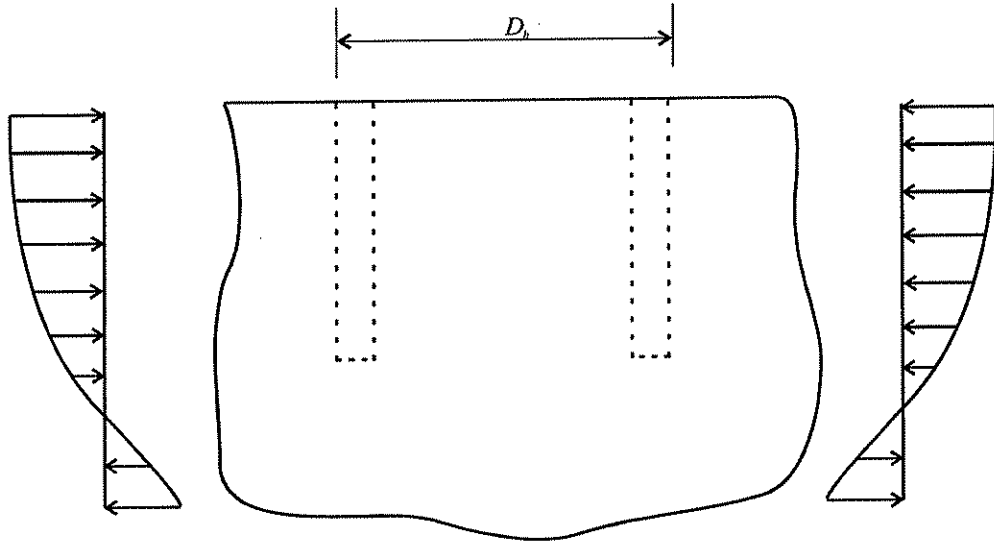
Figure 7.1 Non-uniform in-situ stresses distribution through depth in a structure.
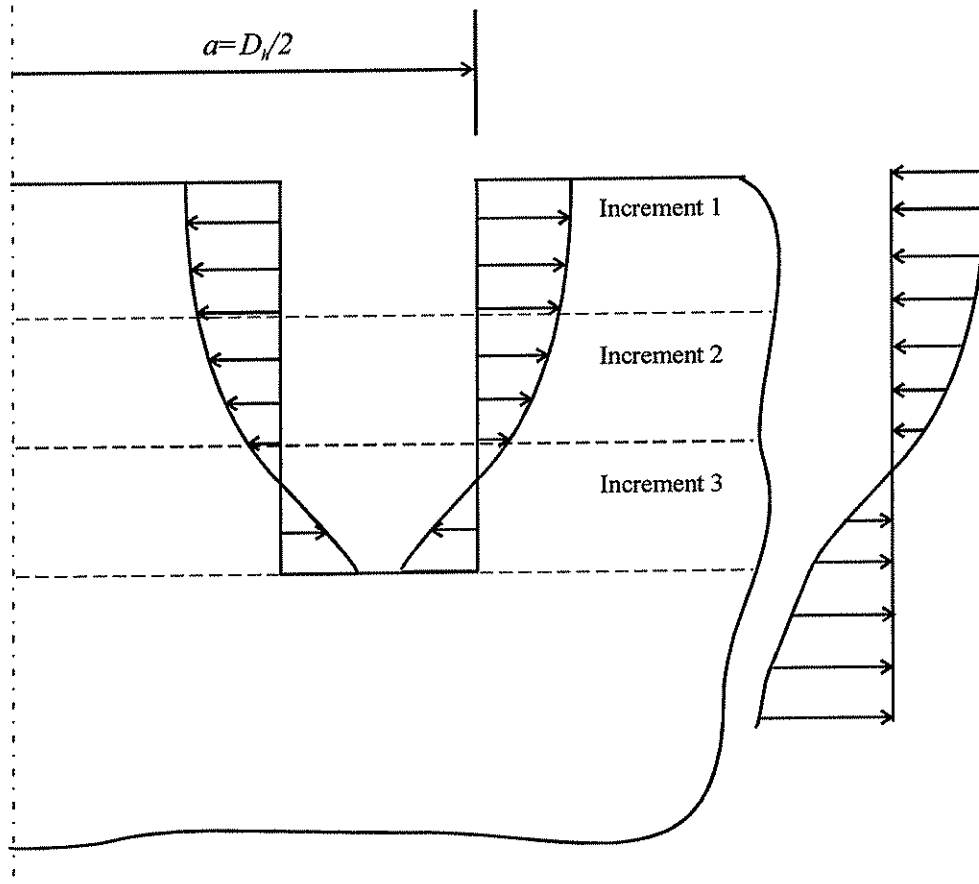
Figure 7.2 Core-hole with relieved in-situ stresses applied as loads to maintain equilibrium (half symmetry of structure is shown).
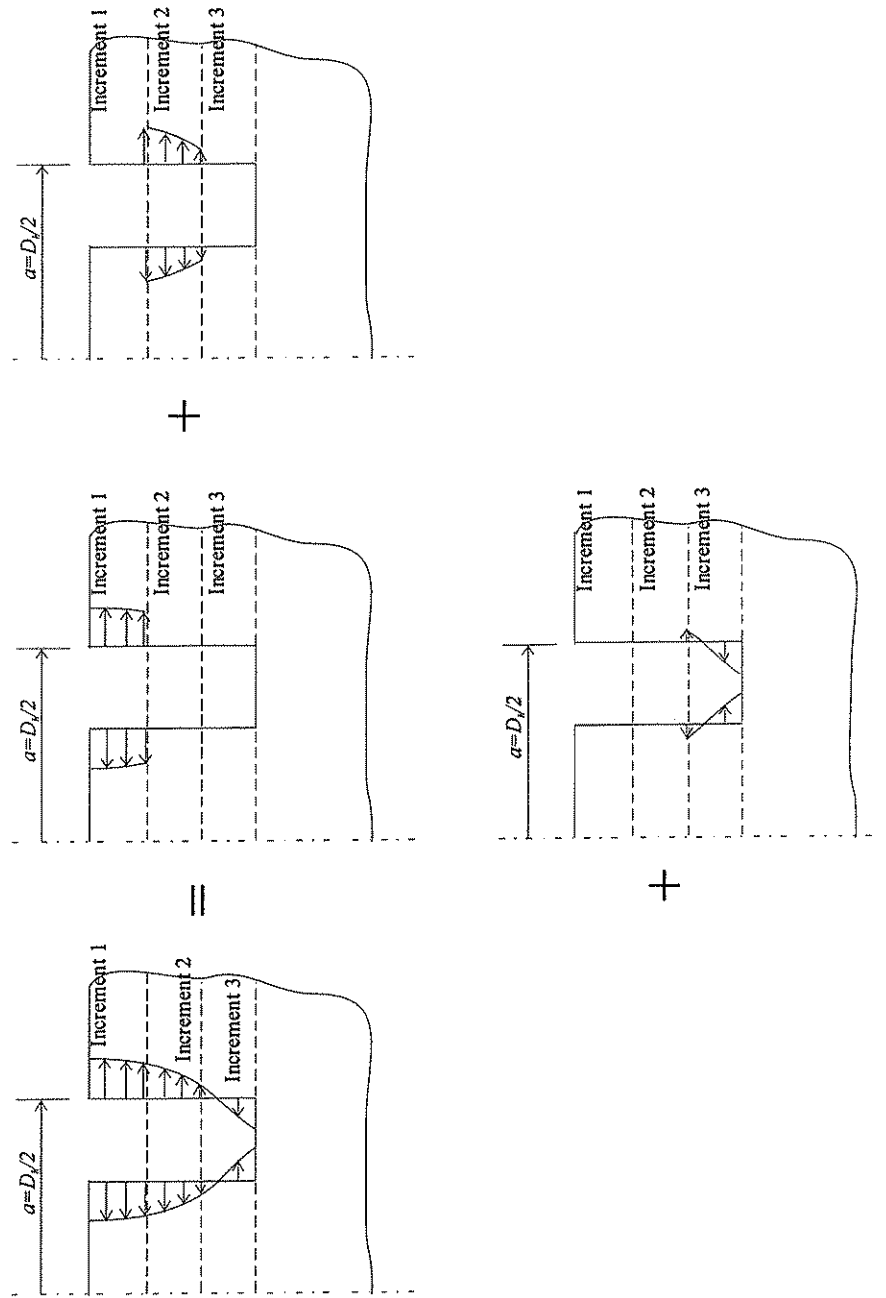
Figure 7.3 Schematic representation of contribution of relieved in-situ stresses to relieved displacements when the core-hole depth is *h*.
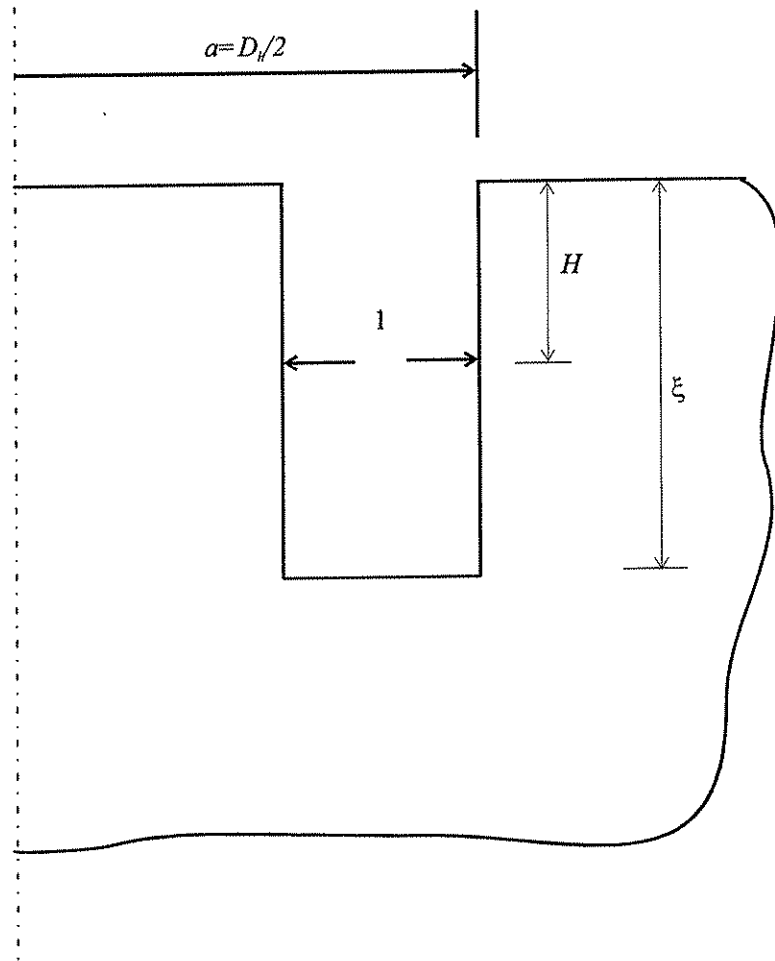
Figure 7.4 Definition of core-hole depth and stress depth.
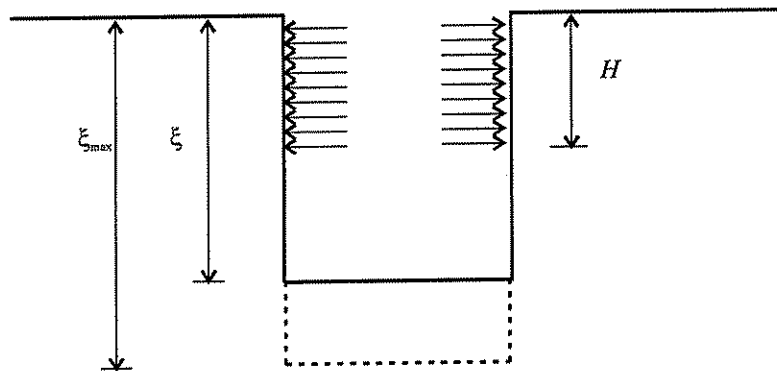
Figure 7.5 Representation of loading in finite element models.

236
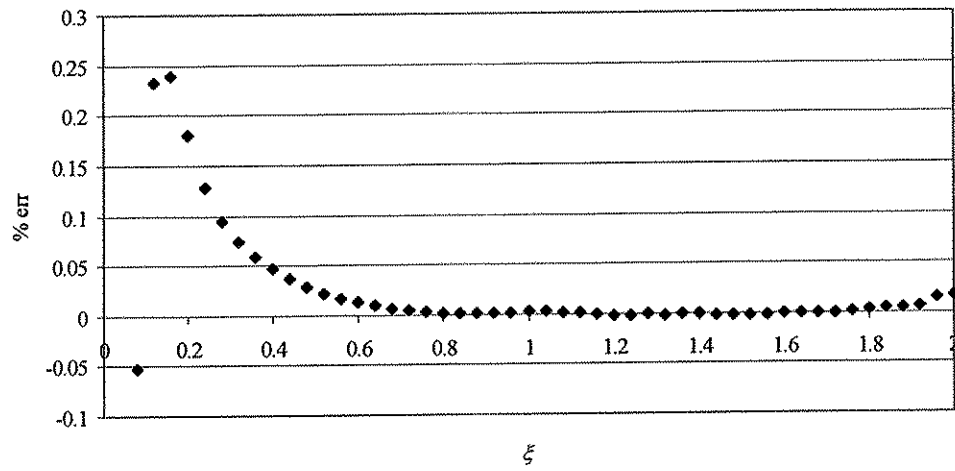
Figure 7.6 Relative residual of coefficient a_{ij} versus core-hole depth ξ for n=10.
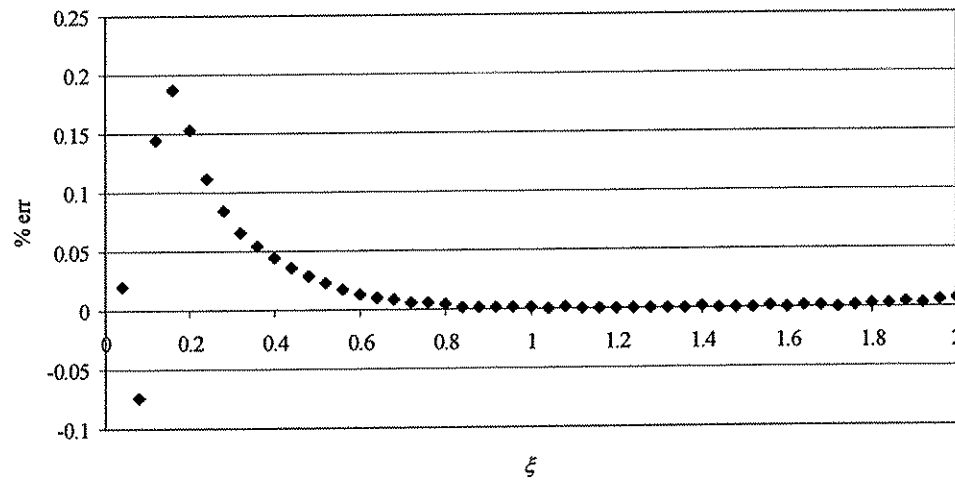
Figure 7.7 Relative residual of coefficient b_{ij} versus core-hole depth ξ for n=10.
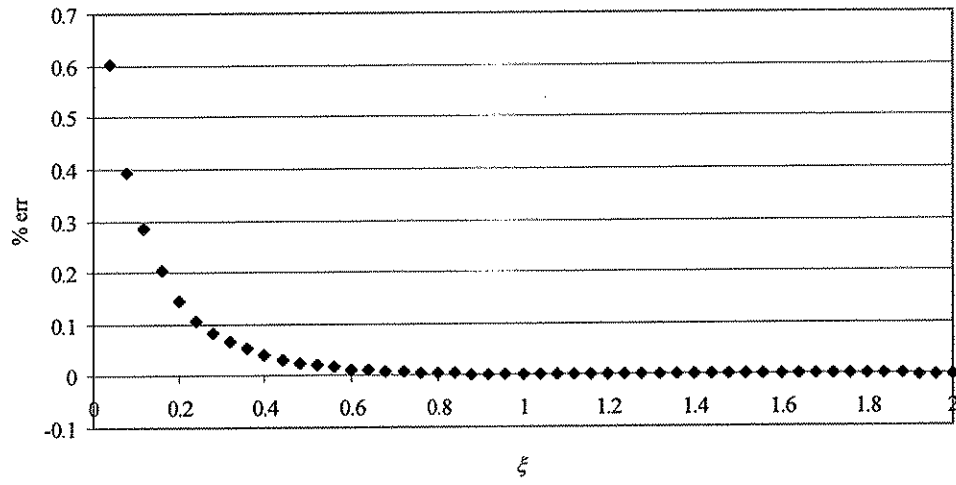
Figure 7.8 Relative residual of coefficient c_{ij} versus core-hole depth ξ for n=10.

i \ j	1	2	3	4	5	6	7	8	9	10
1	0.0817643	8.31569	-17.2705	5.523	38.1131	-75.4365	67.6573	-33.1038	8.55407	-0.915549
2	-6.62251	76.0948	-554.546	1985.11	-3982.17	4791.14	-3533.26	1564	-381.38	39.3709
3	-43.5404	358.433	-379.629	-2941.11	11093.3	-17569.3	15227.2	-7511.87	1981.53	-217.197
4	-85.7514	-673.914	3310.24	-4622.57	-2900.75	16191.3	-20159.4	12129	-3648.42	439.856
5	743.057	-411.815	-1132.44	5662.42	-10949.6	7306.88	1818.14	-4721.32	2187.53	-334.844
6	-2266.47	1235.04	-3068.4	12437.2	-11640.6	-879.016	6482.23	-3271.58	493.181	9.14471
7	4717.34	-876.917	-10868.7	8064.22	2089.3	-128.439	-5705.09	4686.48	-1430.5	152.514
8	-6836.43	10343.1	-2366.36	-2418.66	-680.242	805.555	2180.43	-2381.54	862.13	-108.053
9	3456.87	-5559.42	2450.22	-1257.68	3760.11	-4037.49	1620.97	-49.6397	-128.598	24.3917
10	-2.19045	-2776.59	8632.05	-11639.4	8833.43	-4125.81	1252.14	-268.328	43.5587	-4.11678

a_{ij}

Table 7.1 Coefficients for the calibration constant A_c.

b_{ij}										
i \ j	1	2	3	4	5	6	7	8	9	10
1	0.113734	8.44147	-5.33627	-42.2344	128.904	-176.135	136.191	-61.3272	15.0154	-1.54708
2	-5.51489	73.0781	-535.162	1969.51	-4031.34	4914.59	-3655.78	1627.75	-398.567	41.2702
3	-68.2162	581.458	-1723.15	1022.77	4405.45	-10617.7	10680.9	-5686.81	1570.63	-177.485
4	-110.273	-283.832	3292.91	-8395.49	7307.19	2732.39	-9790.4	7385.75	-2455.81	313.057
5	559.193	-790.892	592.093	4189.3	-10880.9	8104.83	595.973	-3690.1	1768.84	-271.22
6	-1585.56	779.822	-4468.39	12381.3	-11934.7	6047.09	-3335.43	2392.82	-1009.61	160.258
7	3250.83	1989.91	-10177.5	9606.43	-7761.77	7371.72	-4534.85	1266.52	-53.0548	-26.2638
8	-5692.42	5985.94	-3027.37	7691.32	-9456.2	3459.72	1025.72	-1124.76	295.87	-24.4272
9	4221.53	-3456.63	-5198.45	7620.19	-2821.22	-2.53773	-100.78	269.122	-103.245	12.0557
10	-2265.32	4815.78	-3301.67	-3.08577	1234.59	-816.794	322.346	-101.345	22.5262	-2.29523

Table 7.2 Coefficients for the calibration constant B_c.

c_{ij}

i \ j	1	2	3	4	5	6	7	8	9	10
1	-0.086543	-2.92126	3.12	1.61774	-7.63391	8.70057	-5.17963	1.72913	-0.30145	0.0207358
2	1.14677	-12.5722	88.0931	-286.778	525.052	-583.804	402.89	-168.693	39.2543	-3.89454
3	21.6365	-159.493	534.989	-880.476	640.152	56.9773	-446.606	324.327	-102.057	12.3709
4	16.7113	-79.7297	-59.3579	625.206	-917.196	336.21	347.36	-402.17	153.66	-21.1008
5	25.4456	-141.831	515.25	-1559.04	2361.12	-1754.35	520.107	88.2059	-94.8801	17.0986
6	43.3952	-290.092	1480.97	-2461.11	2507.27	-2192.73	1551.58	-731.034	196.274	-22.7171
7	79.577	-990.74	1633.73	-2444.3	3070.8	-1951.98	348.393	201.698	-107.981	15.2051
8	269.621	-130.049	1389.07	-3196.36	2652.59	-1029.67	273.39	-116.265	43.2332	-6.19348
9	-349.09	-492.27	2218.7	-2615.98	1811.87	-952.62	376.225	-90.2222	8.99184	0.0953446
10	623.523	-1845.87	2580.63	-2277.06	1376.78	-566.024	150.248	-23.8857	2.10922	-0.10162

Table 7.3 Coefficients for the calibration constant C_c.

CHAPTER 8

SUMMARY AND CONCLUSIONS

8.1. INTRODUCTION

The objective of this research is to establish the theoretical basis for the core-drilling method for the nondestructive evaluation of stresses in concrete structures. Procedures are developed to calculate in-situ stresses from measured displacements for a variety of test configurations, test object geometries, and in-situ stress states. The equations are first developed for infinite plates and then adapted to bounded objects. The following sections summarize the results and conclusions of this research. The summaries are organized by chapter.

8.2. RESULTS AND CONCLUSIONS FROM CHAPTER 3- DERIVATION OF IN-SITU STRESS EQUATIONS

8.2.1. Uniform Stress State

1. Closed-form relieved displacement equations were derived for a through-hole in an infinite thin plate subjected to a uniform stress state which is uniformly distributed through thickness. These equations calculate the relieved displacements of measurement points in the radial and the tangential directions for a known uniform stress state.

2. Closed-form measured displacement equations were derived for a through-hole in an infinite thin plate subjected to a uniform stress state which is uniformly distributed through thickness. These equations calculate the measured displacements between the two measurement points for a known uniform stress state.

3. Closed-form uniform in-situ stress equations in terms of cartesian stress components were derived for eight Test Configurations for a through-hole in an infinite thin plate. These equations calculate the in-situ stresses σ_{xx}, σ_{yy}, τ_{xy} at the hole location for the known measured displacements.

4. Closed-form uniform in-situ stress equations in terms of principal stresses and direction were derived for eight Test Configurations for a through-hole in an infinite thin plate. These equations calculate the in-situ stresses σ_{max}, σ_{min} and θ at the hole location for the known measured displacements.

242

8.2.2. Linear Gradient Stress State

1. Closed-form relieved displacement equations were derived for a through-hole in an infinite thin plate subjected to a linear gradient stress state which is uniformly distributed through thickness. These equations calculate the relieved displacements of measurement points in the radial and the tangential directions for a known linear gradient stress state.

2. Closed-form measured displacement equations were derived for a through-hole in an infinite thin plate subjected to a linear gradient stress states which is uniformly distributed through thickness. These equations calculate the measured displacements between the two measurement points for a known linear gradient stress state.

3. Closed-form linear gradient in-situ stress equations were derived for five Test Configurations for a through-hole in an infinite thin plate. These equations calculate the in-situ stresses σ_{xx}, σ_{yy}, τ_{xy}, Kx, Ky at the hole location for the known measured displacements.

8.3. RESULTS AND CONCLUSIONS FROM CHAPTER 4 – VERIFICATION OF THEORETICAL FORMULATIONS

1. The closed-form equations for relieved displacements and in-situ stresses derived in Chapter 3 were verified to be correct. The closed-form equations for relieved displacements were verified using finite element analyses. Once these equations were verified, they were then used to verify the closed-form equations for in-situ stresses.

2. For Test Configuration H, the closed-form in-situ stress equations in terms of principal stresses need to be modified when measured displacements $U2 = U3$. The additional equations for $U2 = U3$ are given in Chapter 4.

8.4. RESULTS AND CONCLUSIONS FROM CHAPTER 5 – APPLICATION TO OBJECTS WITH FINITE DIMENSIONS

8.4.1. Relieved Displacements

1. The relieved displacements due to drilling a through-hole are influenced by finite plate thickness. The relieved displacement in the radial direction due to drilling a through-hole in an object with finite thickness is closer to the plane stress solution than the plane strain solution. A maximum error of 3 % is observed when $T_p/D_h = 1$. The relieved displacement in the tangential direction due to drilling a through-hole in an object with finite thickness is influenced significantly by the object thickness T_p. More than a 10 % error is observed as the object thickness varies.

2. The relieved displacements are influenced significantly by core-hole depth when a core-hole is drilled in an object. The errors might be more than 100% at a shallow core-hole depth ($h/r_m < 0.4$), and reduce as core-hole depth increases. The relieved displacements in

243

the radial direction are closer to the closed-form solution when the core-hole depth $h/r_m >$ 2.5. However, the relieved displacement in the tangential direction is not close to the closed-form solution even when the core-hole depth $h/r_m > 6$.

3. The relieved displacements are not influenced significantly by object width variation. Less than 2% error is observed when $W_p/D_h=5$.

8.4.2. Closed-form Uniform In-situ Stress Equations

1. For Test Configurations A, B, C, D, E, and G, the closed-form uniform in-situ stress equations for plane stress assumptions are almost not affected by the object thickness variations when a through-hole is drilled in an object. For Test Configuration F, the closed-form uniform in-situ stress equations for plane stress assumptions can apply to an object when $T_p/D_h< 2$. For Test Configuration H, the closed-form uniform in-situ stress equations for plane stress assumptions can apply to an object when $T_p/D_h< 1$. For Test Configurations A, B, C, D, E, and G, the closed-form uniform in-situ stress equations for plane stress assumptions can apply to an object with a core-hole for $h/r_m > 3$. It is observed that the deeper core-hole depth, the better results are obtained.

2. The closed-form uniform in-situ stress equations can apply to objects with finite width. In particular, the closed-form uniform in-situ stress equations can give less than 1 % error for $W_p/D_h \le 4$. This error increases to 3 % when $W_p/D_h = 3$.

8.4.3. Closed-form Linear Gradient In-situ Stress Equations

1. The closed-form linear gradient in-situ stress equations are affected significantly by thickness variation when a through-hole is drilled in an object. The closed-form linear gradient in-situ stress equations can apply to an object for $T_p/D_h< 0.5$. The closed-form linear gradient in-situ stress equations solutions are affected significantly by core-hole depth h. These equations might give more than 90% error at a shallow core-hole depth ($h/r_m<0.3$). Errors between 5% and 15% were observed for different Test Configurations at $h/r_m=2$.

2. The closed-form linear gradient in-situ stress equations can apply to objects with finite width. In particular, the closed linear gradient in-situ stress equations can give less than 1 % error for $W_p/D_h \le 3$. This error increases to 4-5 % when $W_p/D_h = 2$.

8.5. RESULTS AND CONCLUSIONS FROM CHAPTER 6 – CALIBRATION CONSTANTS

8.5.1.1. Uniform In-situ Stress Equations

1. Relieved displacements due to through-hole drilling in an object subjected equibiaxial stress state are not influenced by thickness variations.

2. The radius of the hole influences the magnitude of the relieved displacements.

3. The maximum displacement release core-hole depth is determined by the radius of the measurement circle. The maximum displacement release core-hole depth is the core-hole depth at which the maximum relieved displacement is reached.

4. There are no closed-form solutions available from theory of elasticity for a through-hole or a core-hole in a thick object because of the complexity of the problem. Semi-analytical equations for relieved displacement and in-situ stresses were developed for objects with finite dimensions and core-hole for in-situ stresses uniformly distributed through the object thickness. This development is done by introducing empirical coefficients called calibration constants A_c, B_c, and C_c.

5. In general, calibration constants A_c, B_c, and C_c are functions of geometric properties and material properties. Accurate analytical definitions for the calibration constants were defined with dimensionless coefficients that make calibration constants material independent.

6. Geometric parameters were reduced by adopting dimensionless quantities. Consequently, the calibration constants for through-hole in thick objects are function of dimensionless geometric properties of T_p/D_h and $k = r_m/a$, and calibration constants for core-hole case are functions of dimensionless geometric properties of $k = r_m/a$, $\xi = h/r_m$. This means that once the calibration constants has been determined for particular dimensionless geometric property, the same calibration constants will apply when the geometric dimensions of the Test Configuration are similarly scaled.

7. Since the calibration constants were made material independent, once the coefficients are determined for particular material properties, the same coefficients will apply when material properties are different.

8. The calibration constants A_c, B_c, and C_c are related with constants A, B, and C. Once the constants A, B, and C are calculated, the in-situ stress equations derived in Chapter 3 can be used.

8.5.2. Linear Gradient In-situ Stress Equations

1. The calibration constants F_c, H_c, I_c and J_c for the linear gradient stress state are not calculated in this work. The concepts of the definition and method of calculation of the calibration constants F_c, H_c, I_c and J_c are same as that for calibration constants A_c, B_c, C_c.

8.6. RESULTS AND CONCLUSIONS FROM CHAPTER 7 – INCREMENTAL CORE-DRILLING METHOD

1. The incremental core-drilling method is developed primarily for applications in which in-situ stresses are non-uniform through the drilling depth. In such cases, the procedure, analytical definition of the calibration constants, and the calibration constant values given

in previous chapters are not applicable. However, using the incremental core-drilling method, it is possible to obtain the in-situ stresses as a function of depth z measured from the specimen surface. The experimental procedure in the incremental core-drilling method is similar to the procedure for the core-drilling method for uniform in-situ stress through the thickness. The incremental core-drilling method involves measuring displacements after successive increments of core-hole depth. Then these measured displacements are related to the in-situ stresses that vary through the depth.

2. Although this method is developed for non-uniform stress state through thickness, it was shown that this method also gives accurate results for a uniform stress state through thickness.

3. Since there is no solution available in closed-form for non-uniform stress through depth, semi-analytical equations for relieved displacement and in-situ stresses were derived for non-uniform in-situ stresses through depth.

4. The constants A, B and C are calculated by numerical analyses. These constants are defined with Influence Functions. Accurate analytical expressions for the Influence Functions for incremental core-drilling method were proposed. These Influence Functions contain coefficients which are calculated by finite element analysis for the dimensionless geometric properties (for example $k = r_m/a$, $\xi = h/r_m$). With the pre-calculated dimensionless coefficients for the particular dimensionless geometric properties, the incremental core-drilling method can be used to calculate the non-uniform stress state through depth. Once these coefficients are calculated for a particular geometric property, these coefficients can apply when geometric properties are similarly scaled.

5. Once the constants A, B, and C are calculated, the in-situ stress equations derived in Chapter 3 can be used.

6. In-situ stresses can be expressed by polynomials of degree c. This allows the calculation of high gradient stress variations of the in-situ stresses through depth.

8.7. FUTURE RESEARCH

This section summarizes future research which follows from the work described in this report.

1. The theoretical basis for the core-drilling method was established based on the assumptions of linear elastic homogenous, isotropic materials. Further research is needed to explore the impact of these assumptions. This may be done experimentally and analytically.

2. Physical tests need to be performed using the core-drilling method. In order to perform these tests, measurement techniques need to be identified that are capable of making the small displacement measurements that are required to successfully apply the core-drilling method. In addition to having sufficient resolution, viable measurement techniques will have to be practical for field applications if they are to be used on actual structures.

3. Calibration constants were calculated for only uniform stress state. The calibration constants for linear gradient stress state need to be calculated.

4. Experimental and analytical investigations need to be performed to evaluate the influence of the presence of steel reinforcement in the concrete and the effects of creep and shrinkage of the concrete.

LIST OF REFERENCES

ABAQUS/ Standard User's Manual [2000], Vol. II Version 6.1.

ANSYS/ User's Manuals [2000] Version 6.1.

Abduner, C. (1982). "Direct Measurement of Stresses in Concrete Structures." Maintenance, Repair, and Rehabilitation of Bridges, International Association for Bridge & Structural Engineering, 39-44.

ASTM D 4623. (1996). "Standard Test Method for Determination of In-Situ Stress in Rock Mass by Overcoring Method." ASTM Standard D 4623 - 94a, American Society for Testing and Materials.

ASTM E 837. (1994). "Standard Test Method for Determining Residual Stresses by the Hole-Drilling Strain-Gage Method." ASTM Standard E 837 - 94a, American Society for Testing and Materials.

Beghini, M. a. B., L. (1998). "Recent Advances in the Hole Drilling Method for Residual Stress Measurement." Journal of Materials Engineering and Performance, 7, 163-172.

Beghini, M. a. B., L. (2000). "Analytical expression of the influence functions for accuracy and versatility improvement in the hole-drilling method." Journal of Strain Analysis, 35, 125-135.

Bijak-Zoochaski, M. (1978). "A Semidestructive Method of Measuring Residual Stresses." VDI-Berichte, No. 313, pp. 469-476.

Cook, R., Malkus, D. S., Plesha, M. E. 1989. Concepts and Applications of Finite Element Analyses, John Wiley & Sons.

Flaman, M. T. a. M., B.H. (1985). "Determination of Residual Stress Variation with Depth by the Hole-Drilling Method." Experimental Mechanics, 25(9), 205-207.

Keeler, B., Mehrabi, A.B., Azizinamini, A., Rohde, J.,. (1994). "Toward Development of a Non-destructive Technique to Measure the Available Prestress in Prestressed Concrete Girders." 12801, University of Nebraska, Lincoln.

Kelsey, R. A. (1956). "Measuring Non-Uniform Residual Stresses by the Hole Drilling Method." Proceedings SESA, 181-194.

248